https://ntrs.nasa.gov/search.jsp?R=19870017663 2020-03-20T09:27:17+00:00Z

Langley
IN-32
93171
P-261

OSU

The Ohio State University

AIRBORNE ANTENNA RADIATION PATTERN CODE USER'S MANUAL

Walter D. Burnside
Jacob J. Kim
Brett Grandchamp
Roberto G. Rojas
Philip Law

The Ohio State University
ElectroScience Laboratory
Department of Electrical Engineering
Columbus, Ohio 43212

Report No. 716199-4
Contract No. NSG-1498
September 1985

National Aeronautics and Space Administration
Langley Research Center
Hampton, VA 23665

(NASA-CR-181249) AIRBORNE ANTENNA RADIATION PATTERN CODE USER'S MANUAL (Ohio State Univ.) 261 p Avail: NTIS HC A12/MF A01 CSCL 20N
N87-27096
Unclas
G3/32 0093171

NOTICES

When Government drawings, specifications, or other data are used for any purpose other than in connection with a definitely related Government procurement operation, the United States Government thereby incurs no responsibility nor any obligation whatsoever, and the fact that the Government may have formulated, furnished, or in any way supplied the said drawings, specifications, or other data, is not to be regarded by implication or otherwise as in any manner licensing the holder or any other person or corporation, or conveying any rights or permission to manufacture, use, or sell any patented invention that may in any way be related thereto.

50272-101

REPORT DOCUMENTATION PAGE

1. REPORT NO.

2.

3. Recipient's Accession No.

4. Title and Subtitle
AIRBORNE ANTENNA RADIATION PATTERN CODE USER'S MANUAL

5. Report Date
September 1985

6.

7. Author(s)
W.D. Burnside, J. Kim, B. Grandchamp, R. Rojas, P. Law

8. Performing Organization Rept. No.
716199-4

9. Performing Organization Name and Address
The Ohio State University
ElectroScience Laboratory
1320 Kinnear Road
Columbus, Ohio 43212

10. Project/Task/Work Unit No.

11. Contract(C) or Grant(G) No
(C) NAG-1498
(G)

12. Sponsoring Organization Name and Address
National Aeronautics and Space Administration
Langley Research Center
Hampton, VA 23665

13. Type of Report & Period Covered

14.

15. Supplementary Notes

16. Abstract (Limit: 200 words)

This report describes the use of a newly developed computer code to analyze the radiation patterns of antennas mounted on a composite ellipsoid and in the presence of a set of finite flat plates. Furthermore, it is shown how the code allows the user to simulate a wide variety of complex electromagnetic radiation problems using the ellipsoid/plates model. The code has the capability of calculating radiation patterns around an arbitrary conical cut specified by the user. The organization of the code, definition of input and output data, and numerous practical examples are also presented. The analysis is based on the Uniform Geometrical Theory of Diffraction (UTD), and most of the computed patterns are compared with experimental results to show the accuracy of this solution.

PRECEDING PAGE BLANK NOT FILMED

17. Document Analysis a. Descriptors

KEY WORDS:

Uniform Geometrical Theory of Diffraction (UTD)
Ray optical technique
Electromagnetic radiation and scattering
Airborne antenna radiation pattern
Computer code user's manual
High frequency analysis
Composite ellipsoid
Experimental verification

b. Identifiers/Open-Ended Terms

c. COSATI Field/Group

18. Availability Statement

19. Security Class (This Report)
Unclassified

20. Security Class (This Page)
Unclassified

21. No. of Pages
247

22. Price

(See ANSI-Z39.18)

See Instructions on Reverse

OPTIONAL FORM 272 (4-77)
(Formerly NTIS-35)
Department of Commerce

TABLE OF CONTENTS

Page

LIST OF TABLES v

LIST OF FIGURES vi

I. INTRODUCTION 1

II. PRINCIPLES OF OPERATION 5

III. DEFINITION OF INPUT DATA 11

COMMAND PART 18

- A. Unit and Frequency Commands 20
    - A1. COMMAND UN 20
    - A2. COMMAND FQ 21
- B. Fuselage Geometry Related Commands 22
    - B1. COMMAND FG 22
    - B2. COMMAND FB 24
    - B3. COMMAND FC 26
- C. Source Geometry Related Commands 27
    - C1. COMMAND SG 27
    - C2. COMMAND SP 32
    - C3. COMMAND LS 33
- D. Plate Geometry Related Commands 38
    - D1. COMMAND PG 38
    - D2. COMMAND PI 41

Page

E. Pattern Cut Related Commands 42

E1. COMMAND PD 42

E2. COMMAND RT 46

F. Specific Terms Related Commands 49

F1. COMMAND TO 49

F2. COMMAND RD 53

F3. COMMAND DD 54

F4. COMMAND RS 55

G. Execute and Output Related Commands 56

G1. COMMAND LP 56

G2. COMMAND PP 56

G3. COMMAND BO 58

G4. COMMAND EX 58

IV. INTERPRETATION OF INPUT DATA 59

V. PROGRAM OUTPUT 68

VI. APPLICATION OF CODE TO SEVERAL SIMPLE EXAMPLES 74

VII. APPLICATION OF CODE TO AIRCRAFT SIMULATIONS 89

REFERENCES 246

LIST OF TABLES

Table Page

I BLOCK DIAGRAM OF THE MAIN PROGRAM 8

II BLOCK DIAGRAM OF THE INPUT DATA ORGANIZATION FOR THE COMPUTER CODE 12

LIST OF FIGURES

Figure		Page
1	Definition of fuselage geometry.	23
2	Definition of antenna phase reference point for computer code. Note that PHS = ϕ_S and ZS = $-|Z_S|$ in the above drawings.	29
3	Source geometry. (Note that RHOA(MS)=ρ_A and PHIA(MS)=ϕ_A)	30
4	Definition of flat plate geometry.	39
5	Definition of pattern axis.	45
6	Definition of rotate-translate coordinate system geometry.	47
7(a)	Data format used to define a flat plate intersecting another flat plate.	64
7(b)	Data format used to define a box structure.	64
7(c)-(f)	Fuselage and wing geometries for aircraft model looking from the front. The antenna is assumed to be on the top portion of the models.	65
7(g)	Data format used to define a flat plate attaching to a fuselage.	66
8	Composite ellipsoid geometry simulating the aircraft fuselage.	67
9(a)	Line printer output for the $E_{\theta p}$ fields of Example 1.	70
9(b)	Line printer output for the $E_{\phi p}$ fields of Example 1.	71
10	Transformed coordinate sysems for the conical pattern cuts.	72
11	A monopole mounted on a composite ellipsoid.	74
12	Radiation pattern of monopole mounted on a composite ellipsoid at frequency .3 GHz. (a) (b) (c) source located at PHS=25°, ZS=3λ (d) (e) source located at PHS=25°, ZS=10λ and fuselage chopped off at ZC2=14λ for (e).	76

Figure Page

13 A bend plate attached to a composite ellipsoid. 77

14 Various GTD terms. 78

15 Roll plane radiation pattern. 84

16 Total solution (S+R+D) after using "PI:" and "PG:" commands. 88

17 Edge to edge plate attachment. 90

18 Edge to surface plate attachment. 90

19 Test locations for the antenna installation on the Boeing 737 aircraft. 94

20 Boeing 737 aircraft. 95

21 Computer simulated model of a Boeing 737 aircraft. The antenna is located at Station 220. 96

22 Roll plane pattern of a $\lambda/4$ monopole mounted at Station 220 on top of a Boeing 737 aircraft. 97

23 Elevation plane pattern of a $\lambda/4$ monopole mounted at Station 220 on top of a Boeing 737 aircraft. 98

24 Azimuth plane pattern of a $\lambda/4$ monopole mounted at Station 220 on top of a Boeing 737 aircraft. 99

25 Azimuthal conical patterns of a $\lambda/4$ monopole mounted at Station 220 on top of a Boeing 737 aircraft. 100

26 Elevation plane pattern of a $\lambda/4$ monopole mounted at Station 250 (off center) on top of a Boeing 737 aircraft. 106

27 Elevation plane pattern of a $\lambda/4$ monopole mounted at Station 305 on top of a Boeing 737 aircraft. 107

28 Computer simulated model for a $\lambda/4$ monopole mounted at Station 222 on the bottom of the fuselage of a Boeing 737 aircraft. 109

29 Elevation plane patterns of an antenna mounted at Station 222 on the bottom of a Boeing 737 aircraft. 110

Figure Page

30 Computer simulated model for a $\lambda/4$ monopole mounted at Station 950 on the bottom of the fuselage of a Boeing 737 aircraft. 114

31 Elevation plane pattern of a $\lambda/4$ monopole mounted at Station 950 on the bottom of a Boeing 737 aircraft. 115

32 KC-135 aircraft. 117

33 Computer simulated model of a KC-135 aircraft. The antenna is located over the wings. 118

34 Computer simulated model of a KC-135 aircraft. The antenna is located forward of the wings. 119

35 Elevation plane pattern for a $\lambda/4$ monopole mounted on a KC-135 aircraft. 121

36 Elevation plane pattern for a circumferential KA-band waveguide mounted on a KC-135 aircraft. 122

37 Elevation plane pattern for an axial KA-band waveguide mounted on a KC-135 aircraft. 123

38 Roll plane pattern for a $\lambda/4$ monopole mounted on a KC-135 aircraft. 124

39 Roll plane pattern for a KA-band circumferential waveguide mounted on a KC-135 aircraft. 125

40 Roll plane pattern for a KA-band axial waveguide mounted on a KC-135 aircraft. 126

41 Azimuth plane pattern for a $\lambda/4$ monopole mounted on a KC-135 aircraft. 127

42 Azimuth plane pattern for a KA-band circumferential waveguide mounted on a KC-135 aircraft. 128

43 Azimuth plane pattern for a KA-band axial waveguide mounted on a KC-135 aircraft. 129

44 Computer simulated model for Lindberg antenna mounted on a KC-135. 131

45 Elevation plane pattern for Lindberg antenna mounted on a KC-135 aircraft. 133

Figure		Page
46	Roll plane pattern for Lindberg antenna mounted on a KC-135 aircraft.	135
47	Azimuth plane pattern for Lindberg antenna mounted on a KC-135 aircraft.	137
48	Azimuth conical pattern (θ_p=45°) for Lindbert antenna mounted on a KC-135 aircraft.	139
49	Cessna 402B.	143
50	Model for Cessna 402B with engines and fuel tanks.	144
51	Roll plane pattern for Cessna 402B model.	145
52	Beechcraft Baron with Antenna in forward location.	148
53	Beechcraft Baron model with engine housings.	149
54	Roll conical pattern (θ_p=80°) for Beechcraft Baron model shown in Figure 53.	150
55	Beechcraft Baron model with rotating propellers on one side.	152
56(a)	Roll conical pattern for the Beechcraft Baron with propeller at 0° (vertical).	154
56(b)	Roll conical pattern for the Beechcraft Baron with propeller at 45°.	155
56(c)	Roll conical pattern for Beechcraft Baron with propeller at 90° (horizontal).	156
56(d)	Roll conical pattern for the Beechcraft Baron with propeller at 135°.	157
57	Variation in the roll conical pattern for the Beechcraft Baron due to the rotation of the propellers.	158
58	Cessna 150.	160
59	Cessna 150 model. Dashed lines are not part of the computer simulation.	161
60	Elevation plane pattern for a Cessna 150 aircraft.	162

Figure Page

61 F-16 fighter aircraft. 167

62 Computer simulated model of a F-16 fighter aircraft. 168

63 Azimuthal conical pattern (θ_p=10°) of a $\lambda/4$ monopole mounted on top of a F-16 fighter aircraft. 169

64 Azimuthal conical pattern (θ_p=20°) of a $\lambda/4$ monopole mounted on top of a F-16 fighter aircraft. 170

65 Azimuthal conical pattern (θ_p=30°) of a $\lambda/4$ monopole mounted on top of a F-16 fighter aircraft. 171

66 Azimuthal conical pattern (θ_p=40°) of a $\lambda/4$ monopole mounted on top of a F-16 fighter aircraft. 172

67 Azimuthal conical pattern (θ_p=45°) of a $\lambda/4$ monopole mounted on top of a F-16 fighter aircraft. 173

68 Azimuthal conical pattern (θ_p=50°) of a $\lambda/4$ monopole mounted on top of a F-16 fighter aircraft. 174

69 Azimuthal conical pattern (θ_p=55°) of a $\lambda/4$ monopole mounted on top of a F-16 fighter aircraft. 175

70 Azimuthal conical pattern (θ_p=60°) of a $\lambda/4$ monopole mounted on top of a F-16 fighter aircraft. 176

71 Azimuthal conical pattern (θ_p=65°) of a $\lambda/4$ monopole mounted on top of a F-16 fighter aircraft. 177

72 Azimuthal conical pattern (θ_p=70°) of a $\lambda/4$ monopole mounted on top of a F-16 fighter aircraft. 178

73 Azimuthal conical pattern (θ_p=75°) of a $\lambda/4$ monopole mounted on top of a F-16 fighter aircraft. 179

74 Azimuthal conical pattern (θ_p=80°) of a $\lambda/4$ monopole mounted on top of a F-16 fighter aircraft. 180

75 Azimuthal conical pattern (θ_p=85°) of a $\lambda/4$ monopole mounted on top of a F-16 fighter aircraft. 181

76 Azimuthal conical pattern (θ_p=90°) of a $\lambda/4$ monopole mounted on top of a F-16 fighter aircraft. 182

77 Azimuthal conical pattern (θ_p=95°) of a $\lambda/4$ monopole mounted on top of a F-16 fighter aircraft. 183

Figure Page

78 Azimuthal conical pattern (θ_p=100°) of a $\lambda/4$ monopole mounted on top of a F-16 fighter aircraft. 184

79 Azimuthal conical pattern (θ_p=105°) of a $\lambda/4$ monopole mounted on top of a F-16 fighter aircraft. 185

80 Azimuthal conical pattern (θ_p=110°) of a $\lambda/4$ monopole mounted on top of a F-16 fighter aircraft. 186

81 Azimuthal conical pattern (θ_p=115°) of a $\lambda/4$ monopole mounted on top of a F-16 fighter aircraft. 187

82 Azimuthal conical pattern (θ_p=120°) of a $\lambda/4$ monopole mounted on top of a F-16 fighter aircraft. 188

83 Elevation plane pattern of a $\lambda/4$ monopole mounted on top of a F-16 fighter. 189

84 Roll plane pattern of a $\lambda/4$ monopole mounted on top of a F-16 fighter aircraft. 190

85 F-4 (Phantom) fighter aircraft. 193

86 Computer simulated model of a F-4 Phantom fighter aircraft. 194

87 Azimuthal conical pattern (θ_p=105°) of a $\lambda/4$ monopole mounted on the belly of a F-4 fighter aircraft. 195

88 A-10 aircraft. 198

89 Computer simulated model of an A-10 aircraft. 199

90 Azimuthal conical pattern (θ_p=105°) of four monopoles mounted on the belly of a A-10 aircraft. 200

91 C-141 aircraft. 202

92 Computer simulated model of a C-141 aircraft. 203

93 Azimuthal conical patterns of a $\lambda/4$ monopole mounted on a C-141 aircraft. 205

94 Elevation plane pattern of a $\lambda/4$ monopole mounted on top of a C-141 aircraft. 210

95 Missile model for an axial slot mounted between two ram jets. 213

Figure Page

96 Roll plane pattern for an axial slot mounted between two ram jets. 214

97 Elevation plane pattern for an axial slot mounted between two ram jets. 215

98 Missile model for an axial slot mounted on a ram jet. 217

99 Roll plane pattern for an axial slot mounted on a ram jet. 218

100 Elevation plane pattern for an axial slot mounted on a ram jet. 219

101 S-band quad antenna locations on the Space Shuttle. 224

102 Computer simulated model for a crossed-slot antenna mounted on top of a Space Shuttle Orbiter. 225

103 Elevation plane patterns for a crossed-slot antenna mounted on top of a Space Shuttle Orbiter. 226

104 Azimuth plane patterns for a crossed-slot antenna mounted on top of a Space Shuttle Orbiter. 227

105 Roll plane radiation patterns for a crossed-slot antenna mounted on top of a Space Shuttle Orbiter. 228

106 Roll conical patterns (θ_p=45°) for a crossed-slot antenna mounted on top of a Space Shuttle Orbiter when the payload bay doors are closed. 229

107 Computer simulated model for a crossed-slot antenna mounted on top of a Space Shuttle Orbiter when the payload bay doors are open. 234

108 Roll conical patterns (θ_p=45°) for a crossed-slot antenna mounted on top of a Space Shuttle Orbiter when the payload bay doors are open. 235

109 Computer simulated model for a crossed-slot antenna mounted on bottom of a Space Shuttle Orbiter. 238

110 Roll conical patterns (θ_p=45°) for a crossed-slot antenna mounted on bottom of a Space Shuttle Orbiter when the payload bay doors are closed. 239

Figure Page

111 Computer simulated model for a crossed-slot antenna mounted on bottom of a Space Shuttle Orbiter when the payload bay doors are open. 244

112 Roll conical patterns (θ_p=45°) for a crossed-slot antenna mounted on bottom of a Space Shuttle Orbiter when the payload bay doors are open. 245

I. INTRODUCTION

If modern aircraft antennas are to function properly, the antenna patterns must meet certain system requirements. The conventional design procedure for an antenna on a particular aircraft has been to evaluate the performance of a candidate antenna system based on numerous scale-model measurements. This approach not only requires a great deal of engineering time and expense, it also has the following drawback.

When the near-field patterns are relatively easy to measure, the far-field patterns are not. To obtain the far-field patterns cost-effectively, there has been a great deal of interest in determining far-field patterns based on near-field pattern measurements. Currently, most of the attention has focused on plane, cylindrical and spherical wave spectrum approaches. However, each of these spectrum approaches is basically an integral transform which in itself can be tedious and expensive. Thus, the following dilemma prevails: far-field patterns are desired but cannot be easily measured directly; near-field patterns are much easier to measure but cannot be simply transformed to the far field.

One approach to solve the above problem is the geometrical theory of diffraction (GTD). It is a high frequency technique which is valid for computing both the near-field and far-field patterns when the source and various scattering centers are separated on the order of a wavelength. The near-field solution can be easily verified by a near-field measurement. Once this near-field verification is accomplished, the solution can be directly extended to the far field without the need of a transformation. The GTD is directly applicable to the near-field pattern prediction because the GTD postulates are not violated in the sense that the receiver is essentially in the far field of each isolated specular point. For instance, the receiver might not be in the far field of a flat plate; yet, it is sufficiently removed from each of the edge diffraction points that the GTD is valid (i.e., the receiver is at least a wavelength away from the isolated diffraction points). Consequently, a GTD solution can effectively solve both the near-field and the far-field airborne antenna patterns.

This Fortran 77 computer code has been developed at Ohio State University to investigate the radiation patterns of antennas mounted on an aircraft fuselage which is modeled by a composite ellipsoid. The computer code is used to compute the near zone and far zone radiated fields for antennas mounted on a composite ellipsoid and in the presence of a set of finite flat plates. The analysis applied in the development of this code is based on the uniform geometrical theory of diffraction (UTD) [1,2,3].

The code allows the user to simulate a wide variety of complex electromagnetic radiation problems using the ellipsoid/plates model. For example, the composite ellipsoid can be used to accurately simulate the fuselage of an aircraft; whereas, the plates are used to represent the wings, stabilizers, stores, etc. Alternatively, the antenna could be mounted directly on a ship mast. In this case the mast could be approximated by the composite ellipsoid with the other ship structures simulated by flat plates. Note that the plates can be attached to the composite ellipsoid and/or to other plates. In fact, the plates can be connected together to form a box. This code is specifically designed to analyze the radiation characteristics of antennas mounted on aircraft configurations.

As with any ray optical solution such as this UTD code, there is a limit to the number of interactions included in the field computation. In this case, the code includes the source, reflected, diffracted, and higher order terms such as the reflected/reflected, reflected/diffracted, diffracted/reflected, and diffracted/diffracted fields. The higher order terms are due to the multiple field interactions between the simulation plates. It assumes that the higher-order diffracted and reflected fields from the composite ellipsoid surface are small and can be neglected. The user may request the code (by using the "TO:" COMMAND) to compute the higher order terms when he thinks they have a significant effect on the results; otherwise, the code will compute first order terms only. This implies that the code can handle structures for which the energy does not significantly bounce back-and-forth across the target. In any event, the code automatically shadows all terms, such that if a higher-order interaction should have been included the resulting pattern will contain a discontinuity. These higher-order terms are normally negligible and can only affect the pattern in rather small sectors. However, if they are significant in some region, the amplitude of the jump is associated with the radiation level of the missing higher-order term. Consequently when the solution fails because of a lack of higher-order terms, it tends to indicate its failure.

The code has the flexibility to handle arbitrary pattern cuts. In addition, an arbitrary antenna type can be analyzed provided the current distribution across the aperture is known. This is done by approximating the distribution by a set of magnetic current elements mounted on or electric currents normal to the composite ellipsoid surface. The magnetic current elements have a cosine distribution along the magnetic current direction and a uniform distribution in the orthogonal direction. The normal electric current represents a monopole provided that its length isn't greater than a quarter wavelength.

The mutual coupling effect for monopole arrays mounted on a fuselage can be handled by thin-wire theory [4], if the region near the array is nearly flat. For engineering purposes, image theory can be applied to calculate the relative current distributions as equivalent dipole arrays. The relative current value on each dipole is then taken to be part of the input data for each monopole source specification. The final pattern is the superposition of the contributions from each individual monopole.

The limitations associated with the computer code result from the basic nature of the analyses. The solution is derived using the UTD, which is a high frequency approach. In terms of the scattering from plate structures this means that each plate should have edges at least a wavelength long. In terms of the composite ellipsoid structure its major and minor radii should be at least a wavelength in extent. In addition, each antenna element should be at least a wavelength from all edges. In some cases, the wavelength limit can be reduced to a quarter wavelength for engineering purposes.

The present code requires approximately 707K bytes of storage. It will run a pattern cut of 360 points for a commercial aircraft model (Example 3, 6 plates included) with one antenna element in approximately 4 minutes on a VAX 11/780 Computer.

This user's manual is designed to give an overall view of the operation of the computer code, to instruct a user in how to use it to model structures, and to show the validity of the code by comparing various computed results against measured data whenever available. Section II describes an overall view of the organization of the program. The definition of the input is given in Section III. How to apply the capabilities of this input data to a practical structure is briefly discussed in Section IV. This includes a clarification of the subtle points of interpreting the input data. The representation of the output is discussed in Section V. Numerous practical airborne antenna problems are presented in Section VI to illustrate the operation, versatility, and validity of the code.

II. PRINCIPLES OF OPERATION

The analytical modeling of complex scattering shapes in order to predict the radiation patterns of antennas has been accomplished using the Uniform Geometrical Theory of Diffraction (UTD) [1,2,3]. This is a high frequency technique that allows a complicated structure to be approximated by basic shapes representing canonical problems in the UTD. These shapes include flat or curved wedges and convex curved surfaces.

The UTD is a ray optical technique, and it, therefore, allows one to gain some physical insight into the various scattering and diffraction mechanisms involved. Consequently, one is able to quickly seek out the dominant mechanisms for a given geometrical configuration and radiation sector. This, in turn, leads to an accurate engineering solution to practical antenna problems. This approach has been used successfully in the past to model aircraft shapes [5,6,7,8,9,10] and ship-like structures [11,12,13].

This section briefly describes the basic operation of this code for the analysis of antennas in an aircraft environment. The present version of the code allows the analysis of objects that can be modeled by flat plates and a composite ellipsoid all of which are built up from the basic canonical problems. These shapes allow one to model a wide variety of structures in the UHF range and above where the scattering structures are large in terms of a wavelength. The general rule is that the lower frequency limit of this solution is dictated by the spacings between the various scattering centers and their overall size. In practice this means that the smallest dimensions should be on the order of a wavelength.

The positive time convention ejωt has been used in this code, and, all the structures are assumed to be perfectly conducting and surrounded by free space.

As mentioned above, the UTD approach is ideal for a general high frequency study of aircraft antennas in that only the most basic structural features of an otherwise very complicated structure need to be modeled. This is because ray optical techniques are used to determine components of the field incident on and diffracted by various structures. Components of the diffracted fields are found using the UTD solutions in terms of the individual rays which are summed with the geometrical optics terms at the field point. The rays from a given scatterer tend to interact with other structures causing various higher-order terms. In this way one can trace out the various possible combinations of rays that interact between scatterers and include only the dominant terms in the solution. Thus, one need only be concerned with the important scattering components and neglect all other higher-order terms. This method leads to accurate and efficient computer codes that can be systematically written and tested.

Complex problems are built up from similar components in terms of a modular computer code. This modular approach is illustrated in the block diagram of the main program shown in Table I. The code is broken up into many subroutines that represent different scattered field components, ray tracing sections, geodesic path algorithms [14,15], plate attachment calculation and shadowing routines. One is referred to Reference [16] for more details on this topic. As can be seen from the flow chart, the code is structured so that all of one type of scattered field is computed at one time for the complete pattern cut so that the amount of core swapping is minimized, thereby, reducing overlaying and increasing efficiency. The results are then, superimposed in the main program as the various segments are executed.

TABLE I

BLOCK DIAGRAM OF THE MAIN PROGRAM

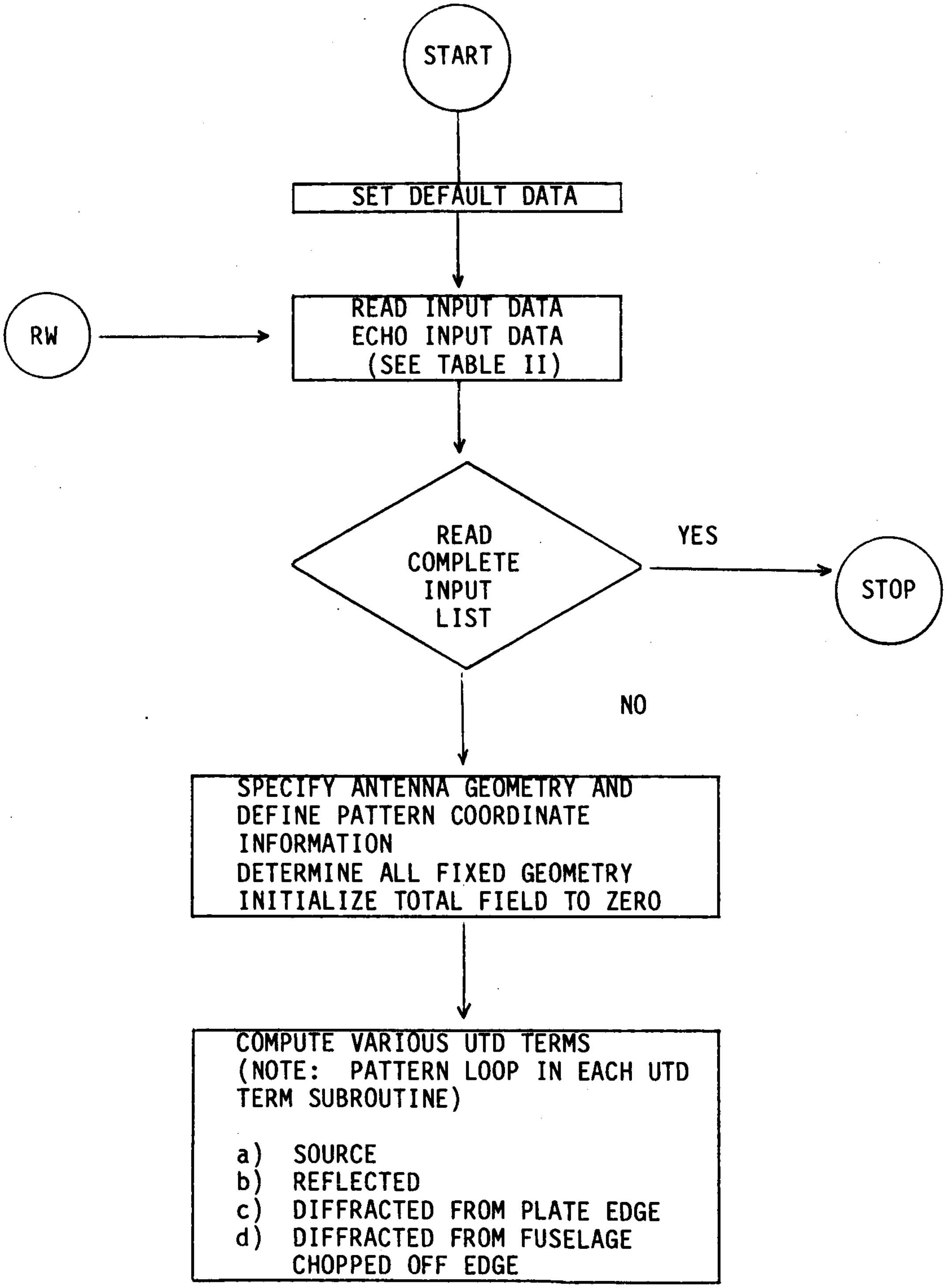
START
SET DEFAULT DATA
RW
READ INPUT DATA
ECHO INPUT DATA
(SEE TABLE II)
READ COMPLETE INPUT LIST
YES
STOP
NO
SPECIFY ANTENNA GEOMETRY AND
DEFINE PATTERN COORDINATE
INFORMATION
DETERMINE ALL FIXED GEOMETRY
INITIALIZE TOTAL FIELD TO ZERO
COMPUTE VARIOUS UTD TERMS
(NOTE: PATTERN LOOP IN EACH UTD
TERM SUBROUTINE)
a) SOURCE
b) REFLECTED
c) DIFFRACTED FROM PLATE EDGE
d) DIFFRACTED FROM FUSELAGE
CHOPPED OFF EDGE

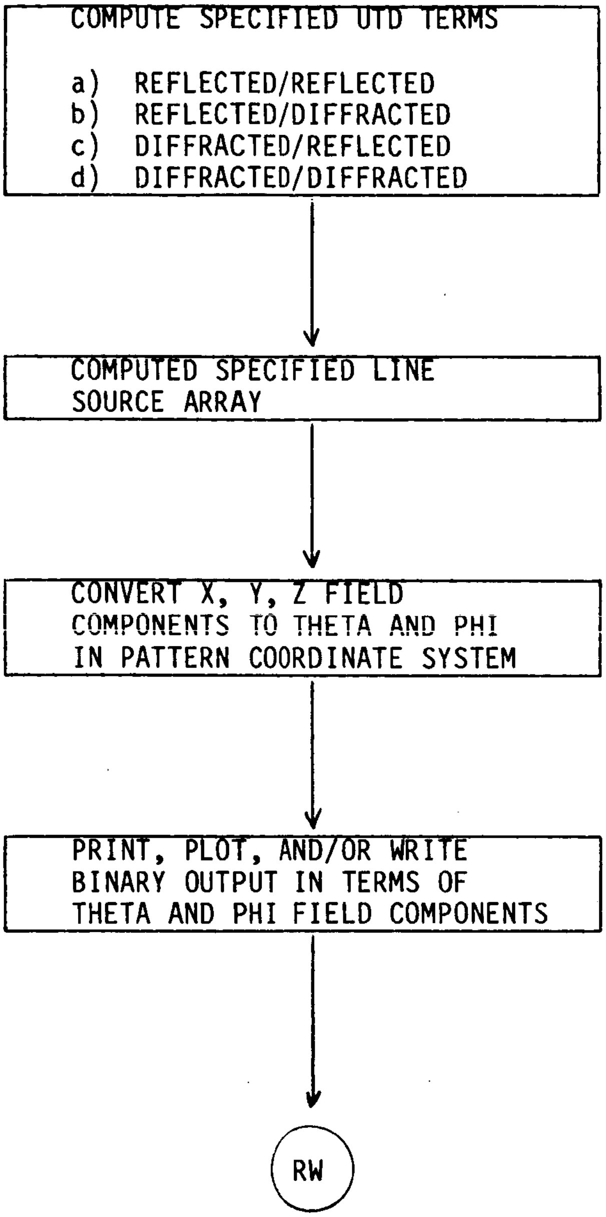
COMPUTE SPECIFIED UTD TERMS
a) REFLECTED/REFLECTED
b) REFLECTED/DIFFRACTED
c) DIFFRACTED/REFLECTED
d) DIFFRACTED/DIFFRACTED
COMPUTED SPECIFIED LINE SOURCE ARRAY
CONVERT X, Y, Z FIELD COMPONENTS TO THETA AND PHI IN PATTERN COORDINATE SYSTEM
PRINT, PLOT, AND/OR WRITE BINARY OUTPUT IN TERMS OF THETA AND PHI FIELD COMPONENTS
RW

The subroutines for each of the scattered field components are all structured in the same basic way. First, the ray path is determined from the source to a particular scatterer and subsequently to the observation point using either the laws of reflection or diffraction. Each ray path, assuming one is possible, is then checked to see if it is shadowed by any structure along the complete ray path. If it is shadowed, the field is not computed and the code proceeds to the next scatterer or observation point. If the path is not interrupted, the scattered field is computed using the appropriate UTD solutions. The fields are then superimposed in the main program. This shadowing process is often speeded up by making various decisions based on bounds associated with the geometry of the structure. This type of knowledge is used wherever possible.

The shadowing of rays is a very important part of the UTD scattering code. It is obvious that this approach leads to various discontinuities in the resulting pattern; however, the UTD diffraction coefficients are designed to smooth out the discontinuities in the field such that a continuous field is obtained. When a scattered field is not included in the result, the lack of its presence is apparent. This can be used to advantage in analyzing complicated problems. Obviously, in a complex problem not all the possible scattered fields can be included. In the UTD code the importance of the neglected terms are determined by the size of the so-called gliches or jumps in the pattern trace.

If the gliches are small, no additional terms are needed for a good engineering solution. If the gliches are large, it may be necessary to include more terms in the solution. In any case the user has a gauge with which he can examine the accuracy of the results and is not falsely led into believing a result is correct when in fact there could be an error associated with neglecting a higher order interaction term.

The brief discussion of the operation of the scattering code given above should help the user get a feel for the overall code so he might better understand the code's capabilities and interpret its results. The code is designed, however, so that a general user can run the code without knowing all the details of its operation. Yet, he must become familiar with the input/output details which will be discussed in the next three sections.

III. DEFINITION OF INPUT DATA

The method used to input data into the computer code is presently based on a command word system. This is especially convenient when more than one problem is to be analyzed during a computer run. The code stores the previous input data such that one need only input that data which needs to be changed from the previous execution. Also, there is a default list of data so for any given problem the amount of data that needs to be input has been shortened. The organization of the input data is illustrated in Table II.

In this system, all linear dimensions may be specified in either meters, inches, or feet; whereas, all angular dimensions are in degrees. All the dimensions are eventually referred to a fixed cartesian

TABLE II

BLOCK DIAGRAM OF THE INPUT DATA ORGANIZATION FOR THE COMPUTER CODE

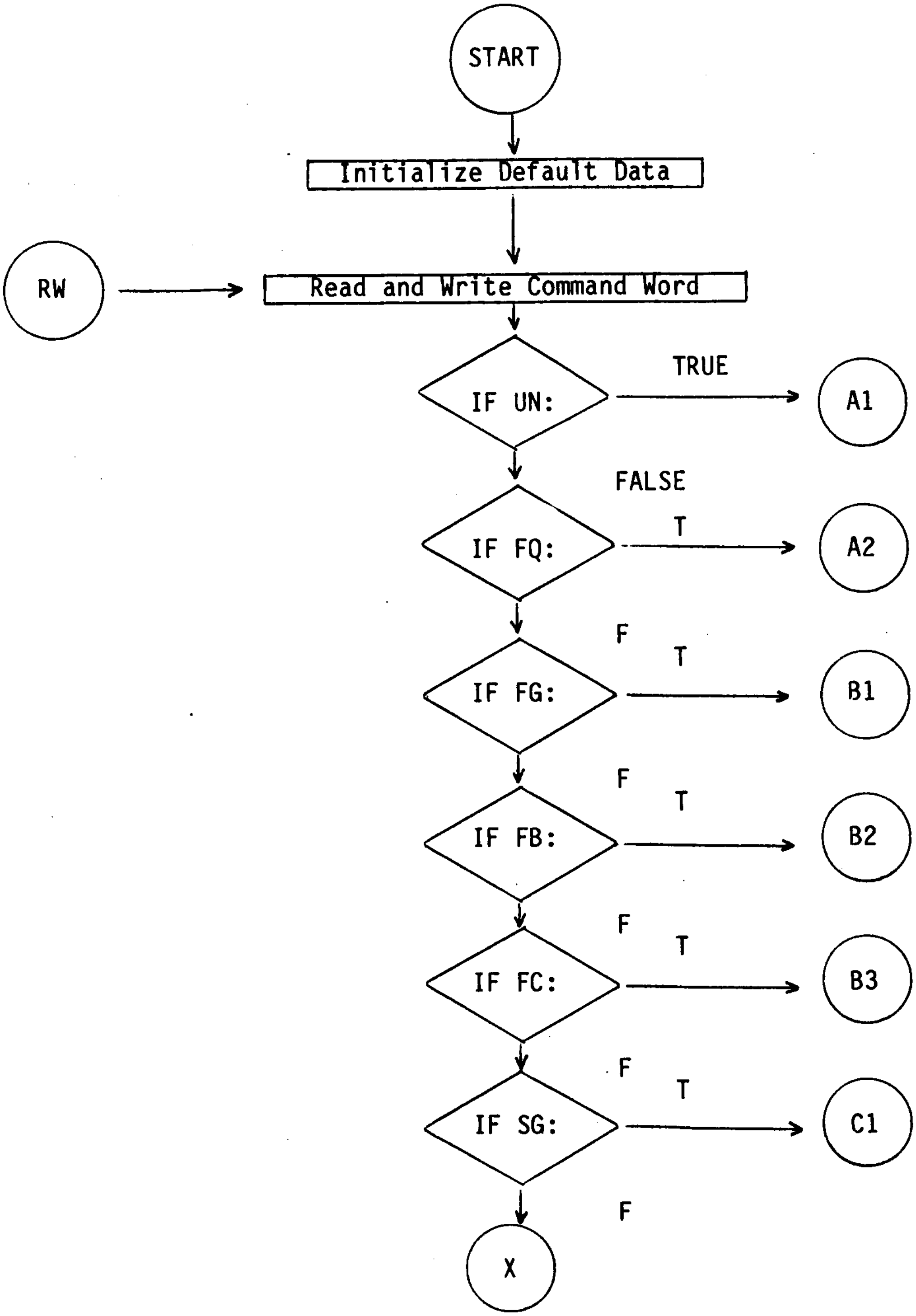
START
Initialize Default Data
RW
Read and Write Command Word
IF UN:
TRUE
A1
FALSE
IF FQ:
T
A2
F
IF FG:
T
B1
F
IF FB:
T
B2
F
IF FC:
T
B3
F
IF SG:
T
C1
F
X

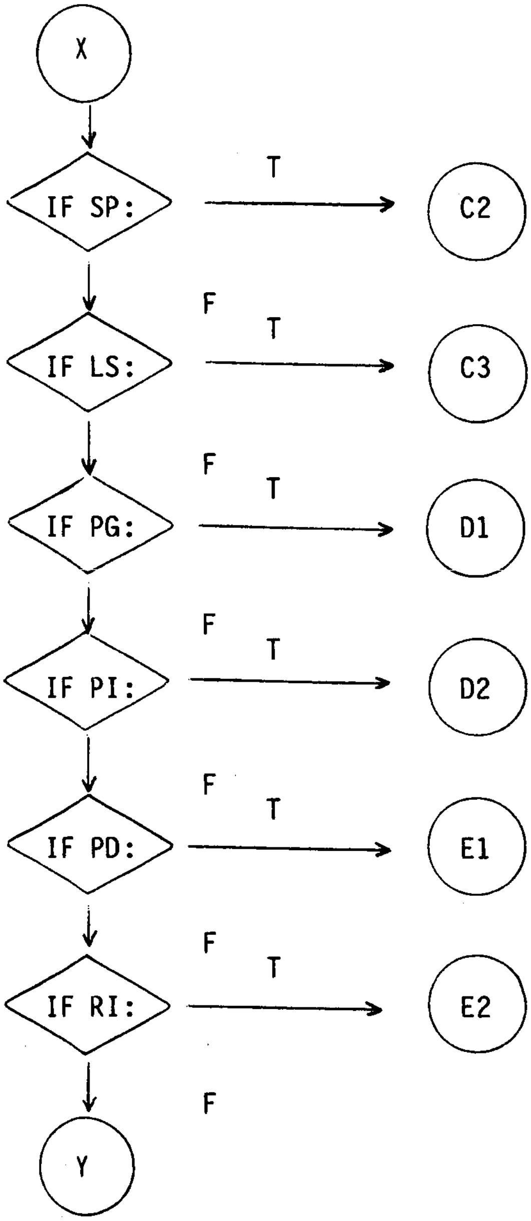
X
IF SP:
T
C2
F
IF LS:
T
C3
F
IF PG:
T
D1
F
IF PI:
T
D2
F
IF PD:
T
E1
F
IF RI:
T
E2
F
Y

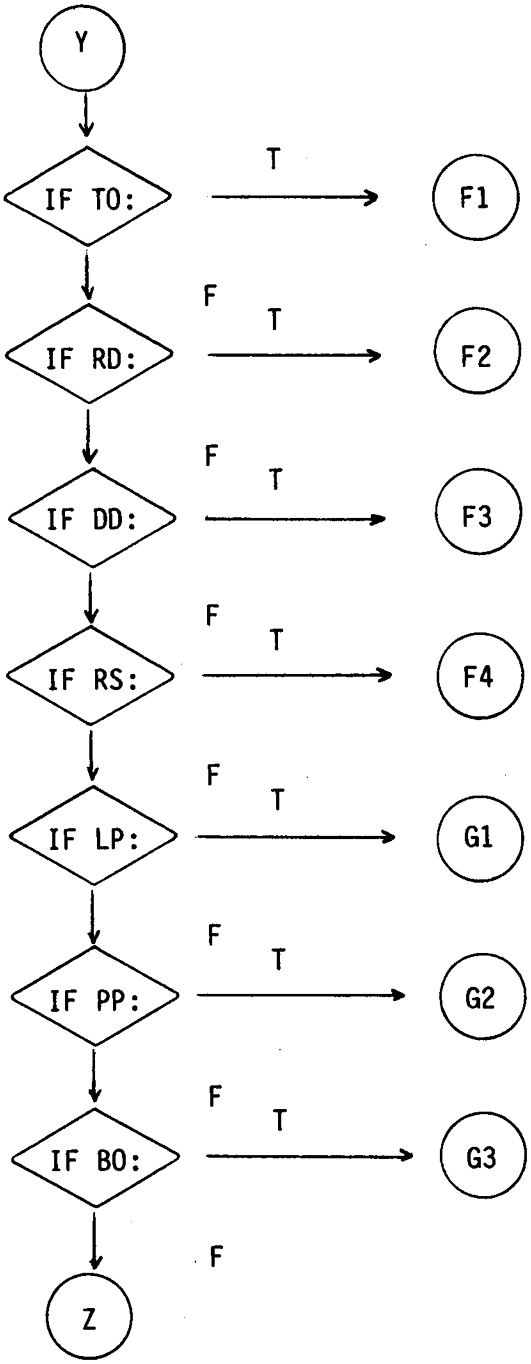
Y
IF TO:
T
F1
F
IF RD:
T
F2
F
IF DD:
T
F3
F
IF RS:
T
F4
F
IF LP:
T
G1
F
IF PP:
T
G2
F
IF BO:
T
G3
F
Z

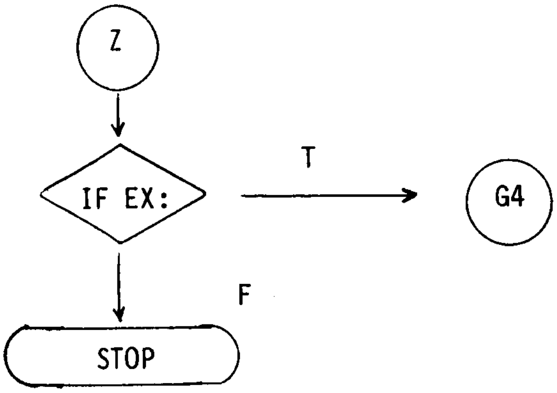
Z
IF EX:
T
G4
F
STOP

coordinate system used as a common reference for the source and structure. The reference coordinate system is located at the origin of the composite ellipsoid. There is, however, a geometry definition coordinate system that may be defined using the "RT:" command. This command enables the user to rotate and translate the coordinates relative to the reference coordinate system and is used to input plate geometry in terms of the best coordinate system for this particular substructure. Once the "RT:" command is used, all the input following the command will be in that rotated and translated coordinate system until the "RT:" command is called again. The only exception to this is that the composite ellipsoid will always be in the reference coordinate system. See below for more details. There is also a separate coordinate system that can be used to define the pattern coordinates. This is discussed in more detail in Section III-C in terms of the "PD:" command.

It is felt that the maximum usefulness of the computer code can be achieved using it on an interactive computer system. As a consequence, all input data are defined in free format such that the operator need only put commas or spaces between the various input variables. This allows the user on an interactive terminal to avoid the problems associated with typing in the field length associated with a fixed format. This method also is useful on batch processing computers. Note that all read statements are made on unit #5, i.e., READ (5,*), where the "*" symbol refers to free format. Other machines, however, may have different symbols representing free format.

In all the following discussions associated with logical variables a "T" will imply true, and an "F" will imply false. The complete words true and false need not be input since most compilers just consider the first character in determining the state of the logical variable.

The following list defines in detail each command word and the variables associated with them. Section VI will give specific examples using this input method. Note that the program halts execution by sensing the end-of-file mark associated with the input data stream.

COMMAND PART:

A. Unit and Frequency Commands:

A1. COMMAND UN: Set Linear Units Used for Input

A2. COMMAND FQ: Frequency Input

B. Fuselage Geometry Related Commands:

B1. COMMAND FG: Fuselage Geometry Input

B2. COMMAND FB: Fuselage Blockage Modeled by Plates

B3. COMMAND FC: Fuselage Chopped Off

C. Source Geometry Related Commands:

C1. COMMAND SG: Source Geometry Input

C2. COMMAND SP: Superposition Fields from Several Sources

C3. COMMAND LS: Line Source Distribution Along Z-axis Used in Array Pattern

D. Plate Geometry Related Commands:

D1. COMMAND PG: Plate Geometry Input

D2. COMMAND PI: Initialize Number of Plates to be Retained

E. Pattern Cut Related Commands:

E1. COMMAND PD: Conical Pattern Data Desired

E2. COMMAND RT: Translate and/or Rotate Coordinates

F. Specific Calculation Related Commands:

F1. COMMAND TO: Test Data Generation Option

F2. COMMAND RD: Reflection/Diffraction Included in Computation

F3. COMMAND DD: Double Diffraction Included in Computation

F4. COMMAND RS: Reset Input Data to Default Case

G. Execute and Output Related Commands:

G1.	COMMAND LP:	Line Printer Listing of Results
G2.	COMMAND PP:	Pen Plot of Results
G3.	COMMAND BO:	Binary Outputs of E-THETA and E-PHI Pattern Results
G4.	COMMAND EX:	Execute Program

A. Unit and Frequency Commands:

A1. COMMAND UN:

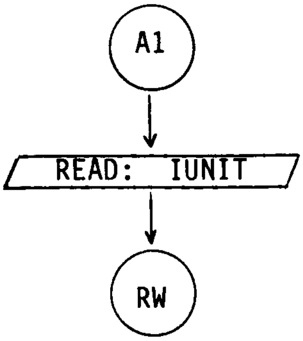

This command enables the user to specify the units used for all following linear dimensions in the input data list. Note that this command should be defined before the other geometry-related commands.

1. READ: IUNIT

   a) IUNIT: This is an integer variable that defines the units. If

$$\text{IUNIT} = \begin{cases} 1 \rightarrow \text{meters} \\ 2 \rightarrow \text{feet} \\ 3 \rightarrow \text{inches} \end{cases}$$

   The default is 1.

A2. COMMAND FQ:

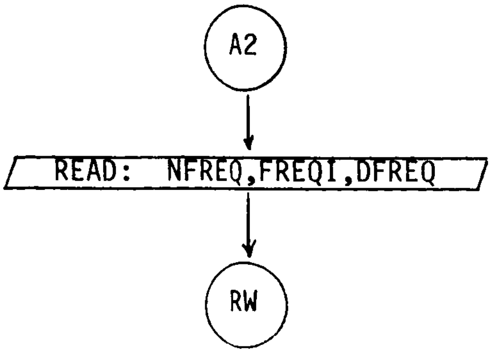

This command enables the user to specify the operating frequencies of the antennas.

1. READ: NFREQ, FREQI, DFREQ
   a) NFREQ: This is an integer variable that specifies the number of different frequencies.

   b) FREQI, DFREQ: They are real variables that specify the start and increment of the frequency loop, respectively, in Gigahertz.

   The default is N=1, FREQI=.2997925, and DFREQ=.2997925.

B. Fuselage Geometry Related Commands:

B1. COMMAND FG:

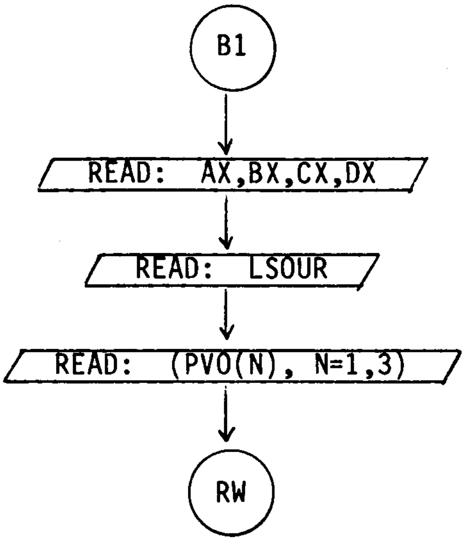

This command enables the user to model the fuselage by a composite ellipsoid. (See Section IV for more details in defining fuselage geometry.)

1. READ: AX,BX,CX,DX

   a) AX,BX,CX,DX: These are real variables that specify the semi-minor axes of the composite ellipsoid used to model the fuselage as shown in Figure 1. Note that the cross-section and profile of an ellipsoid is an ellipse.

2. READ: LSOUR

a) LSOUR: This is a logical variable defined by T or F. It is used to indicate if one wishes to define the location of the origin about which pattern is taken at the phase reference of antennas.

The default is LSOUR = •FALSE•

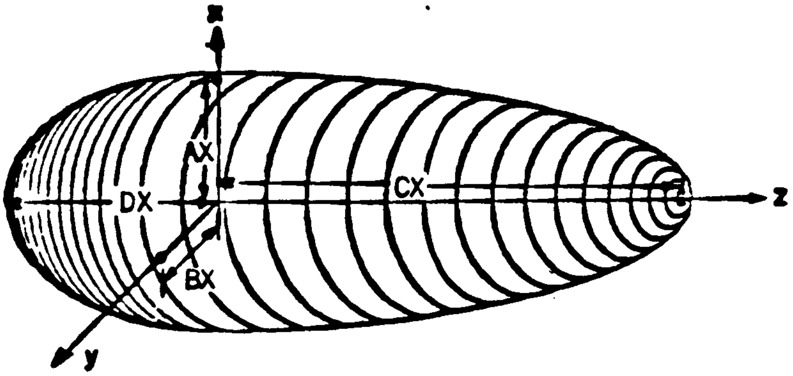

Figure 1. Definition of fuselage geometry.

3. READ: (PVO(N), N=1,3)

a) PVO(N): This is a real dimensioned array that defines the location of the origin about which the pattern is taken, i.e., PVO(N) = (x,y,z). Note PVO(N) is not used when LSOUR is .TRUE. but it must be input.

B2. COMMAND FB:

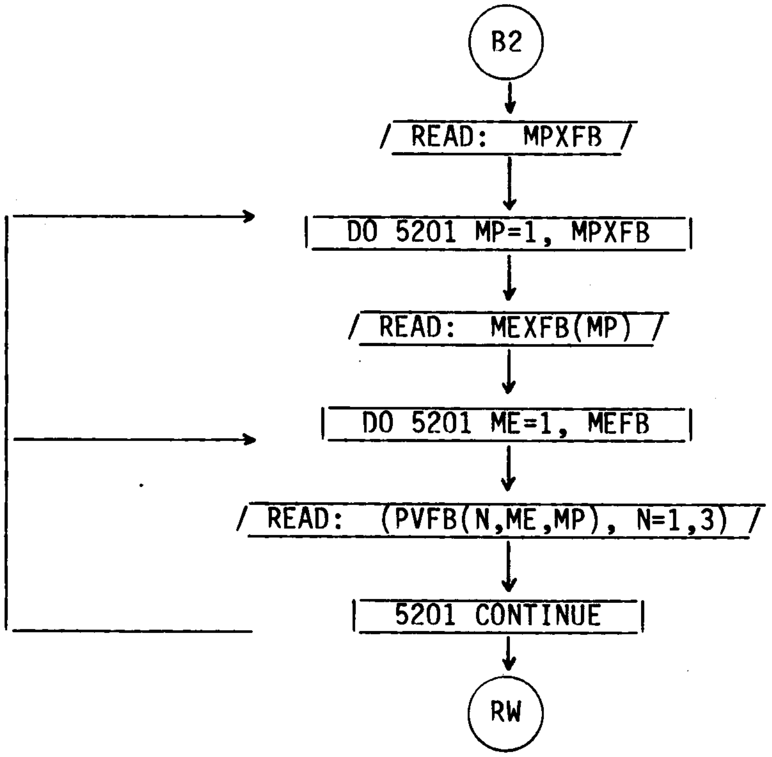
B2
READ: MPXFB
DO 5201 MP=1, MPXFB
READ: MEXFB(MP)
DO 5201 ME=1, MEFB
READ: (PVFB(N,ME,MP), N=1,3)
5201 CONTINUE
RW

This command enables the user to model the fuselage blockage by plates. The blockage plates prevent the rays from passing through the fuselage and contributing to the field calculations. Note that these plates only shadow energy, i.e., they don't scatter energy.

1. READ: MPXFB

MPXFB: This is an integer variable which defines the maximum number of plates to be used in modeling the fuselage blockage. MPXFB can not exceed 2! Normally, one uses two plates, i.e., one horizontal and the other vertical. Their contour is a best fit match to the top and side profiles of the fuselage.

2. READ: MEXFB(MP)

MEXFB(MP): This is a dimensioned integer variable which defines the maximum number of corners of each fuselage blockage plate. MEXFB(MP) can not exceed 6!

3. READ: (PVFB(N,ME,MP), N=1,3)

PVFB(N,ME,MP): This is a triply dimensioned real variable. It is used to specify the location of the MEth corner of the MPth plate. It is input on a single line with the real numbers being the X,Y,Z coordinates of the corner which corresponds to N=1,2,3, respectively, in the array. For example, if the first plate and 2nd corner is located at x=2, y=0, z=20, then it is represented by

PVFB(1,2,1)=2.

PVFB(2,2,1)=0.

PVFB(3,2,1)=20.

This data is input as: 2., 0., 20.

B3. COMMAND FC:

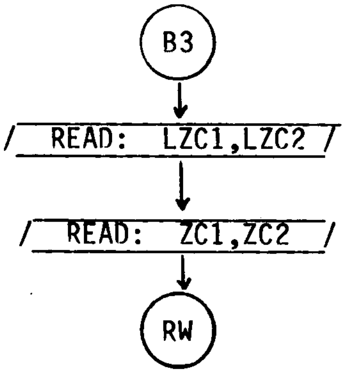

This command enables the user to chop off the fuselage. This command is ueful in modeling the radome bulk/head portion of an aircraft fuselage. Using this command the fuselage ellipsoid is cut at right angles to the z-axis which forms an abrupt termination of the fuselage.

1. READ: LZC1,LZC2

   LZC1/LZC2: These are logical variables defined by T or F. They are used to indicate if the fuselage will be chopped off in the ZC1/ZC2 location.

2. READ: ZC1, ZC2

ZCI/ZC2: This is a real variable which defines positive/ negative Z location at which the fuselage is chopped, respectively. Note ZCI(ZC2) can be any number when LZC1(LZC2) is .FALSE.

C. Source Geometry Related Commands:

C1. COMMAND SG:

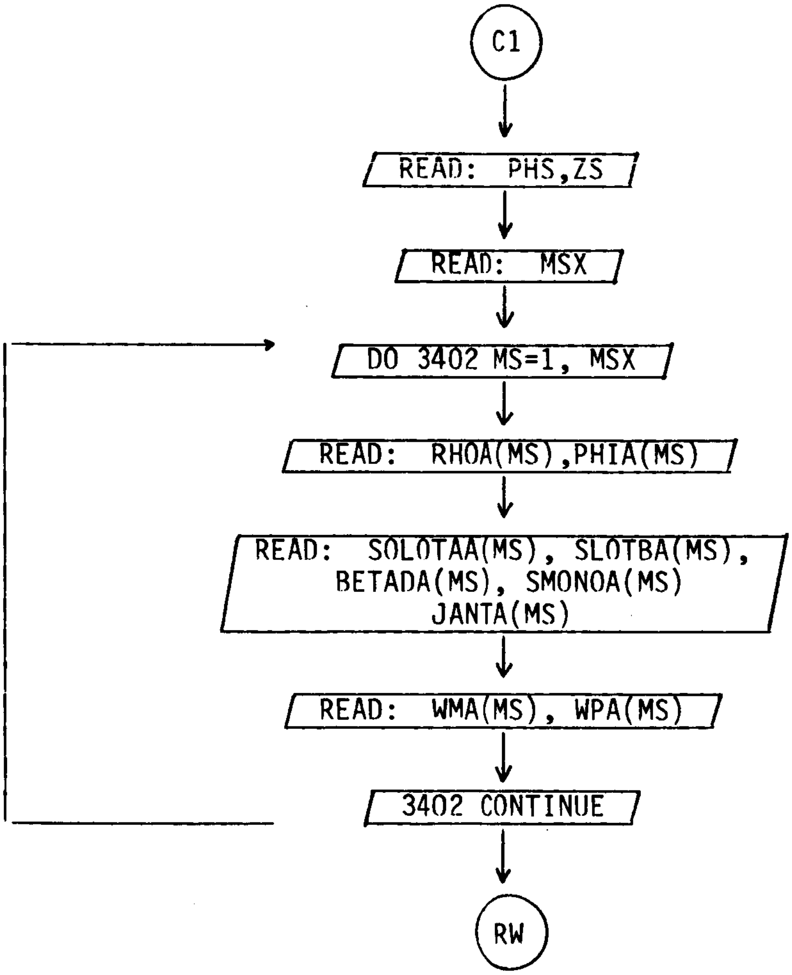
C1
READ: PHS,ZS
READ: MSX
DO 3402 MS=1, MSX
READ: RHOA(MS),PHIA(MS)
READ: SOLOTAA(MS), SLOTBA(MS), BETADA(MS), SMONOA(MS) JANTA(MS)
READ: WMA(MS), WPA(MS)
3402 CONTINUE
RW

This command enables the user to specify the location and type of antenna to be used. The geometry is illustrated in Figure 2.

1. READ: PHS,ZS

   PHS,ZS: These are real variables used to specify the phi-angle (in degrees) and Z location of the antenna phase reference point. (Refer to Figure 2) Note: $-90° < PHS < 90°$.

2. READ: MSX

   MSX: This is an integer variable which defines the maximum number of elemental radiators to be considered during execution of the program. Presently, $1 < MSX < 10$.

3. READ: RHOA(MS), PHIA(MS)

   a) RHOA(MS): This is a dimensioned real variable which defines the distance that a single antenna element is positioned away from the antenna phase reference point. It is shown in Figure 3 in terms of ρ_A.

   b) PHIA(MS): This is a dimensioned real variable used to specify the angle (ϕ_A is in degrees) relative to the antenna coordinates shown in Figure 3.

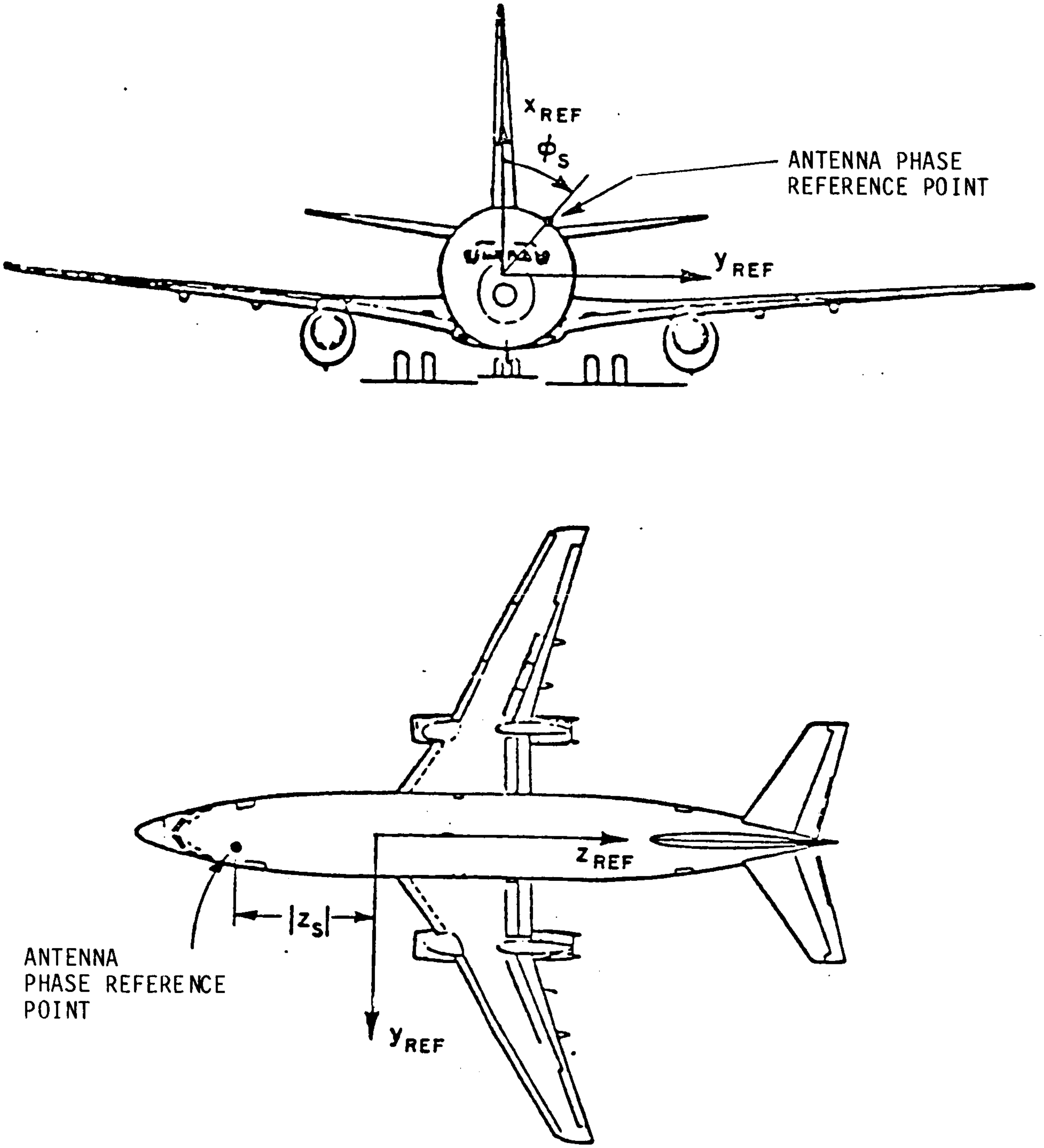
X REF
φS
ANTENNA PHASE
REFERENCE POINT
Y REF
Z REF
|ZS|
ANTENNA
PHASE REFERENCE
POINT
Y REF

Figure 2. Definition of antenna phase reference point for computer code. Note that PHS = ϕ_s and ZS = - $|Z_s|$ in the above drawings.

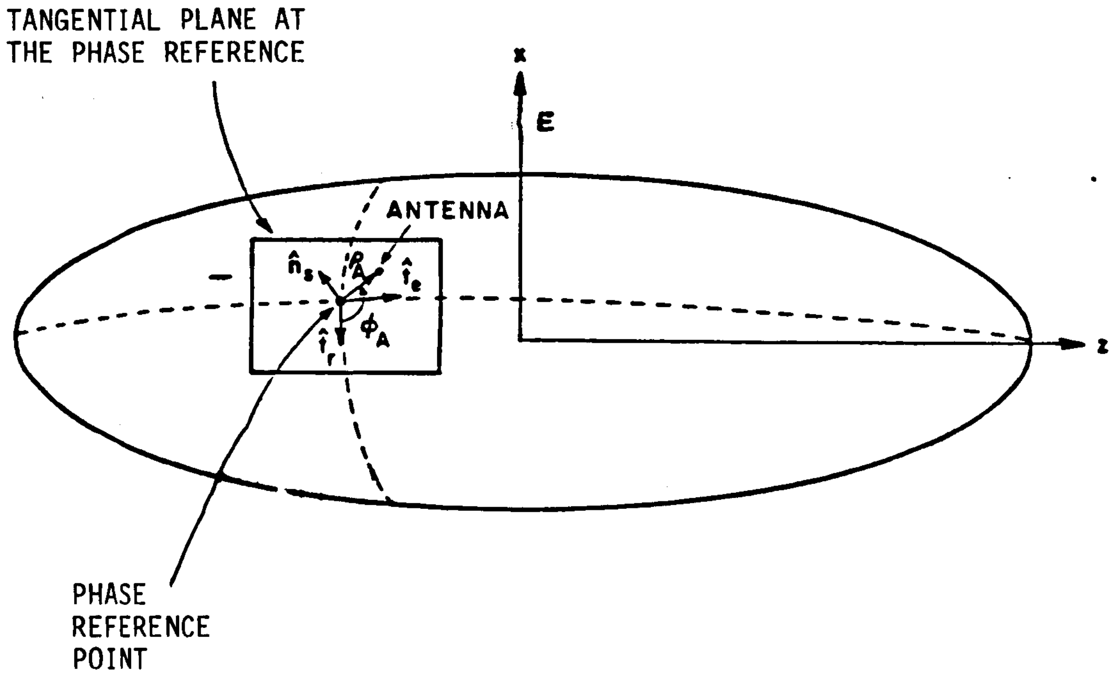
TANGENTIAL PLANE AT THE PHASE REFERENCE
x
E
ANTENNA
$\hat{n}_s$
ρ_A
$\hat{t}_e$
ϕ_A
$\hat{t}_r$
z
PHASE REFERENCE POINT

Figure 3. Source geometry.
(Note that RHOA(MS)=ρ_A and PHIA(MS)=ϕ_A)

4. READ: SLOTAA(MS), SLOTBA(MS), BETADA(MS), SMONOA(MS), JANTA(MS)

a) SLOTAA(MS), SLOTBA(MS): These are real variables uesed to specify the narrow (parallel with E field) and broad (perpendicular to E field) dimensions of the slot in specified units.

b) BETADA(MS): This is a real variable used to specify the angle (in degrees) of the slot relative to the fuselage axis. If BETADA=0, then it is an axial slot. If BETADA=90., then it is a circumferential slot.

c) SMONOA(MS): This is a real variable used to specify the length of the monopole in specified units. Note that SMONOA should not exceed a quarter wavelength.

d) JANTA(MS): This is an integer variable used to specify the type of antenna considered in the computation:

$$\text{JANTA} = \begin{cases} 1 \rightarrow \text{arbitrary oriented slot} \\ 3 \rightarrow \text{radial monopole.} \end{cases}$$

5. READ: WMA(MS), WPA(MS)

a) WMA(MS), WPA(MS): These are real variables used to specify the magnitude and phase (in degrees) of the excitation of the MSth antenna. If an array is used, then the excitation including the coupling effect on the radiators may be obtained using a thin-wire [4] as shown in the results section.

C2. COMMAND SP:

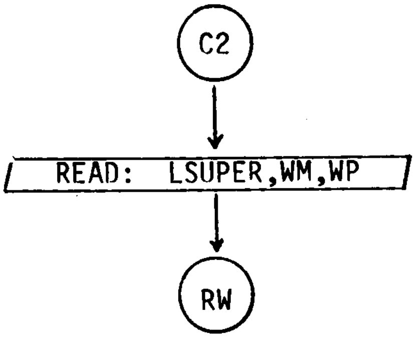

This command enables the user to superimpose the fields calculated for several sources. But, one should note that this command can be used only when sources are operating at the same frequency. Note that the fields are superimposed with each execution of the program if LSUPER = TRUE.

1. READ: LSUPER,WM,WP

a) LSUPER: This is a logical variable defined by T or F. It is to indicate if one wishes to superimpose fields or not.

b) WM,WP: These real variables are used to specify the magnitude and phase (in degrees) of the source relative to the first source in the superposition string.

C3. COMMAND LS:

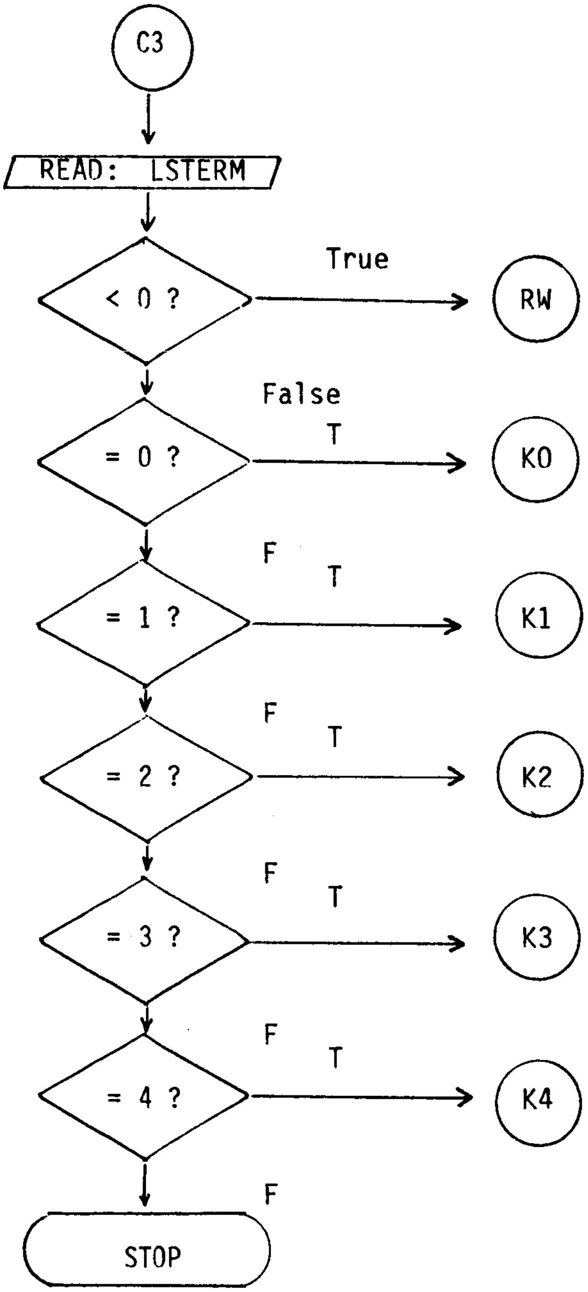
C3
READ: LSTERM
< 0 ?
True
RW
False
= 0 ?
T
K0
F
= 1 ?
T
K1
F
= 2 ?
T
K2
F
= 3 ?
T
K3
F
= 4 ?
T
K4
F
STOP

COMMAND LS (continued)

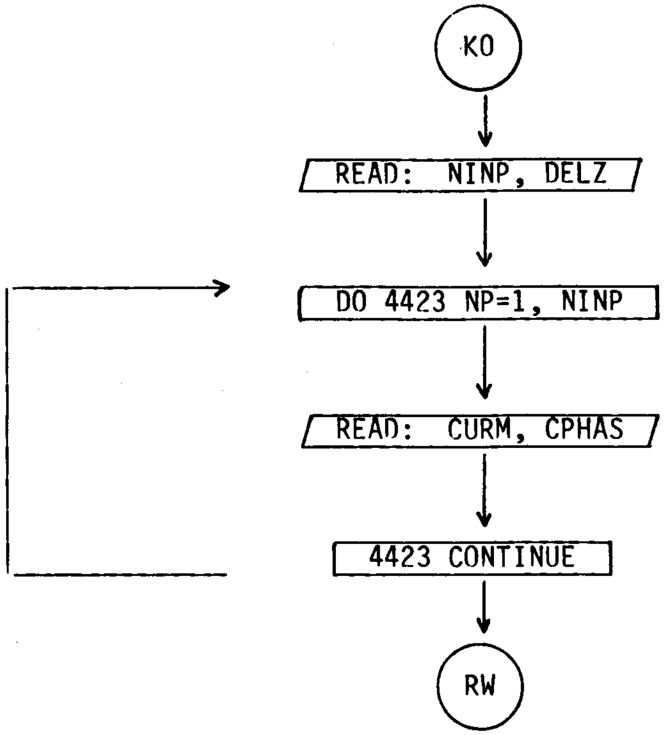
K0
READ: NINP, DELZ
DO 4423 NP=1, NINP
READ: CURM, CPHAS
4423 CONTINUE
RW

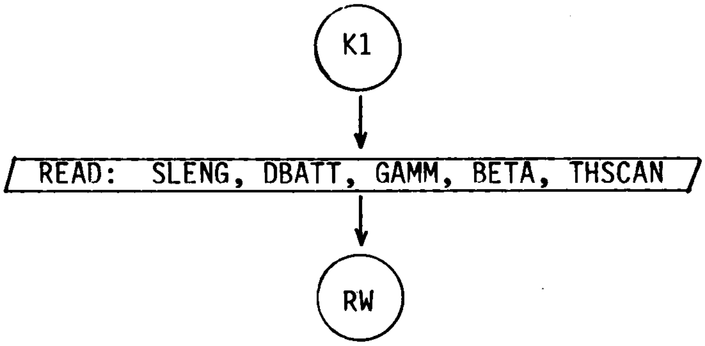
K1
READ: SLENG, DBATT, GAMM, BETA, THSCAN
RW

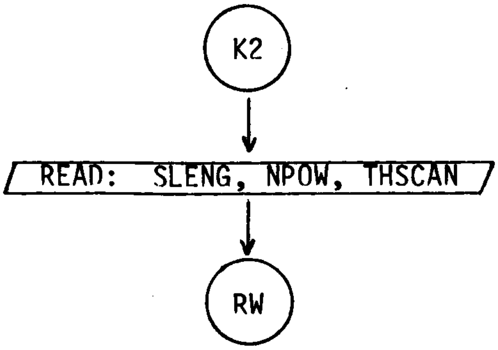
K2
READ: SLENG, NPOW, THSCAN
RW

COMMAND LS (continued)

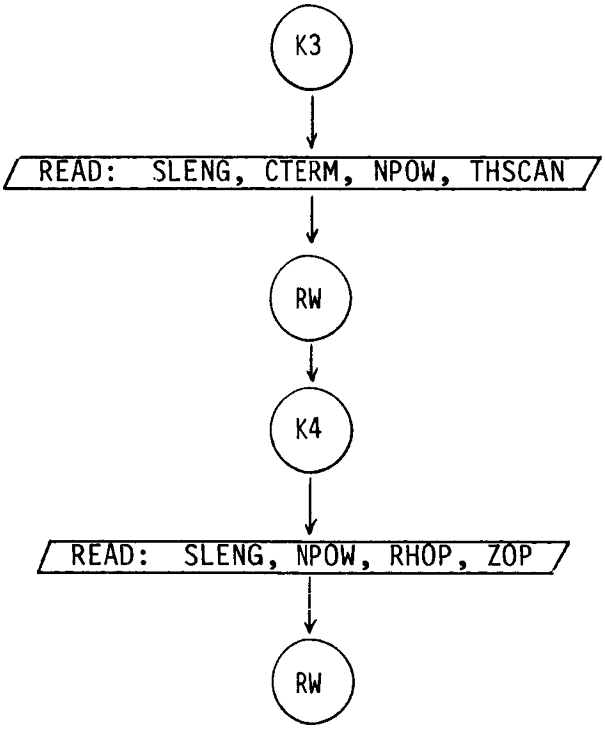
K3
READ: SLENG, CTERM, NPOW, THSCAN
RW
K4
READ: SLENG, NPOW, RHOP, ZOP
RW

This command enables the user to specify a line source distribution along the z-axis. It is used in an array pattern multiplication analysis. This command applies only when one has a uniform geometry along the axis of the fuselage.

1. READ: LSTERM
   a) LSTERM: This is an integer variable that indicates the type of line source distribution treated. The current distribution and, therefore, the following inputs vary according to the following table.

LSTERM=0: $$I(z) = \sum_{N=1}^{NINP} |I_N|\, e^{j\phi_N}\ \delta(z-(N-1/2)\Delta z)$$

READ: NINP,DELZ

READ: CURM,CPHAS

LSTERM=1: $$I(z) = \left[e^{-\alpha z} + \Gamma e^{-j\beta} e^{-\alpha(2L-z)} \right] e^{-jkz\cos\theta_s}$$

READ: SLENG,DBATT,GAMM,BETA,THSCAN

LSTERM=2: $$I(z) = \left\{ 1 - \left[\frac{2(z-L/2)}{L} \right]^2 \right\}^N e^{-jkz\cos\theta_s}$$

READ: SLENG,NPOW,THSCAN

LSTRM=3: $$I(z) = \left[\left(\cos \frac{\pi z}{L}\right)^N + C \right] e^{-jkz\cos\theta_s}$$

READ: SLENG,CTERM,NPOW,THSCAN

LSTERM=4: $$I(z) = \left(\cos \frac{\pi z}{L}\right)^N e^{-jk(\rho-\rho_0)}$$

where $\rho = \sqrt{\rho_0^2 + (z-z_0)^2}$

READ: SLENG,NPOW,RHOP,ZOP

The input data is interpreted as follows:

a) NINP: This is an integer variable that defines the number of current samples.

b) DELZ: This is a real variable (Δz) that defines the current sample spacing in wavelengths.

c) CURM,CPHAS: These are real variables that define the magnitude ($|I|_N$) and phase (ϕN) of the current elements.

d) SLENG: This is a real variable (L) that defines the length of the linear array, in wavelengths.

e) DBATT: This is a real variable that defines the attenuation (in dB) along the total length (SLENG) of the array.
Note that α is related to DBATT.

f) GAMM,BETA: These are real variables (Γ and β) that define the magnitude and phase (in degrees) of the reflection coefficient at the end of the traveling wave antenna (LSTERM=1).

g) THSCAN: This is a real variable that defines the scan angle (in degrees) of the array.

h) NPOW: This is an integar variable (N) that defines the exponent in the previous equations.

i) CTERM: This is a real variable that defines the constant (C) in the previous equations.

j) RHOP,ZOP: These are real variables that define the phase distribution across an aperture. Note that RHOP and ZOP are specified in wavelengths. In terms of the previous definition for the case (LSTERM=4) RHOP=ρ_0 and ZOP=Z_0.

D. Plate-Geometry Related Commands:

D1. COMMAND PG:

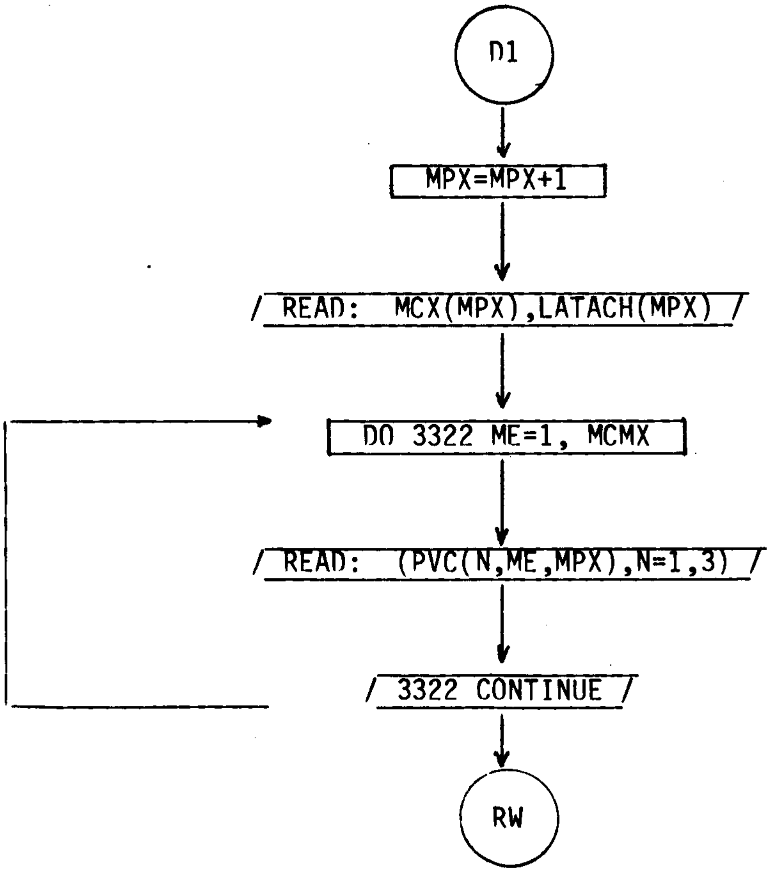
D1
MPX=MPX+1
READ: MCX(MPX),LATACH(MPX)
DO 3322 ME=1, MCMX
READ: (PVC(N,ME,MPX),N=1,3)
3322 CONTINUE
RW

This command enables the user to define the geometry of the flat plate structures to be considered. The geometry is illustrated in Figure 4. It can be called repeatedly up to 25 times. If the higher order terms (R/R, R/D, D/R, D/R) are not defined, it can be extended up to 26. Note that each side of the chopped-off fuselage is automatically counted as three plates in the computer code when the "FC:" command is used. See Section IV for further details in defining the corner locations.

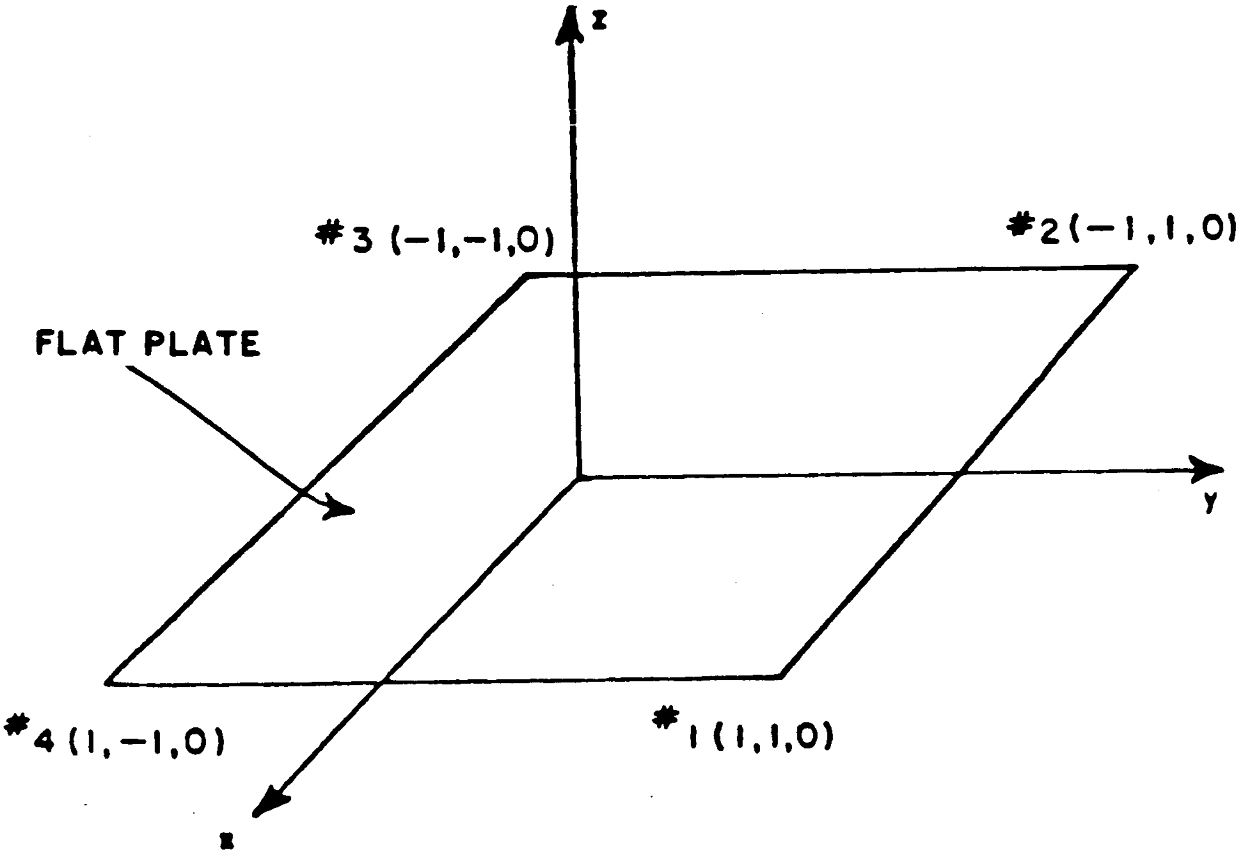

Figure 4. Definition of flat plate geometry.

1. READ MCX(MPX),LATACH(MPX)

a) MCX(MPX): This is a dimensioned integer variable. It is ued to define the number of corners (or edges) on the MPXth plate. Presently, 1<MCX(MPX)<6 with 1<MPX<25.

b) LATACH(MPX): This is a logical variable defined by T or F. It is used to indicate if the MPXth plate is attached to the fuselage (T) or not (F). If it is true, the first and last corners of attached plates should be specified on or near the fuselage. If they are not attached, the program will automatically attach the first and last corners.

2. READ: (PVC(N,ME,MPX),N=1,3)

As stated earlier, the locations of the corners of the flat plates are input in terms of the x, y, z coordinates in the specified cartesian coordinate system.

a) PVC(N,ME,MPX): This is a triply dimensioned real variable. It is used to specify the location of the MEth corner of the MPXth plate. It is input on a single line with the real numbers being the x, y, z coordinates of the corner which correspond to N=1,2,3, respectively, in the array. For example, the array will contain the following for plate #1 and corner #2 located at x=2, y=4, z=6:

$$PVC(1,2,1) = 2$$

$$PVC(2,2,1) = 4$$

$$PVC(3,2,1) = 6$$

This data is input as: 2., 4., 6.

Considering the flat plate structure given in Figure 4, the input data is given by

1., 1., 0. : corner #1
-1., 1., 0. : corner #2
-1.,-1., 0. : corner #3
1.,-1., 0. : corner #4

plate #1

Presently, $1 \leq MPX \leq 25$

$$1 \leq ME \leq 6$$

$$1 \leq N \leq 3$$

Note that the limits on the number of plates, and corners are only due to the size of the arrays.

D2. COMMAND PI:

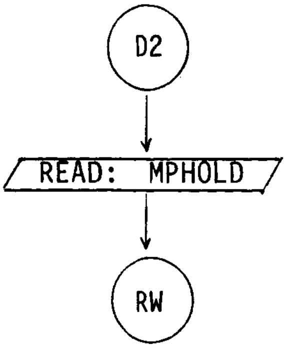

This command enables the user to specify those consecutive plates which will remain for the next calculation. Its useful when one simulates a complicated model by many plates and wants to know the effect of eliminating some plates from a configuration. The usage is illustrated in example 2.

1. READ: MPHOLD

MPHOLD: This is a real variable used to specify the number of plates to be retained for the next calculation. One should note that the first MPHOLD plates are retained. For example, if MPHOLD=2, then plates #1 and #2 remain in the input data list for the next computation.

E. Pattern Cut Related Commands:

E1. COMMAND PD:

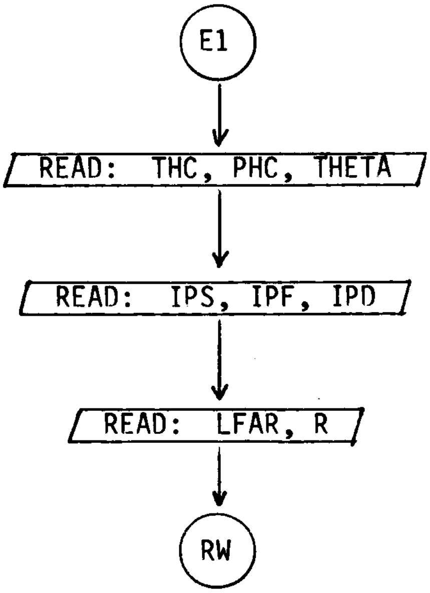

This command enables the user to define the pattern axis of rotation, the angular range, and the range from origin to receiver for the desired conical pattern.

This set of data is associated with the conical pattern desired during execution of the program. The pattern axis is defined by the spherical angles (THC,PHC) as illustrated in Figure 5. These angles define a radial vector direction which points in the direction of the pattern axis of rotation. These angles actually set-up a new coordinate system in relation to the reference coordinates. The new cartesian coordinates defined by the subscript "p" are found by first rotating about the z-axis the angle PHC and, then, about the y_p-axis the angle THC. The pattern is, then, taken in the "p" coordinate system in terms of spherical angles. The theta angle of the pattern taken about the z_p-axis is defined by THETA. The phi angle is defined by the next read statement. In the present form the program will compute any conical pattern in which THETA is used as the conical pattern angle about the z_p-axis for the complete pattern calculation.

As an aid in setting up the "p" coordinate system the following set of equations give the relationships between (THC, PHC) and the x_p, y_p, and z_p-axes:

$$\hat{x}_p = \cos(\mathrm{PHC})\sin(\mathrm{THC}+90°)\hat{x}+\sin(\mathrm{PHC})\sin(\mathrm{THC}+90°)\hat{y}+\cos(\mathrm{THC}+90°)\hat{z}$$

$$\hat{y}_p = \cos(\mathrm{PHC}+90°)\hat{x}+\sin(\mathrm{PHC}+90°)\hat{y}$$

and

$$\hat{z}_p = \cos(\mathrm{PHC})\sin(\mathrm{THC})\hat{x}+\sin(\mathrm{PHC})\sin(\mathrm{THC})\hat{y}+\cos(\mathrm{THC})\hat{z}$$

where $0 \leq \text{THC} \leq 180°$ and $0 \leq \text{PHC} \leq 360°$. Note that the "p" axes are defined as radial vector directions in a spherical coordinate system. In its present form it should be noted that the user may not be able to define the x_p-axis at the starting location that he desired. In addition, the rotation of the pattern may be in the opposite sense using this approach. However, these problems can be easily overcome with properly written plot routines.

1. READ: THC,PHC,THETA
   - a) THC,PHC: These are real variables. They are input in degrees and define the axis of rotation about which a conical pattern will be computed (see Figure 5.).
   - b) THETA: This is a real variable. It is input in degrees and ued to define the conical angle (θ_p) about the axis of rotation for the desired pattern.

2. READ: IPS,IPF,IPD
   - a) IPS,IPF,IPD: These are integer variables used to define angles in degrees. They are, respectively, the beginning, ending, and incremental values of the phi pattern angle (ϕ_p).

As a result of the input given by the two previous read statements, the user has completely defined the desired conical pattern to be computed during execution of the program.

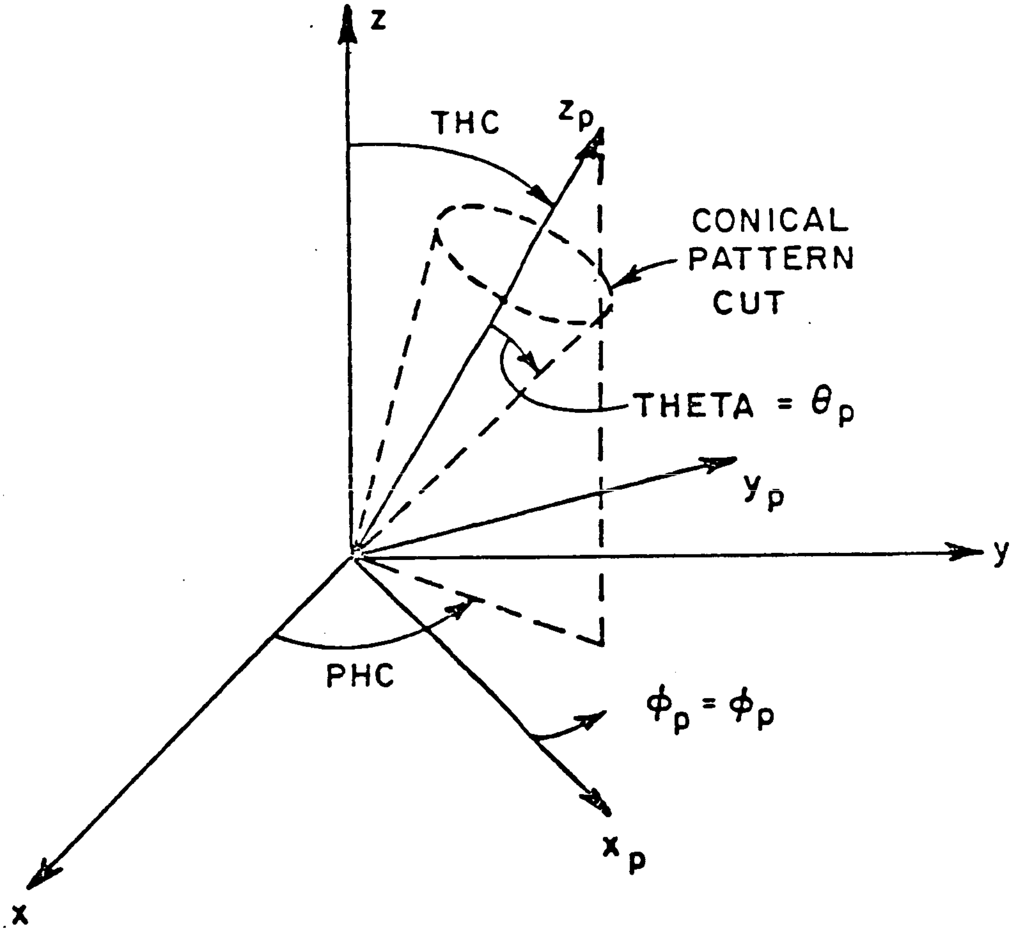
z
THC
z_p
CONICAL PATTERN CUT
THETA = θ_p
y_p
y
PHC
$\phi_p = \phi_p$
x_p
x

Figure 5. Definition of pattern axis.

3. READ: LFAR,R

a) LFAR: This is a logical variable defined by T or F. It is used to specify if the far field pattern is desired or not.

b) R: This is a real variable which is used to define the range in linear units from the origin to the receiver. Note R can be any number when LFAR is .TRUE. in that it is not used in the calculation.

E2. COMMAND RT:

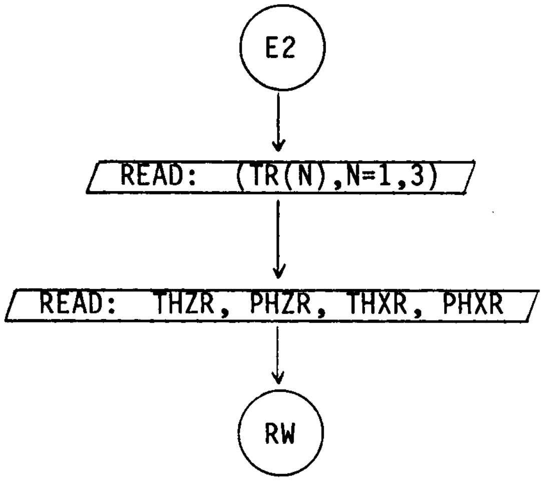

This command enables the user to translate and/or rotate the coordinate system used to define the input data in order to simplify the specification of the plate geometry. The geometry is illustrated in Figure 6.

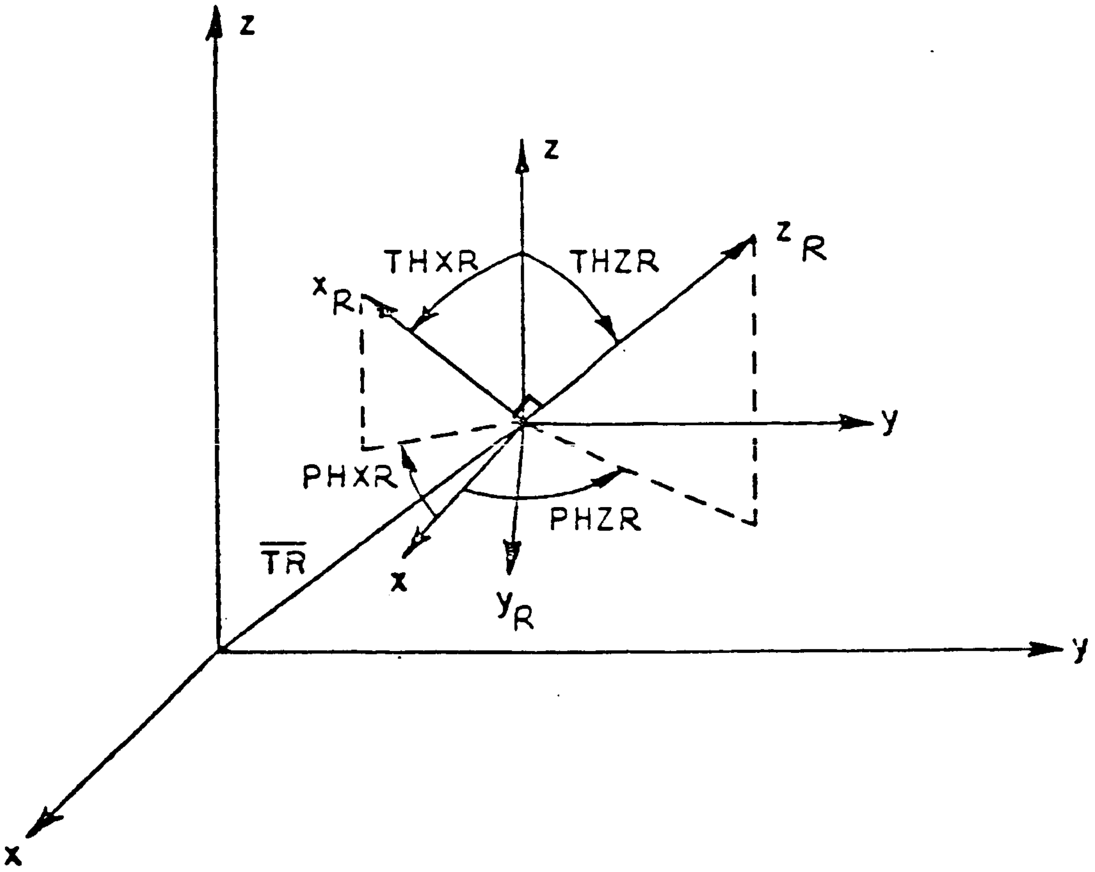
z
z
THXR
THZR
z_R
x_R
y
PHXR
PHZR
$\overline{TR}$
x
y_R
y
x

Figure 6. Definition of rotate-translate coordinate system geometry.

1. READ: (TR(N), N=1,3)

   a) TR(N): This is a dimensioned real variable. It is used to specify the origin of the new coordinate system to be used to input the data for the plate structures. It is input on a single line with the real numbers being the x,y,z coordinates of the new origin which corresponds to N=1,2,3, respectively.

2. READ: THZR, PHZR, THXR, PHXR

   a) THZR,PHZR: These are real variables. They are input in degrees as spherical angles that define the z_R-axis of the new coordinate system as if it was a radial vector in the reference coordinate system (see Figure 6).

   b) THXR,PHXR: These are real variables. They are input in degrees as spherical angles that define the x_R-axis of the new coordinate system as if it was a radial vector in the reference coordinate system (see Figure 6).

The new x_R-axis and z_R-axis must be defined orthogonal to each other. If they are not, the program aborts with a warning. The new y_R-axis is found from the cross product of the x_R and z_R axes. All the subsequent inputs will be made relative to this new coordinate system, which is shown as (x_R, y_R, z_R) unless command "RT:" is called again and redefined. It is always defined relative to the reference coordinate system.

F. Specific Terms Related Commands:

F1. COMMAND TO:

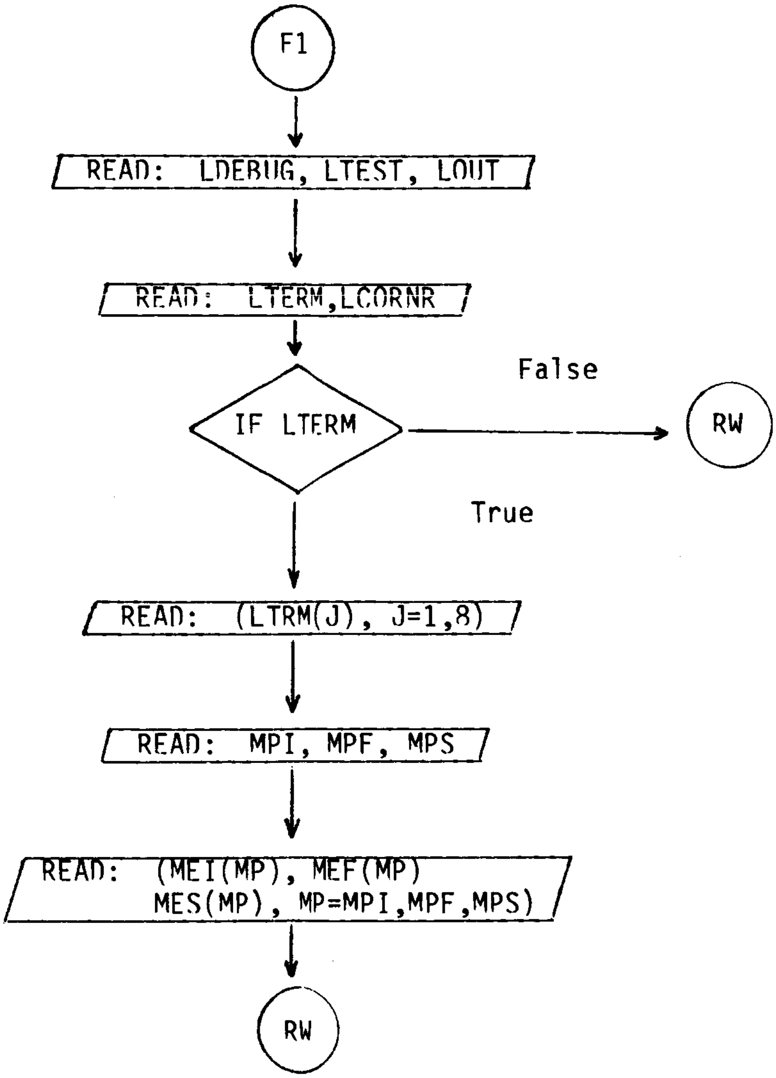
F1
READ: LDEBUG, LTEST, LOUT
READ: LTERM,LCORNR
IF LTERM
False
RW
True
READ: (LTRM(J), J=1,8)
READ: MPI, MPF, MPS
READ: (MEI(MP), MEF(MP)
MES(MP), MP=MPI,MPF,MPS)
RW

This command enables the user to obtain an extended output of various intermediate quantities in the computer code. This is useful in testing the program or in analyzing the contributions from various scattering mechanisms in terms of the total solution.

1. READ: LDEBUG, LTEST, LOUT
   - a) LDEBUG: This is a logical variable defined by T or F. It is ued to debug the program if errors are suspected within the program. If set true, the program prints out data on unit #6 associated with each of its internal operations. These data can, then, be compared with previous data which are known to be correct. It is, also, used to insure initial operation of the code. Only one pattern angle is considered. (normally set false)
   - b) LTEST: This is a logical variable defined by T or F. It is used to test the input/output associated with each subroutine. The data written out on unit #6 is associated with the window variables of the subroutine. They are written out each time the subroutine is called. It is, also, used to insure initial operation of the code. Only one pattern angle is considered. (normally set false)

c) LOUT: This is a logical variable defined by T or F. It is used to output data on unit #6 associated with the main program. It is also used to initially insure proper operation. It can be used to examine the various components of the pattern. (normally set false)

2. READ: LTERM,LCORNR

a) LTERM: This is a logical variable defined by T or F. It is used to tell the code whether or not individual terms are desired during the computation. (normally set false)

b) LCORNR: This is a logical variable defined by T or F. It is used to tell the code whether or not corner diffraction is desired during the computation. (normally set true)

3. READ: (LTRM(J), J=1,8)

a) LTRM(J): These are logical variables defined by T or F to specify a set of individual scattering components that are to be included in the scattered field computation. The components are defined by the following number designations:

J=1: source field
J=2: single reflected field

J=3: single diffracted field

J=4: diffracted field from chopped fuselage

J=5: double reflected field

J=6: reflected-diffracted field

J=7: diffracted-reflected field

J=8: double diffracted field

The default values are $\text{LTERM(J)} = \begin{cases} \text{.TRUE.} & \text{for } 1,2,3,4 \\ \text{.FALSE.} & \text{for } 5,6,7,8. \end{cases}$

(Note: To get the reflected-diffracted and/or double diffracted field one must accompany this command with COMMAND "RD:" and/or "DD:", respectively.)

4. READ: MPI,MPF,MPS

   a) MPI,MPF,MPS: These are integer variables to define the plates used in the computation, where

      MPI = initial plate

      MPF = final plate, and

      MPS = increment in plates going from initial to final plate.

(Note: MPI=1, MPF=3, and MPS=2 imply plates 1 and 3 are included in the computation.)

5. READ: (MEI(MP), MEF(MP), MES(MP), MP=MPI,MPF,MPS)

   a) MEI(MP),MEF(MP),MES(MP): These are dimensioned integer variables to define the edges on the MPth plate used in the computation, where

MEI(MP) = initial edge on plate MP

MEF(MP) = final edge on plate MP, and

MES(MP) = increment in edges going from MEI(MP) to MEF(MP).

F2. COMMAND RD:

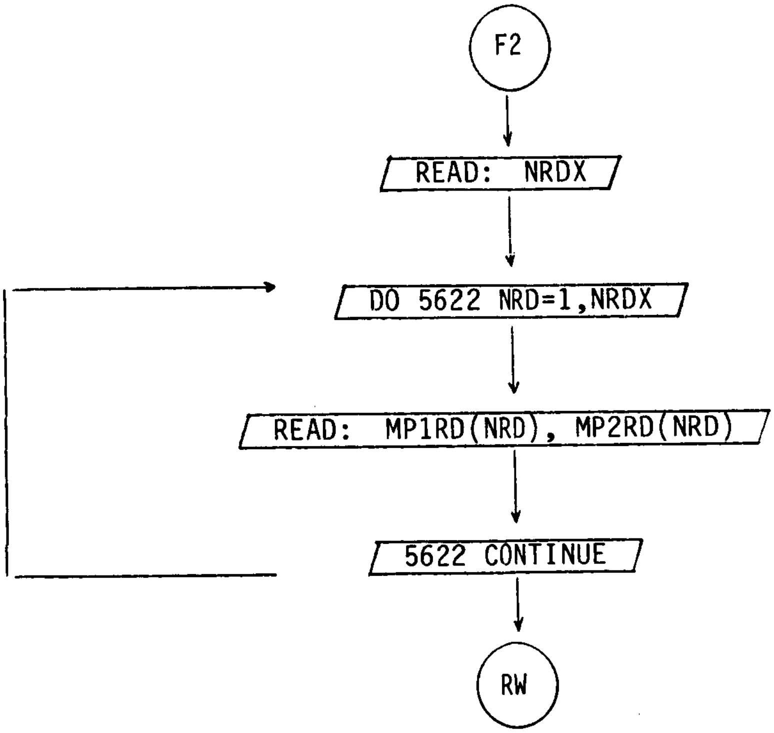
F2
READ: NRDX
DO 5622 NRD=1,NRDX
READ: MP1RD(NRD), MP2RD(NRD)
5622 CONTINUE
RW

1. READ: NRDX

NRDX: This is a real variable used to specify the number of reflection-diffraction terms desired. Presently, $0 \leq NRDX \leq 40$.

2. READ: MP1RD(NRD), MP2RD(NRD)

MP1RD(NRD): This is an integer dimensioned array used to specify the plate number from which the first reflection occurs.

MP2RD(NRD): This is an integer dimensioned array used to specify the plate number from which the diffraction occurs.

(Note: The usage of this command is illustrated in example 2.)

F3. COMMAND DD:

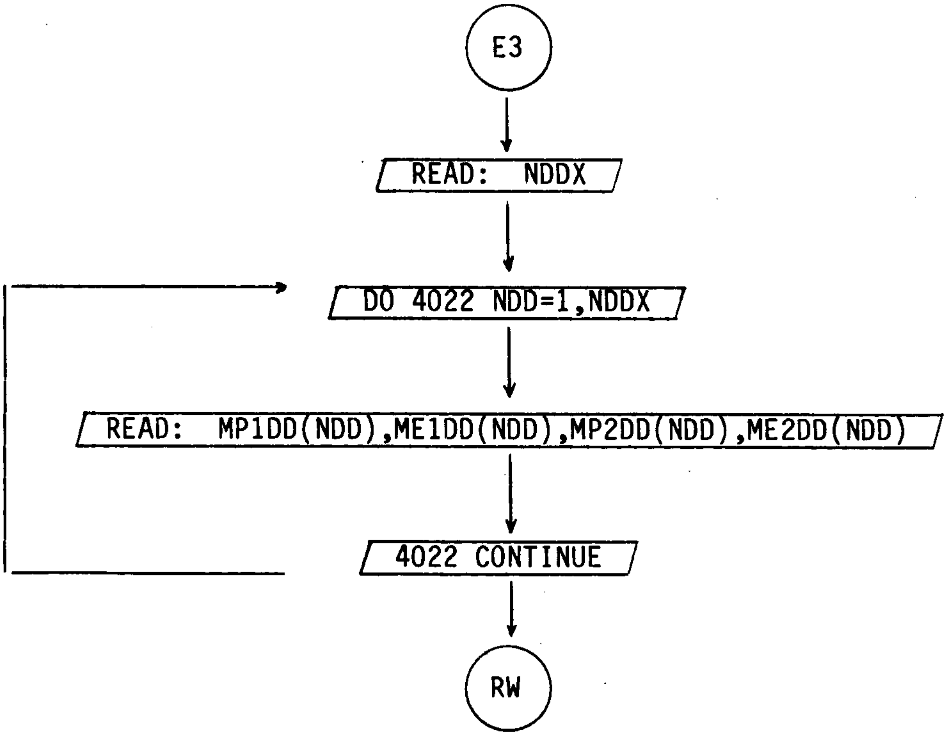
E3
READ: NDDX
DO 4022 NDD=1,NDDX
READ: MP1DD(NDD),ME1DD(NDD),MP2DD(NDD),ME2DD(NDD)
4022 CONTINUE
RW

1. READ: NDDX

   a) NDDX: This is an integer variable that specifies the total number of double diffraction terms desired: Presently, $0 \leq NDDX \leq 10$.

2. READ: MP1DD(NDD), ME1DD(NDD), MP2DD(NDD), ME2DD(NDD)

   a) MP1DD(NDD), ME1DD(NDD): These are integer dimensioned arrays used to specify the plate and edge number, respectively, from which the first diffraction occurs.

   b) MP2DD(NDD), ME2DD(ND): These are integer dimensioned arrays used to specify the plate and edge number, respectively, from which a second diffraction occurs.

(Note: The usage of this command is illustrated in example 2.)

F4. COMMAND RS:

This command enables the user to reset the input data to the default case. There is no input data associated with this command.

G. Execute and Output Related Commands:

G1. COMMAND LP:

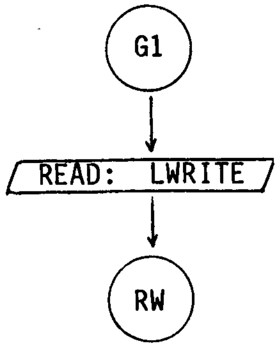
G1
READ: LWRITE
RW

This command enables the user to obtain a line printer listing of the total fields ($E_{\theta p}$, $E_{\phi p}$).

1. READ: LWRITE

LWRITE: This is a logical variable defined by T or F. It is used to indicate if a line printer output is desired or not.

G2. COMMAND PP:

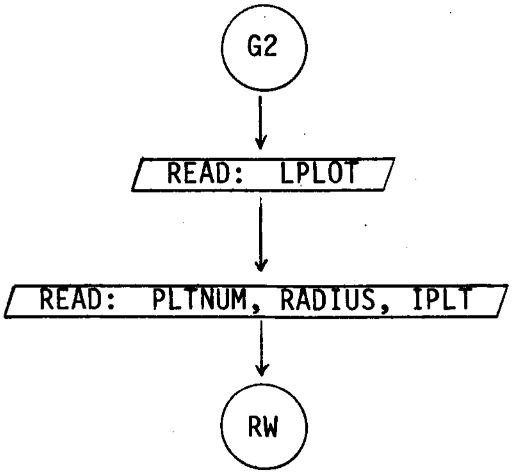
G2
READ: LPLOT
READ: PLTNUM, RADIUS, IPLT
RW

This command enables the user to obtain a pen plot of the total fields ($E_{\theta p}$, $E_{\phi p}$).

1. READ: LPLOT

   LPLOT: This is a logical variable defined by T or F. It is used to indicate if pen plot is desired or not.

2. READ: PLTNUM, RADIUS, IPLT

   a) PLTNUM: This is a real variable used to indicate the type of polar plot desired, such that

$$\text{PLTNUM} = \begin{cases} 1 \rightarrow \text{E-THETA and E-PHI are plotted separately.} \\ 2 \rightarrow \text{E-THETA and E-PHI are plotted in the same} \\ \quad \text{plot.} \\ 3 \rightarrow \text{Both 1 and 2.} \end{cases}$$

   b) RADIUS: This is a real variable that is used to specify the radius of the polar plot.

   c) IPLT: This is an integer variable that indicates the type of polar plot desired, such that

$$\text{IPLOT} = \begin{cases} 1 \rightarrow \text{field plot} \\ 2 \rightarrow \text{power plot} \\ 3 \rightarrow \text{dB plot} \end{cases}$$

G3. COMMAND BO:

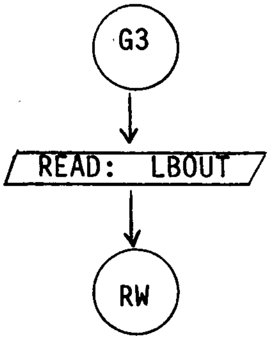

This command enables the user to obtain a binary output of the complex E-THETA and E-PHI patterns values. This output is useful if one wishes to input the aircraft code results into another program. This might be useful, for example, to study array patterns. One can run each array element individually, and then process the array pattern by appropriately adjusting the amplitude and phase of each element pattern. In this way numerous array patterns can be obtained without running the aircraft code excessively.

1. READ: LBOUT

   a) LBOUT: This is a logical variable defined by T or F. It is used to indicate if the binary output is desired or not. The output format is specified within the source listing of the code.

G4. COMMAND EX:

This command is used to execute the code so that the total fields may be computed. After execution the code returns for another possible command word.

This concludes the definition of all the input parameters to the program. The program would, then, run the desired data and output the results on unit #6. However, as with any sophisticated program, the definition of the input data is not sufficient for one to fully understand the operation of the code. In order to overcome this difficulty the next section discusses how the input data is interpreted and used in the program.

IV. INTERPRETATION OF INPUT DATA

This computer code is written to require a minimum amount of user information such that the burden associated with a complex geometry will be organized internal to the computer code. For example, the operator need not instruct the code that two plates are attached to form a convex or concave structure. The code flags this situation by recognizing that two plates have a common set of corners (i.e., a common edge). So if the operator wishes to attach two plates together he needs only define the two plates as though they were isolated. However, the two plates will have two identical corners. All the geometry information associated with plates having common edges is then generated by the code. The present code also will allow a plate to intersect another plate as shown in Figure 7(a). It is necessary that the corners defining the attachment be positioned a small amount through the plate surface to which it is being connected. Note that the edges of the two intersecting plates should be no closer than a quarter wavelength.

In defining the plate corners it is necessary to be aware of a subtlety associated with simulating convex or concave structures in which two or more plates are used in the computation. This problem results in that each plate has two sides. If the plates are used to simulate a closed or semi-closed structure, then possibly only one side of the plate will be illuminated by the antenna. Consequently, the operator must define the data in such a way that the code can infer which side of the plate is illuminated by the antenna. This is accomplished by defining the plate according to the right-hand rule. As one's fingers of the right hand follow the edges of the plate around in the order of their definition, his thumb should point toward the illuminated region above the plate. To illustrate this constraint associated with data format, let us consider the definition of a rectangular box. In this case, all the plates of the box must be specified such that they satisfy the right-hand rule with the thumb pointing outward as illustrated in Figure 7 (b). If this rule were not satisfied for a given plate, then the code would assume that the antenna is within the box as far as the scattering from that plate is concerned.

In the "PG:" command, if LATACH(MPX)=T (i.e., the plate is attached to the fuselage), the program assumes that the first and last plate corners (PVC(N,1,MPX) and PVC(N,MCMX,MPX)) are to be attached to the fuselage. The user must define the geometry accordingly.

The plates can be attached to the ellipsoid as illustrated in Figure 7(c) and (d). However, when the plates are attached on the lower half of the ellipsoid, the y component of the first and last corners are set equal to the y dimension of the ellipsoid center line as shown in Figure 7(e) and (f). It is important to note that the user need not exactly attach the first and last corners to the fuselage because the code will extend the edges and reset the first and final corner points on the fuselage as shown in Figure 7(g).

In the "FG:" command, the composite ellipsoid is constructed from two ellipsoid sections positioned back to back and connected together such that its surface is continuous and smooth at the cross-section of the source location. The composite ellipsoid semi-major/minor axes are defined by AX, BX, CX and DX. The source location is defined by Z_s and ϕ_s. The case in which the source is positioned to the right of the coordinate system origin (Z_s positive) as shown in Figure 8(a). It is assumed here that both the right and left ellipsoid coordinate systems are coincident. Then, the right side ellipsoid semi-major/minor axes and the source location are defined as

$$(a_F,\ b_F,\ c_F,\ V_{es},\ V_{rs}) = (AX,\ BX,\ CX,\ V_{es},\ V_{rs})$$

where

$$V_{es} = \cdot \arcsin (Z_s/CX) \quad \text{and} \quad V_{rs} = \frac{AX \sin (\phi_s)}{BX \cos (\phi_s)} \quad .$$

The parameters for the left side ellipsoid are given by the following:

$$a'_F = \frac{AX \cos (V_{es})}{\cos (V'_{es})}$$

$$b_F' = \frac{BX \cos (V_{es})}{\cos (V_{es}')}$$

and

$$c_F' = DX + Z_{sh}$$

where

$$V_{es}' = \arcsin \left[\left[\frac{CX \cos V_{es}}{\tan (V_{es}) (DX + Z_s)} +1 \right]^{-1} \right]$$

and

$$Z_{sh} = \frac{Z_s - DX \sin (V_{es}')}{1 + \sin (V_{es}')} \quad .$$

Note that Z_{sh} is the distance between the right and left ellipsoid coordinate origins as shown in Figure 8.

For the case when the source is to the left of the origin (Z_s negative as shown in Figure 8(b), the left ellipsoid semi-major/minor axes and source location are defined as

$$(a_F', b_F', c_F', V_{es}, V_{rs}) = (AX, BX, DX, V_{es}, V_{rs})$$

where

$$V_{es} = \arcsin (\frac{Z_s}{DX}) \quad \text{and} \quad V_{rs} = \frac{AX \sin (\phi_s)}{BX \cos (\phi_s)} \quad .$$

The parameters for the right ellipsoid are given by

$$a_F = \frac{AX \cos (V_{es})}{\cos (V_{es}')}$$

$$b_F = \frac{BX \cos (V_{es})}{\cos (V_{es}')}$$

and

$$c_F = CX - Z_{sh}$$

where

$$V_{es}' = \arcsin \left[\left[\frac{DX \cos V_{es}}{\tan V_{es} (CX + Z_s)} - 1 \right]^{-1} \right]$$

and

$$Z_{sh} = \frac{Z_s - CX \sin (V_{es}')}{1 + \sin (V_{es}')} \quad .$$

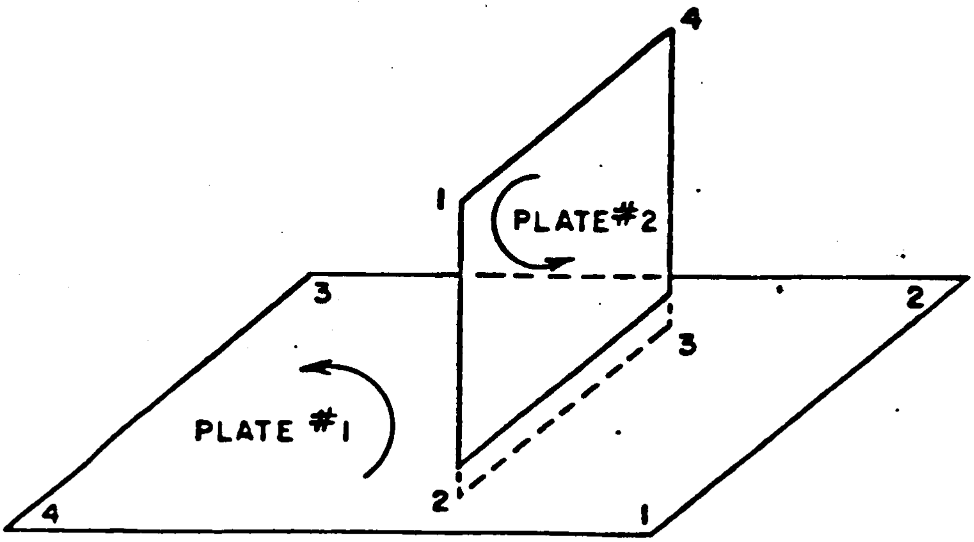
4
1
PLATE#2
3
2
3
PLATE #1
2
4
1

Figure 7(a). Data format used to define a flat plate intersecting another flat plate.

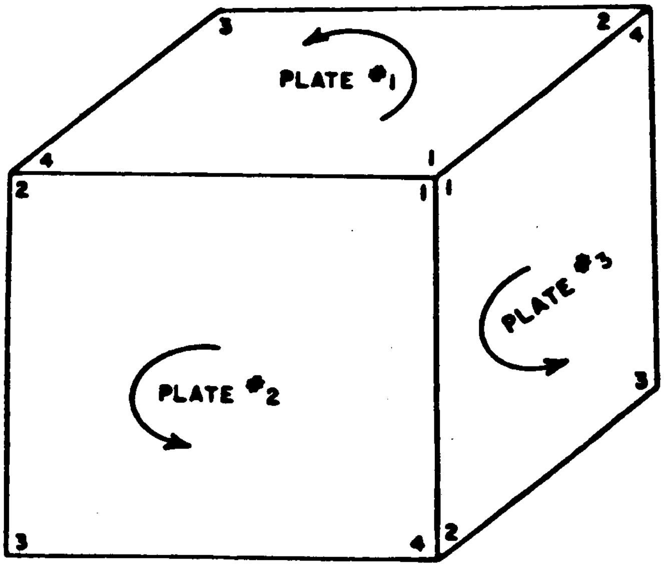
3
2
4
PLATE #1
4
1
2
1
1
PLATE #3
PLATE #2
3
3
4
2

Figure 7(b). Data format used to define a box structure.

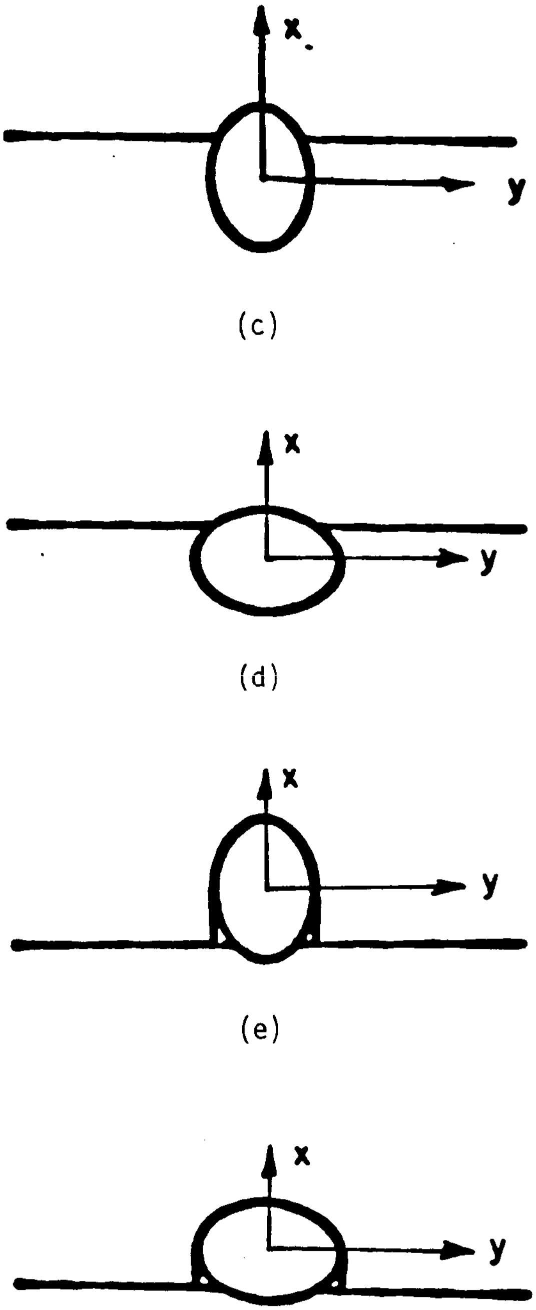

(c)

(d)

(e)

(f)

Figure 7(c)-(f). Fuselage and wing geometries for aircraft model looking from the front. The antenna is assumed to be on the top portion of the models.

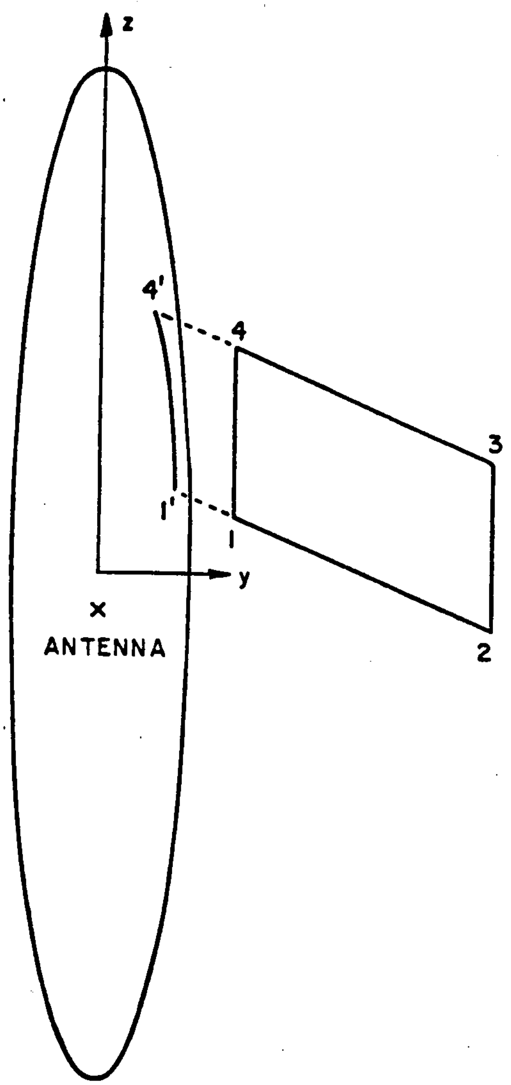
z
4'
4
3
1'
1
y
x
ANTENNA
2

Figure 7(g). Data format used to define a flat plate attaching to a fuselage.

(a) WHEN ZS ≥ 0,

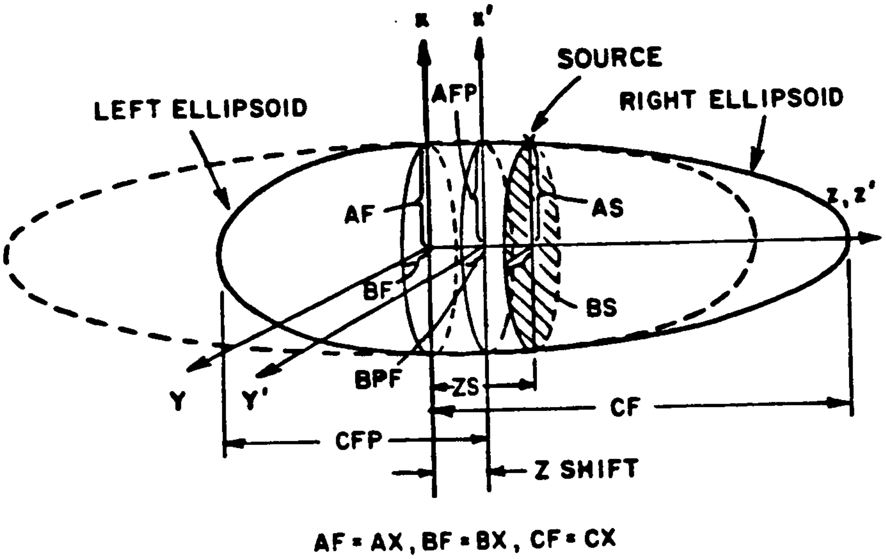
x
x'
SOURCE
LEFT ELLIPSOID
AFP
RIGHT ELLIPSOID
AF
AS
z, z'
BF
BS
BPF
Y
Y'
ZS
CF
CFP
Z SHIFT
AF = AX, BF = BX, CF = CX

(b) WHEN ZS < 0,

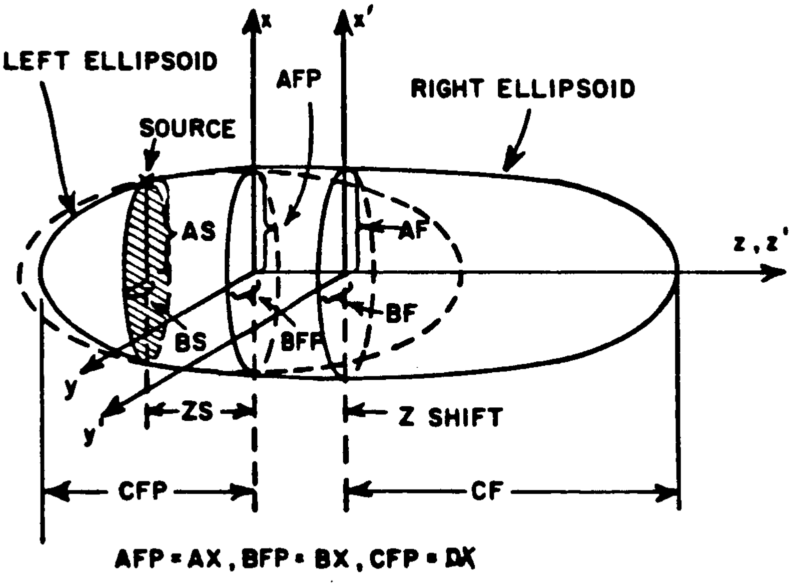
x
x'
LEFT ELLIPSOID
AFP
RIGHT ELLIPSOID
SOURCE
AS
AF
z, z'
BF
BS
BFP
y
y'
ZS
Z SHIFT
CFP
CF
AFP = AX, BFP = BX, CFP = DX

Figure 8. Composite ellipsoid geometry simulating the aircraft fuselage.

Using the "SG:" command, it is necessary that -90° $\leq$ PHS(MS) $\leq$ 90°. In case the antenna is placed on the bottom part of the fuselage, the user must redefine the geometry such that ϕ_s PHS(MS) falls within the required angular range. This requires turning the aircraft upside-down.

The code simulates fuselage blockage by using "FB:" COMMAND. If this command is activated, the code will determine if a ray strikes a fuselage blockage plate. If so, it will set that field component to zero. Thus, the shadowing effect of the fuselage can be simulated in this way. It is assumed that the higher-order diffraction and reflection fields from the fuselage are small in which case they are neglected. Thus, even though higher-order interactions between structures and the fuselage are not added in the computation, their absence will be apparent in the results.

Finally, it must be kept in mind that the antenna should be kept at least a wavelength away from any diffracting edge. In fact all dimensions should be at least a wavelength.

V. PROGRAM OUTPUT

The basic output option from the computer code is a line printer listing of the results. If LWRITE=T in the input data list, the program will automatically generate a line printer output of the complex field values as shown in Figure 9. Recall that the results of the program are the $E_{\theta p}$ and $E_{\phi p}$ radiation pattern values. In order to again describe these pattern components, let us consider the various principal plane patterns treated in the previous section. The computer code allows for a rotation of coordinates such that one can take a pattern about the spherical angles (THC, PHC). The geometry that applies for each of the roll, elevation, and azimuth patterns used in the next section is illutrated in Figure 10. Note that the θp and ϕp angles are defined relative to the rotated pattern coordinates and that they change as THC and PHC are changed. Thus, $E_{\theta p}$ is the theta component of the field (i.e., $E_{\theta p}=\vec{E}\cdot\hat{\theta}_p$) in the pattern coordinate system. Likewise, $E_{\phi p}=\vec{E}\cdot\hat{\phi}_p$). The total radiated electric field is denoted by $\vec{E}$.

In addition to the printed results, one has the option of obtaining a set of polar patterns. If LPLOT=T in the input data list, using the "PP:" command, the program will automatically plot the $E_{\theta p}$ and $E_{\phi p}$ polar patterns. These patterns are plotted such that the outer ring corresponds to the pattern maximum in each case. This polar plot routine was used to plot the data presented in the next section.

One more output option is to get the binary output of the $E_{\theta p}$ and $E_{\phi p}$ patterns. If LBOUT=T in the input data list, using the "BO:" command, the program will automatically write the $E_{\theta p}$ and $E_{\phi p}$ results on unit number #11, i.e., WRITE (11). Note that this unit number increases one by one (i.e., #12, #13, ...) for each additional execution. This is a very useful output when one wishes to interface this program with another one.

ORIGINAL PAGE IS
OF POOR QUALITY

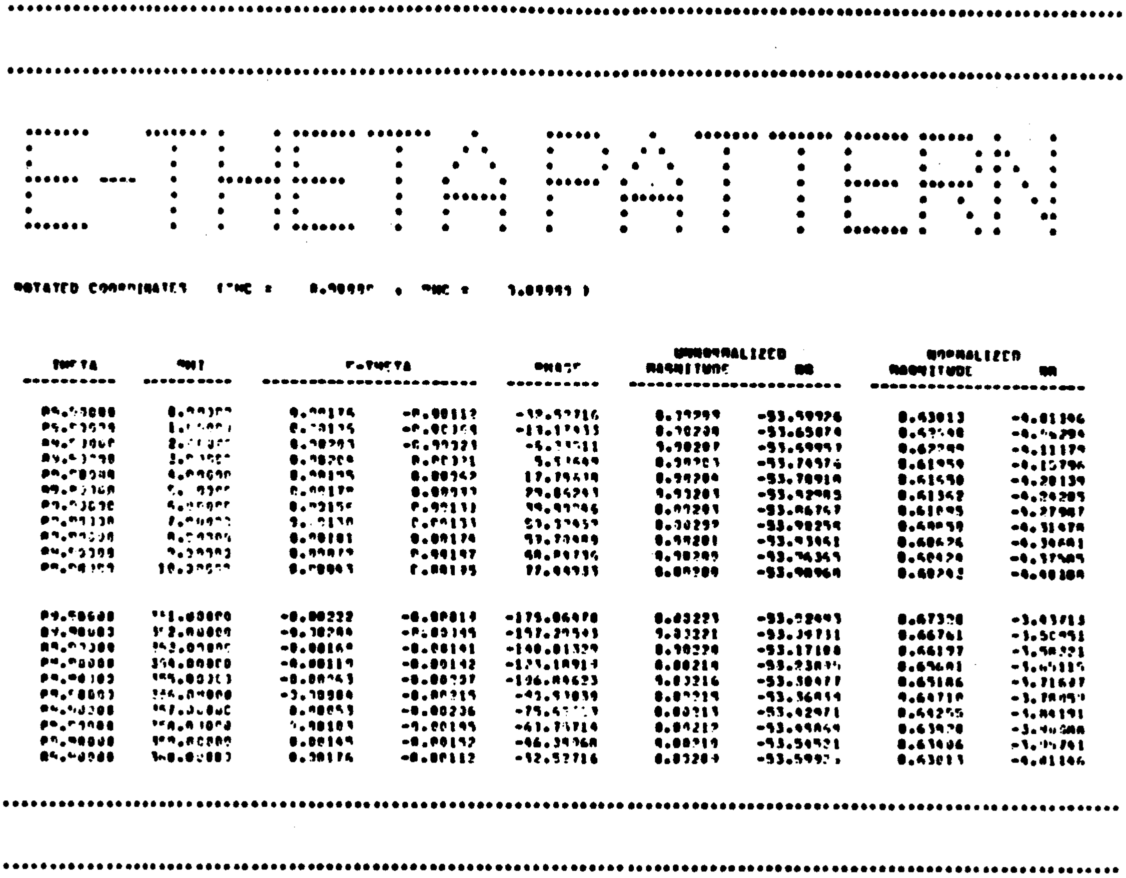

E-THETA PATTERN

ROTATED COORDINATES

THETA PHI E-THETA PHASE UNNORMALIZED MAGNITUDE DB NORMALIZED MAGNITUDE DB

Figure 9(a). Line printer output for the $E_{\theta p}$ fields of Example 1.

ORIGINAL PAGE IS
OF POOR QUALITY

```
..............................................................................................

..............................................................................................

E-PHI PATTERN

ROTATED COORDINATES  (THC =   0.00000 ,  PHC =   0.00000 )

                                                                    UNNORMALIZED                 NORMALIZED
   THETA        PHI              E-PHI                PHASE       MAGNITUDE       DB         MAGNITUDE       DB
----------   ----------   ----------------------   ----------   ------------------------   ------------------------

 89.90000      0.00000    -0.21050     0.12979     149.55362     0.24675    -12.15486     0.29152    -10.70678
 89.90000      1.00000    -0.22134     0.07239     161.91291     0.23290    -12.65873     0.27508    -11.21168
 89.90000      2.00000    -0.21800     0.02080     174.76041     0.21899    -13.19232     0.25868    -11.74490
 89.90000      3.00000    -0.20352    -0.02332    -172.93352     0.20509    -13.76127     0.24329    -12.31318
 89.90000      4.00000    -0.18093    -0.06199    -161.13099     0.19124    -14.36852     0.22591    -12.92144
 89.90000      5.00000    -0.15336    -0.08911    -149.81754     0.17741    -15.02033     0.20954    -13.57345
 89.90000      6.00000    -0.12559    -0.10711    -139.05915     0.16560    -15.72045     0.19528    -14.27438
 89.90000      7.00000    -0.09345    -0.11664    -128.69077     0.14941    -16.48967     0.17648    -15.04134
 89.90000      8.00000    -0.06627    -0.11890    -119.13959     0.13605    -17.12770     0.16271    -15.67316
 89.90000      9.00000    -0.04181    -0.11990    -110.93930     0.12227    -18.25333     0.14446    -16.80651
 89.90000     10.00000    -0.02144    -0.10539    -101.50500     0.10855    -19.28877     0.12822    -17.84193


 89.90000    351.00000     0.37048     0.03954       5.99724     0.37274     -8.56032     0.44055     -7.11914
 89.90000    352.00000     0.32862     0.14457      23.71738     0.35891     -8.89990     0.42405     -7.45172
 89.90000    353.00000     0.26368     0.22331      43.54841     0.34555     -9.25435     0.40726     -7.80097
 89.90000    354.00000     0.17602     0.27318      57.82943     0.33090     -9.61544     0.39091     -8.15736
 89.90000    355.00000     0.08610     0.30455      74.17953     0.31659     -9.99132     0.37397     -8.54324
 89.90000    356.00000    -0.00025     0.30236      90.04677     0.30236    -10.38913     0.35744     -8.93582
 89.90000    357.00000    -0.07674     0.27411     105.42252     0.28468    -10.79464     0.34033     -9.36660
 89.90000    358.00000    -0.13956     0.23710     120.39170     0.27452    -11.22917     0.32449     -9.77721
 89.90000    359.00000    -0.18329     0.18335     134.67941     0.26069    -11.67738     0.30797    -10.22896
 89.90000    360.00000    -0.21050     0.12979     148.55362     0.24675    -12.15486     0.29152    -10.70678

..............................................................................................

..............................................................................................
```

Figure 9(b). Line printer output for the $E_{\phi p}$ fields of Example 1.

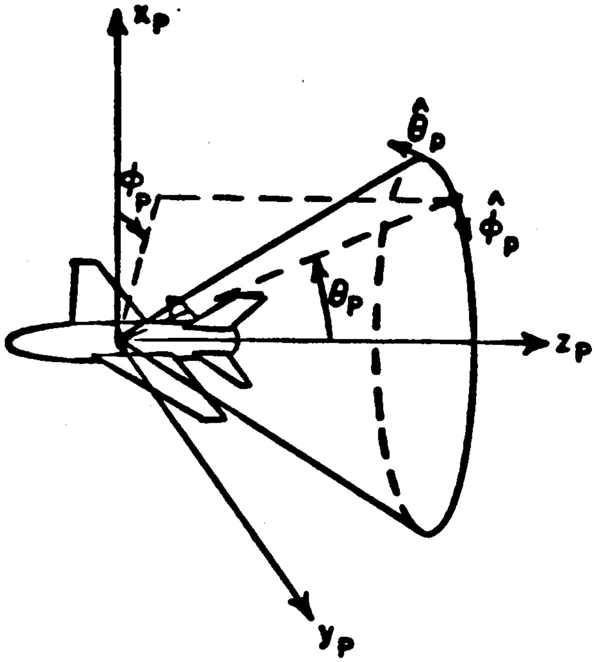
x_p
$\hat{\theta}_p$
ϕ_p
$\hat{\phi}_p$
θ_p
z_p
y_p

(a) ROLL PLANE COORDINATES (THC=0°, PHC=0°)

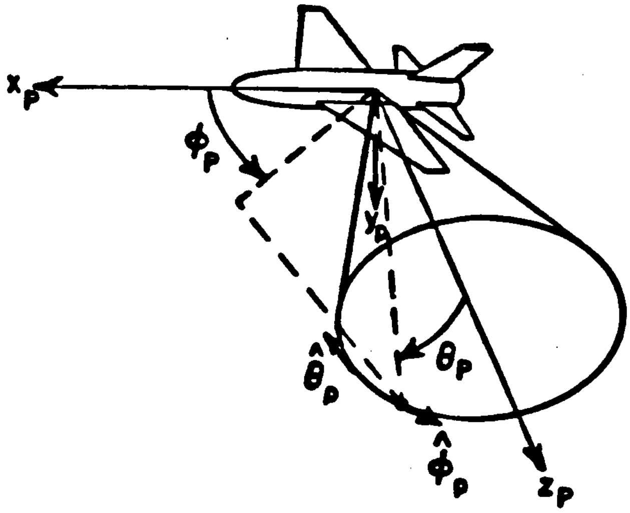
x_p
ϕ_p
y_p
θ_p
$\hat{\theta}_p$
$\hat{\phi}_p$
z_p

(b) ELEVATION PLANE COORDINATES (THC=90°, PHC = 90°)

Figure 10. Transformed coordinate systems for the conical pattern cuts.

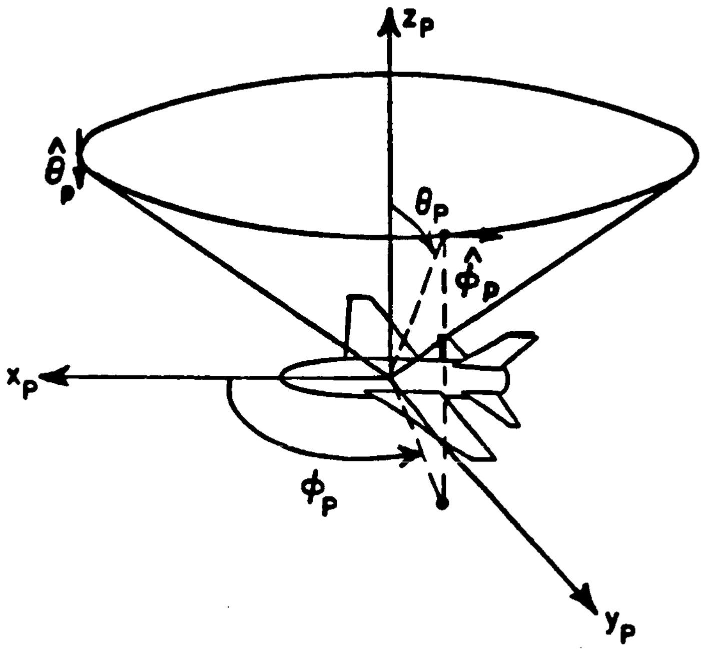
z_p
$\hat{\theta}_p$
θ_p
$\hat{\phi}_p$
x_p
ϕ_p
y_p

(c) AZIMUTH PLANE COORDINATES (THC = 90°, PHC = 0°)

Figure 10. (Continued).

VI. APPLICATION OF CODE TO SEVERAL SIMPLE EXAMPLES

The following two examples are used to illustrate some features and demonstrate the usage of the basic COMMANDS of the computer code. The effect of higher order terms in the solution is shown in example 2. Note that the patterns are plotted in decibels with each division being 10 dB and that the labeling is not included.

Example 1. Consider the radiation pattern of an antenna mounted on a composite ellipsoid for different pattern cuts. This example illustrates the usage of the COMMAND "FC:" and its effect on the pattern. The geometry is shown in Figure 11.

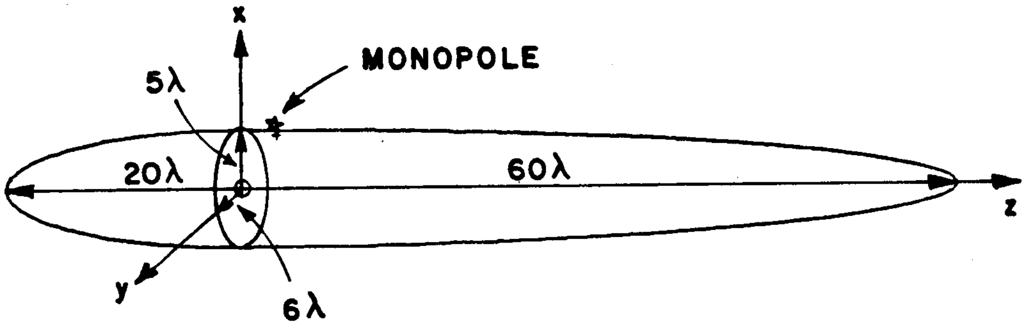

(a) SIDE VIEW

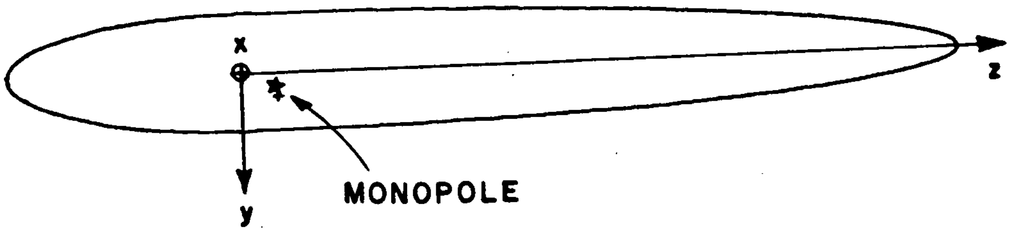

(b) TOP VIEW

Figure 11. A monopole mounted on a composite ellipsoid.

The input data is given by:

```
FG:
5.,6.,60.,20.
F
0.,0.,0.
SG:MONOPOLE
25.,3.
1
0.,0.
.4,.8,0.,.25,3
1.,0.
PD: ROLL PLANE (FAR FIELD)
0.,0.,90.
0,360,1
T,1000.
PP:
T
2,1.,3
EX:
PD:AZIMUTH PLANE  (FAR FIELD)
90.,0.,90.
0,360,1
T,1000.
EX:
PD: ELEVATION PLANE  (FAR FIELD)
90.,90.,90.
0,360,1
T,1000.
EX:
SG: MONOPOLE
25.,-10.
1
0.,0.
.4,.8,0.,.25,3
1.,0.
EX:
FC: FUSELAGE CHOPPED OFF
F,T
40.,-14.
EX:
```

The computed results are shown in Figure 12.

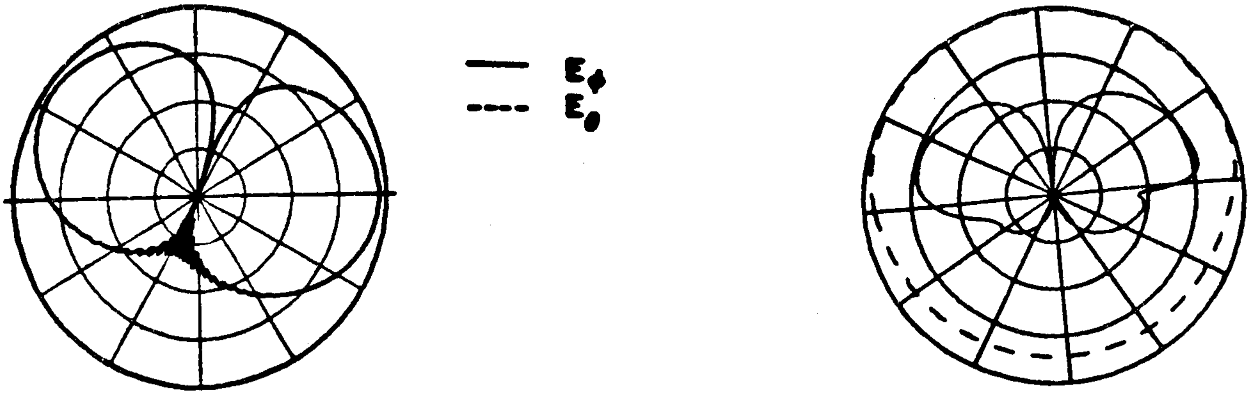

(a) θ_c=0°, ϕ_c=0°, θ_p=90°

(b) θ_c=90°, ϕ_c=0°, θ_p=90°

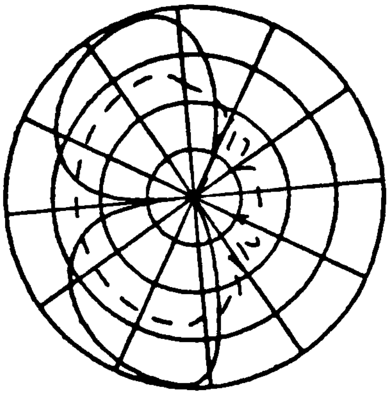

(c) θ_c=90°, ϕ_c=90°, θ_p=90°

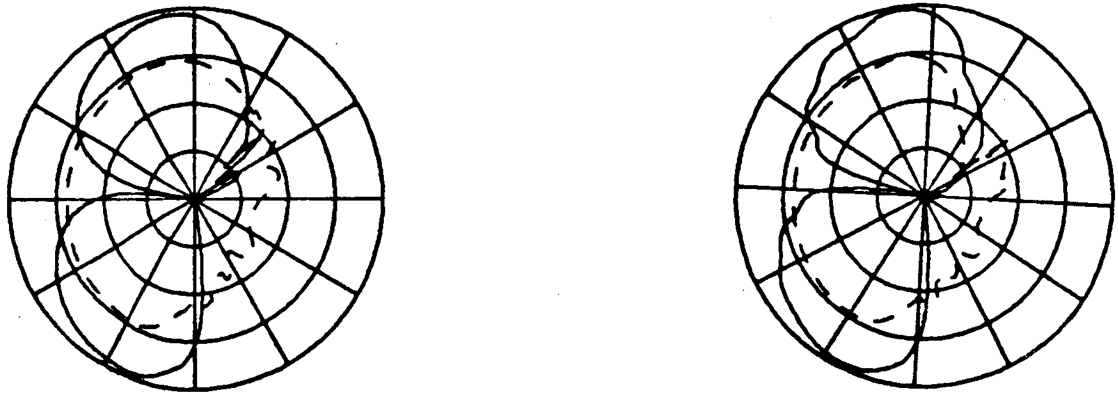

(d) θ_c=90°, ϕ_c=90°, θ_p=90°

(e) θ_c=90°, ϕ_c=90°, θ_p=90°

Figure 12. Radiation pattern of monopole mounted on a composite ellipsoid at frequency .3 GHz. (a) (b) (c) source located at PHS=25°, ZS=3λ (d) (e) source located at PHS=25°, ZS=10λ and fuselage chopped off at ZC2=-14λ for (e).

Example 2: Consider the roll plane radiation pattern for a bent plate attached to a composite ellipsoid (5' x 6', 50' x 50'). The geometry is shown in Figure 13. The usage of "TO:" and "PI:" commands and their effect on the radiation pattern will be shown in this example. Various GTD terms involved in the computation are shown in Figure 14.

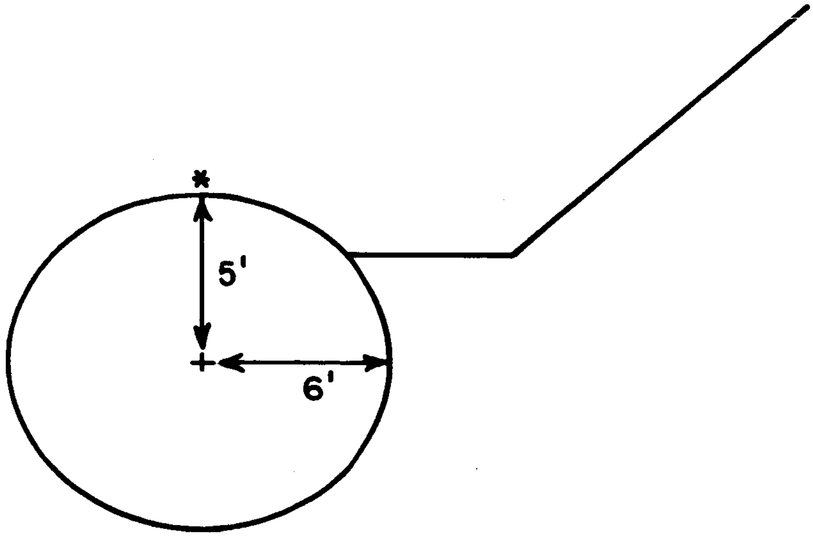

Figure 13. A bend plate attached to a composite ellipsoid.

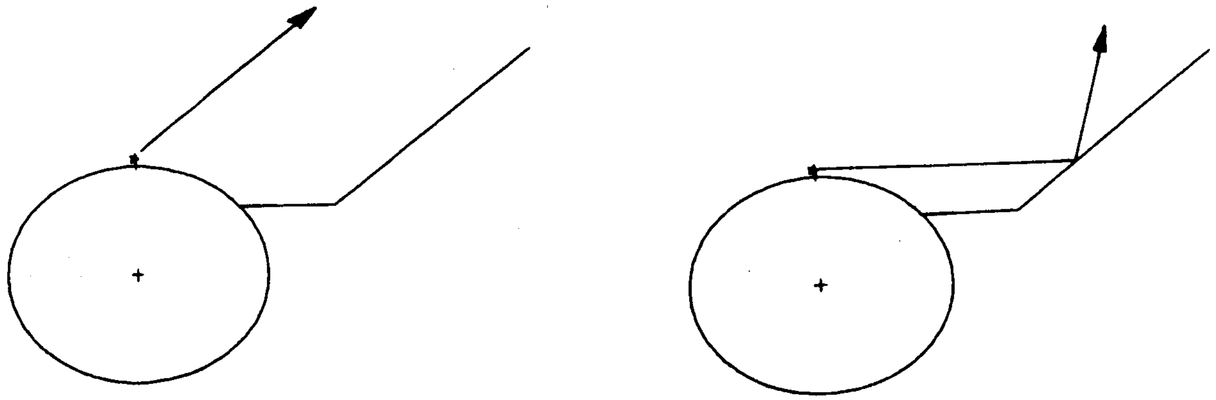

source field

reflected field

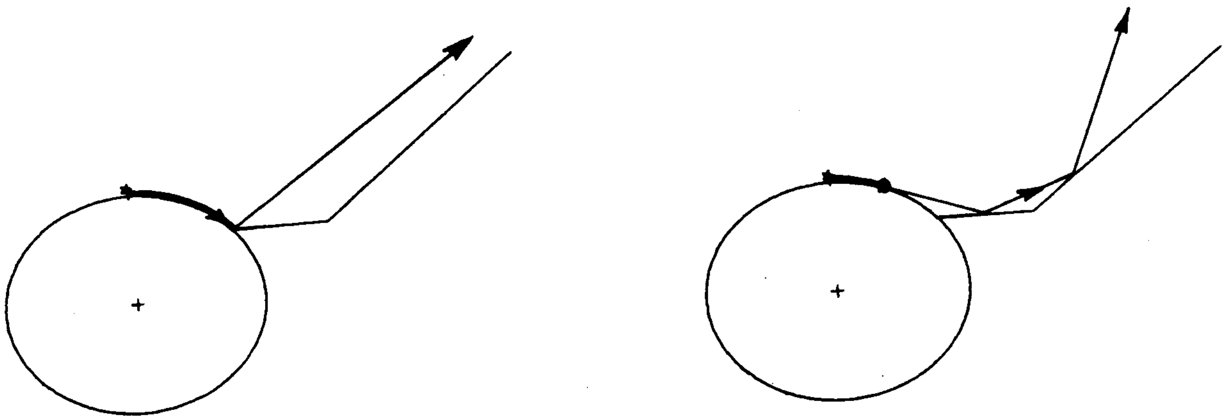

diffracted field

reflected-reflected field

Figure 14. Various GTD terms.

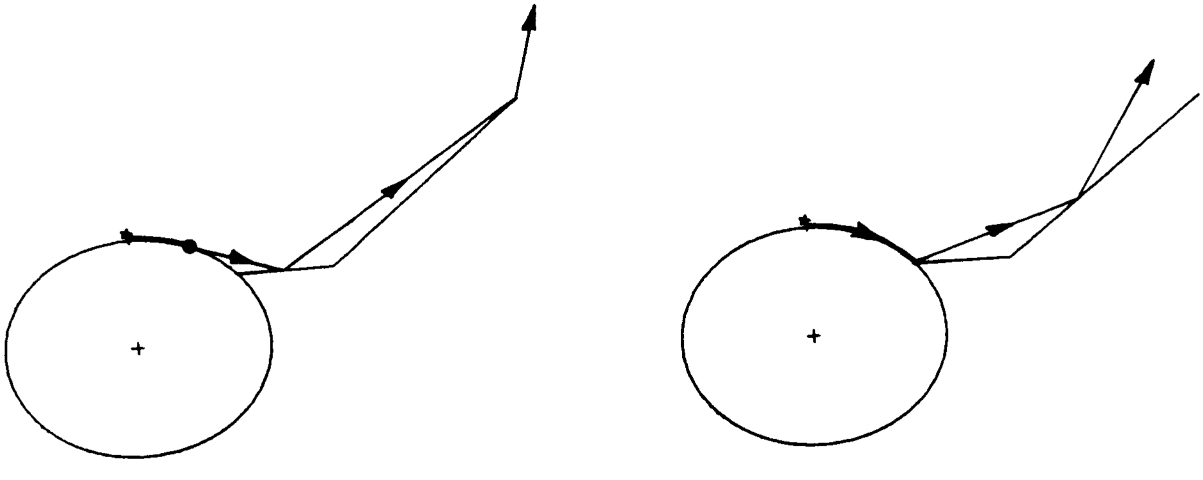

reflected-diffracted
field

diffracted-reflected
field

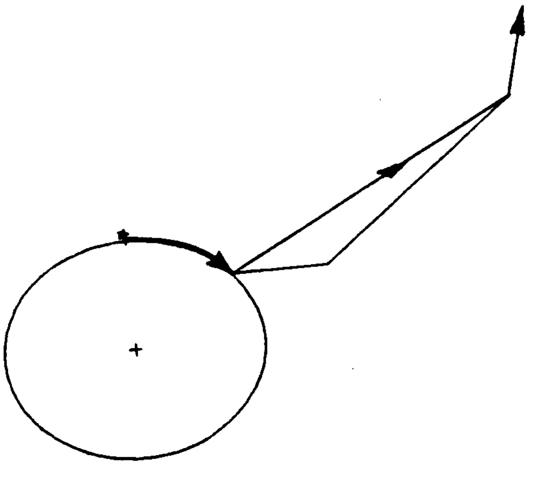

diffracted-diffracted field

Figure 14. (Continued).

The input data is given by:

```
UN: FEET
2
FQ: 1GHz
1,1.,1.
FG:
5.,6.,50.,50.
F
0.,0.,0.
FB:
2
4
4.5,0.,20.
4.5,0.,-20.
-4.5,0.,-20.
-4.5,0.,20.
4
0.,-5.5,20.
0.,5.5,20.
0.,5.5,-20.
0.,-5.5,-20.
SG: MONOPOLE
0.,0.
1
0.,0.
.4,.8,0.,.25,3
1.,0.
PP: PEN PLOT
T
1,1.35,3
PD: ROLL PLANE (NEAR FIELD)
0.,0.,90.
0,360,1
F,1000.
PG:
4,T
3.,6.,-20.
3.,9.,-20.
3.,9.,20.
3.,6.,20.
PG:
4,F
3.,9.,-20.
10.,18.,-20.
10.,18.,20.
3.,9.,20.
RD:
1
1,2
DD:
4
2,4,2,2
1,4,2,2
2,2,1,4
2,2,2,4
TO: TOTAL FIELD (INCLUDE DOUBLE TERMS)
F,F,F
T,T
T,T,T,F,T,T,T,T
1,2,1
1,4,1
1,4,1
EX:
TO: SOURCE FIELD ONLY
F,F,F
T,T
T,F,F,F,F,F,F,F
1,2,1
1,4,1
1,4,1
EX:
TO: REFLECTED FIELD ONLY
F,F,F
T,T
F,T,F,F,F,F,F,F
1,2,1
1,4,1
1,4,1
EX:
TO: DIFFRACTED FIELD ONLY
F,F,F
T,T
F,F,T,F,F,F,F,F
1,2,1
1,4,1
1,4,1
EX:
TO: S+R
F,F,F
T,T
T,T,F,F,F,F,F,F
1,2,1
1,4,1
1,4,1
EX:
```

```
TO: S+R+D (ONLY FIRST ORDER TERM INCLUDE)
F,F,F
T,T
T,T,T,F,F,F,F,F
1,2,1
1,4,1
1,4,1
EX:
TO: DOUBLE REFLECTION (R/R)
F,F,F
T,T
F,F,F,F,T,F,F,F
1,2,1
1,4,1
1,4,1
EX:
TO: S+R+R/R
F,F,F
T,T
T,T,F,F,T,F,F,F
1,2,1
1,4,1
1,4,1
EX:
TO: REFLECTION/DIFFRACTION TERM (R/D)
F,F,F
T,T
F,F,F,F,F,T,F,F
1,2,1
1,4,1
1,4,1
EX:
TO: R/R+R/D
F,F,F
T,T
F,F,F,F,T,T,F,F
1,2,1
1,4,1
1,4,1
EX:
TO: S+R+D+R/R+R/D
F,F,F
T,T
T,T,T,F,T,T,F,F
1,2,1
1,4,1
1,4,1
EX:
```

```
TO: DIFFRACTION/REFLECTION TERM (D/R)
F,F,F
T,T
F,F,F,F,F,F,T,F
1,2,1
1,4,1
1,4,1
EX:
TO: S+R+D+R/R+R/D+D/R
F,F,F
T,T
T,T,T,F,T,T,T,F
1,2,1
1,4,1
1,4,1
EX:
TO: DOUBLE DIFFRACTION TERM (D/D)
F,F,F
T,T
F,F,F,F,F,F,F,T
1,2,1
1,4,1
1,4,1
EX:
TO: D/R+D/D
F,F,F
T,T
F,F,F,F,F,F,T,T
1,2,1
1,4,1
1,4,1
EX:
TO: ALL DOUBLE TERM
F,F,F
T,T
F,F,F,F,T,T,T,T
1,2,1
1,4,1
1,4,1
EX:
TO:
F,F,F
T,T
T,T,T,F,F,F,F,F
1,2,1
1,4,1
1,4,1
PI: TAKE OFF SECOND PLATE
1
PG: ADD ONE PLATE
4,T
3.,-6.,20.
3.,-9.,20.
3.,-9.,-20.
3.,-6.,-20.
PP:
T
1.,2.,3
EX:
```

The computed results are shown in Figures 15 and 16. Note that each pattern in Figure 15 is normalized to the same level so that one can see the relative significance of each term. An interesting result is shown in Figure 15(e) where the source and the reflected field are superimposed. These two terms form the classical "Geometrical Optics" (GO) solution. However, one should note that the GO solution is far from being complete as one can observe from the discontinuities in the pattern. Even when the first order terms of the GTD solution are superimposed, as shown in Figure 15(f), the pattern is still rough. Therefore, higher order terms which are in Figures 15(g) to 15(p) are added to eliminate the discontinuities. The final result is shown in Figure 15(a). It is clear that these higher terms can be significant in certain regions of the pattern as shown in Figure 15(p). In the last execution the geometry is modified by removing one plate and adding another as shown in Figure 16.

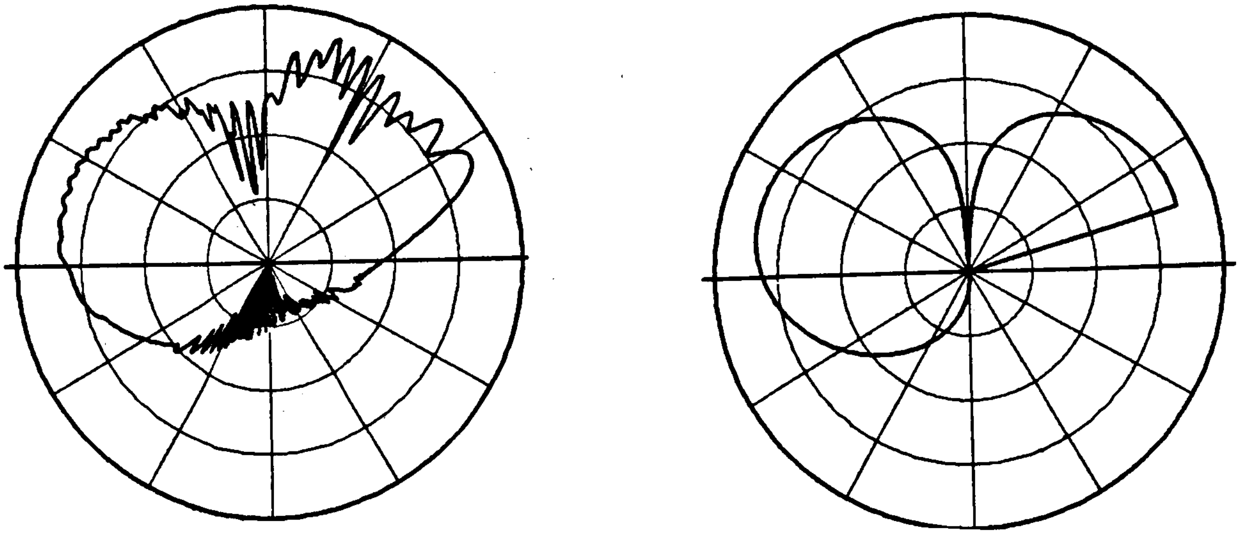

(a) total solution
(S+R+D+R/R+R/D+D/R+D/D)

(b) source field (S)

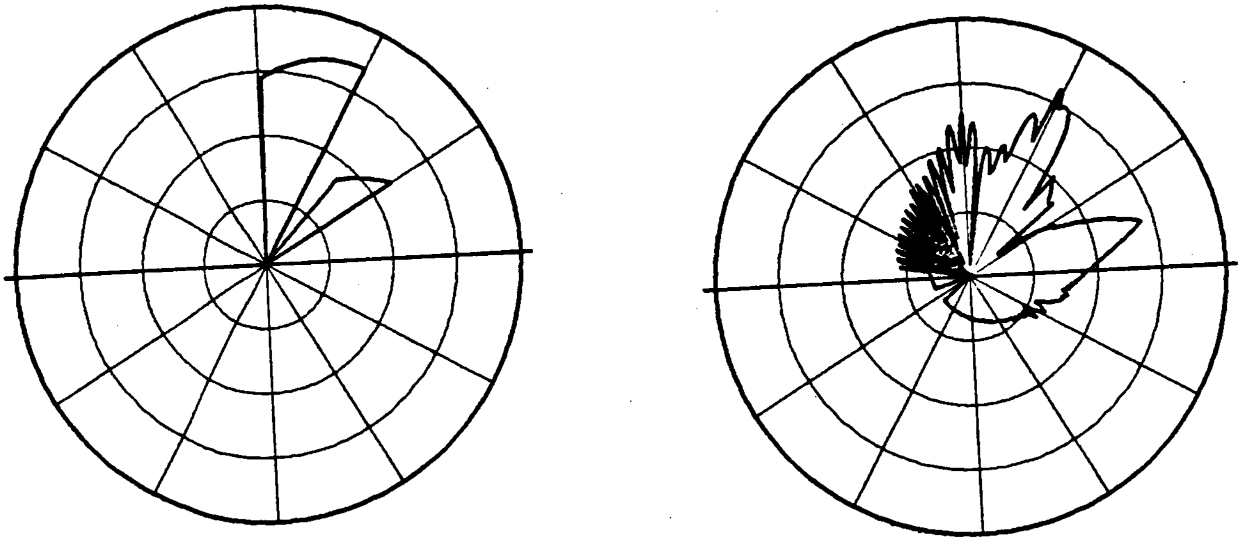

(c) reflected field (R)

(d) diffracted field (D)

Figure 15. Roll plane radiation pattern.

ORIGINAL PAGE IS
OF POOR QUALITY

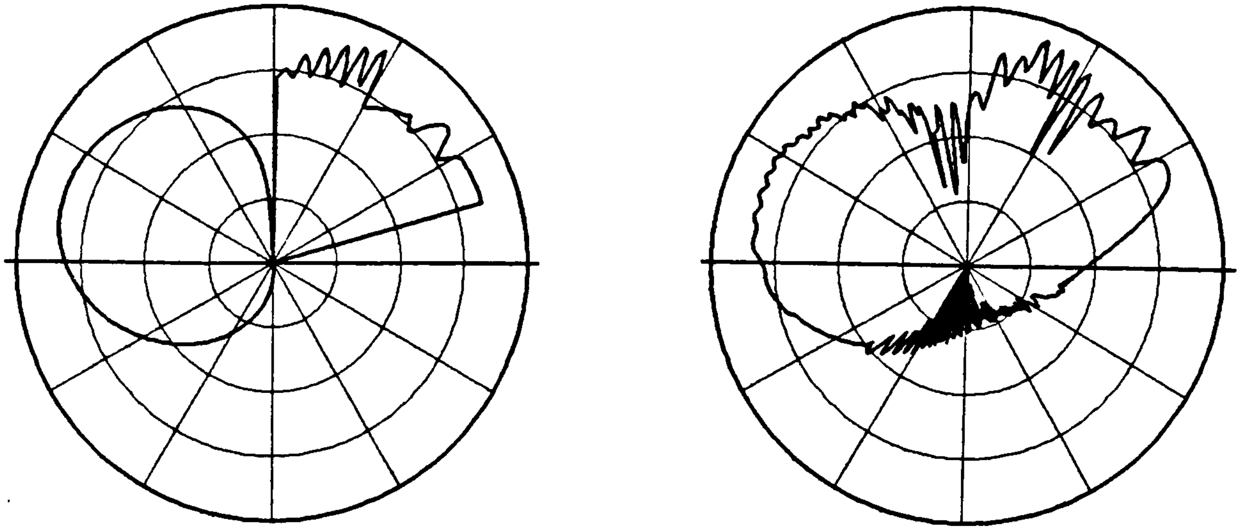

(e) S + R

(f) S + R + D

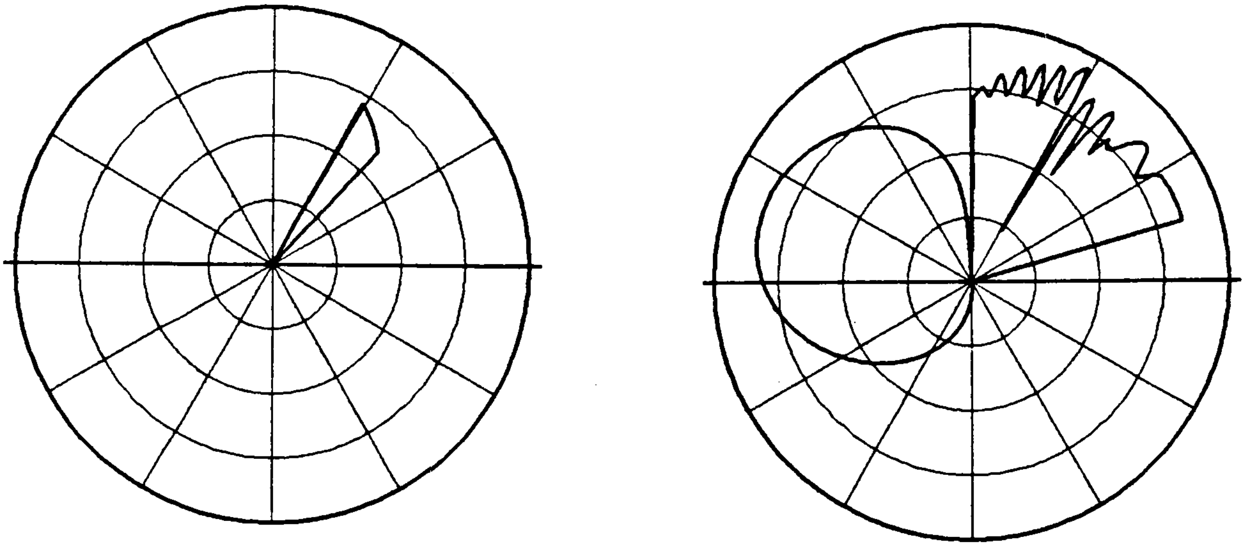

(g) reflected/reflected field (R/R)

(h) S + R + R/R

Figure 15. (Continued).

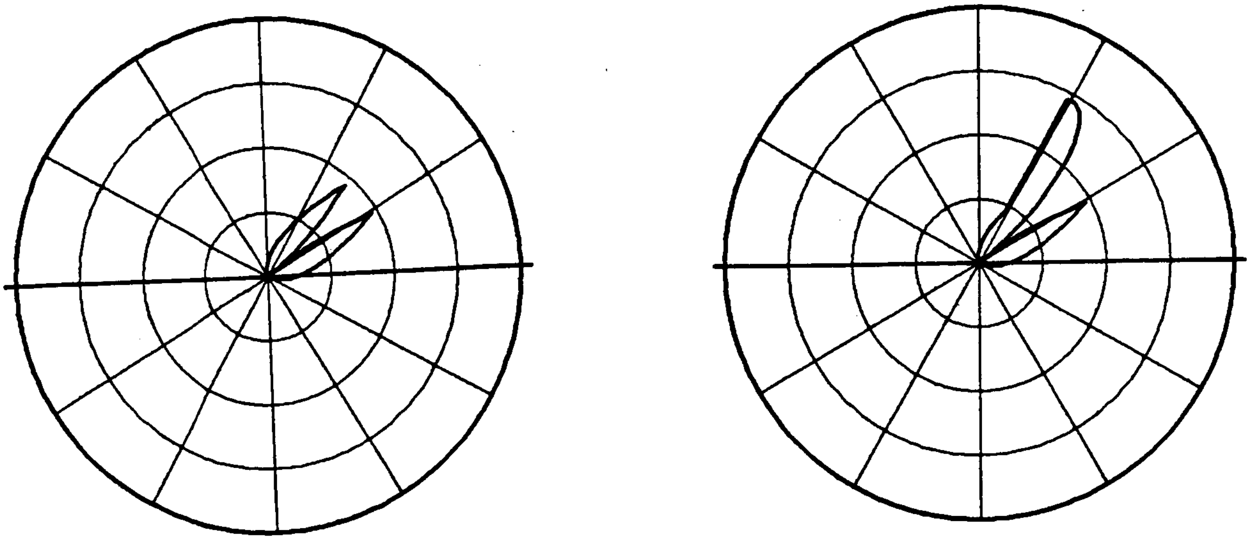

(f) reflected/diffracted field (R/D)

(j) R/R + R/D

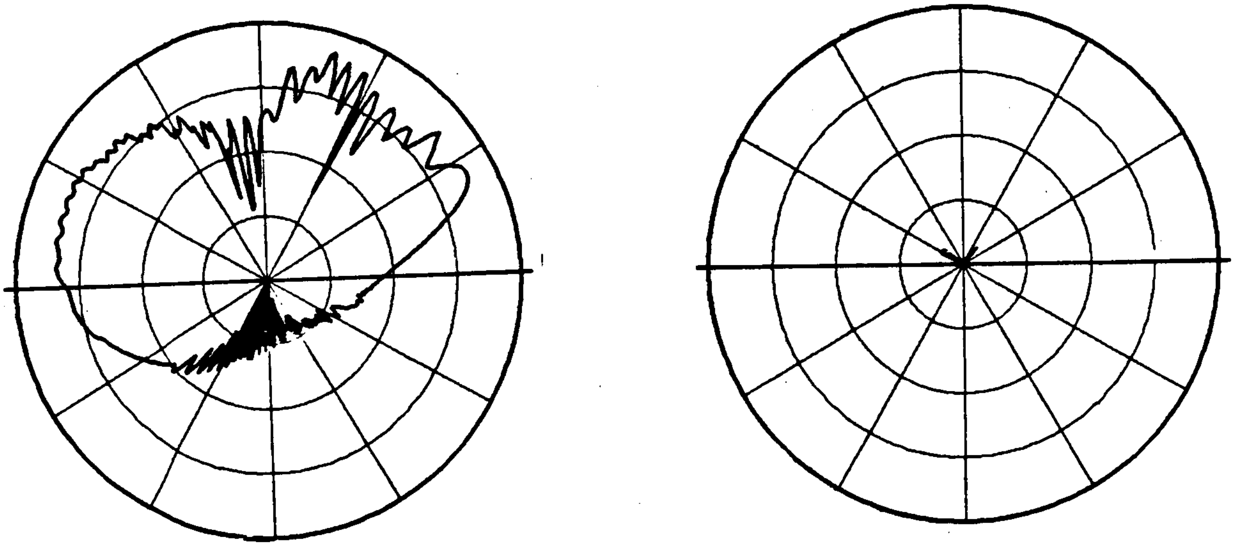

(k) S + R + D + R/R + R/D

(l) diffracted/reflected field (D/R)

Figure 15. (Continued).

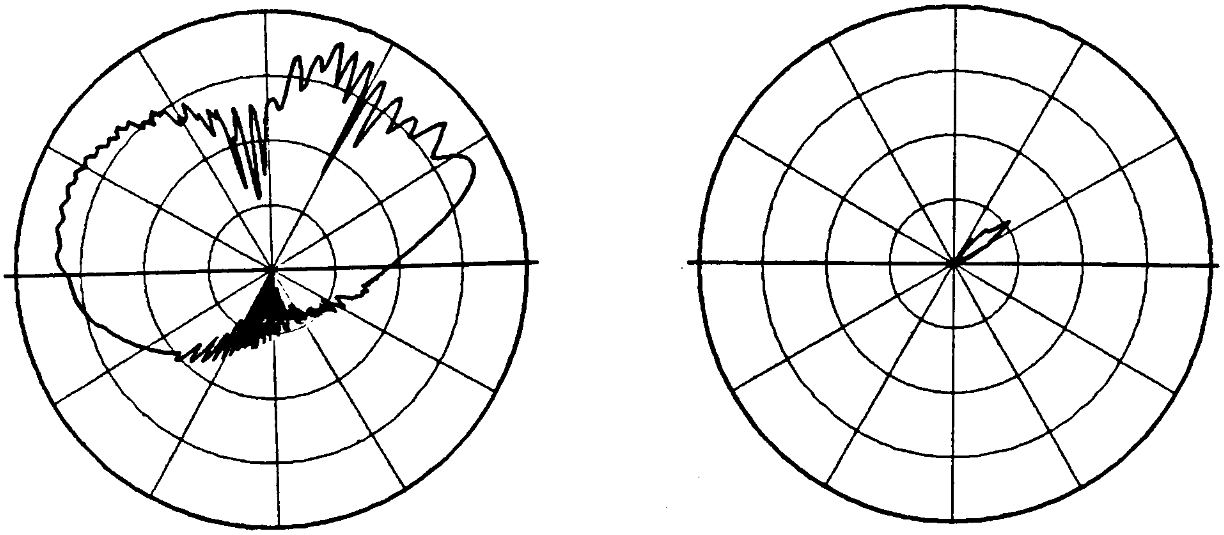

(m) S + R + R/R + R/D + D/R

(n) diffracted/diffracted field (D/D)

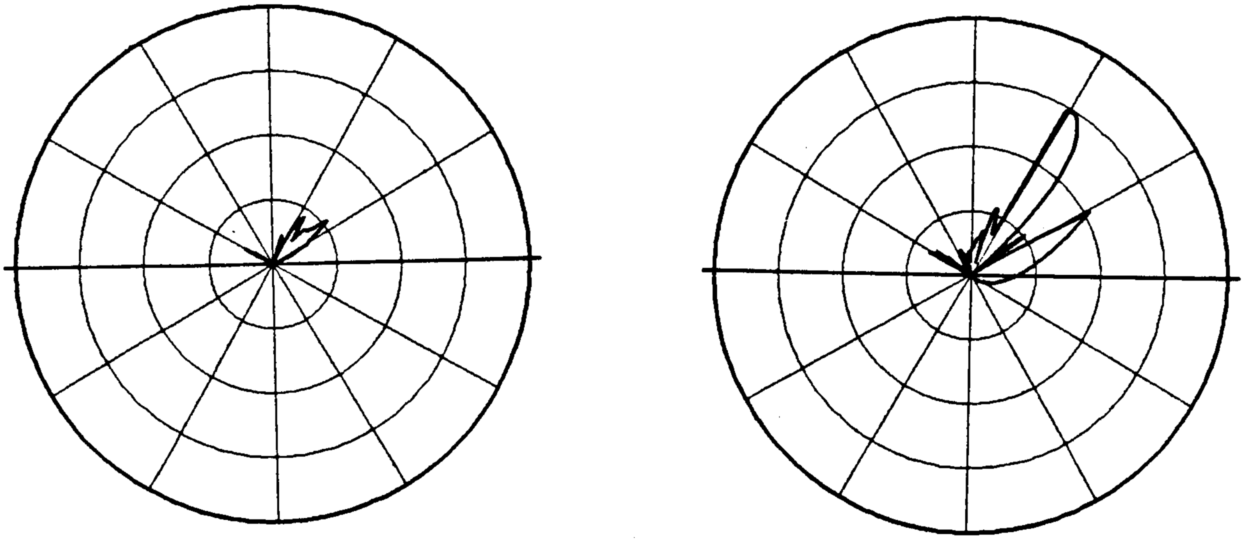

(o) D/R + D/D

(p) second order interaction GTD terms (R/R + R/D + D/R + D/D)

Figure 15. (Continued).

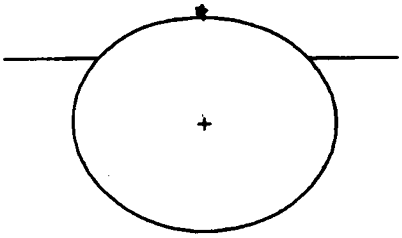

(a)

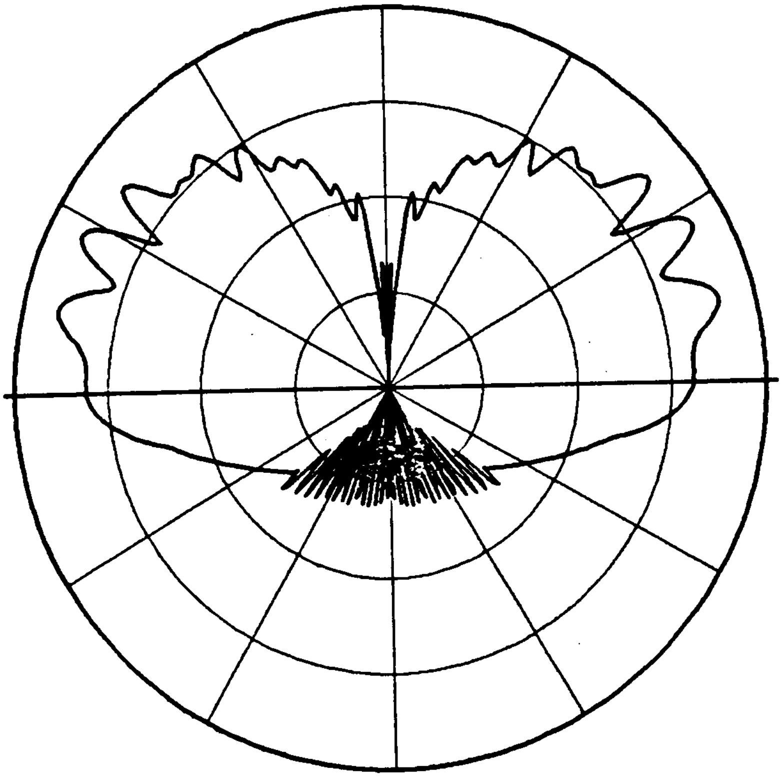

(b)

Figure 16. Total solution (S+R+D) after using "PI:" and "PG:" commands.

VII. APPLICATION OF CODE TO AIRCRAFT SIMULATIONS

To begin any simulation of an aircraft, one needs to start with a set of scale model drawings. A typical aircraft model consists of a composite ellipsoid fuselage plus flat plates simulating the other structures such as wings, stabilizers, etc. One can also use the "COMMAND FC:" to model the radome part of the aircraft. The radome is constructed of low dielectric constant material such that it is assumed to be totally transparent in these calculations.

A wide variety of aircraft computer models such as commercial, private, military aircrafts and the space shuttle are given in the following examples. They serve to illustrate the use capability, and validity of this general numerical solution.

To begin the simulation procedure, one first finds the composite ellipsoid parameters for the aircraft fuselage. The ellipsoid surface should simulate the fuselage surface as accurately as possible near the antenna location. Once the composite ellipsoid dimensions are specified the plates are added to the model.

This code allows for two different methods for defining one plate to be attached to another: 1) edge to edge attachment and 2) edge to surface attachment. Edge to edge attachment, as illustrated in Figure 17 often requires that a plate edge be defined as two or three colinear edges as the program identifies this mode of attachment only by finding two identical pairs of corners. Note that the corners must be consecutive on both plates which means there actually exists an edge

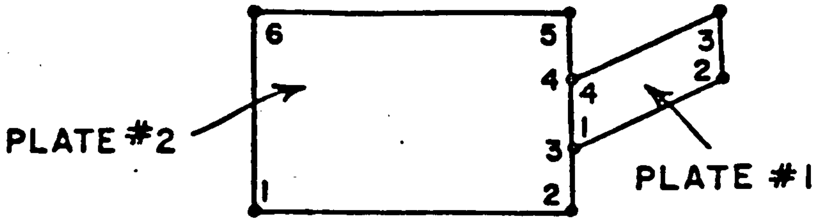
6
5
4
3
2
1
PLATE #2
3
2
4
1
PLATE #1

Figure 17. Edge to edge plate attachment.

between them. In the case to surface attachment, one plate is defined as penetrating a short distance through the surface of the second plate as illustrated in Figure 18. The program then defines the new junction edge and eliminates the smaller portion of plate #1 behind plate #2. Here care must be taken to assure that the new junction edge is completely contained within the bounds of plate #2, and no where nearer than a quarter wavelength or so to an edge of plate #2.

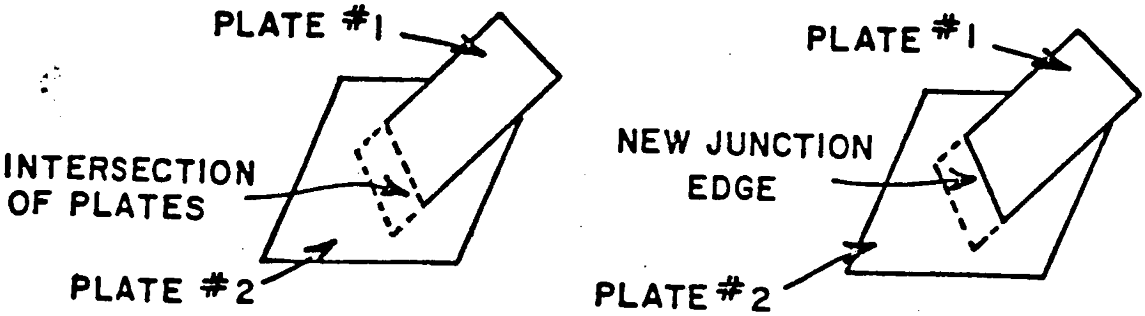
PLATE #1
INTERSECTION
OF PLATES
PLATE #2
PLATE #1
NEW JUNCTION
EDGE
PLATE #2

Figure 18. Edge to surface plate attachment.

One thing which should be noted is that the attaching of the wings, stabilizers, and plates to the fuselage is automatically done by the computer as illustrated in Figure 7(g). Thus, the user need not worry about generating the correct input data to perform this task.

Example 3: Simulation of Boeing 737

In this example, monopole and slot antennas are mounted on the fuselage of a Boeing 737 aircraft at various stations as shown in Figure 19.

A λ/4 monopole mounted at station 220 just above the cockpit as shown in Figure 19. The line drawing of the 737 is shown in Figure 20 and the computer model based on the input data is shown in Figure 21. The input data is as follows:

```
UN:INCHES
3
FQ: 3.18 GHZ
1,3.18,1.
FG: BOEING 737 (STATION 220)
77.,74.,830.,308.56
F
0.,0.,0.
SG: MONOPOLE
0.,-278.
1
0.,0.
1.537,3.074,0.,.928525,3
1.,0.
PG: RIGHT WING
4,T
1.,75.,67.952
1.,536.93,316.14
1.,536.93,379.86
1.,75.,240.26
PG: LEFT WING
4,T
1.,-75.,240.26
1.,-536.93,379.86
1.,-536.93,316.14
1.,-75.,67.952
PG: VERTICAL STABILIZER
4,T
77.,8.25,618.55
284.147,8.25,819.056
284.147,0.,683.696
77.,0.,483.19
```

```
PG: VERTICAL STABILIZER
4,T
77.,0.,483.19
284.147,0.,683.696
284.147,-8.25,819.056
77.,-8.25,618.55
PG: NOSE
4,T
5.5,-10.,-308.56
-.1,-10.,-321.6
-.1,0.,-321.6,
5.5,0.,-308.56
PG: NOSE
4,T
5.5,0.,-308.56
-.1,0.,-321.6
-.1,10.,-321.6
5.5,10.,-308.56
PP: POLAR PLOT IN DB
T
1,1.5,3
PD: ROLL PLANE
0.,0.,89.8
0,360,1
F,6000.
EX:
PD: ELEVATION PLANE
90.,90.,89.8
0,360,1
F,6000.
EX:
```

```
PD: AZIMUTH PLANE
93.,0.,89.8
0,360,1
F,6000.
EX:
PD: AZIMUTH PLANE
93.,0.,50.
0,360,1
F,6000.
EX:
PD: AZIMUTH PLANE
93.,0.,60.
0,360,1
F,6000.
EX:
PD: AZIMUTH PLANE
93.,0.,70.
0,360,1
F,6000.
EX:
```

```
PD: AZIMUTH PLANE
93.,0.,80.
0,360,1
F,6000.
EX:
PD: AZIMUTH PLANE
93.,0.,100.
0,360,1
F,6000.
EX:
PD: AZIMUTH PLANE
93.,0.,110.
0,360,1
F,6000.
EX:
PD: AZIMUTH PLANE
93.,0.,120.
0,360,1
F,6000.
EX:
```

The three principle plane results are shown in Figures 22 to 24 and found to be in very good agreement with measurements. The experimental work was performed by the technical staff at NASA (Hampton, Virginia) using a 1/11th scale model of a Boeing 737 aircraft. It is noted that the measured results have some asymmetry in the patterns. This could be attributed to misalignment of the monopole with respect to the surface normal or the movement of the model due to shifting weight during the measurement. This misalignment of the monopole (approximately 3° tilted to the nose section from the actual surface normal) was detected by the calculated evaluation plane pattern and various azimuth plane patterns. To compensate this misalignment in the comparison with measured patterns, the conical pattern axis rotated 3° to the nose section was used in the following pattern calculations for the Station 220 case. The various azimuth plane patterns for this antenna location are computed and shown in Figures 25(a) to (g). In each case, the calculated results compare very favorably with the measurements.

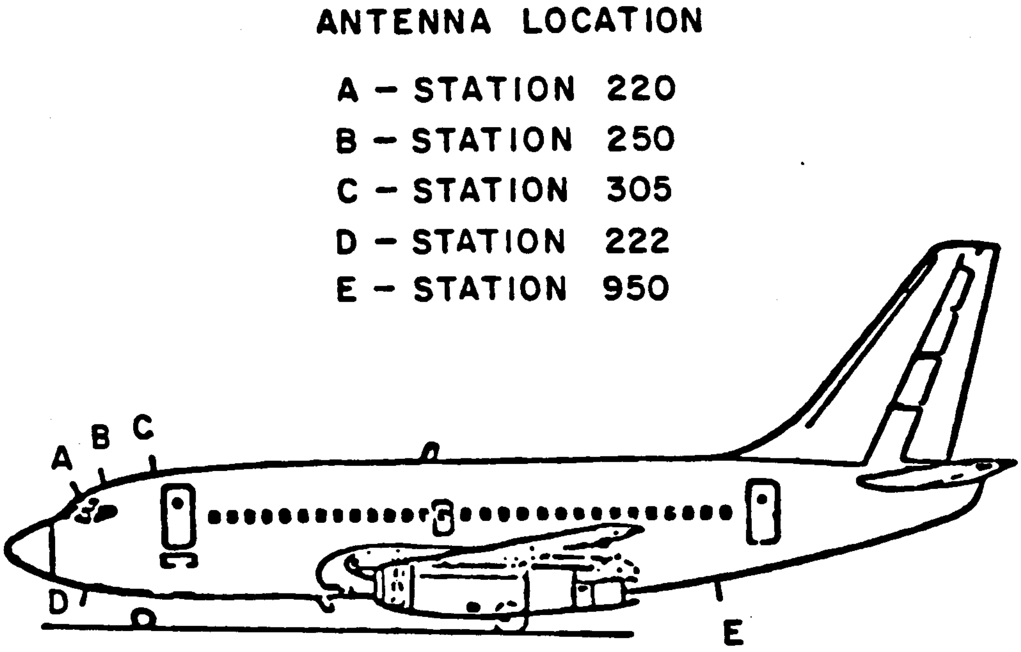
ANTENNA LOCATION
A - STATION 220
B - STATION 250
C - STATION 305
D - STATION 222
E - STATION 950
A
B
C
D
E

Figure 19. Test locations for the antenna installation on the Boeing 737 aircraft.

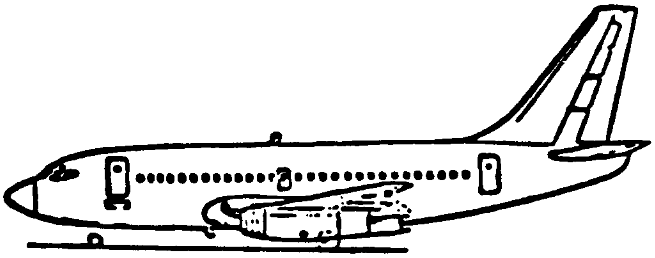

(a) SIDE VIEW

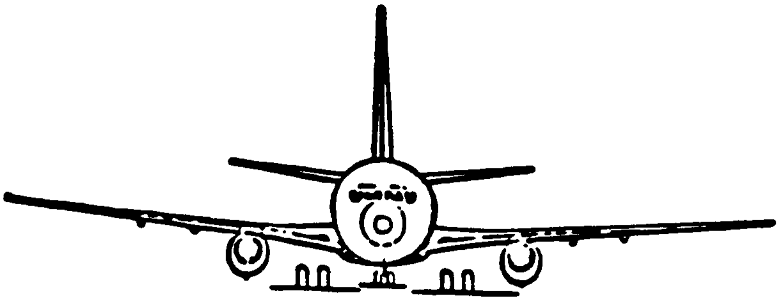

(b) FRONT VIEW

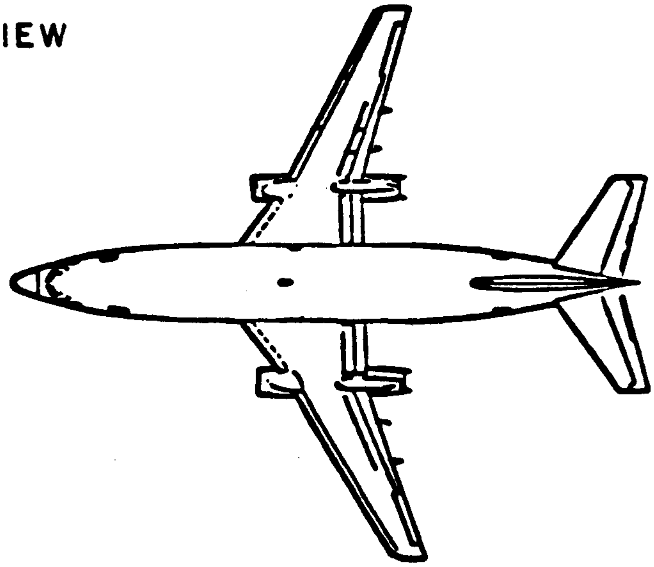

(c) TOP VIEW

Figure 20. Boeing 737 aircraft.

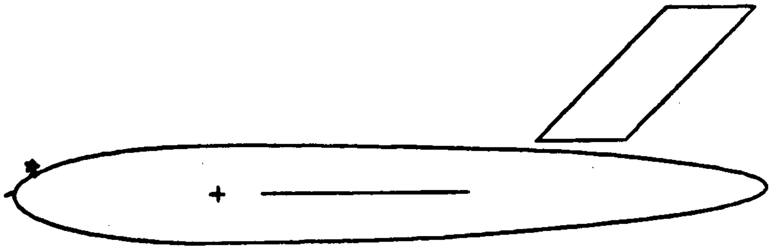

(a) SIDE VIEW

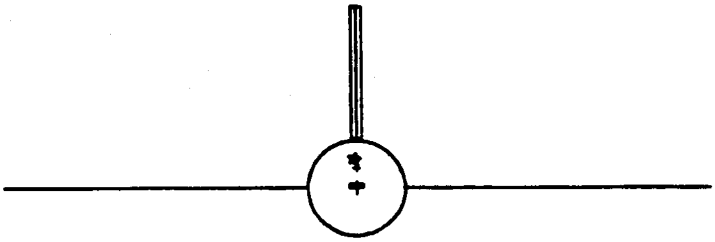

(b) FRONT VIEW

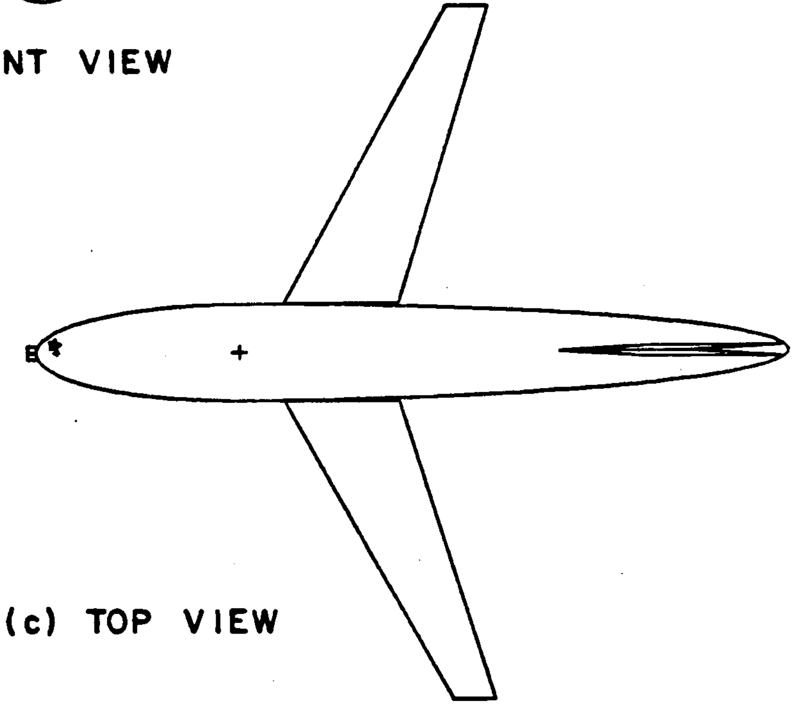

(c) TOP VIEW

Figure 21. Computer simulated model of a Boeing 737 aircraft. The antenna is located at Station 220.

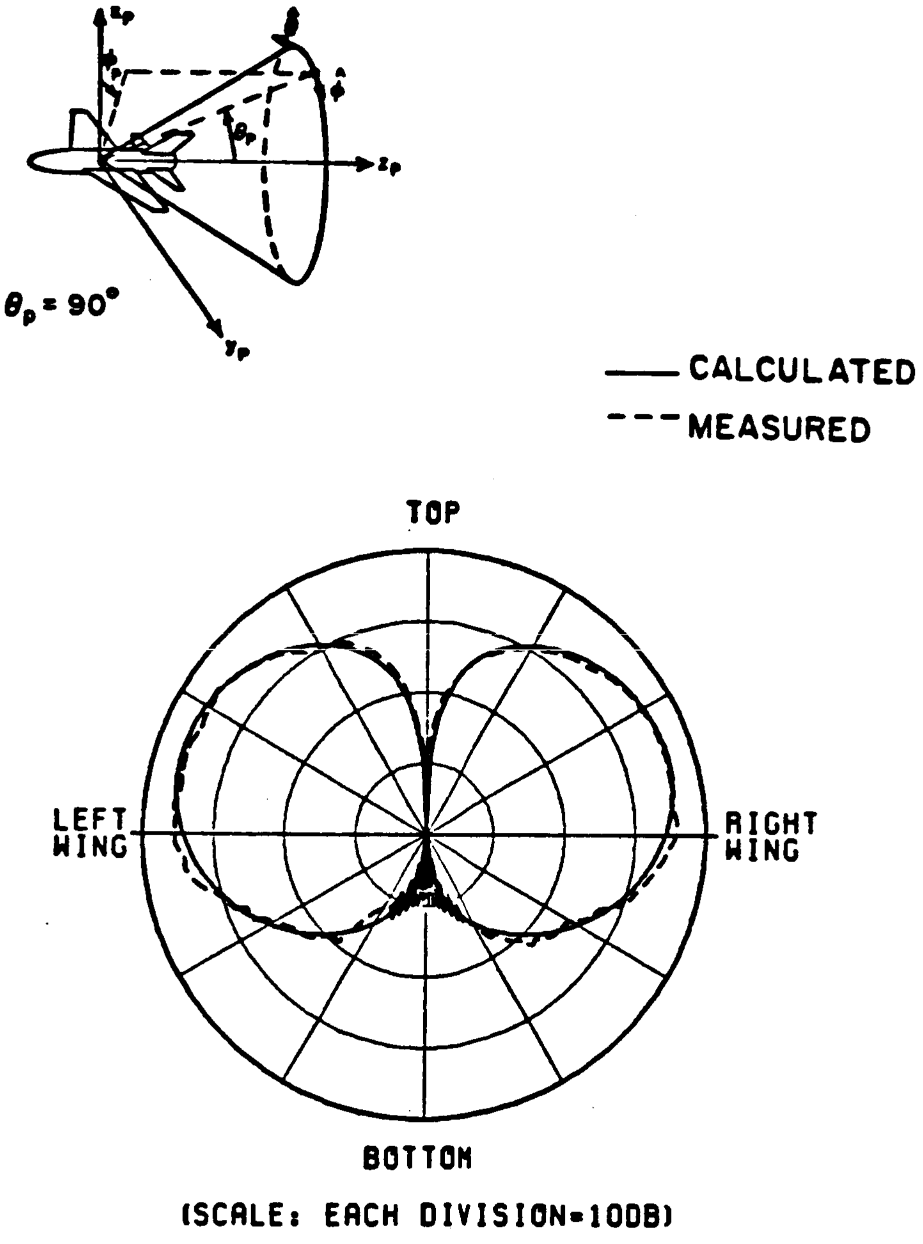

Figure 22. Roll plane pattern of a $\lambda/4$ monopole mounted at Station 220 on top of a Boeing 737 aircraft.

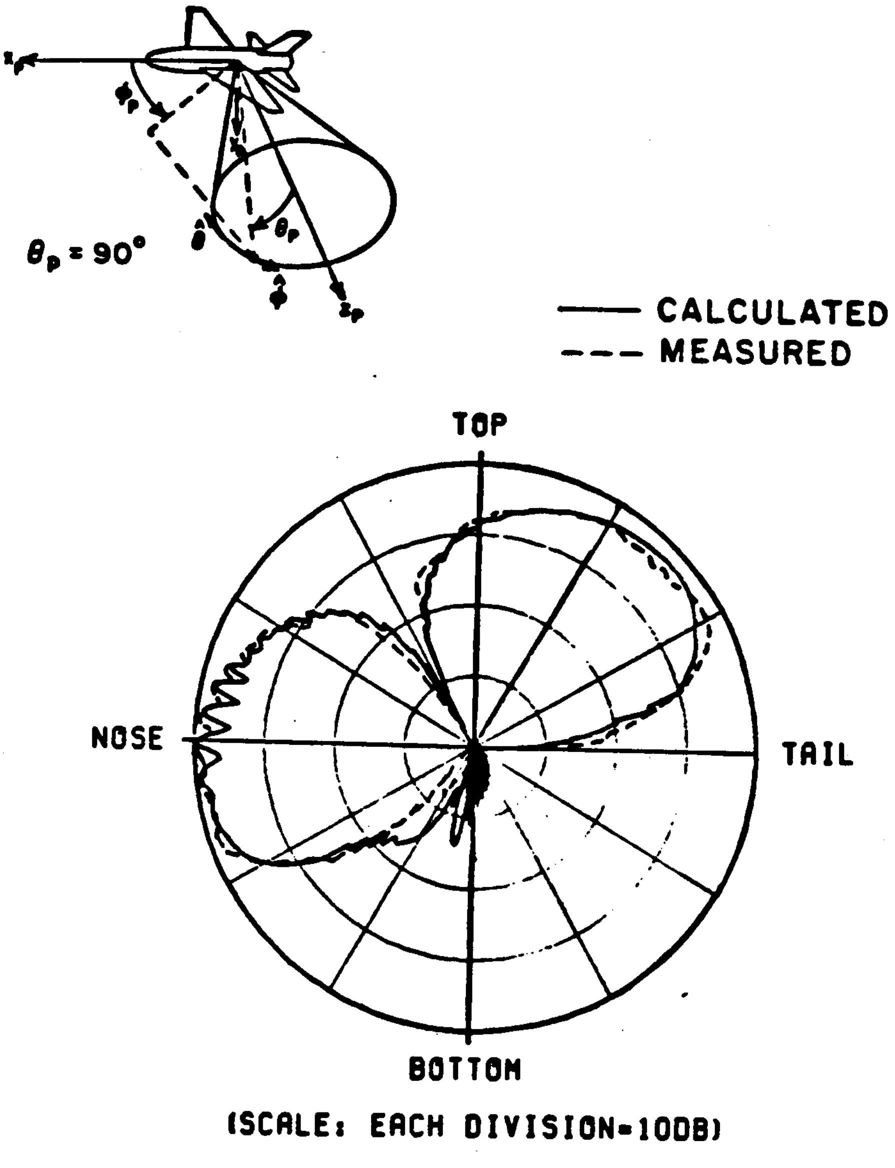

Figure 23. Elevation plane pattern of a $\lambda/4$ monopole mounted at Station 220 on top of a Boeing 737 aircraft.

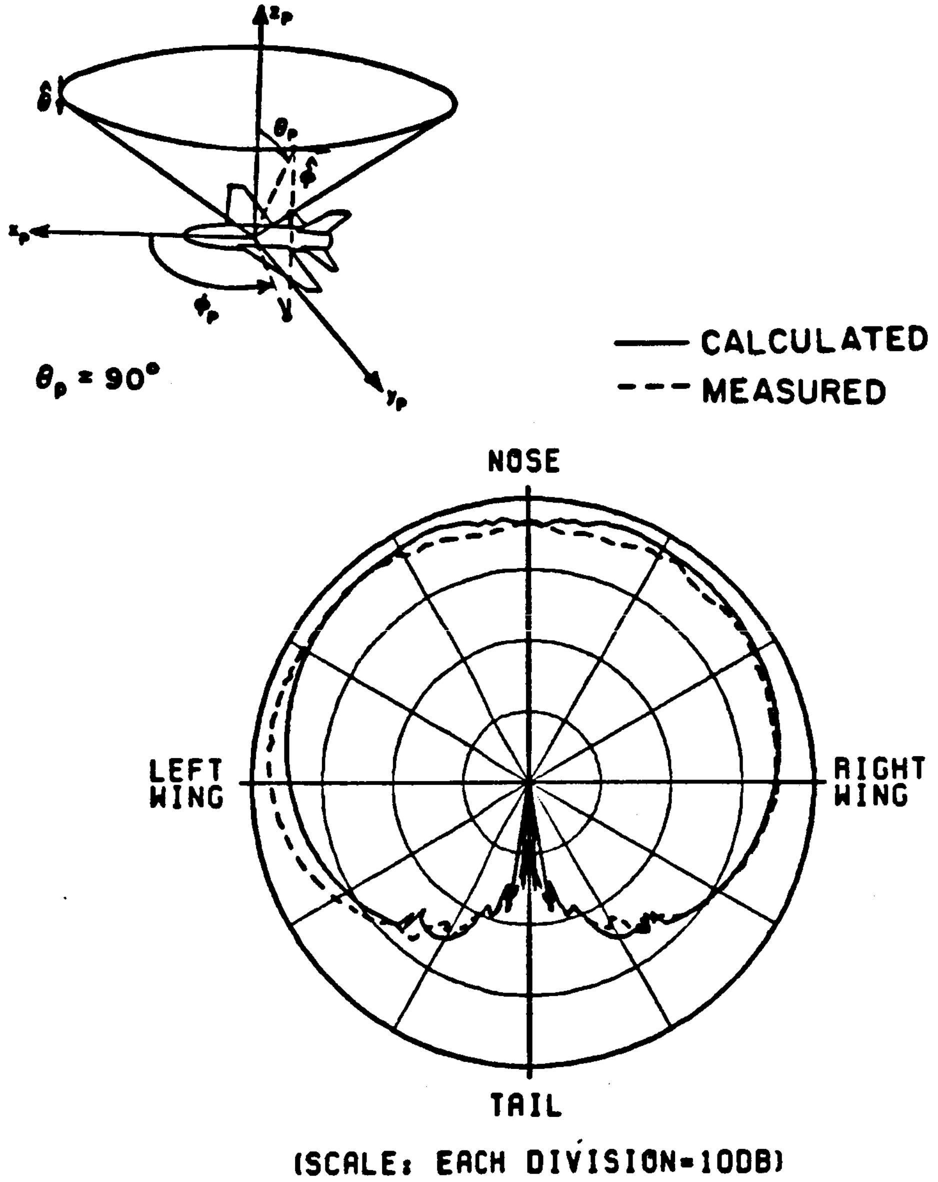

Figure 24. Azimuth plane pattern of a $\lambda/4$ monopole mounted at Station 220 on top of a Boeing 737 aircraft.

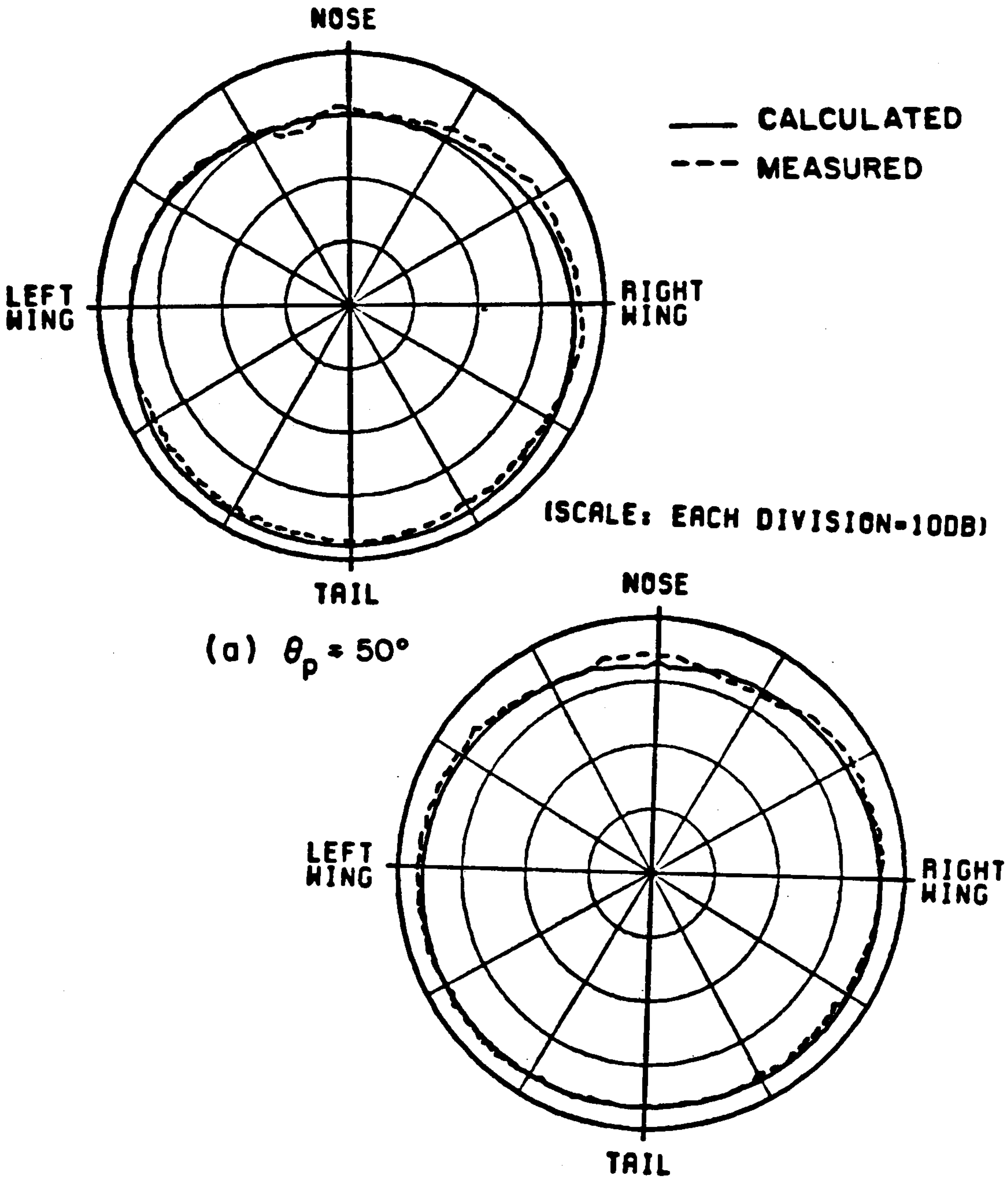

(a) $\theta_p = 50°$

(b) $\theta_p = 60°$

Figure 25. Azimuthal conical patterns of a $\lambda/4$ monopole mounted at Station 220 on top of a Boeing 737 aircraft.

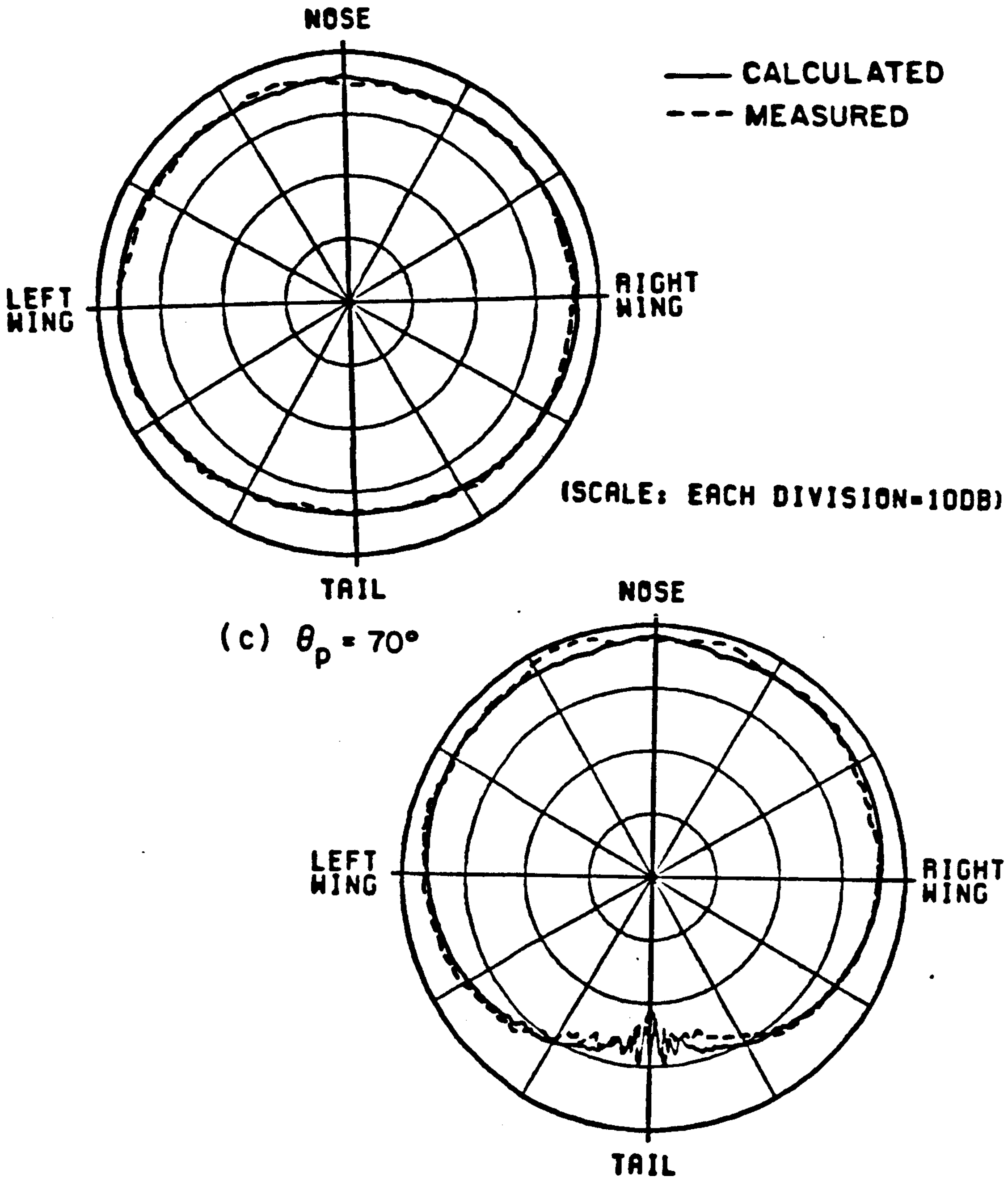

(c) $\theta_p = 70°$

(d) $\theta_p = 80°$

Figure 25. (Continued).

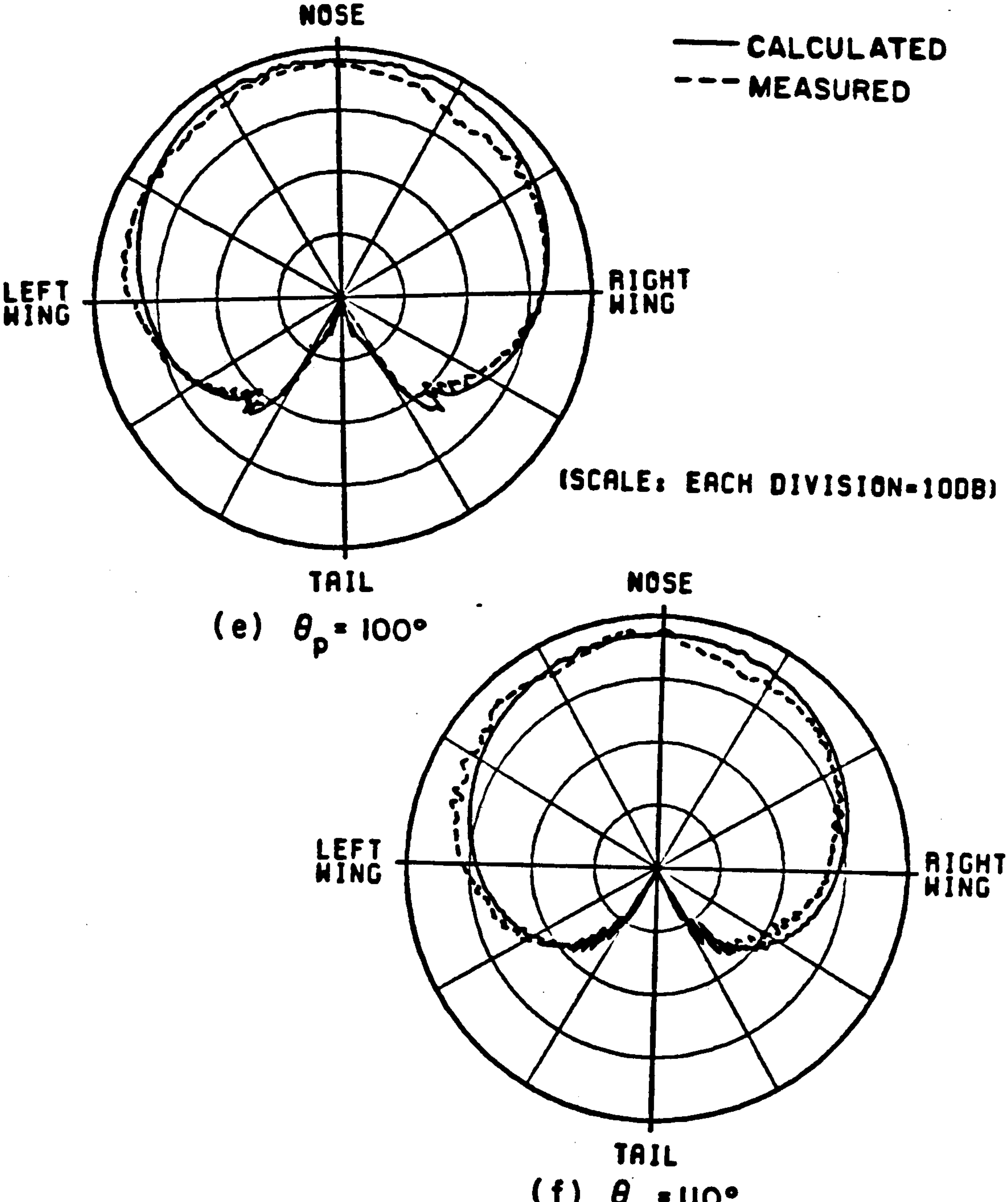

(e) $\theta_p = 100°$

(f) $\theta_p = 110°$

Figure 25. (Continued).

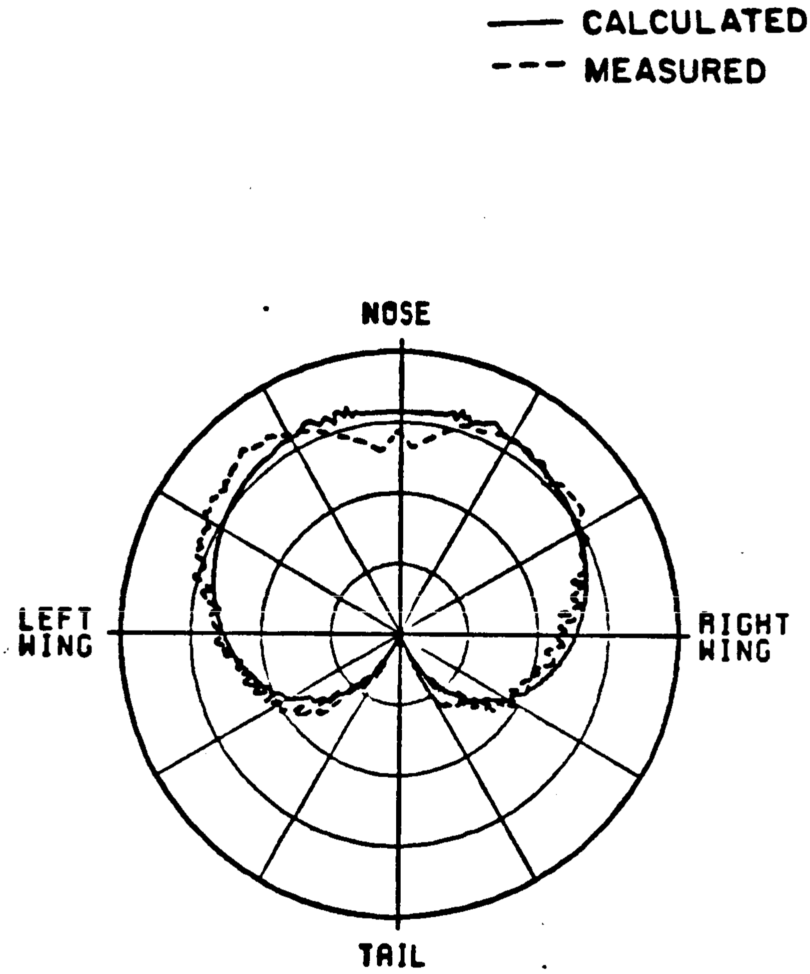

(SCALE: EACH DIVISION=10DB)

(g) $\theta_p = 120°$

Figure 25. (Continued).

The next two cases, a λ/4 monopole is mounted at stations 250 and 305 on top of the fuselage of the Boeing 737 aircraft. The input data is as follows:

```
UN: INCHES
3
FQ: 3.18 GHZ
1,3.18,1.
FG: BOEING 737
77.,74.,830.,308.56
F
0.,0.,0.
SG: MONOPOLE (STATION 250)
2.9,-248.
1
0.,0.
1.537,3.074,0.,.928525,3
1.,0.
PG: VERTICAL STABILIZER
4,T
77.,8.25,618.55
284.147,8.25,819.056
284.147,0.,683.696
77.,0.,483.19
PG: VERTICAL STABILIZER
4,T
77.,0.,483.19
284.147,0.,683.696
284.147,-8.25,819.056
77.,-8.25,618.55
PG: NOSE
4,T
5.5,-10.,-308.56
-.1,-10.,-321.6
-.1,0.,-321.6,
5.5,0.,-308.56
PG: NOSE
4,T
5.5,0.,-308.56
-.1,0.,-321.6
-.1,10.,-321.6
5.5,10.,-308.56
PP: POLAR PLOT IN DB
T
1,1.5,3
PD: ELEVATION PLANE
90.,90.,90.
0,360,1
F,6000.
EX:
```

The only difference in the input data for the case when the monopole is at station 305 is in the specification of the source geometry. The source geometry for station 305 is given by the following:

```
SG:  MONOPOLE 737 (STATION 305)
0.,-193.
1
0.,0.
1.537,3.074,0.,.928525,3
1.,0.
```

It is noted that the antenna at Station 250 is mounted 4" off the fuselage centerline. Both calculated and experimental results for Stations 250 and 305 are presented in Figures 26 and 27, respectively. The results reveal good agreement between the theoretical predictions and scale model measurements.

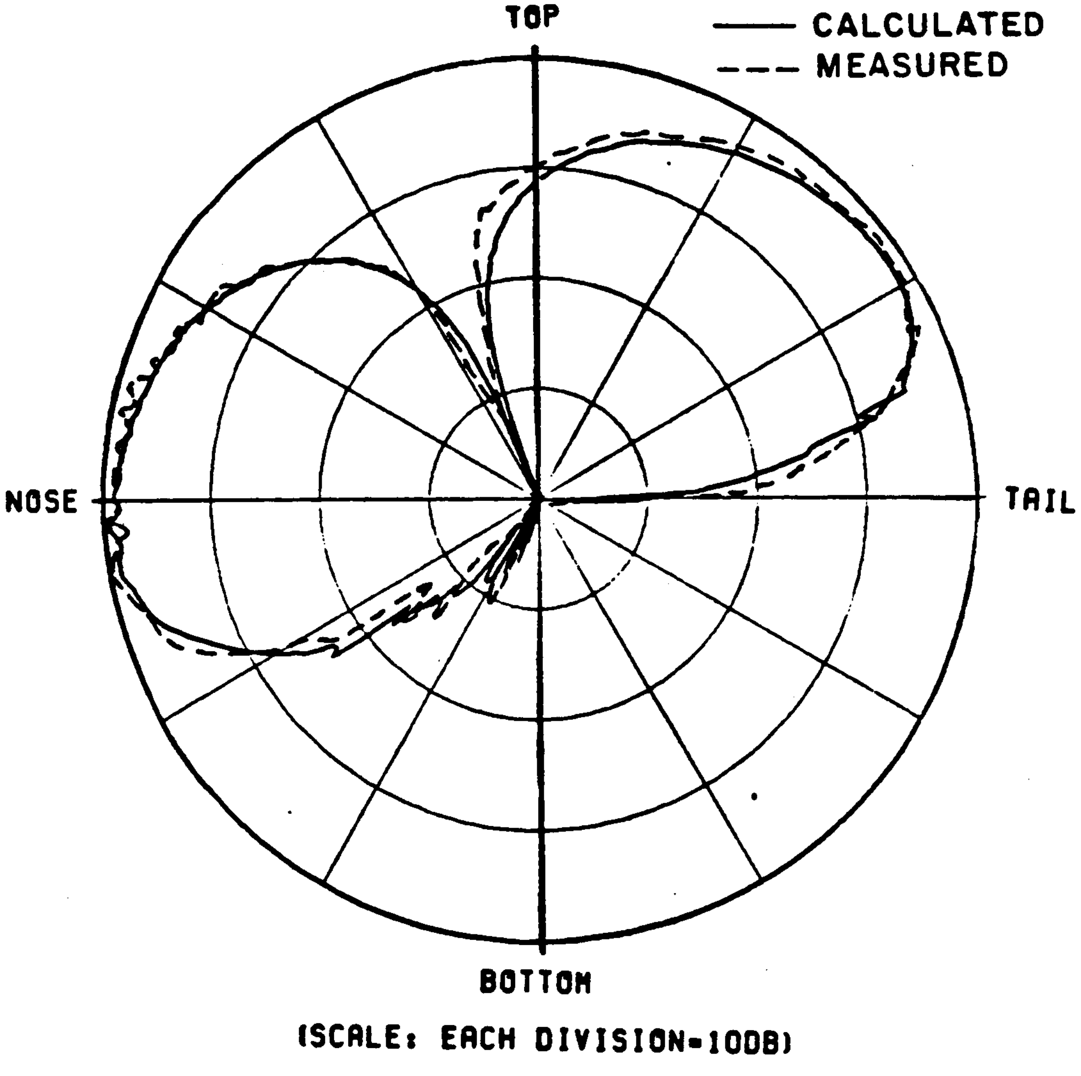

Figure 26. Elevation plane pattern of a λ/4 monopole mounted at Station 250 (off center) on top of a Boeing 737 aircraft.

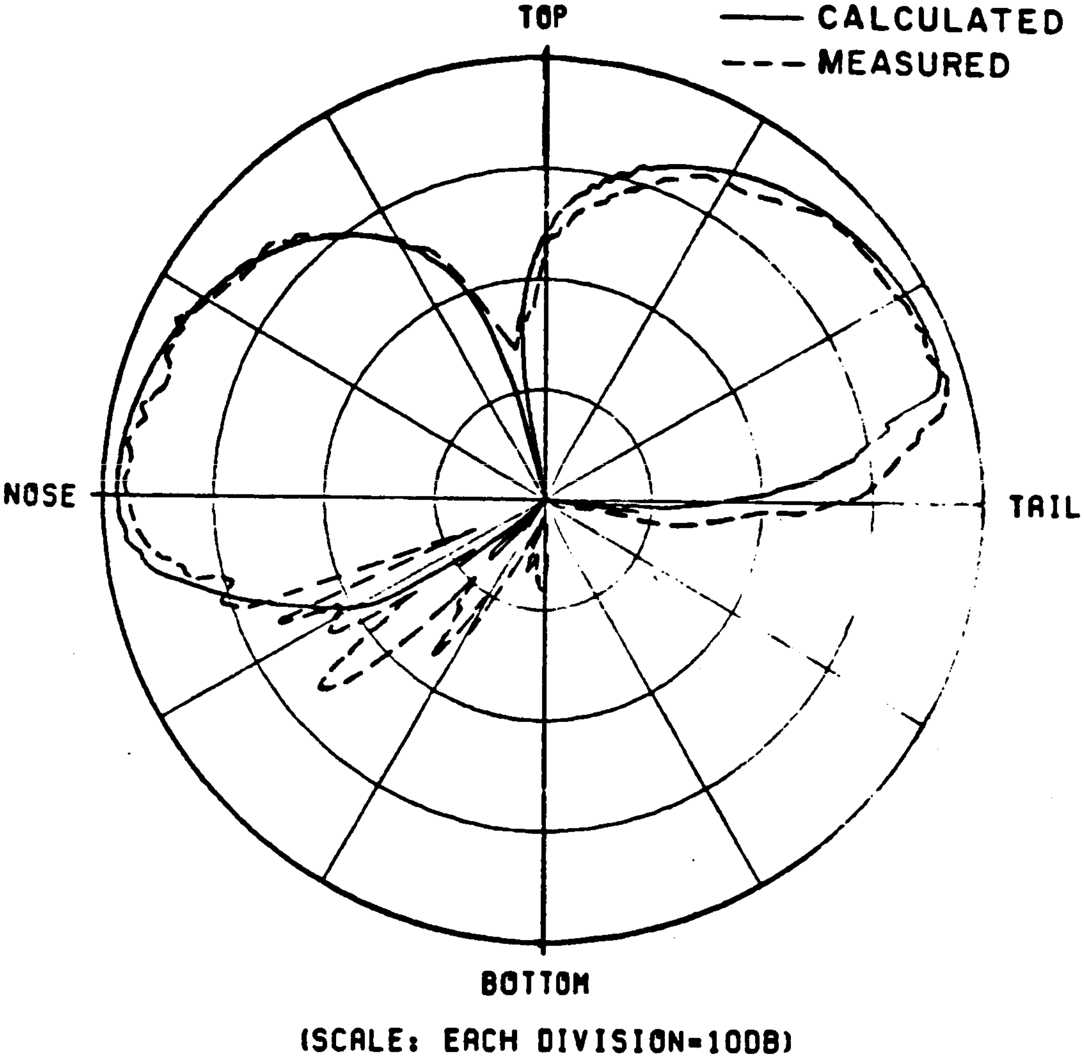

Figure 27. Elevation plane pattern of a λ/4 monopole mounted at Station 305 on top of a Boeing 737 aircraft.

The next antenna location considered on the Boeing 737 aircraft, is station 222 on the bottom of the fuselage just behind the nose. The computer simulated model for this case is shown in Figure 28. The input data is as follows:

```
UN: INCHES
3
FQ: 3.18 GHZ
1,3.18,1.
FG: BOEING 737 (STATION 222)
66.,55.,785.,232.52
F
0.,0.,0.
SG: MONOPOLE
0.,-144.6
1
0.,0.
1.537,3.074,0.,.928525,3
1.,0.
```

```
FC: FUSELAGE CHOPPED-OFF
F,T
0.,-186.97
PP: POLAR PLOT IN DB
T
1,2.46,3
PD: ELEVATION PLANE
90.,90.,90.
0,360,1
F,6000.
EX:
```

Axial and circumferential slot antennas are also analyzed for station 222. The source geometry input data for these two cases are given by the following:

```
SG: AXIAL SLOT
0.,-144.6
1
0.,0.
1.537,3.074,0.,.928525,1
1.,0.
```

```
SG: CIRCUMFERENTIAL SLOT
0.,-144.6
1
0.,0.
1.537,3.074,90.,.928525,1
1.,0.
```

The calculated elevation plane patterns for the monopole, axial slot and circumferential slot at station 222 are compared with measured patterns in Figures 29(a) through (c), and they are found to be in very good agreement.

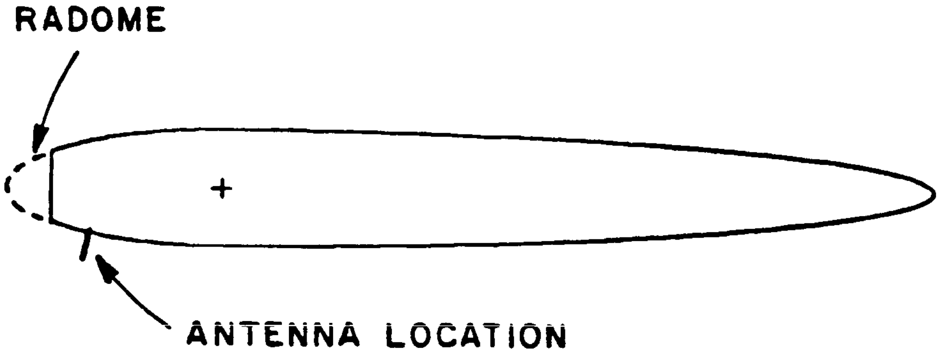
RADOME
+
ANTENNA LOCATION

Figure 28. Computer simulated model for a $\lambda/4$ monopole mounted at Station 222 on the bottom of the fuselage of a Boeing 737 aircraft.

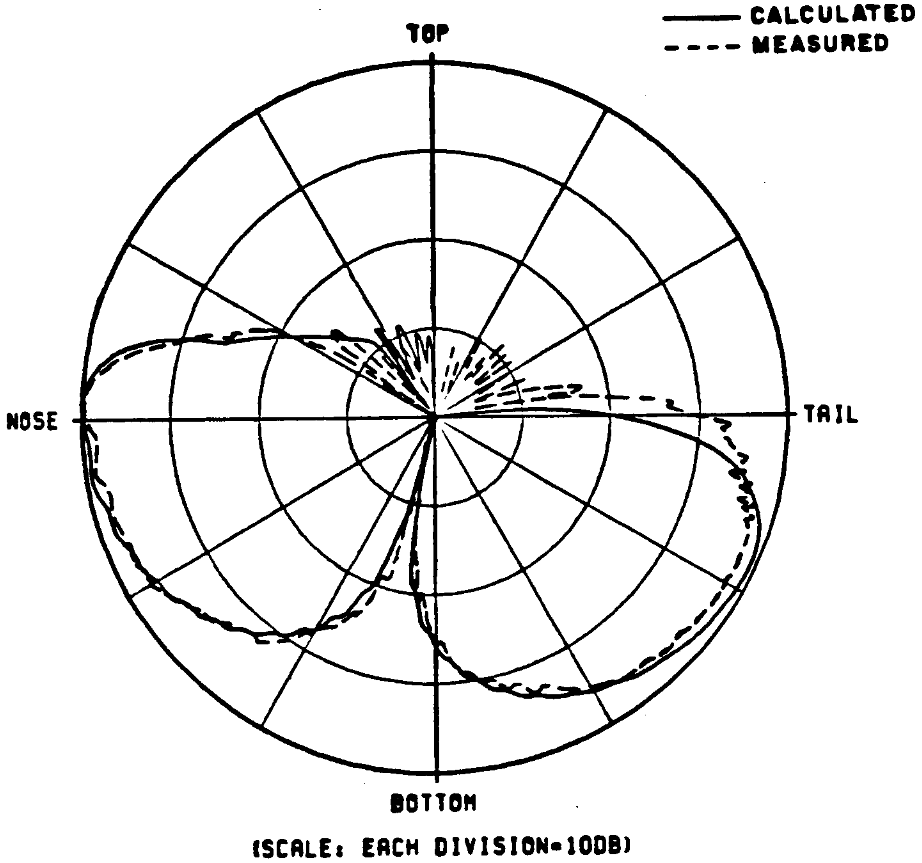

(a) a λ/4 monople case

Figure 29. Elevation plane patterns of an antenna mounted at Station 222 on the bottom of a Boeing 737 aircraft.

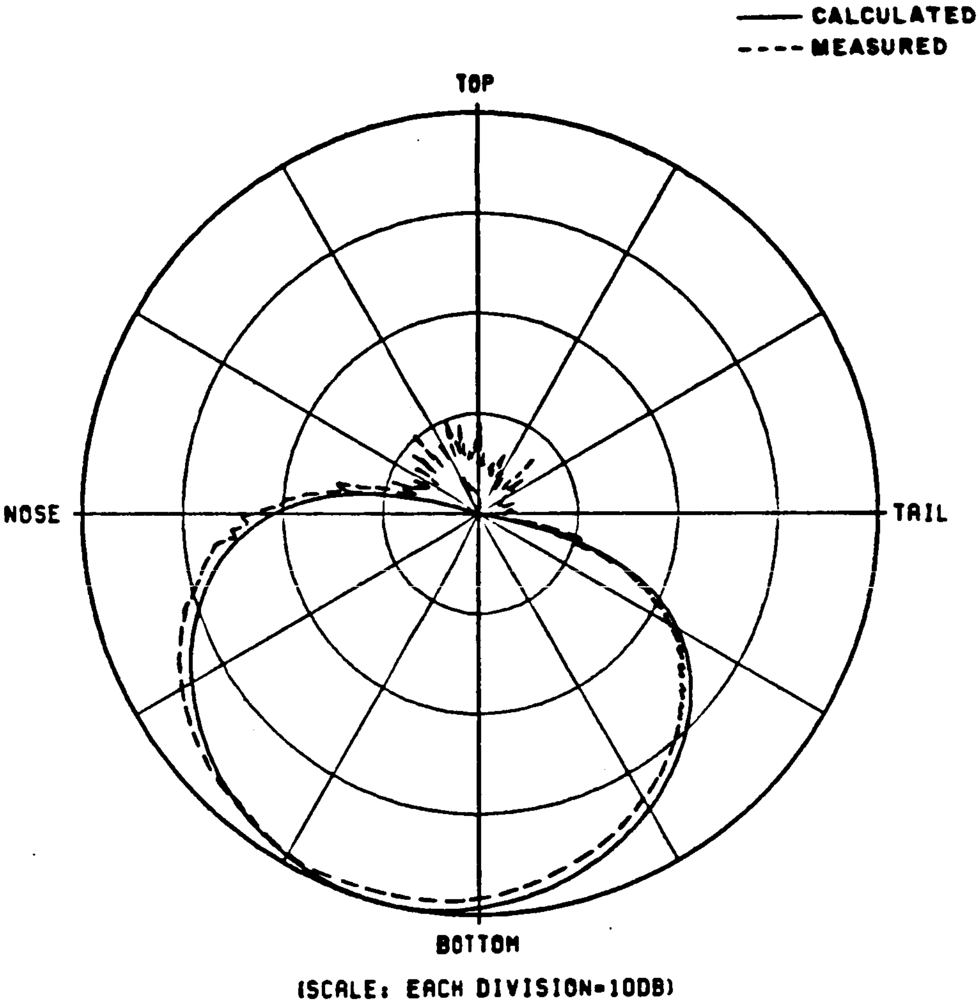

(b) an axial slot case

Figure 29. (Continued).

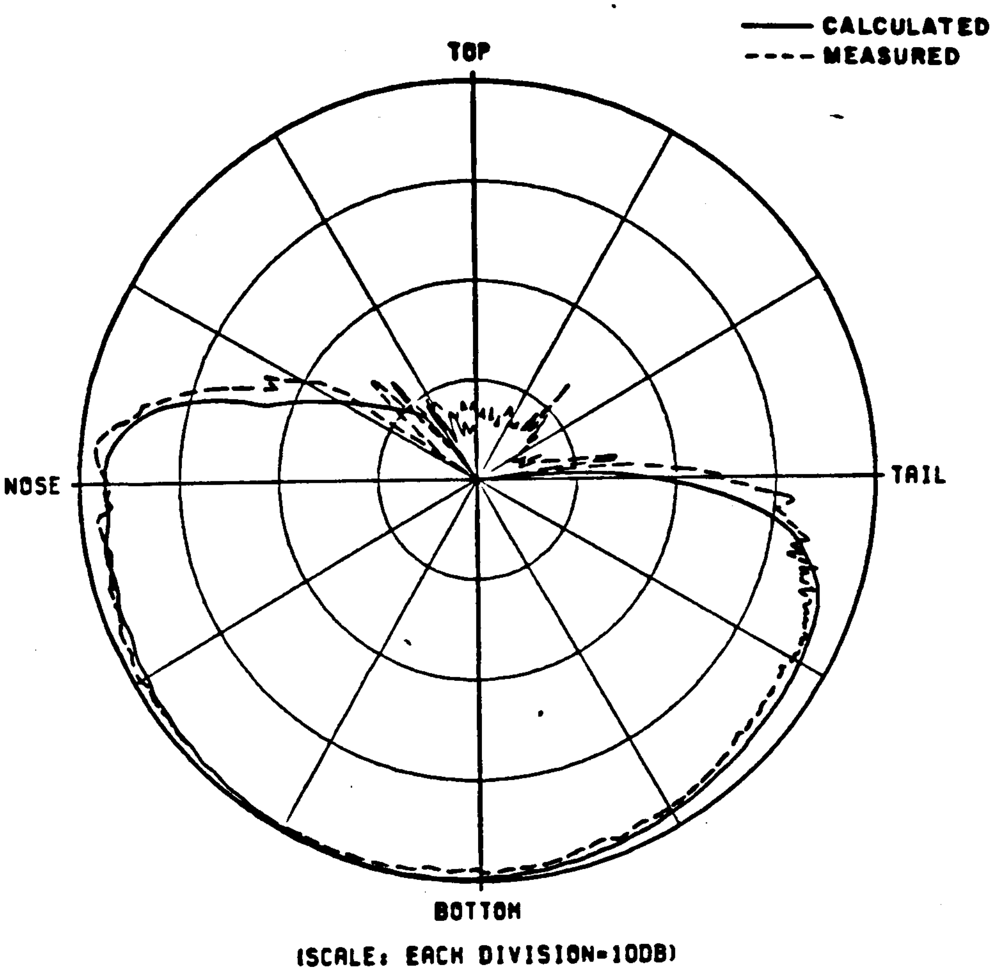

(c) a circumferential slot case

Figure 29. (Continued).

Finally, a λ/4 monopole is located at station 950 on the bottom of the fuselage at the rear of the Boeing 737 aircraft. The computer simulated model for this case is shown in Figure 30. The input data is as follows:

```
UN: INCHES
3
FQ: 3.18 GHZ
1,3.18,1.
FG: BOEING 737 (STATION 950)
77.,74.,580.,200.
F
0.,0.,0.
SG: MONOPOLE
0.,300.
1
0.,0.
1.537,3.074,0.,.928525,3
1.,0.
PG: RIGHT WING
4,T
8.1,75.,-118.
33.9,536.93,140.
40.,536.93,201.
30.6,75.,107.
PG: LEFT WING
4,T
30.6,-75.,107.
40.,-536.93,201.
33.9,-536.93,140.
8.1,-75.,-118.
PG: HORIZONTAL STABILIZER
4,T
-18.1,66.,443.
-6.3,207.,561.
-0.4,207.,620.
-5.,66.,574.
PG: HORIZONTAL STABILIZER
4,T
-5.,-66.,574.
-0.4,-207.,620.
-6.3,-207.,561.
-18.1,-66.,443.
PP: POLAR PLOT IN DB
T
1,2.38,3
PD: ELEVATION PLANE
90.,90.,90.
0,360,1
F,6000.
EX:
```

The elevation plane radiation pattern is computed and found to be in very good agreement with the measured pattern as shown in Figure 31.

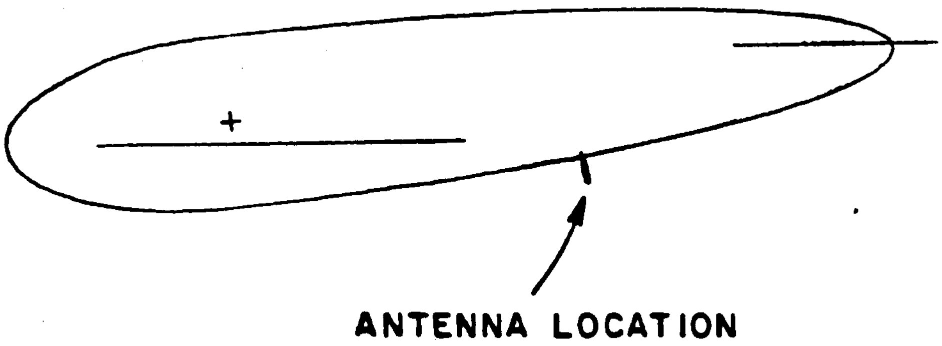
+
ANTENNA LOCATION

Figure 30. Computer simulated model for a $\lambda/4$ monopole mounted at Station 950 on the bottom of the fuselage of a Boeing 737 aircraft.

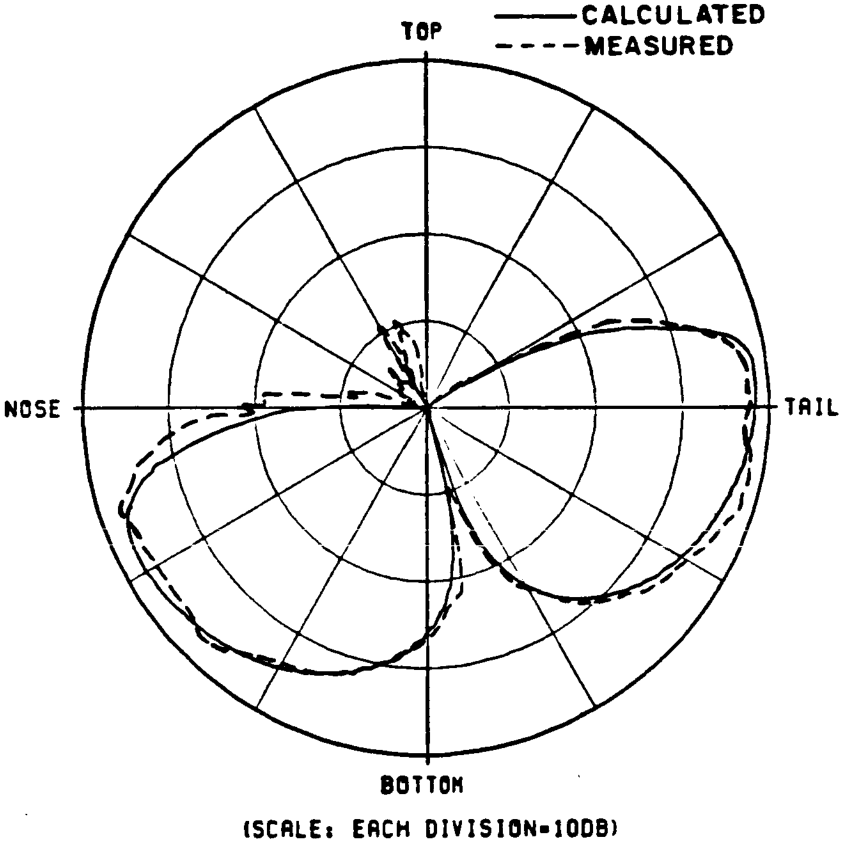

Figure 31. Elevation plane pattern of a λ/4 monopole mounted at Station 950 on the bottom of a Boeing 737 aircraft.

Example 4: Simulation of the KC-135 Aircraft

In this example a monopole, axial slot and circumferential slot antennas mounted both over and forward of the wings are studied on a KC-135 aircraft. The line drawings of the KC-135 are shown in Figure 32. The computer simulated models based on the input data are shown in Figures 33 and 34.

The input data for the monopole mounted over the wings is as follows:

```
UN: INCHES
3
FQ: 34.92 GHZ
1,34.92,1.
FG: KC-135 FUSELAGE GEOMETRY
3.3,3.,72.,8.
F
0.,0.,18.81
SG: MONOPOLE OVER WING
0.,18.81
1
0.,0.
.140,.200,90.,.0845,3
1.,0.
PG: RIGHT WING
4,T
-.5,3.,12.31
-.5,28.5,36.41
-.5,28.5,40.41
-.5,3.,24.61
PG: LEFT WING
4,T
-.5,-3.,24.61
-.5,-28.5,40.41
-.5,-28.5,36.41
-.5,-3.,12.31
PG: VERTICAL STABILIZER
4,T
2.946,.5,55.672
14.076,.5,64.205
14.076,0.,58.025
2.946,0.,49.492
PG: VERTICAL STABILIZER
4,T
2.946,0.,49.492
14.076,0.,58.025
14.076,-.5,64.205
2.946,-.5,55.672
PG: NOSE
4,T
1.39,-1.36,-7.35
1.275,-1.36,-9.
1.37,0.,-9.
1.485,0.,-7.35
PG: NOSE
4,T
1.485,0.,-7.35
1.37,0.,-9.
1.275,1.36,-9.
1.39,1.36,-7.35
PD: ELEVATION PLANE
90.,90.,90.
0,360,1
T,1000.
PP: PEN PLOT
T
1,1.71,3
EX:
PD: ROLL PLANE
0.,0.,90.
0,360,1
T,1000.
EX:
PD: AZIMUTH PLANE
90.,0.,90.2
0,360,1
T,1000.
EX:
```

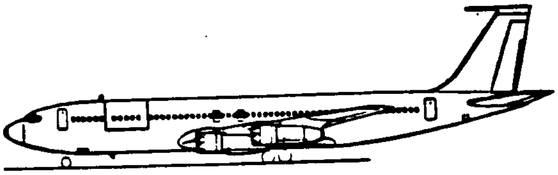

(a) SIDE VIEW

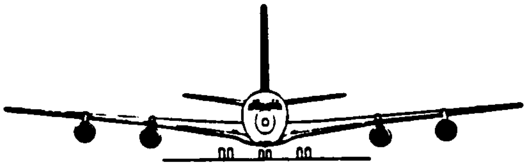

(b) FRONT VIEW

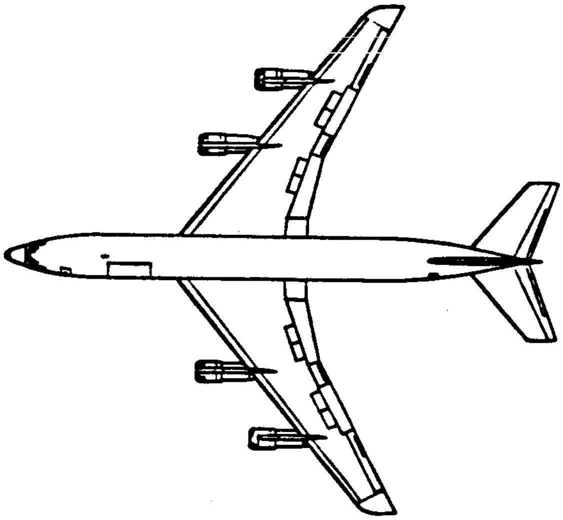

(c) TOP VIEW

Figure 32. KC-135 aircraft.

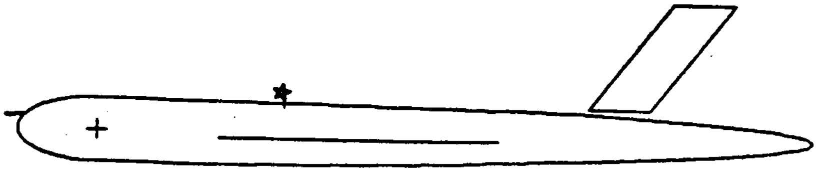

(a) SIDE VIEW

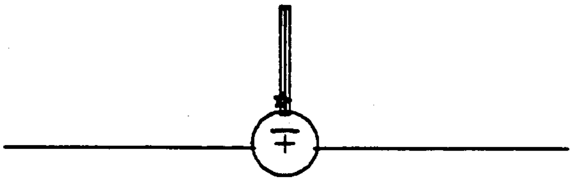

(b) FRONT VIEW

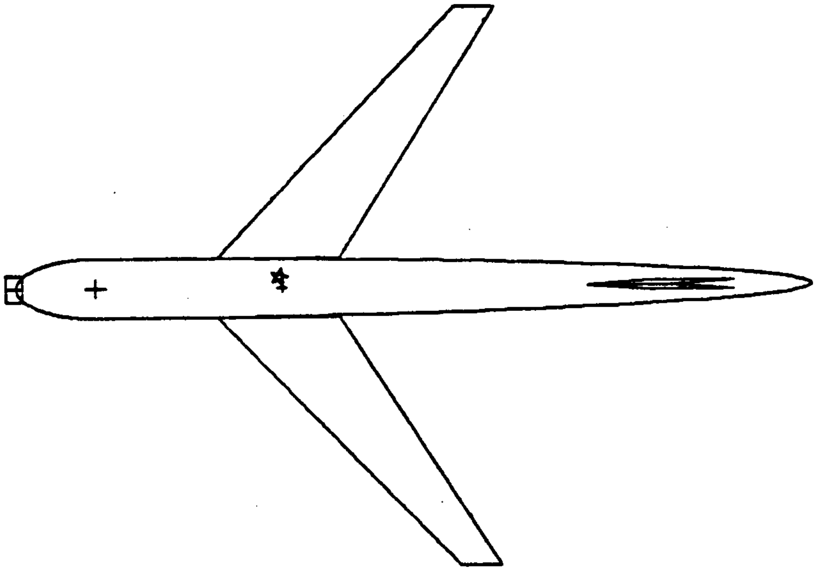

(c) TOP VIEW

Figure 33. Computer simulated model of a KC-135 aircraft. The antenna is located over the wings.

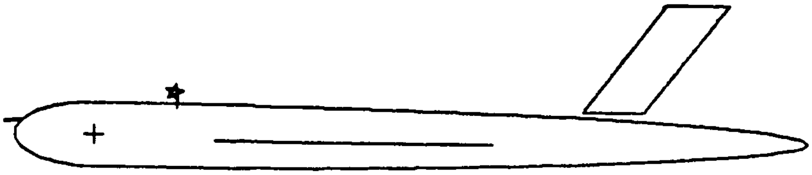

(a) SIDE VIEW

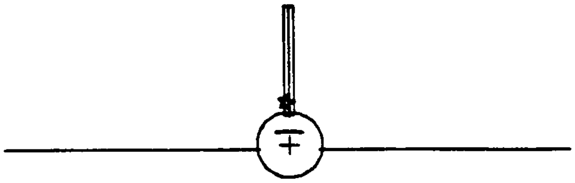

(b) FRONT VIEW

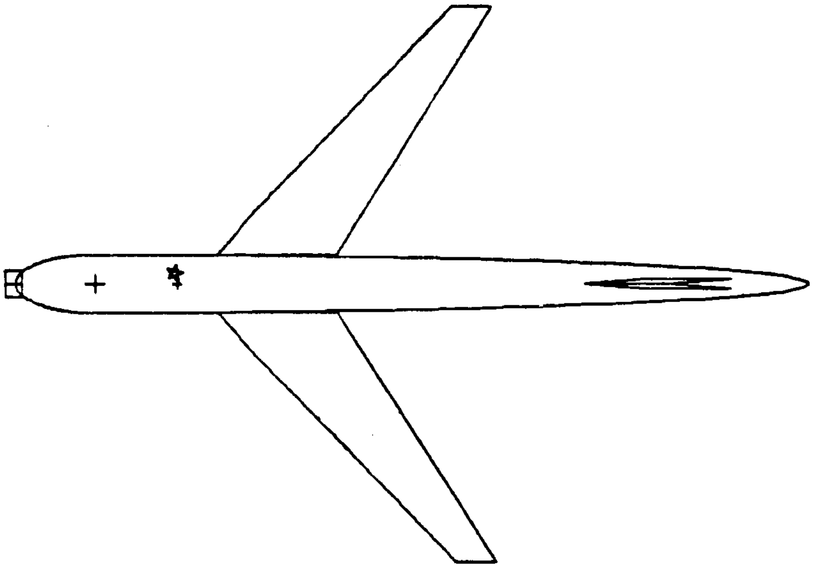

(c) TOP VIEW

Figure 34. Computer simulated model of a KC-135 aircraft. The antenna is located forward of the wings.

The radiation patterns of different antenna configurations on the KC-135 may be obtained simply by changing the source geometry command. The other source locations are specified as follows:

```
SG: MONOPOLE FORWARD OF WINGS
0.,8.34
1
0.,0.
.140..280.90.,.0845,3
1.,0.
```

```
SG: AXIAL SLOT FORWARD OF WINGS
0.,8.34
1
0.,0.
.140..280.0.,.0845,1
1.,0.
```

```
SG: CIRCUMFERENTIAL SLOT FORWARD OF WINGS
0.,8.34
1
0.,0.
.140,.280.90.,.0845,1
1.,0.
```

```
SG: AXIAL SLOT OVER WINGS
0.,18.81
1
0.,0.
.140,.280,0.,.0845,1
1.,0.
```

```
SG: CIRCUMFERENTIAL SLOT OVER WINGS
0.,18.81
1
0.,0.
.140,.280,90.,.0845,1
1.,0.
```

The elevation, roll and azimuth plane patterns for a short monopole, a circumferential KA-band waveguide and an axial KA-band waveguide mounted forward and over the wings are shown in Figures 35 to 43.

The computed results are found to be in very good agreement with the measurements in the elevation and roll planes. The precision pattern measurements (elevation and roll plane patterns) using the 1/25 scale model were taken at NASA (Hampton, Virginia). Measured data was not available for the azimuth plane.

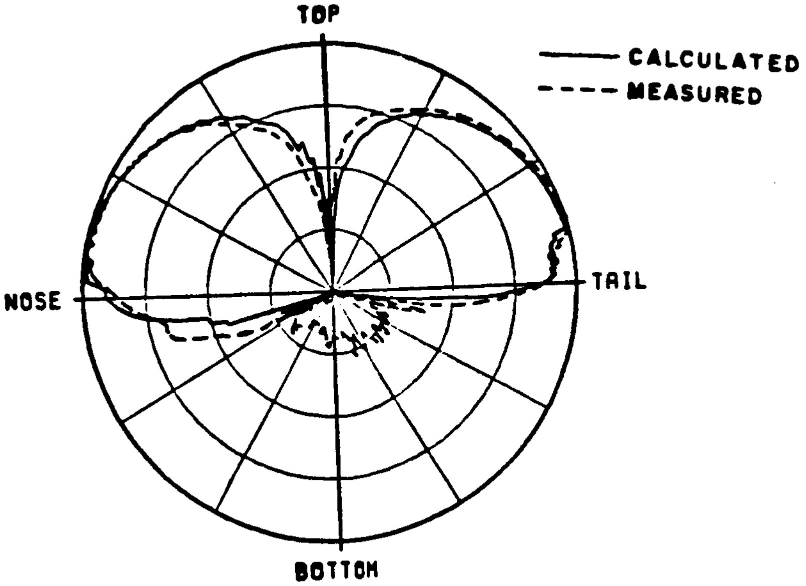

(a) Antenna mounted forward of wings

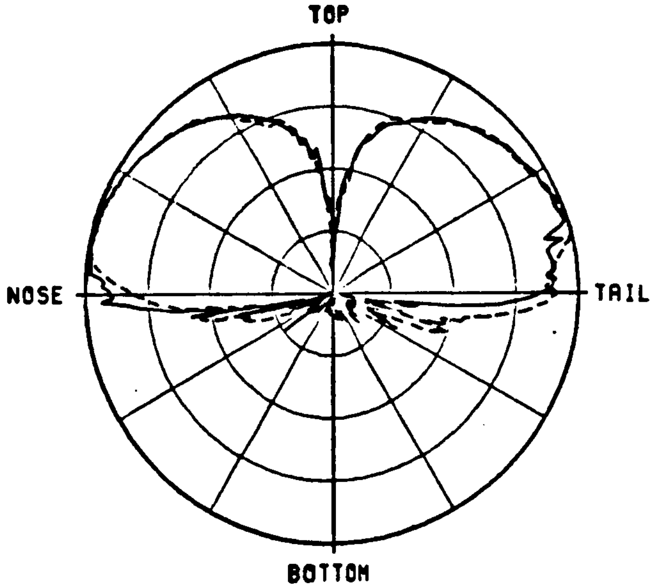

(SCALE: EACH DIVISION=10DB)

(b) Antenna mounted over wings

Figure 35: Elevation plane pattern for a $\lambda/4$ monopole mounted on a KC-135 aircraft.

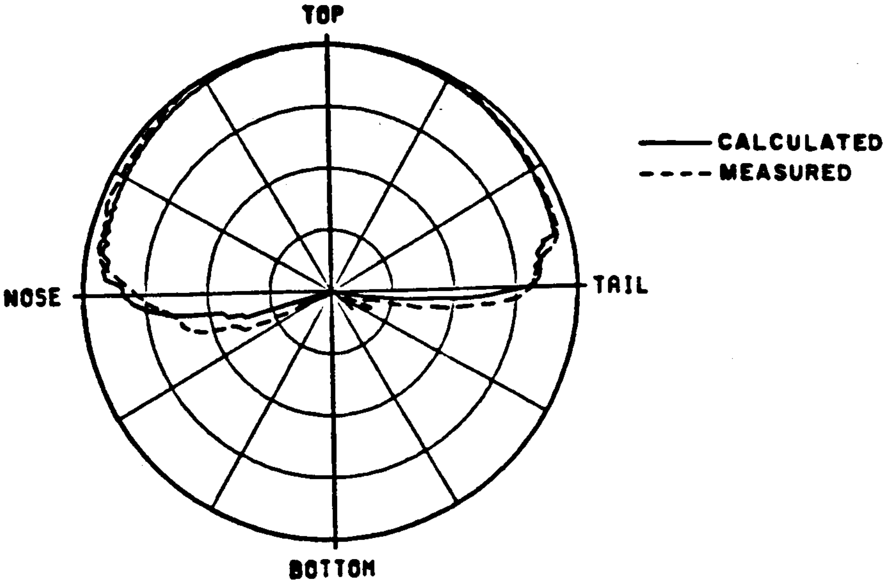

(a) Antenna mounted forward of wings

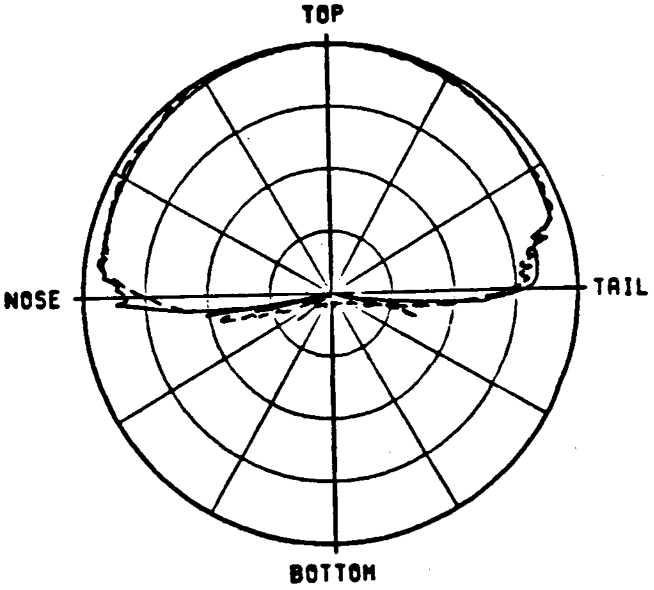

(SCALE: EACH DIVISION=10DB)

(b) Antenna mounted over wings

Figure 36. Elevation plane pattern for a circumferential KA-band waveguide mounted on a KC-135 aircraft.

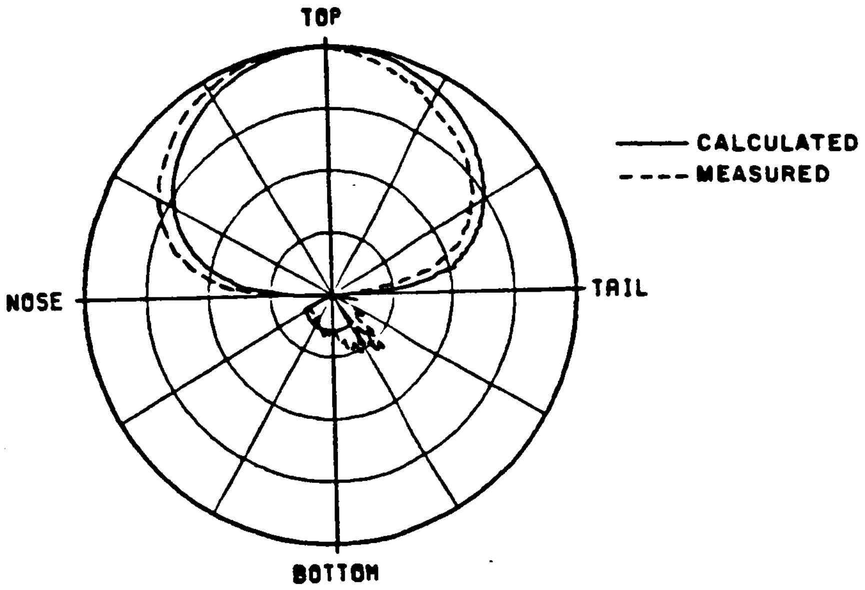

(a) Antenna mounted forward of wings

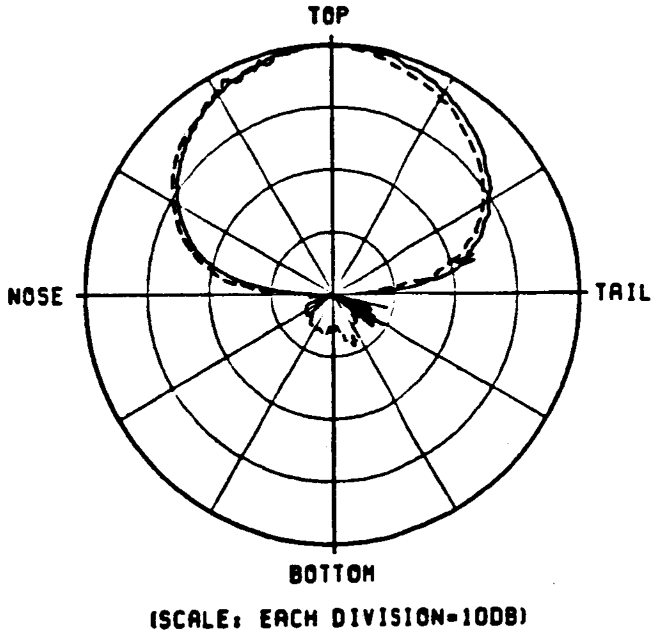

(b) Antenna mounted over wings

Figure 37. Elevation plane pattern for an axial KA-band waveguide mounted on a KC-135 aircraft.

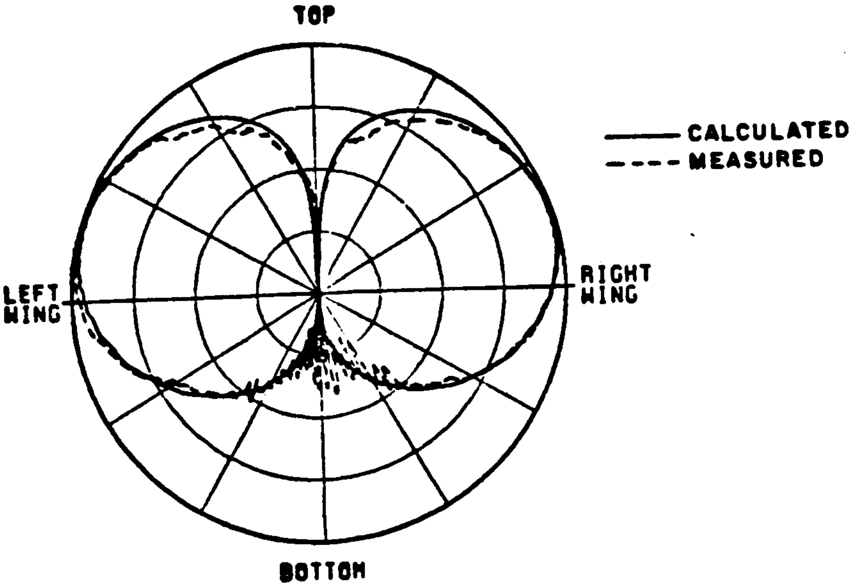

(a) Antenna mounted forward of wings

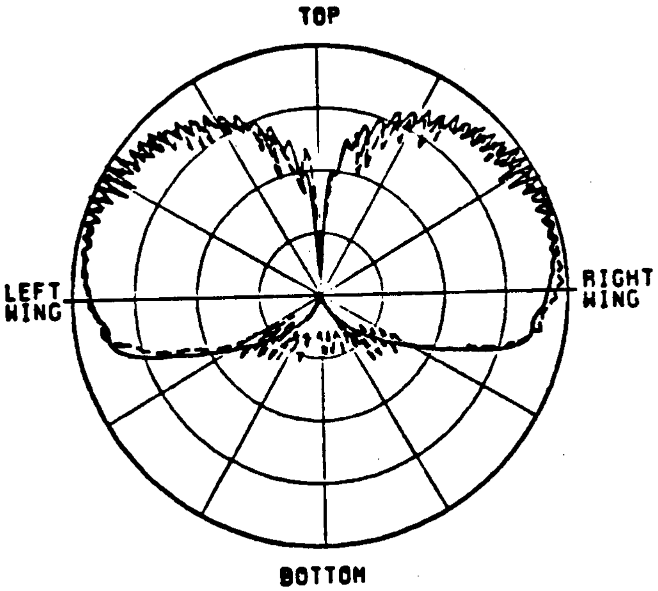

(SCALE: EACH DIVISION=10DB)

(b) Antenna mounted over wings

Figure 38. Roll plane pattern for a $\lambda/4$ monopole mounted on a KC-135 aircraft.

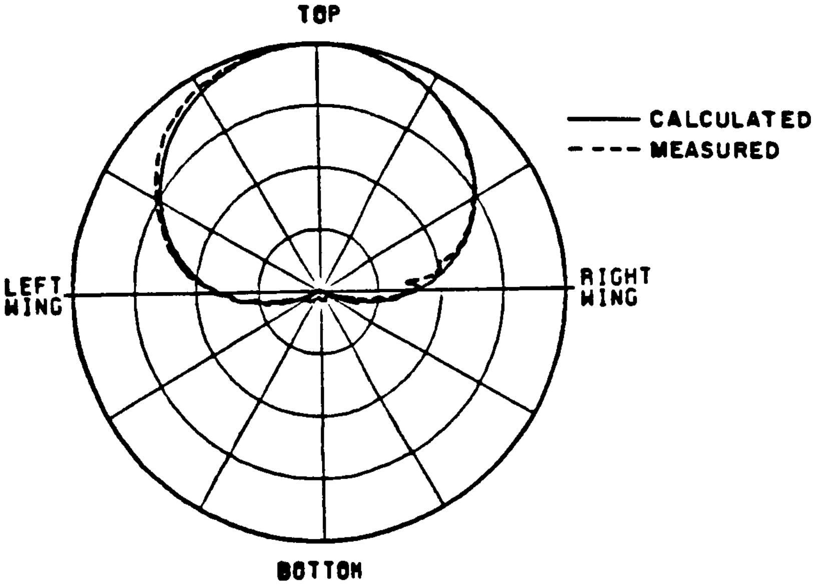

(a) Antenna mounted forward of wings

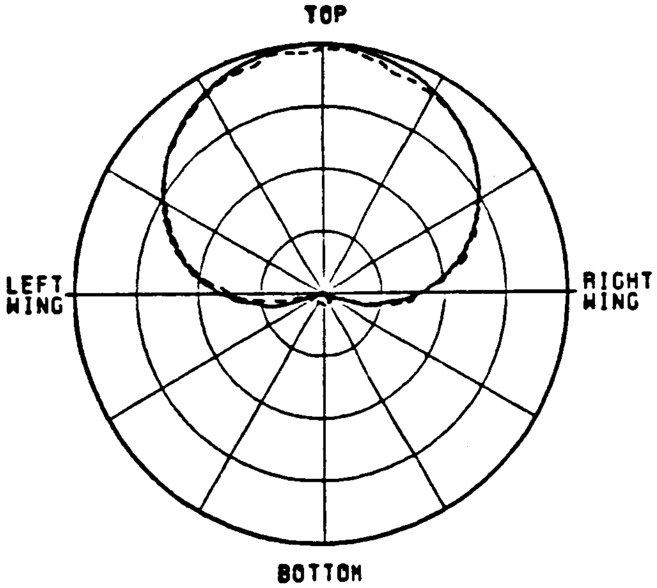

(SCALE: EACH DIVISION=10DB)

(b) Antenna mounted over wings

Figure 39. Roll plane pattern for a KA-band circumferential waveguide mounted on a KC-135 aircraft.

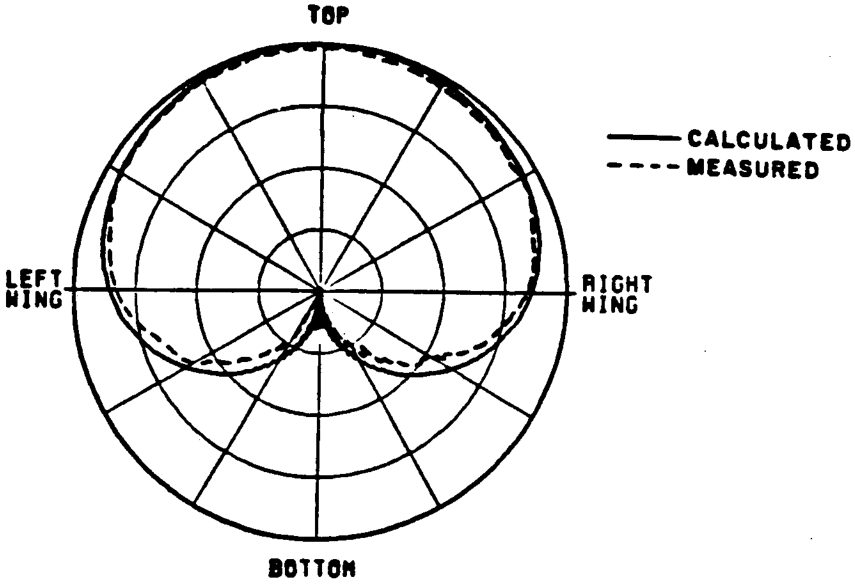

(a) Antenna mounted forward of wings

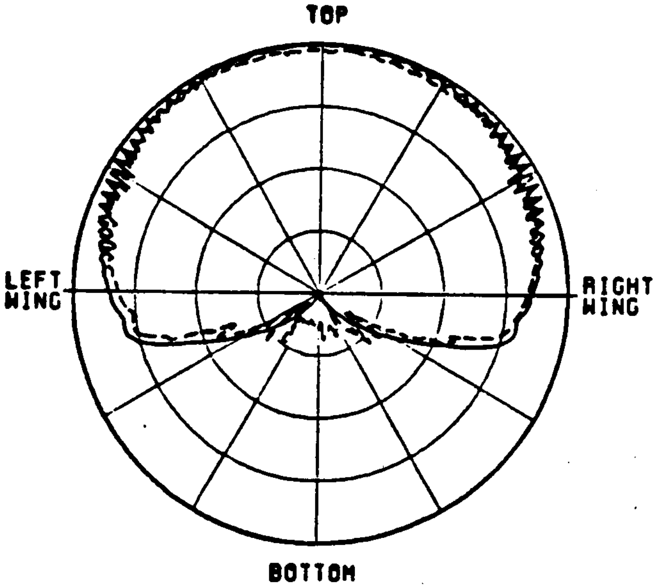

(SCALE: EACH DIVISION=10DB)

(b) Antenna mounted over wings

Figure 40. Roll plane pattern for a KA-band axial waveguide mounted on a KC-135 aircraft.

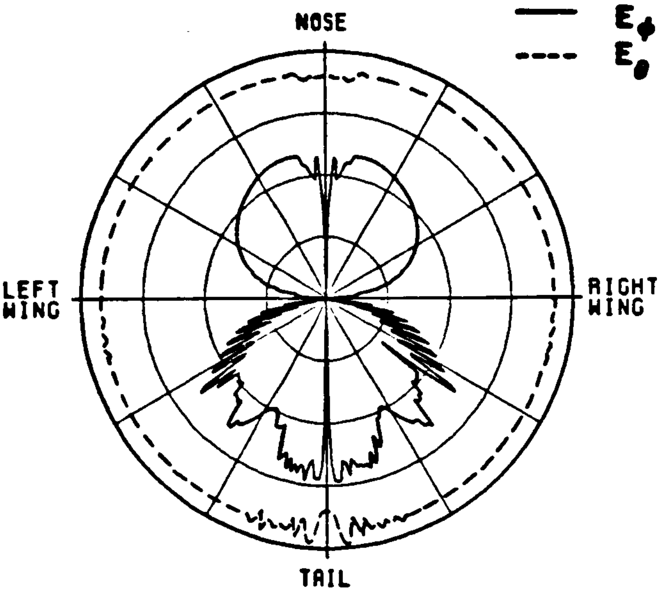

(a) Antenna mounted forward of wings

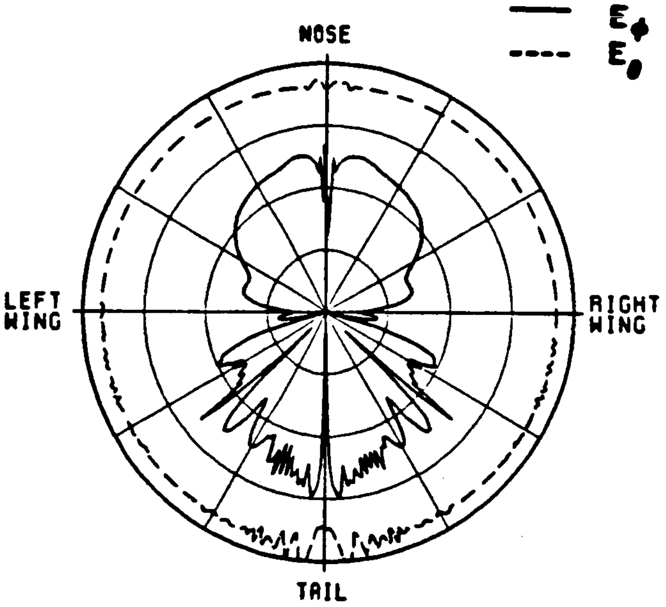

(SCALE: EACH DIVISION=10DB)

(b) Antenna mounted over wings

Figure 41. Azimuth plane pattern for a λ/4 monopole mounted on a KC-135 aircraft.

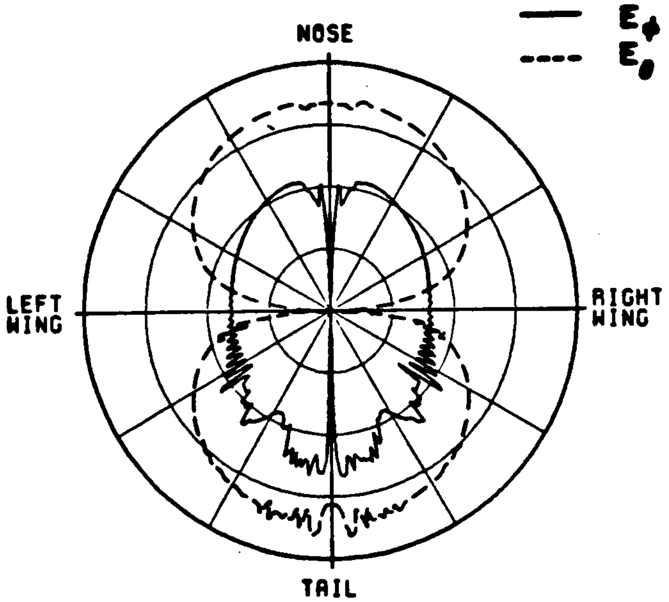

(a) Antenna mounted forward of wings

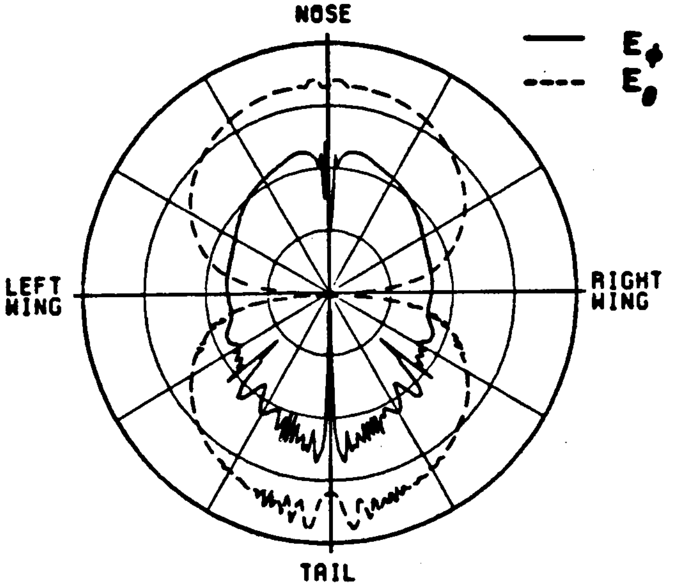

(SCALE: EACH DIVISION=10DB)

(b) Antenna mounted over wings

Figure 42. Azimuth plane pattern for a KA-band circumferential waveguide mounted on a KC-135 aircraft.

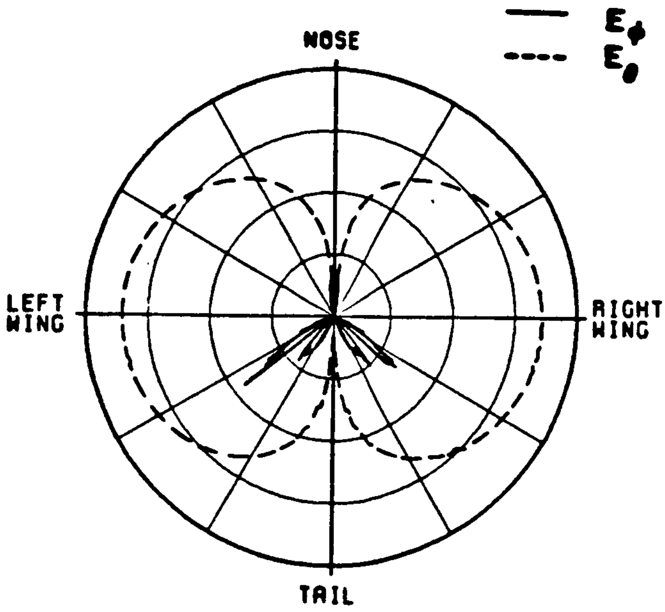

(a) Antenna mounted forward of wings

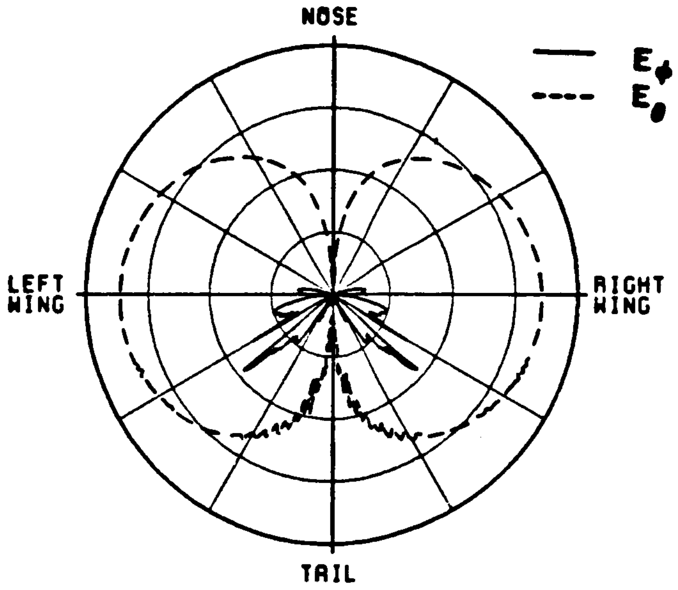

(SCALE: EACH DIVISION=10DB)

(b) Antenna mounted over wings

Figure 43. Azimuth plane pattern for a KA-band axial waveguide mounted on a KC-135 aircraft.

Example 5: Simulation of a Lindberg Antenna Mounted on a KC-135

A Lindberg crossed slot antenna mounted on the fuselage of a KC-135 is studied in this example. The line drawing of the KC-135 aircraft was shown in Figure 32. The computer simulated model based on the input data is shown in Figure 44. The input data is as follows:

```
UN: INCHES
3
FQ: 6.25 GHZ
1,6.25,1.
FG: KC-135 FUSELAGE GEOMETRY
3.3,3.,72.,8.
F
0.,0.,18.81
SG: LINDBERG CROSSED-SLOT
0.,2.25
2
0.,0.
.07375,1.475.0.,.0845,1
1.,0.
0.,0.
.07375,1.475,90.,.0845,1
1.,90:
PG: RIGHT WING
4,T
-.5,3.,12.31
-.5,28.5,36.41
-.5,28.5,40.41
-.5,3.,24.61
PG: LEFT WING
4,T
-.5,-3.,24.61
-.5,-28.5,40.41
-.5,-28.5,36.41
-.5,-3.,12.31
PG: VERTICAL STABILIZER
4,T
2.946,.5,55.672
14.076,.5,64.205
14.076.0.,58.025
2.946,0.,49.492
```

```
PG: VERTICAL STABILIZER
4,T
2.946,0.,49.492
14.076,0.,58.025
14.076,-.5,64.205
2.946,-.5,55.672
PG: NOSE
4,T
1.39,-1.36,-7.35
1.275,-1.36,-9.
1.37,0.,-9.
1.485,0.,-7.35
PG: NOSE
4,T
1.485,0.,-7.35
1.37,0.,-9.
1.275,1.36,-9.
1.39,1.36,-7.35
PD: ELEVATION PLANE
90.,90.,90.
0,360,1
T,1000.
PP: PEN PLOT
T
1,1.625,3
EX:
PD: ROLL PLANE
0.,0.,90.2
0,360,1
T,1000.
EX:
PD: AZIMUTH PLANE
90.,0.,90.
0,360,1
T,1000.
EX:
PD: 45°CONICAL CUT
90.,0.,45.
0,360,1
T,1000.
EX:
```

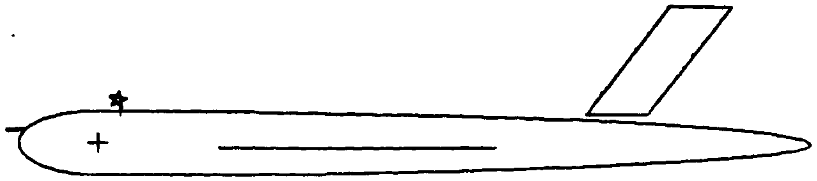

(a) SIDE VIEW

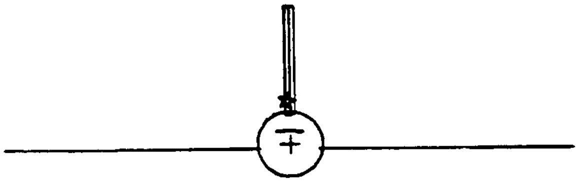

(b) FRONT VIEW

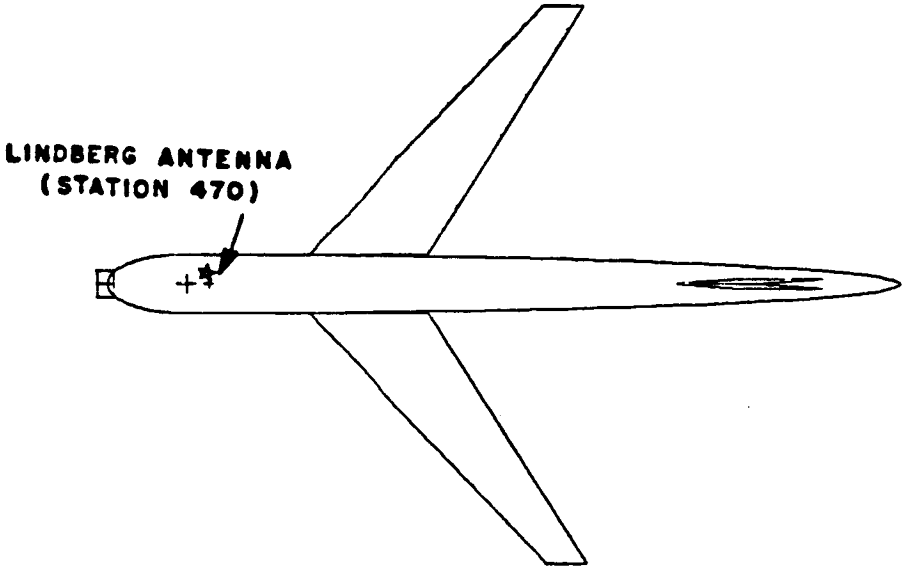
LINDBERG ANTENNA
(STATION 470)

(c) TOP VIEW

Figure 44. Computer simulated model for Lindberg antenna mounted on a KC-135.

Various calculated patterns along with the measured results taken from reference [17] are presented in Figures 45 to 48. Again, good agreement is obtained. The gain level in each case is adjusted to compare with measurements. The E_θ pattern corresponds to the vertical component, E_ϕ to the horizontal component and E_{cp} to the circularly polarized field.

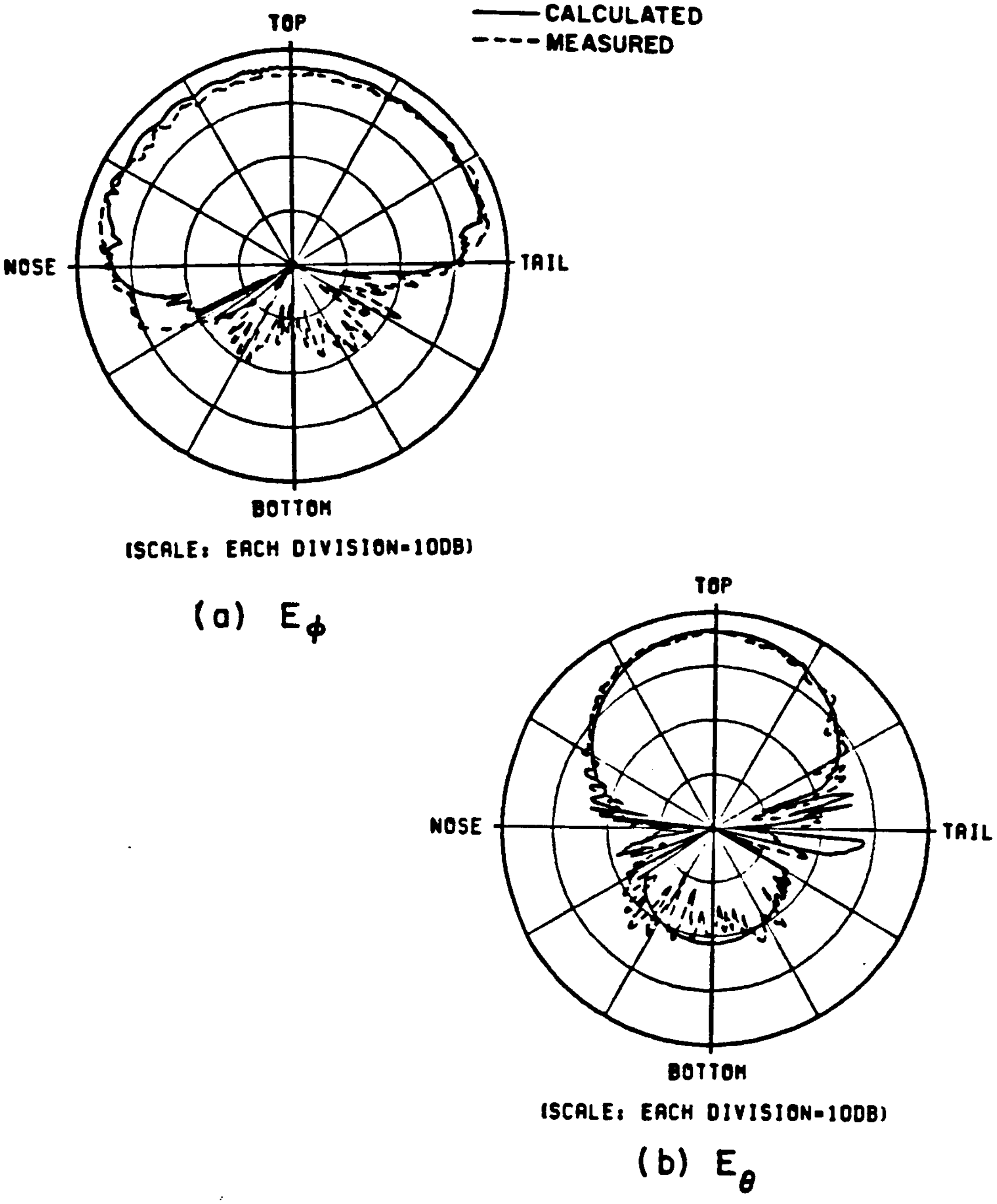

(a) E_ϕ

(b) E_θ

Figure 45. Elevation plane pattern for Lindberg antenna mounted on a KC-135 aircraft.

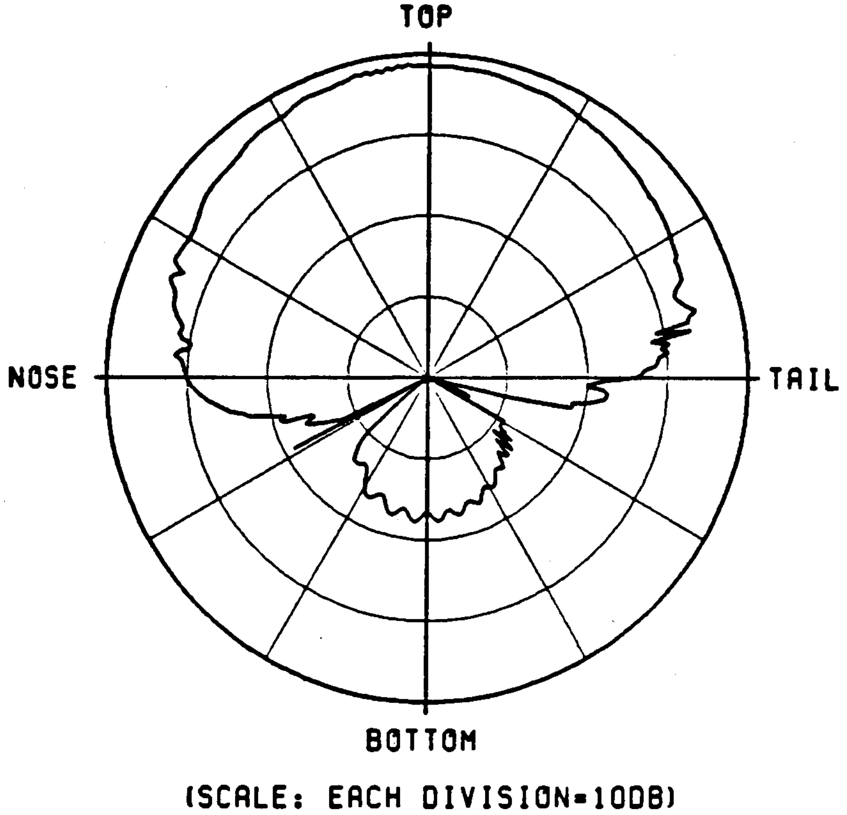

(c) E_{cp}

Figure 45. (Continued).

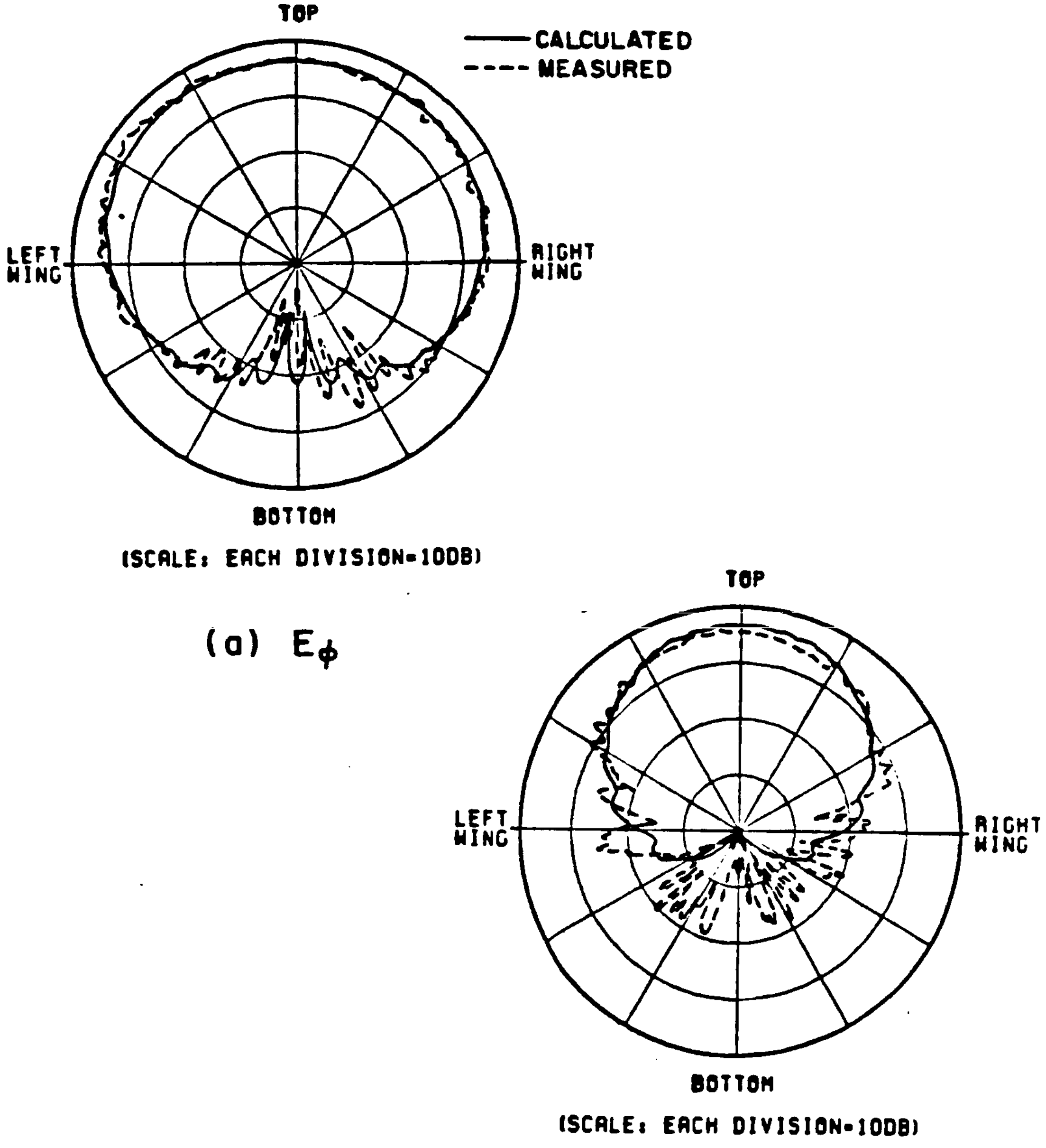

(a) E_ϕ

(b) E_θ

Figure 46. Roll plane pattern for Lindberg antenna mounted on a KC-135 aircraft.

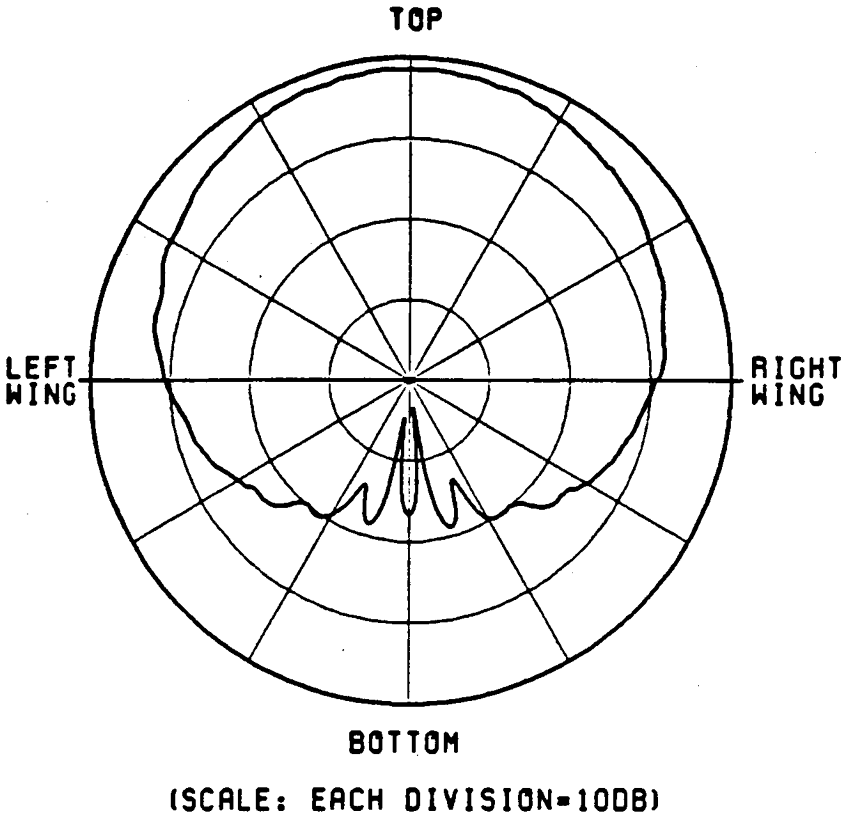

(c) E_{cp}

Figure 46. (Continued).

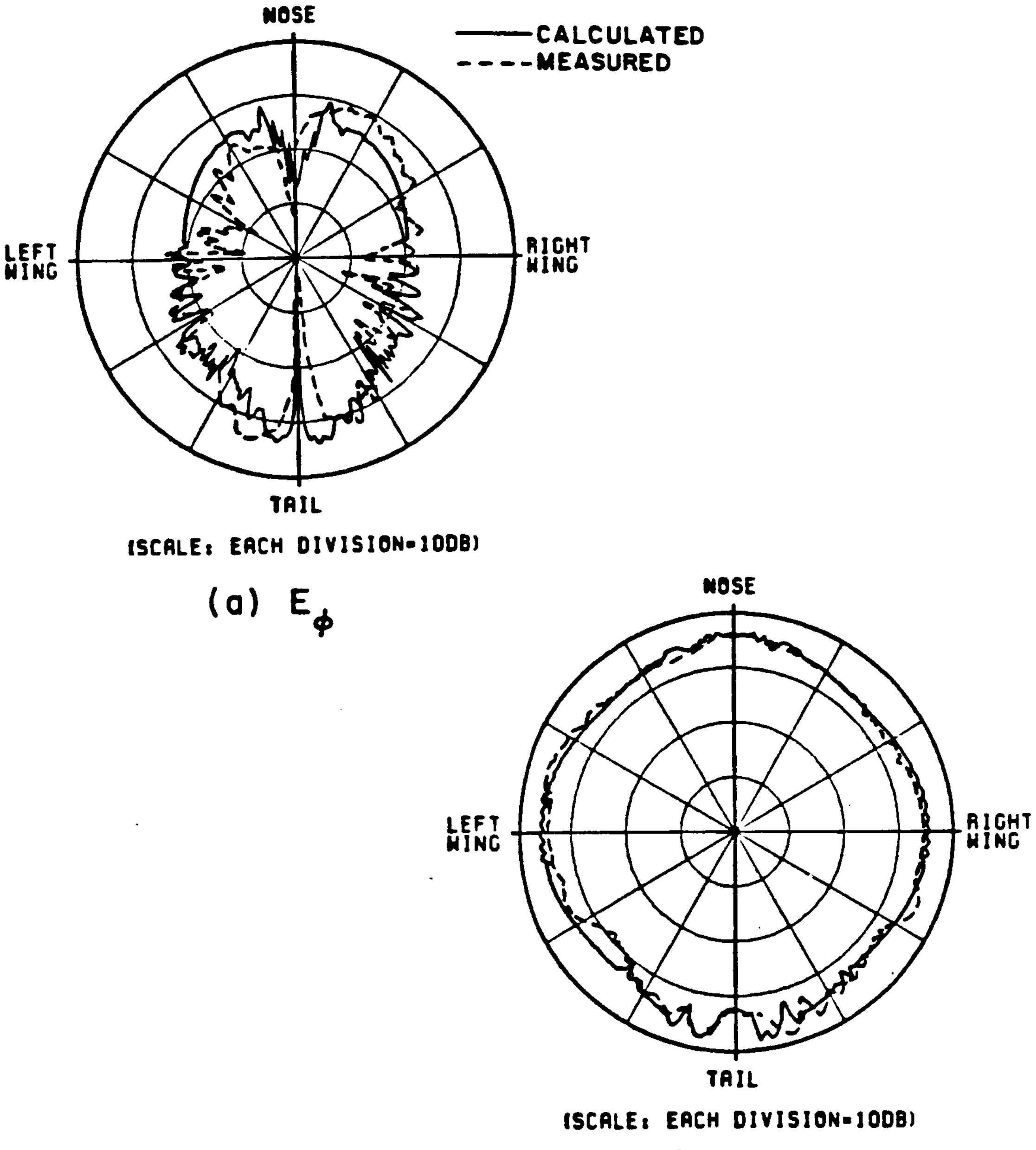

(a) E_ϕ

(b) E_θ

Figure 47. Azimuth plane pattern for Lindberg antenna mounted on a KC-135 aircraft.

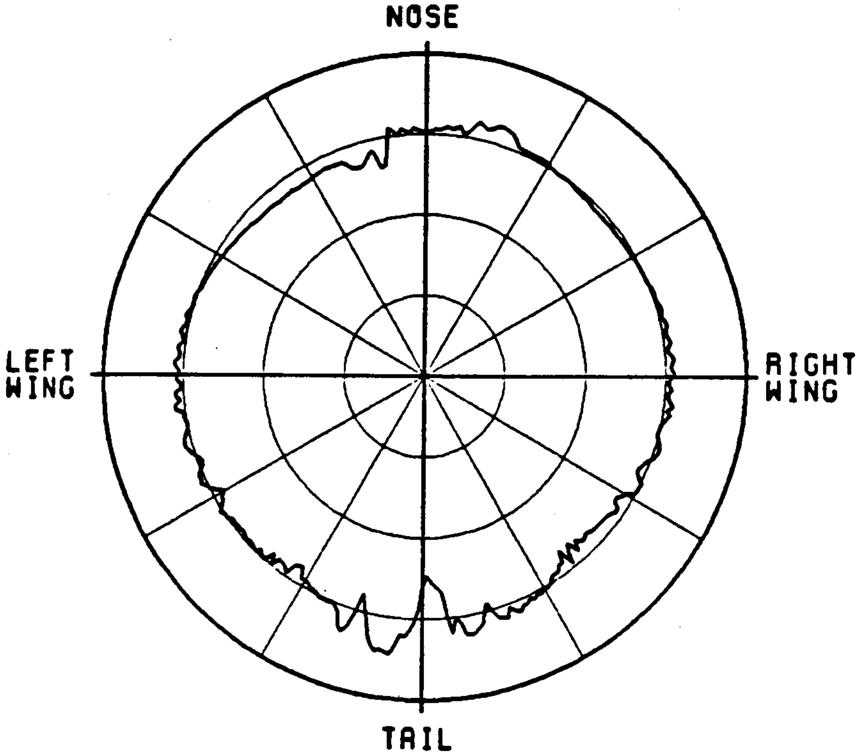

(SCALE: EACH DIVISION=10DB)

(c) E_{cp}

Figure 47. (Continued).

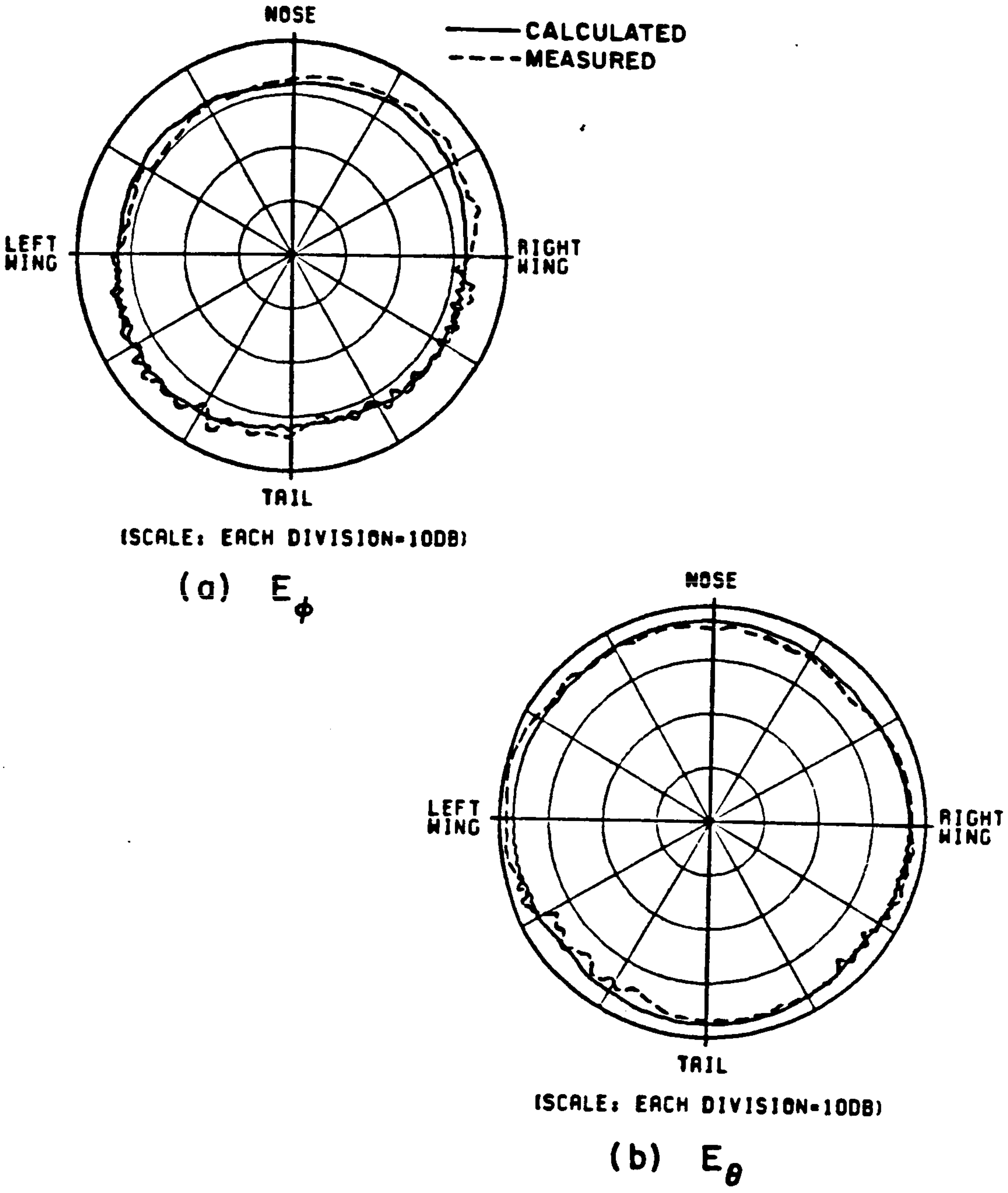

(a) E_ϕ

(b) E_θ

Figure 48: Azimuth conical pattern θ_p=45°) for Lindbert antenna mounted on a KC-135 aircraft.

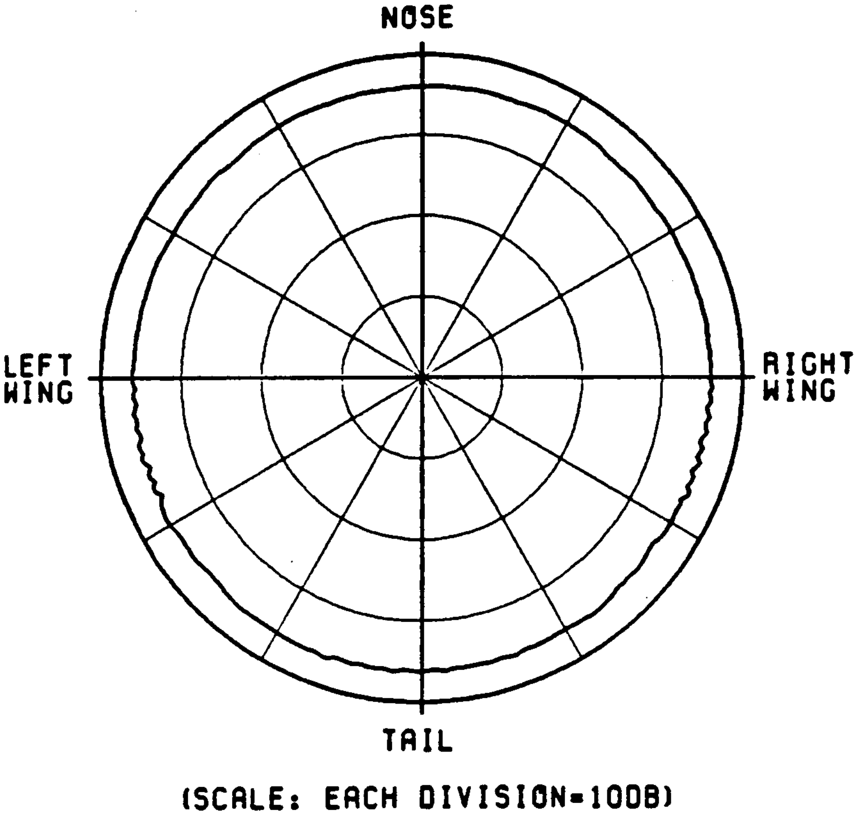

(c) E_{cp}

Figure 48. (Continued).

Example 6: Simulation of Cessna 402B

In this example a monopole antenna is mounted on the fuselage of a Cessna 402B aircraft just above the cockpit. The line drawing of the Cessna 402B is shown in Figure 49, and the computer model based on the input data is shown in Figure 50. The input data is as follows:

```
UN: INCHES
3
FQ: FIVE GIGAHERTZ
1,5.,1.
FG: CESSNA 402B
8.2,26.,285.,152.
F
0.,0.,0.
SG: MONOPOLE
0.,-10.
1
0.,0.
.414,.828,0.,.25,3
1.,0.
FG: LEFT WING (INNER PART)
4,T
-41.8,26.0,0.
-36.8,68.,0.
-36.8,68.,65.
-41.8,26.,65.
FG: RIGHT WING (INNER PART)
4,T
-41.8,-26.,65.
-36.8,-68.,65.
-36.8,-68.,0.
-41.8,-26.0,0.
FG: LEFT ENGINE (RIGHT SIDE)
6,F
-36.8,68.,0.
-36.8,68.,-40.
-21.8,68.,-40.
-21.8,68.,85.
-36.8,68.,85.
-36.8,68.,65.
FG:RIGHT ENGINE (LEFT SIDE)
6,F
-36.8,-68.,0.
-36.8,-68.,65.
-36.8,-68.,85.
-21.8,-68.,85.
-21.8,-68.,-40.
-36.8,-68.,-40.
FG: LEFT ENGINE (TOP)
4,F
-21.8,68.,-40.
-21.8,106.,-40.
-21.8,106.,85.
-21.8,68.,85.
FG:RIGHT ENGINE (TOP)
4,F
-21.8,-68.,-40.
-21.8,-68.,85.
-21.8,-106.,85.
-21.8,-106.,-40.
FG: LEFT ENGINE (LEFT SIDE)
6,F
-36.8,106.,65.
-36.8,106.,85.
-21.8,106.,85.
-21.8,106.,-40.
-36.8,106.,-40.
-36.8,106.,0.
```

```
FG: RIGHT ENGINE (RIGHT SIDE)
6,F
-36.8,-106.,65.
-36.8,-106.,0.
-36.8,-106.,-40.
-21.8,-106.,-40.
-21.8,-106.,85.
-36.8,-106.,85.
FG: LEFT ENGINE (FRONT)
4,F
-21.8,68.,-40.
-36.8,68.,-40.
-36.8,106.,-40.
-21.8,106.,-40.
FG: RIGHT ENGINE (FRONT)
4,F
-21.8,-68.,-40.
-21.8,-106.,-40.
-36.8,-106.,-40.
-36.8,-68.,-40.
FG: LEFT WING (OUTER PART)
4,F
-36.8,106.,0.
-26.8,213.,0.
-26.8,213.,50.
-36.8,106.,65.
FG:RIGHT WING (OUTER PART)
4,F
-36.8,-106.,0.
-36.8,-106.,65.
-26.8,-213.,50.
-26.8,-213.,0.
FG: LEFT FUEL TANK PLATE #1
4,F
-26.8,213.,0.
-14.8,219.,-32.
-14.8,219.,82.
-26.8,213.,50.
FG: RIGHT FUEL TANK PLATE #1
4,F
-26.8,-213.,0.
-26.8,-213.,50.
-14.8,-219.,82.
-14.8,-219.,-32.
FG: LEFT FUEL TANK PLATE #2
4,F
-14.8,219.,-32.
-8.8,235.,0.
-8.8,235.,50.
-14.8,219.,82.
FG: RIGHT FUEL TANK PLATE #2
4,F
-14.8,-219.,-32.
-14.8,-219.,82.
-8.8,-235.,50.
-8.8,-235.,0.
PD: ROLL PLANE
0.,0.,90.
0,360,1
F,4200.
PP:
T
1,2.5,3
EX:
```

The calculated roll plane radiation pattern shown in Figure 51 is found to be in good agreement with the measured pattern.

Experimental results were obtained from NASA (Hampton, Virginia), using the 1/7 scale model at a range of 50 feet.

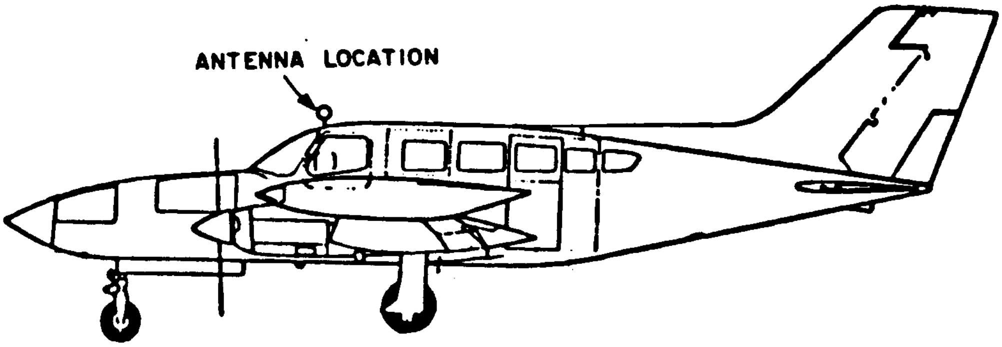
ANTENNA LOCATION

(a) SIDE VIEW

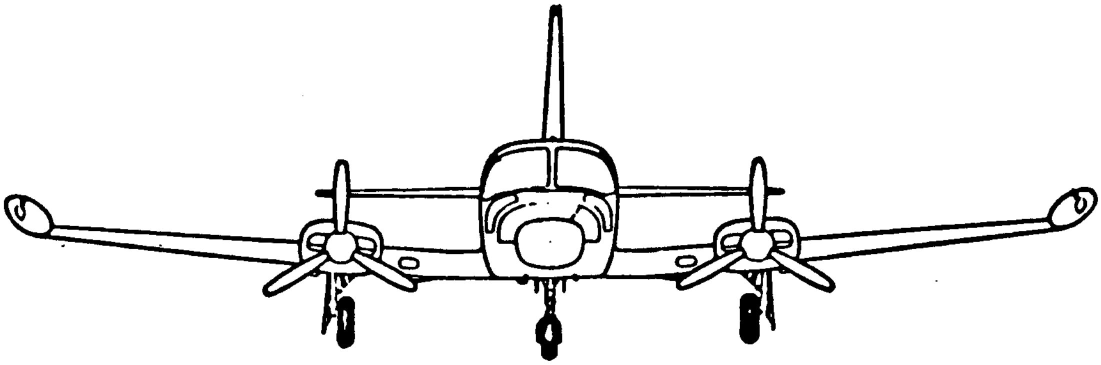

(b) FRONT VIEW

Figure 49. Cessna 402B.

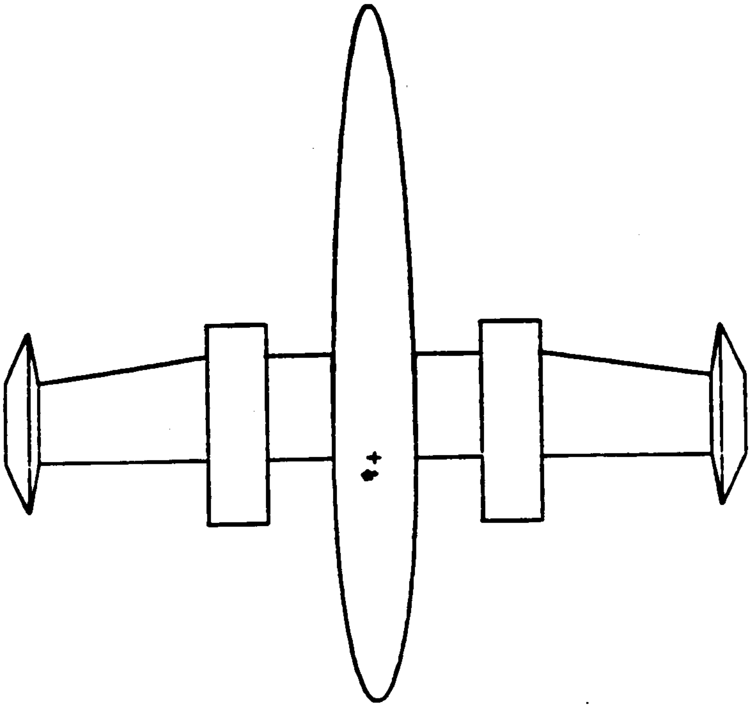

(a) TOP VIEW

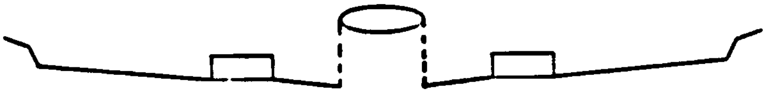

(b) FRONT VIEW

Figure 50. Model for Cessna 402B with engines and fuel tanks.

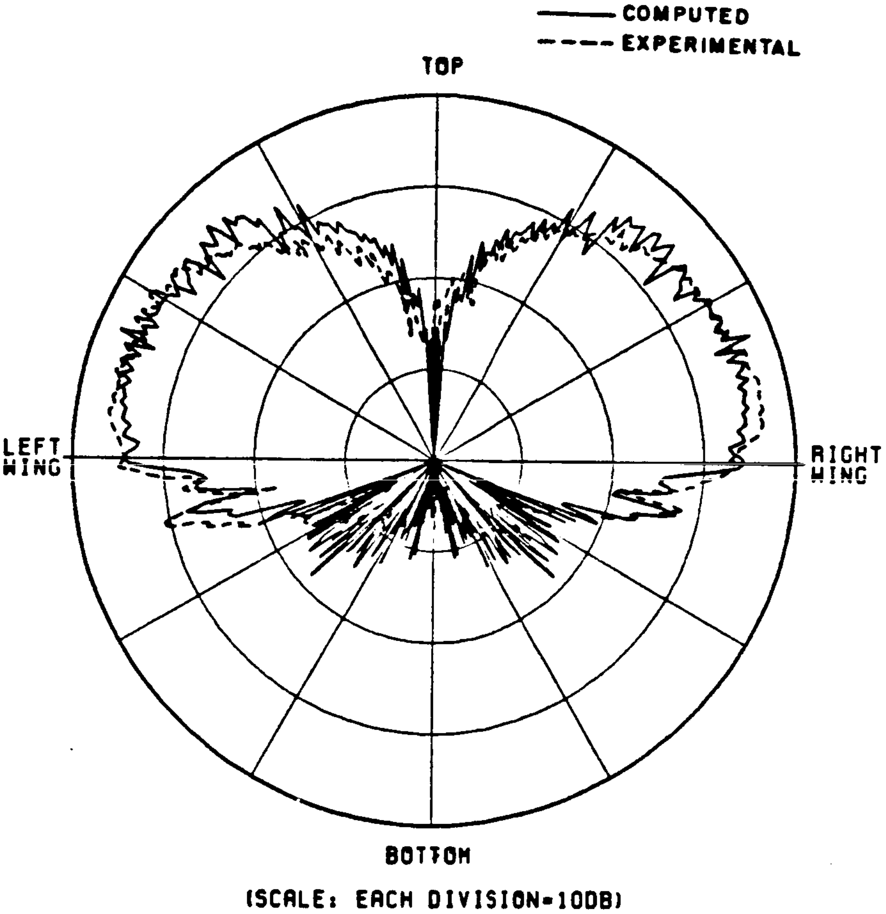

Figure 51. Roll plane pattern for Cessna 402B model.

Example 7: Simulation of Beechcraft Baron

Consider a λ/4 monopole mounted forward of the cockpit of a Beechcraft Baron aircraft as shown in Figure 52. The computer model based on the input data is shown in Figure 53. The input data is as follows:

```
UN:INCHES
3
FQ: FIVE GIGAHERTZ
1,5.,1.
PG: BEECHCRAFT BARON
15.5,23.2,206.5,117.5
F
0.,0.,0.
SG: MONOPOLE
0.,-77.
1
0.,0.
.414,.828,0.,.25,3
1.,0.
PG: LEFT WING
4,T
-10.,23.5,-20.
10.,227.,-10.
10.,227.,27.
-10.,23.5,60.
PG: LEFT ENGINE (RIGHT SIDE)
6,F
-5.6,50.5,-62.
8.4,50.5,-62.
8.4,50.5,20.
-8.6,50.5,20.
-8.6,50.5,-8.5
-5.6,50.5,-8.5
PG: LEFT ENGINE (TOP)
4,F
8.4,50.5,-62.
11.4,84.5,-62.
11.4,84.5,20.
8.4,50.5,20.
```

```
PG: LEFT ENGINE (FRONT)
4,F
-2.6,84.5,-62.
11.4,84.5,-62.
8.4,50.5,-62.
-5.6,50.5,-62.
PG: RIGHT WING
4,T
-10.,-23.5,60.
10.,-227.,27.
10.,-227.,-10.
-10.,-23.5,-20.
PG: RIGHT ENGINE (LEFT SIDE)
6,F
-5.6,-50.5,-62.
-5.6,-50.5,-8.5
-8.6,-50.5,-8.5
-8.6,-50.5,20.
8.4,-50.5,20.
8.4,-50.5,-62.
PG: RIGHT ENGINE (TOP)
4,F
8.4,-50.5,-62.
8.4,-50.5,20.
11.4,-84.5,20.
11.4,-84.5,-62.
PG: RIGHT ENGINE (RIGHT SIDE)
6,F
-5.6,-84.5,20.
-5.6,-84.5,-7.
-2.6,-84.5,-7.
-2.6,-84.5,-62.
11.4,-84.5,-62.
11.4,-84.5,20.
```

```
PG: LEFT ENGINE (LEFT SIDE)
6,F
-5.6,84.5,20.
11.4,84.5,20.
11.4,84.5,-62.
-2.6,84.5,-62.
-2.6,84.5,-7.
-5.6,84.5,-7.
```

```
PG: RIGHT ENGINE (FRONT)
4,F
-2.6,-84.5,-62.
-5.6,-50.5,-62.
8.4,-50.5,-62.
11.4,-84.5,-62.
PD: ROLL PLANE
0.,0.,80.
0,360,1
F,4200.
PP:
T
1,2.5,3
EX:
```

The conical roll plane radiation pattern is shown in Figure 54.

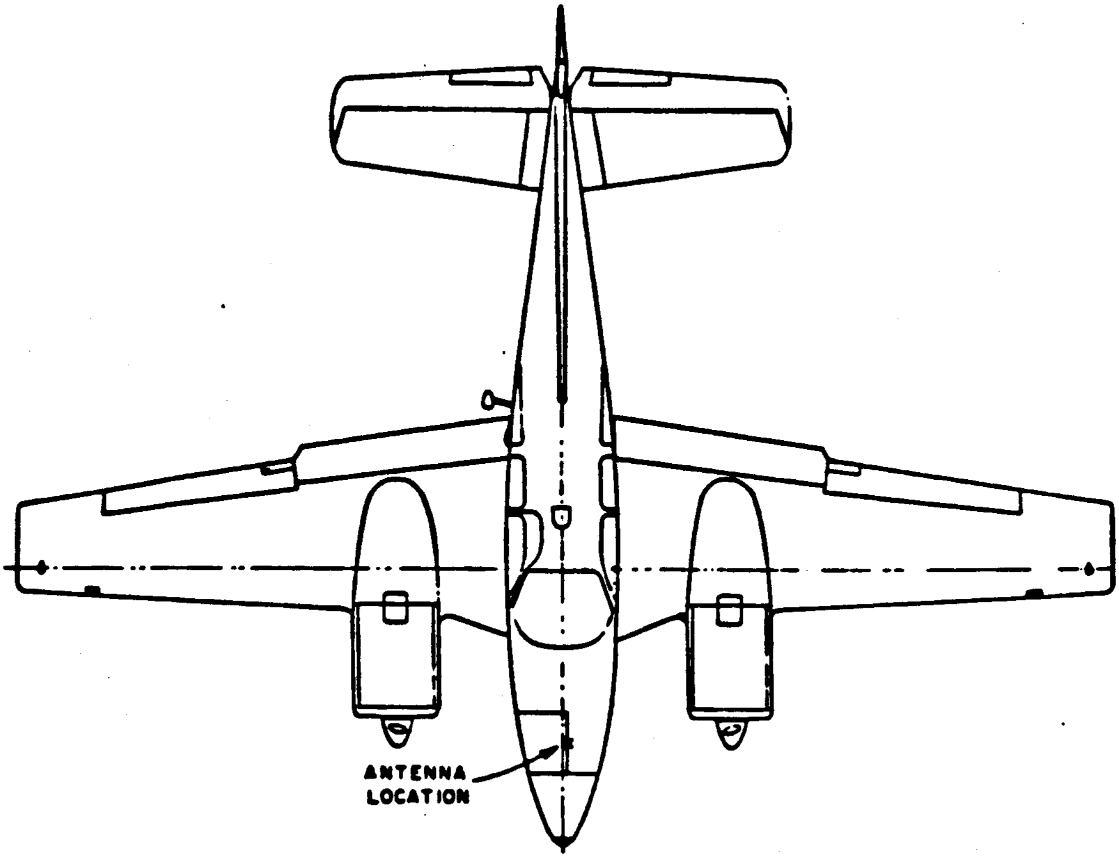
ANTENNA LOCATION

(a) TOP VIEW

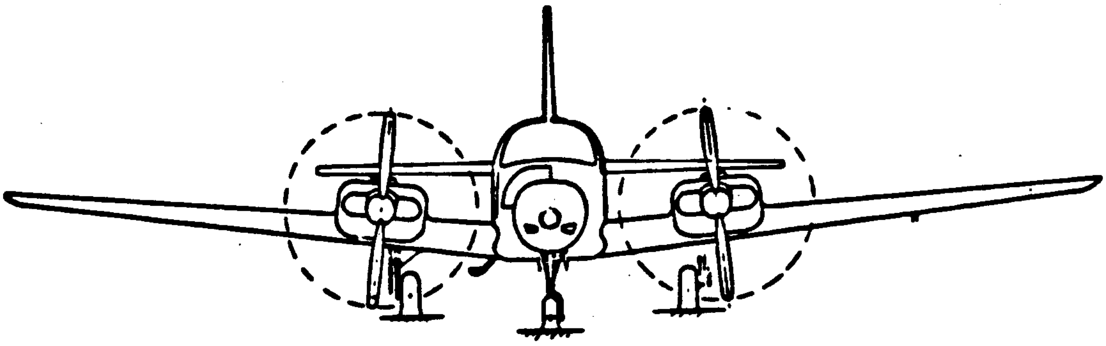

(b) FRONT VIEW

Figure 52. Beechcraft Baron with Antenna in forward location.

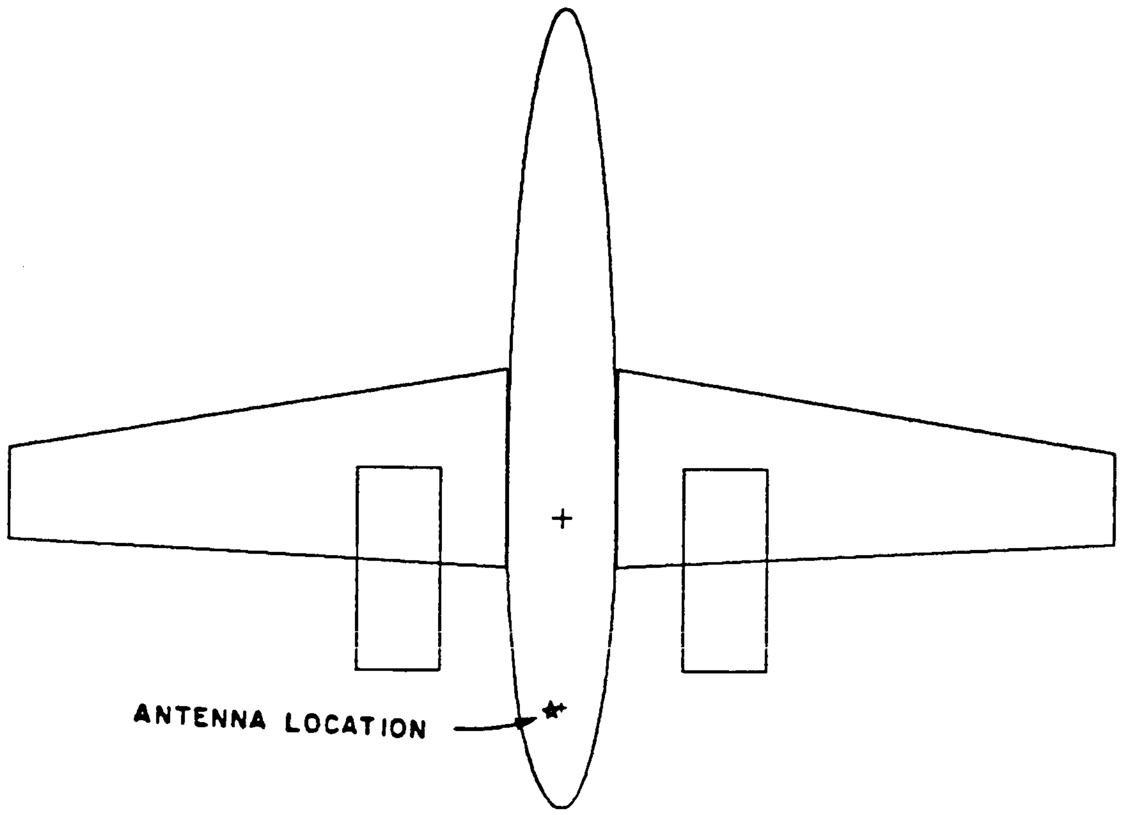
ANTENNA LOCATION

(a) TOP VIEW

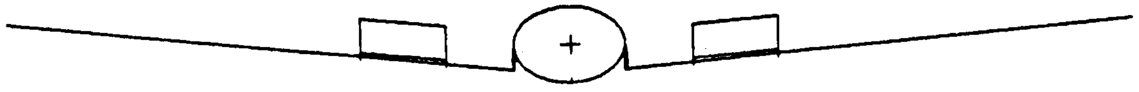

(b) FRONT VIEW

Figure 53. Beechcraft Baron model with engine housings.

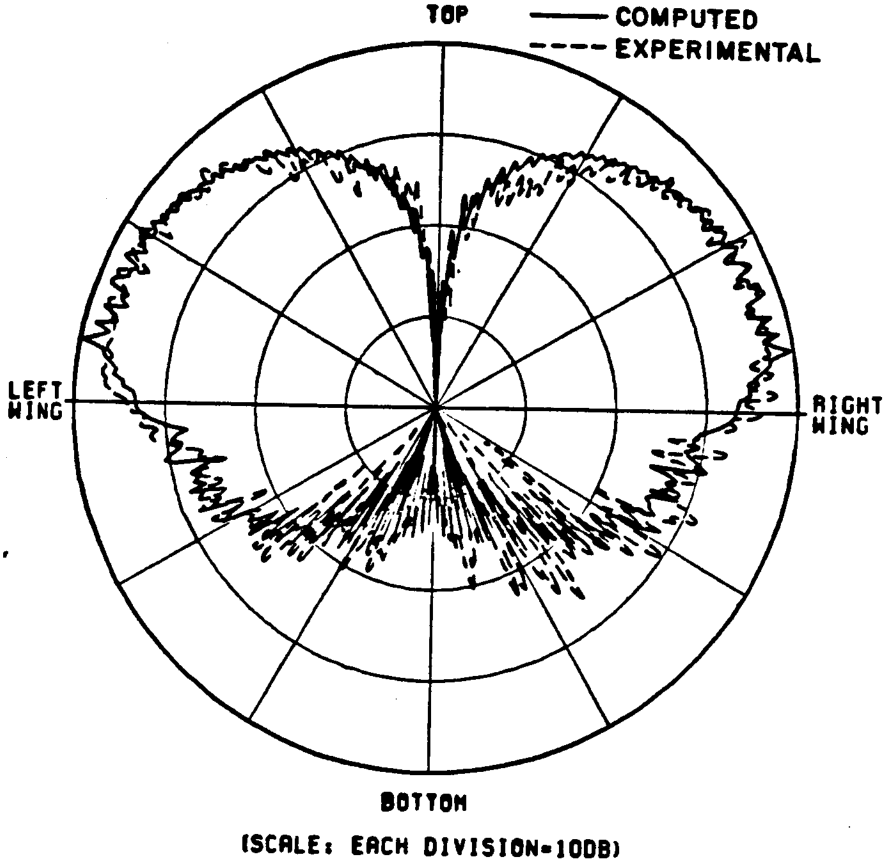

Figure 54. Roll conical pattern (θ_p=80°) for Beechcraft Baron model shown in Figure 53.

Next, let us consider the effect of the rotating propellers in the front of the engines. It is necessary to check the scattering due to the rotation of the propellers because they are close to the antenna. Four different positions (i.e., 0°, 45°, 90°, 135°) of the stationary propellers are chosen to simulate the rotating motion of the propellers as shown in Figure 55. For simplicity, only the left propeller is considered here. The input data for the four different propellers are as follows:

```
PG: PROPELLOR (TOP) AT 0°
3,F
2.9,-67.5,-66.
42.9,-70.,-65.
42.9,-65.,-67.
PG: PROPELLOR (BOTTOM) AT 0°
3,F
2.9,-67.5,-66.
-37.1,-70.,-67.
-37.1,-65.,-65.
```

```
PG: PROPELLOR (TOP) AT 45°
3,F
2.9,-67.5,-66.
29.414,-97.554,-65.
32.954,-94.014,-67.
PG: PROPELLOR (BOTTOM) AT 45°
3,F
2.9,-67.5,-66.
-27.154,-40.986,-67.
-24.384,-37.446,-65.
```

```
PG: PROPELLOR (TOP) AT 90°
3,F
2.9,-67.5,-66.
0.4,-107.5,-65.
5.4,-107.5,-67.
PG: PROPELLOR (BOTTOM) AT 90°
3,F
2.9,-67.5,-66.
0.4,-27.5,-65.
5.4,-27.5,-67.
```

```
PG: PROPELLOR (TOP) AT 135°
3,F
2.9,-67.5,-66.
32.954,-40.986,-65.
29.414,-37.446,-67.
PG: PROPELLOR (BOTTOM) AT 135°
3,F
2.9,-67.5,-66.
-23.614,-97.554,-67.
-27.154,-94.014,-65.
```

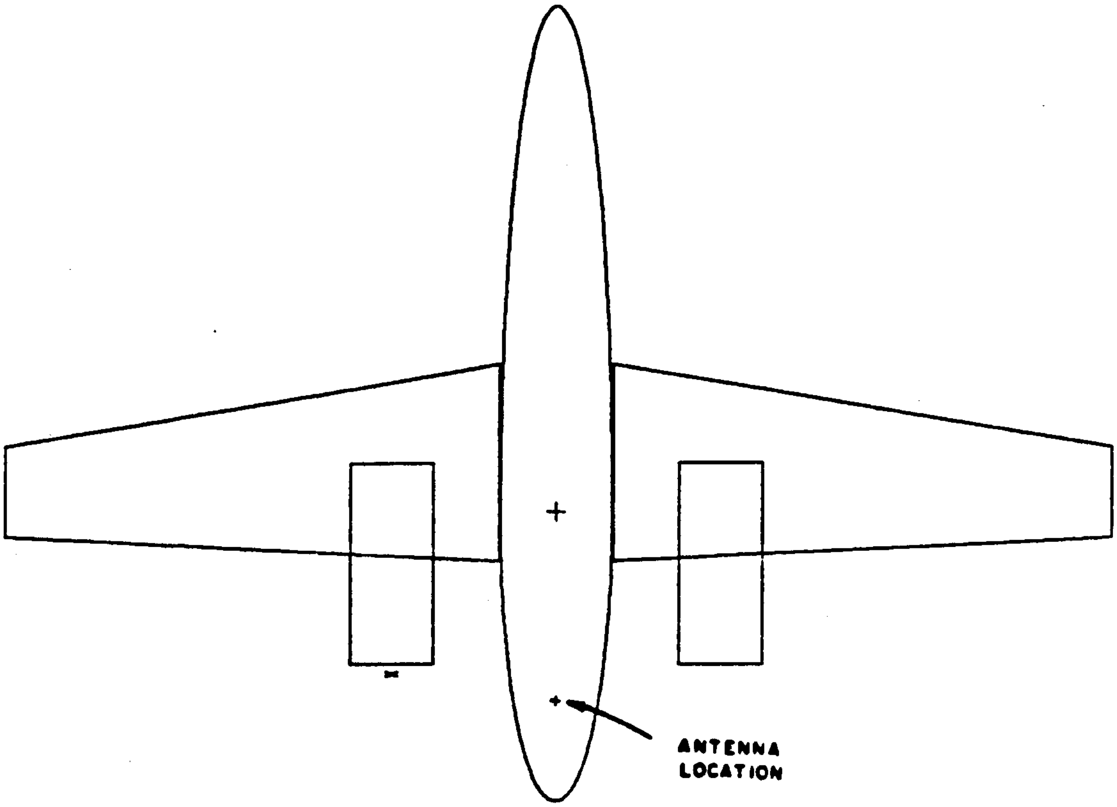
ANTENNA
LOCATION

(a) TOP VIEW

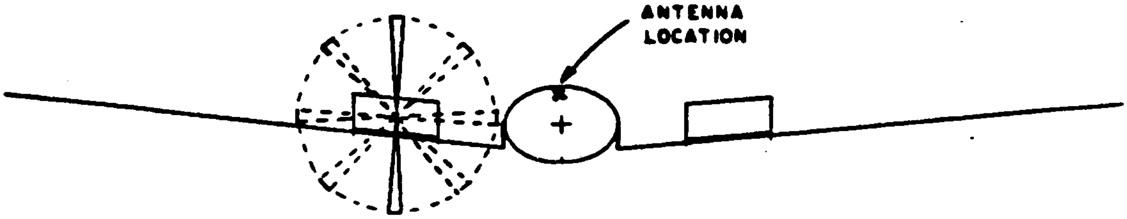
ANTENNA
LOCATION

(b) FRONT VIEW

Figure 55. Beechcraft Baron model with rotating propellers on one side.

The calculated conical roll plane radiation patterns for the four different propeller positions are shown in Figures 56(a) through (d).

The roll plane pattern in Figure 57 is a combination of the four previous patterns. The width of the pattern line indicates the variation of the radiation pattern due to the rotation of the propellers.

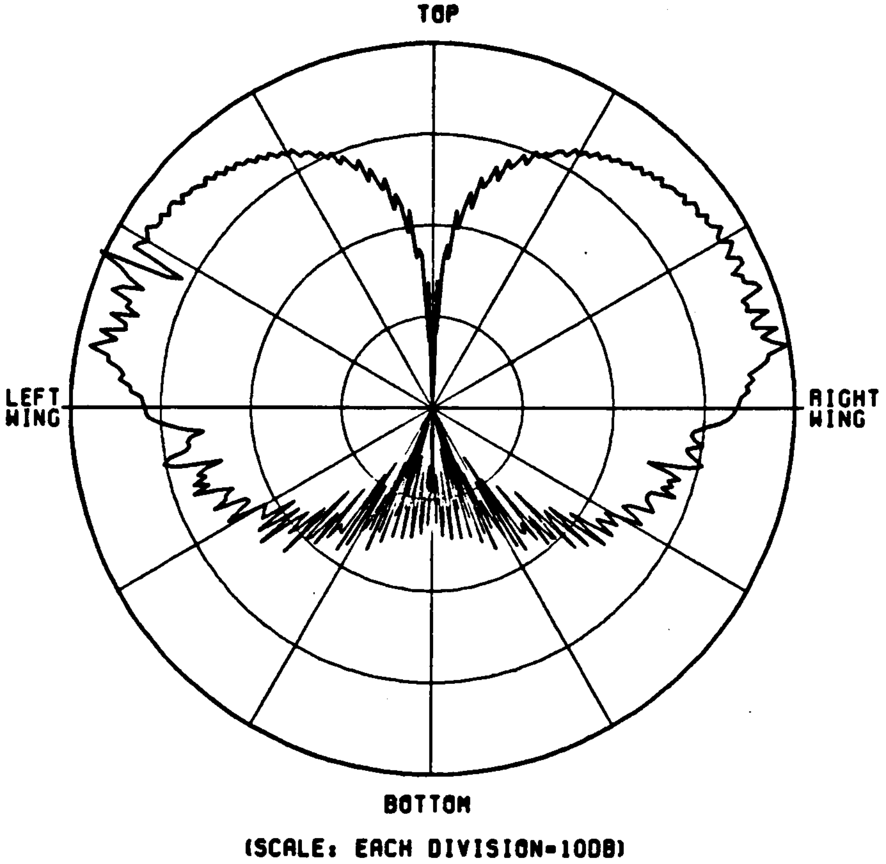

Figure 56(a). Roll conical pattern for the Beechcraft Baron with propeller at 0° (vertical).

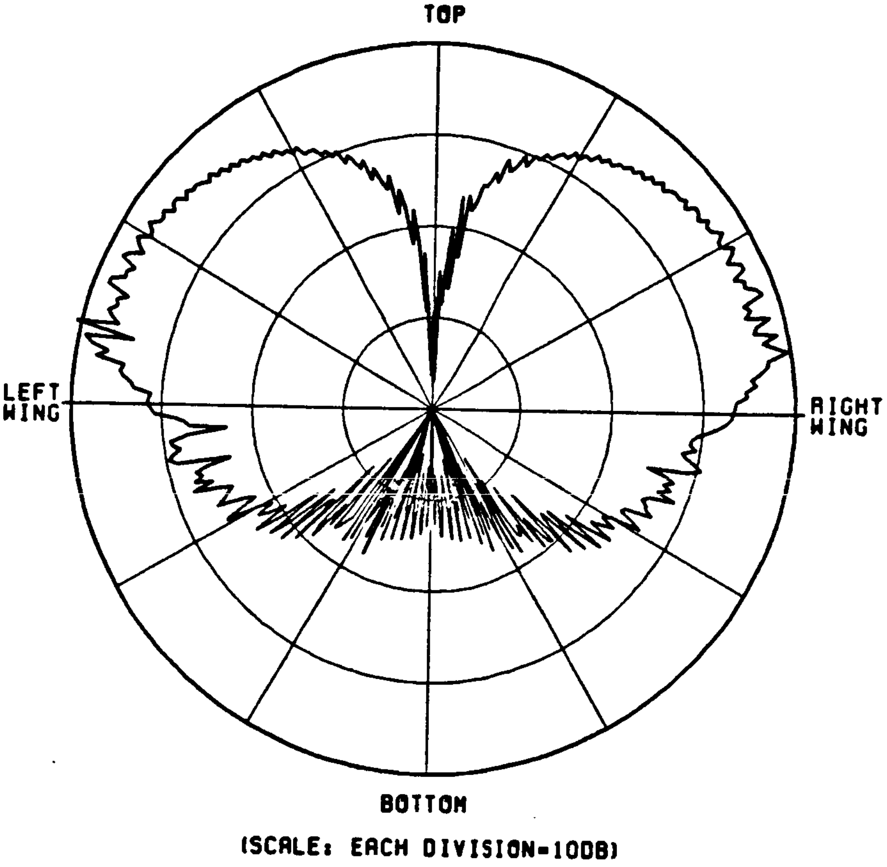

Figure 56(b). Roll conical pattern for the Beechcraft Baron with propeller at 45°.

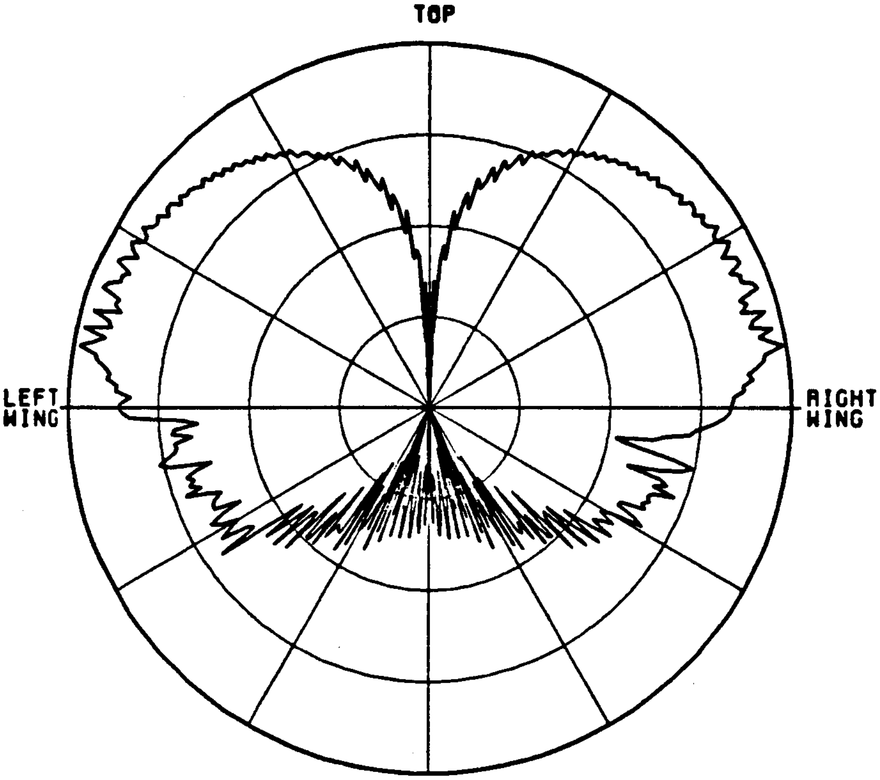

(SCALE: EACH DIVISION=10DB)

Figure 56(c). Roll conical pattern for Beechcraft Baron with propeller at 90° (horizontal).

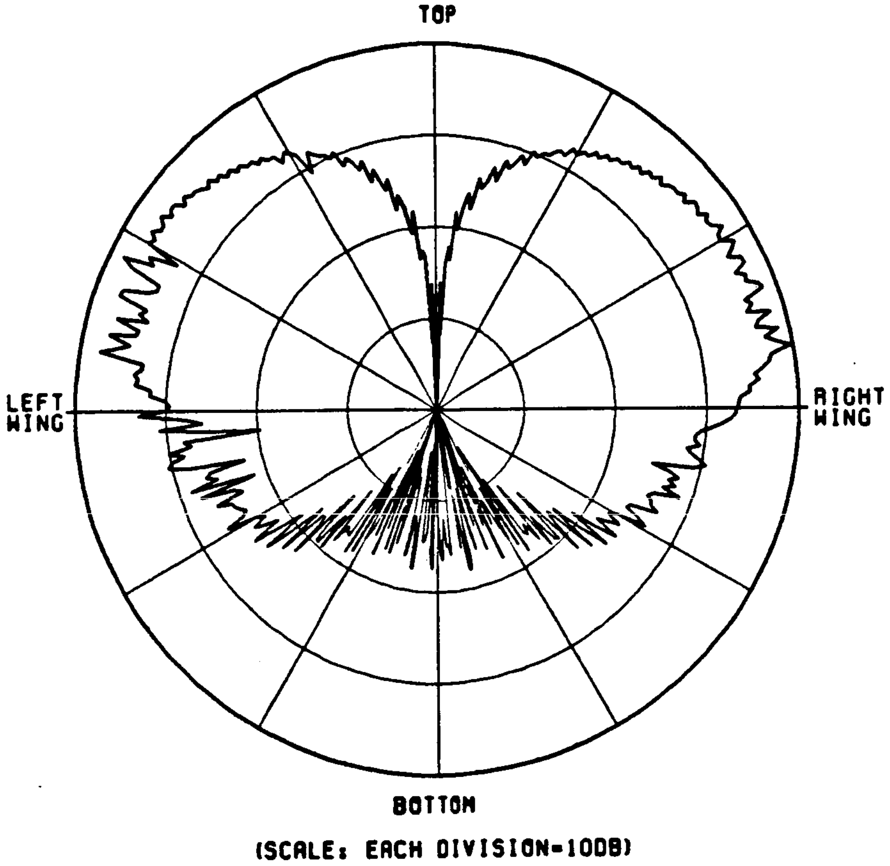

Figure 56(d). Roll conical pattern for the Beechcraft Baron with propeller at 135°.

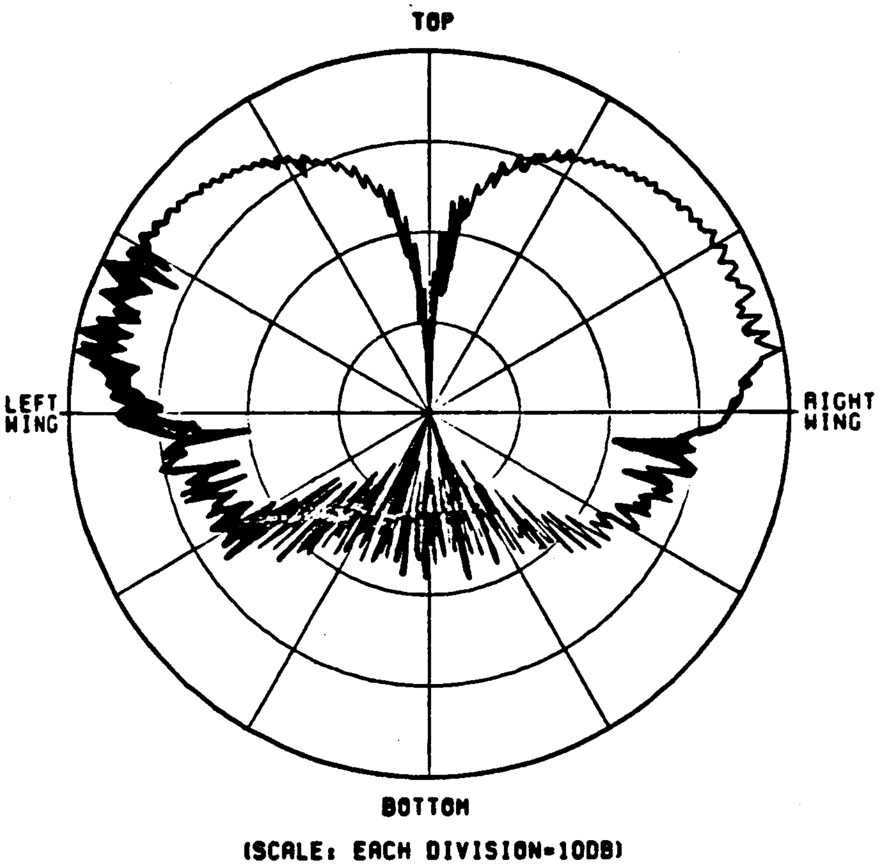

Figure 57. Variation in the roll conical pattern for the Beechcraft Baron due to the rotation of the propellers.

Example 8: Simulation of the Cessna 150 Aircraft

In this example, a monopole antenna is mounted forward on the wings of a Cessna 150 aircraft. A different approach was taken in the modeling of the Cessna 150 aircraft due to the position of the antenna and the shape of the wings. The wings are simulated by the composite ellipsoid and two flat plates are attached to simulate the nose and fuselage of the aircraft. The line drawing of the Cessna 150 is shown in Figure 58, and the computer model based on the input data is shown in Figure 59. The input data is as follows:

```
UN: INCHES
3
FQ: FIVE GIGAHERTZ
1,5.,1.
FG: CESSNA 150 WING
3.5,25.,250.,250.
F
0.,0.,0.
FC: SQUARE OFF WING TIPS
T,T
196.25,-196.25
SG: MONOPOLE MOUNTED ON WING
86.,0.
1
0.,0.
.414,.828,0.,.25,3
1.,0.
PG: NOSE PLATE
4,T
-17.35,32.53,-17.52
-27.35,82.4,-15.18
-27.35,82.4,15.18
-17.35,32.53,17.52
```

```
PG: FUSELAGE PLATE
4,T
-18.67,-25.2,14.93
10.,-152.,3.17
10.,-152.,-3.17
-18.67,-25.2,-14.93
PD: ELEVATION PLANE AS REFERED TO THIS MODEL
0.,0.,90.
0,360,1
F,4200
PP: PEN PLOT
T
1,1.925,3
EX:
```

The resulting elevation plane pattern for this model is shown in Figure 60. Although the magnitude of the ripple is not quite perfect, it is of the correct spatial frequency, and the general shape of the pattern is good.

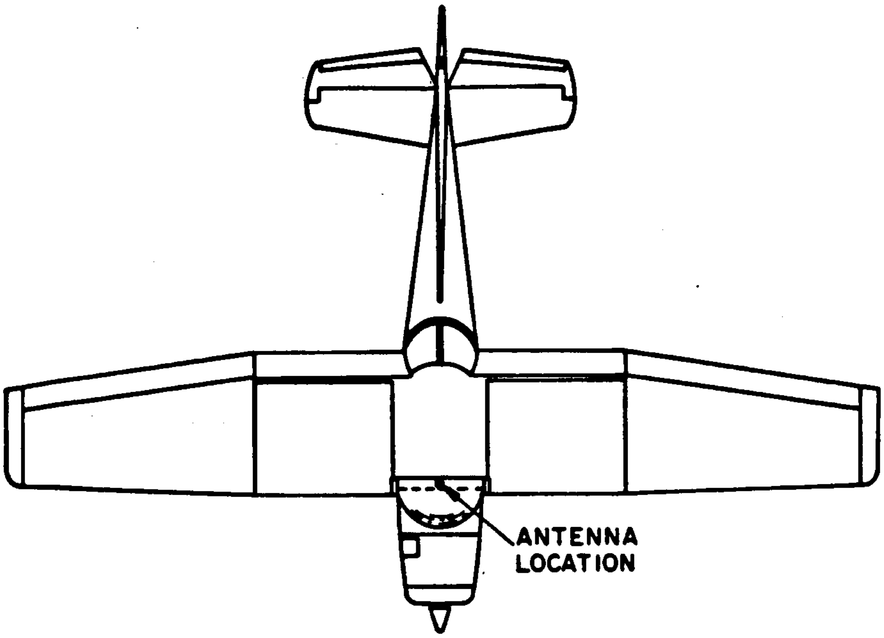
ANTENNA
LOCATION

(a) TOP VIEW

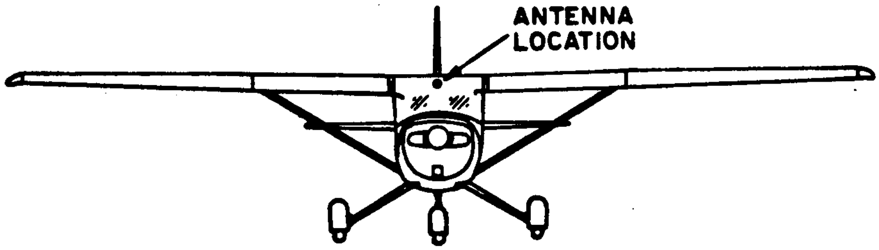
ANTENNA
LOCATION

(b) FRONT VIEW

Figure 58. Cessna 150.

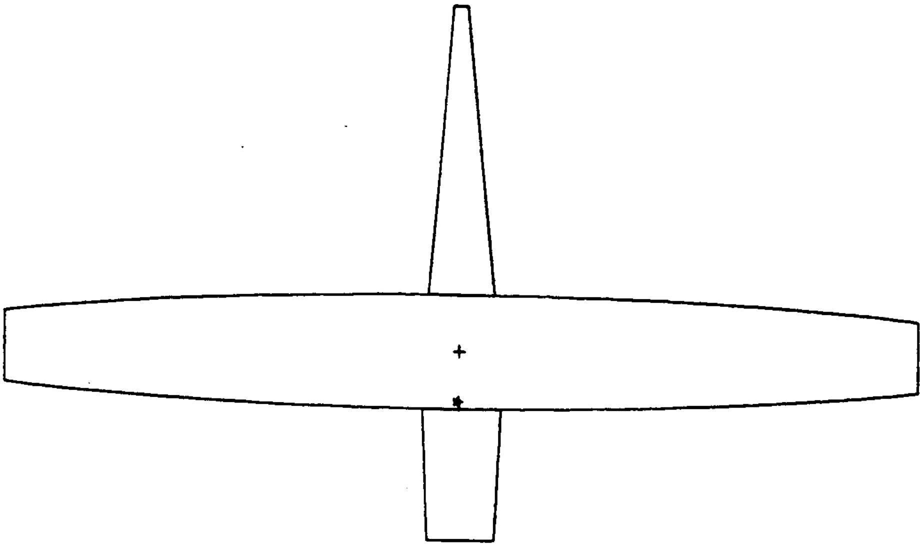

(a) Top view.

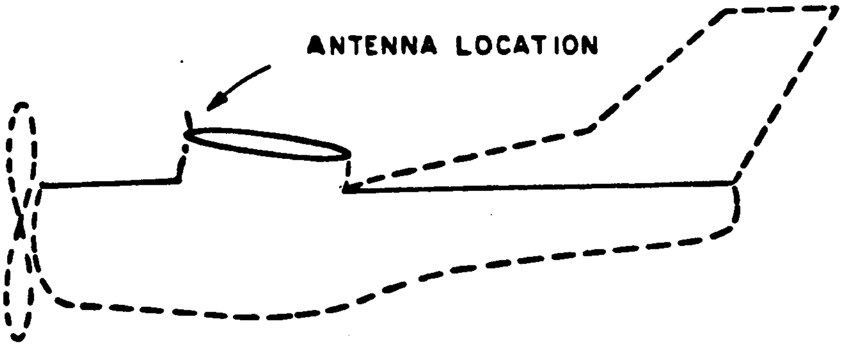
ANTENNA LOCATION

(b) Side view.

Figure 59. Cessna 150 model. Dashed lines are not part of the computer simulation.

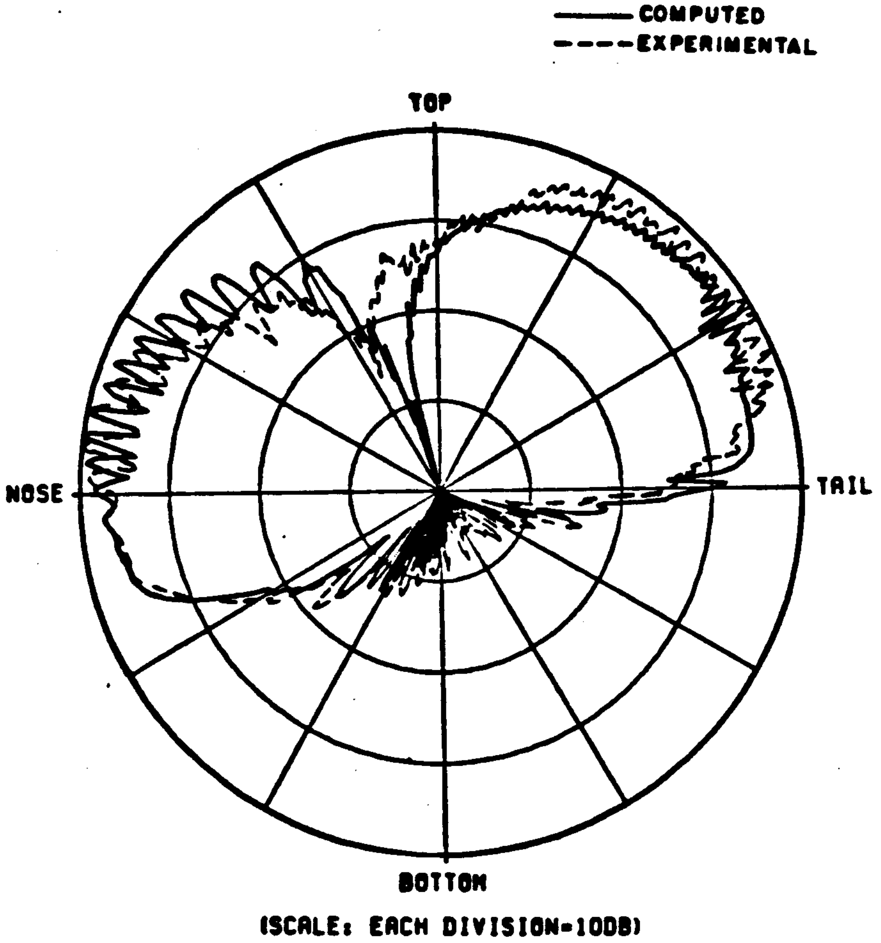

Figure 60. Elevation plane pattern for a Cessna 150 aircraft.

Example 9: Simulation of F-16 Fighter Aircraft

Consider a TACAN antenna mounted on the top of a F-16 fighter aircraft as shown in Figure 61 and operated at a frequency of 0.96 GHz. A composite ellipsoid and a total of 12 plates are used to simulate the structure of the aircraft. The computer model is illustrated in Figure 62. Note that the radome of the F-16 is simulated as a truncated fuselage. The measured data was obtained by General Dynamics using a quarter scale model of the F-16. The input data is as follows:

```
UN:IN INCHES
3
FG:F16A FUSELAGE GEOMETRY AT STATION 250
21.5,23.,400.,250.
F
0.,0.,0.
FC:
T,T
300.,-185.
FQ:FREQUENCY
1,0.96,1.
SG:SOURCE GEOMETRY
0.,13.25
1
0.,0.
0.,0.,0.,3.0758,3
1.,0.
PG:CURVATURE SIMULATED PLATE #1 ON POS. SIDE
6,T
8.2046,22.4421,-61.
2.1418,36.5,-61.
-4.0866,50.942,-8.6
-5.4054,54.,8.743
-5.4054,54.,158.95
8.2046,22.4421,158.95
PG:CURVATURE SIMULATED PLATE #2 ON POS. SIDE
5,T
8.2046,22.4421,158.95
-5.4054,54.,158.95
-6.2805,54.,209.084
-7.6944,54.,290.084
5.9156,22.4421,290.084
```

```
PG:  CURVATURE SIMULATE
     PLATE #3 ON POS. SIDE

3,T
0.5,19.2,-150.
2.1418,36.5,-61.
8.2046,22.4421,-61.
```

```
PG:WING ON POS. SIDE
4,F
-5.4054,54.,8.743
-5.4054,180.,114.47
-5.4054,180.,158.95
-5.4054,54.,158.95
PG:HORIZONTAL STABILIZER ON POS. SIDE
4,F
-5.4054,54.,219.7958
-5.4054,109.101,266.031
-5.4054,109.101,290.084
-5.4054,54.,290.084
PG:VERTICAL STABILIZER ON NEG. SIDE
4,T
20.,0.,160.
120.,0.,261.
120.,-3.4,298.
20.,-6.8,234.
PG:VERTICAL STABILIZER ON POS. SIDE
4,T
20.,6.8,234.
120.,3.4,298.
120.,0.,261.
20.,0.,160.
PG:CURVATURE SIMULATED PLATE #1 ON NEG. SIDE
6,T
8.2046,-22.4421,158.95
-5.4054,-54.,158.95
-5.4054,-54.,8.743
-4.0866,-50.942,-8.6
2.1418,-36.5,-61.
8.2046,-22.4421,-61.
PG:CURVATURE SIMULATED PLATE #2 ON NEG. SIDE
5,T
5.9156,-22.4421,290.084
-7.6944,-54.,290.084
-6.2805,-54.,209.084
-5.4054,-54.,158.95
8.2046,-22.4421,158.95
PG:CURVATURE SIMULATED PLATE #3 ON NEG. SIDE
3,T
8.2046,-22.4421,-61.
2.1418,-36.5,-61.
0.5,-19.2,-150.
PG:WING ON NEG. SIDE
4,F
-5.4054,-54.,158.95
-5.4054,-180.,158.95
-5.4054,-180.,114.47
-5.4054,-54.,8.743
```

```
PG:HORIZONTAL STABILIZER ON NEG. SIDE
4,F
-5.4054,-54.,290.084
-5.4054,-109.101,290.084
-5.4054,-109.101,266.031
-5.4054,-54.,219.7958
PP:POLAR PLOT IN DB
T
1,2.81,3
PD:AZIMUTH PLANE CUT
90.,0.,10.
0,360.,1
T,50000.
EX:EXECUTE
PD:AZIMUTH PLANE CUT
90.,0.,20.
0,360.,1
T,50000.
EX:EXECUTE
PD:AZIMUTH PLANE CUT
90.,0.,30.
0,360.,1
T,50000.
EX:EXECUTE
I
I
I
PD:AZIMUTH PLANE CUT
90.,0.,115.
0,360.,1
T,50000.
EX:EXECUTE
PD:AZIMUTH PLANE CUT
90.,0.,120.
0,360.,1
T,50000.
EX:EXECUTE
```

```
PD:ELEVATION PLANE CUT
90.,90.,90.
0,360.,1
T,50000.
EX:EXECUTE
PI:
9
PD:ROLL PLANE CUT
0.,0.,90.
0,180.,1
T,50000.
TO:
F,F,F
T,T
T,T,T,T,T,T,T,T
1,9,1
2,6,1
1,5,1
1,3,2
1,4,1
1,4,1
1,4,1
1,4,1
2,3,1
1,3,2
DD:
5
1,6,1,3
1,6,4,1
1,6,4,4
4,1,1,6
4,4,1,6
RD:
1
1,4
EX:EXECUTE
```

To show the complete volumetric radiation patterns, the various azimuthal conical patterns are calculated as shown in Figures 63 through 82. In each case, both the principal and cross polarizations are considered. The elevation plane and roll plane patterns are also shown in Figure 83 and 84, respectively. All the above calculated results compare favorably with the measurements. It is noted that since the cockpit section simulation is not complete in our model, one cannot expect good agreement between the calculated and measured results in the nose region since the cockpit is part of the radiation path. In addition, the ripple above the aircraft in the elevation pattern are most likely created by the cockpit which is not simulated in this model.

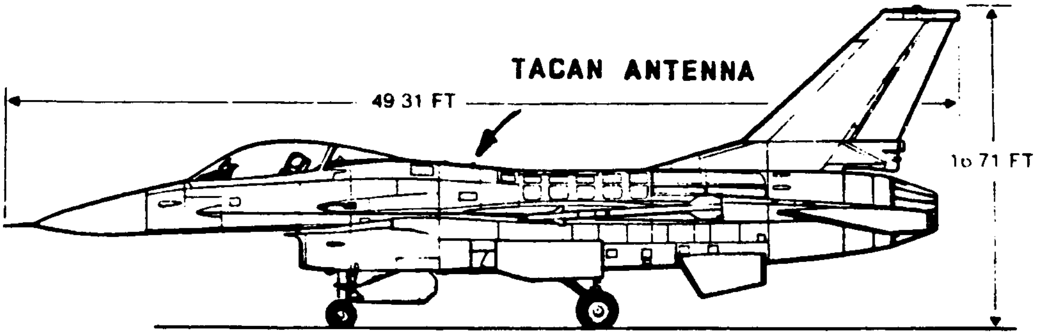
TACAN ANTENNA
49 31 FT
16 71 FT

(a) SIDE VIEW

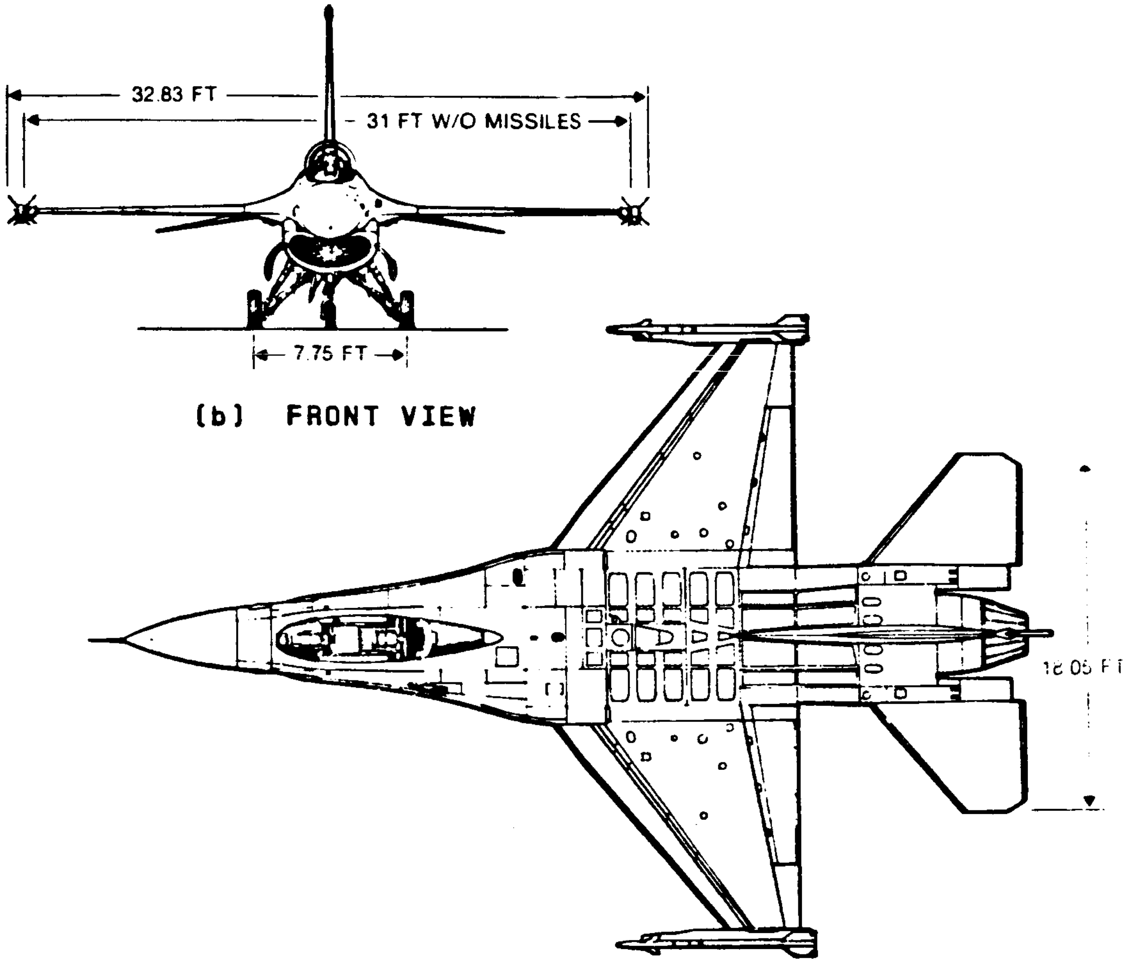
32.83 FT
31 FT W/O MISSILES
7.75 FT
18 05 FT

(b) FRONT VIEW

(c) TOP VIEW

Figure 61. F-16 fighter aircraft.

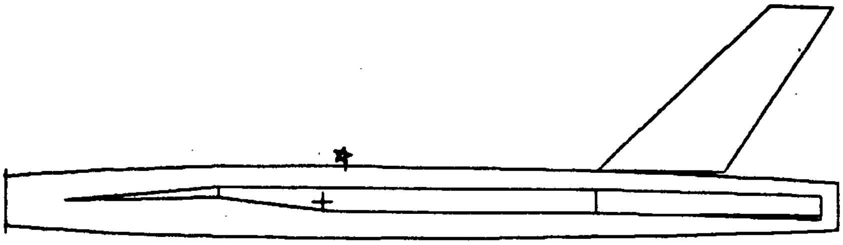

(a) SIDE VIEW

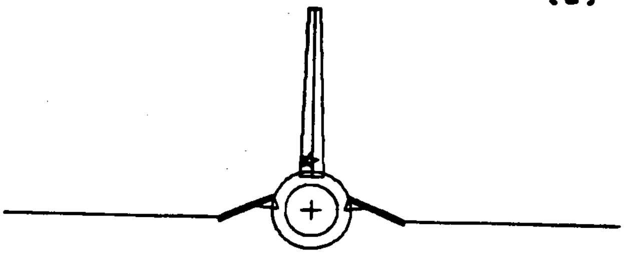

(b) FRONT VIEW

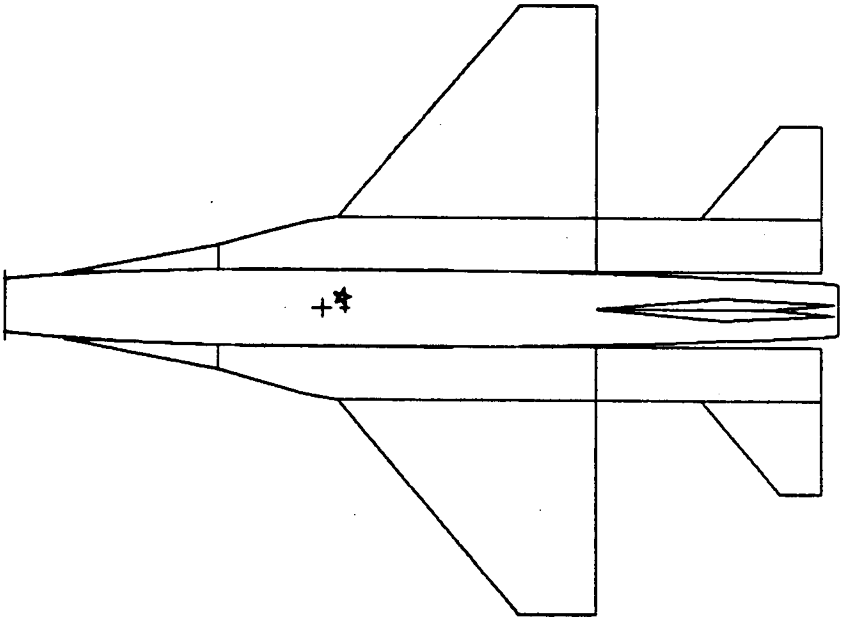

(c) TOP VIEW

Figure 62. Computer simulated model of a F-16 fighter aircraft.

ORIGINAL PAGE IS
OF POOR QUALITY

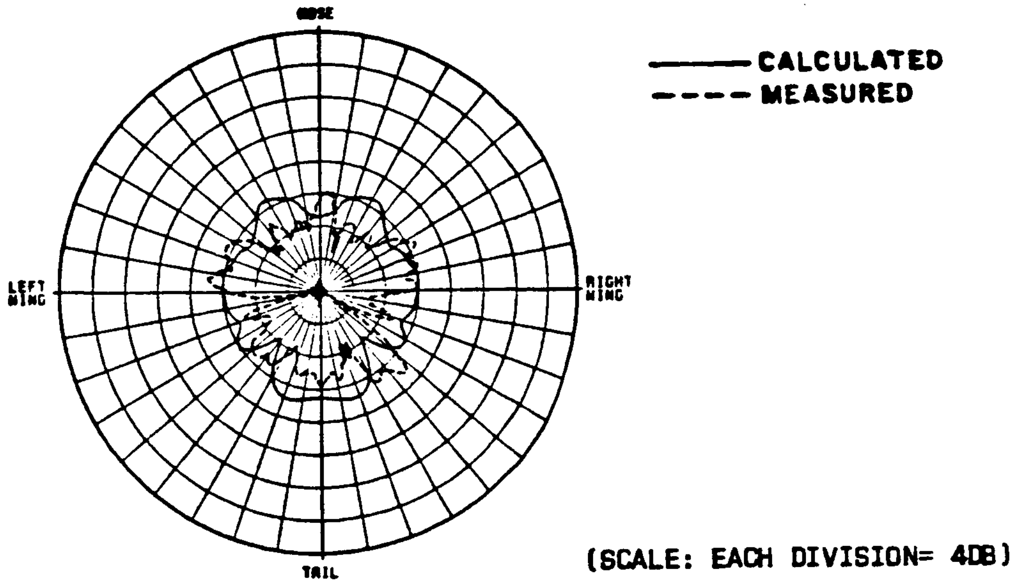

(a) E_θ

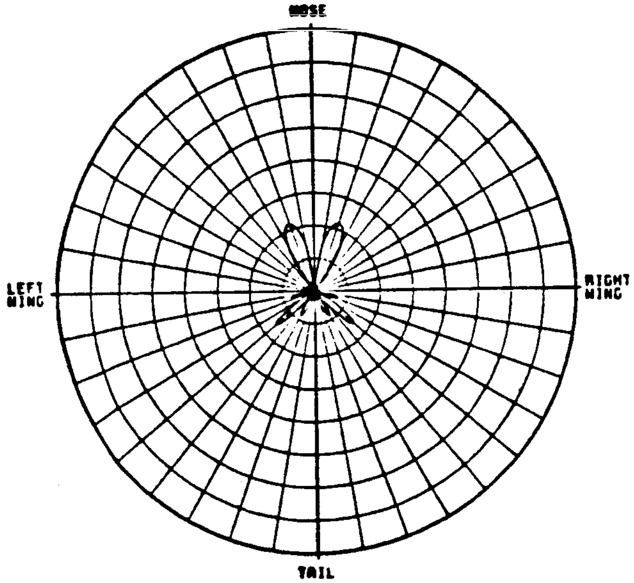

(b) E_ϕ

Figure 63. Azimuthal conical pattern (θ_p=10°) of a $\lambda/4$ monopole mounted on top of a F-16 fighter aircraft.

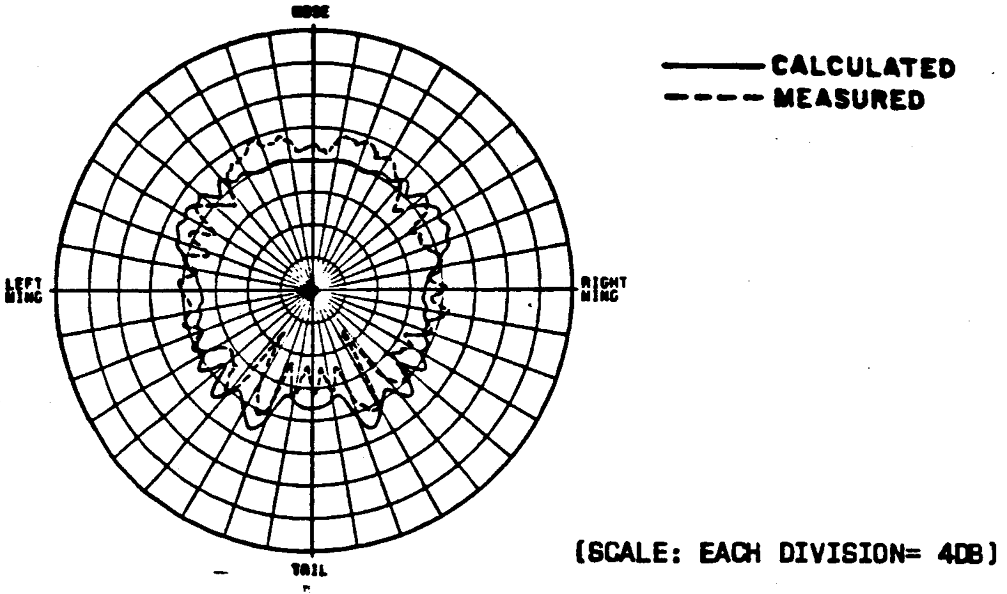

(a) E_θ

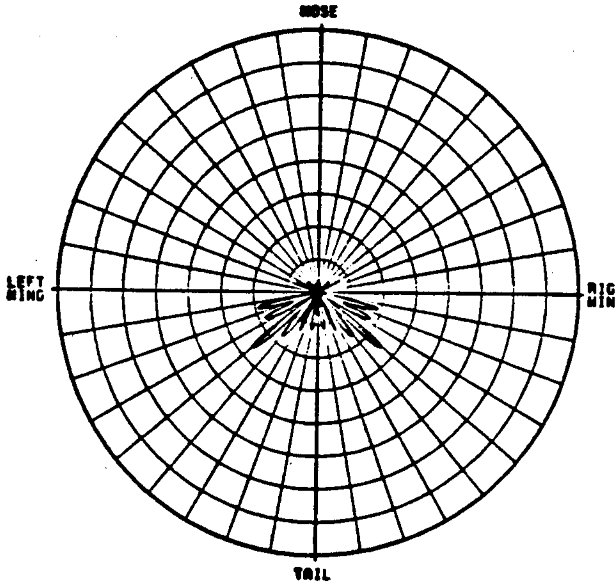

(b) E_ϕ

Figure 64. Azimuthal conical pattern (θ_p=20°) of a $\lambda/4$ monopole mounted on top of a F-16 fighter aircraft.

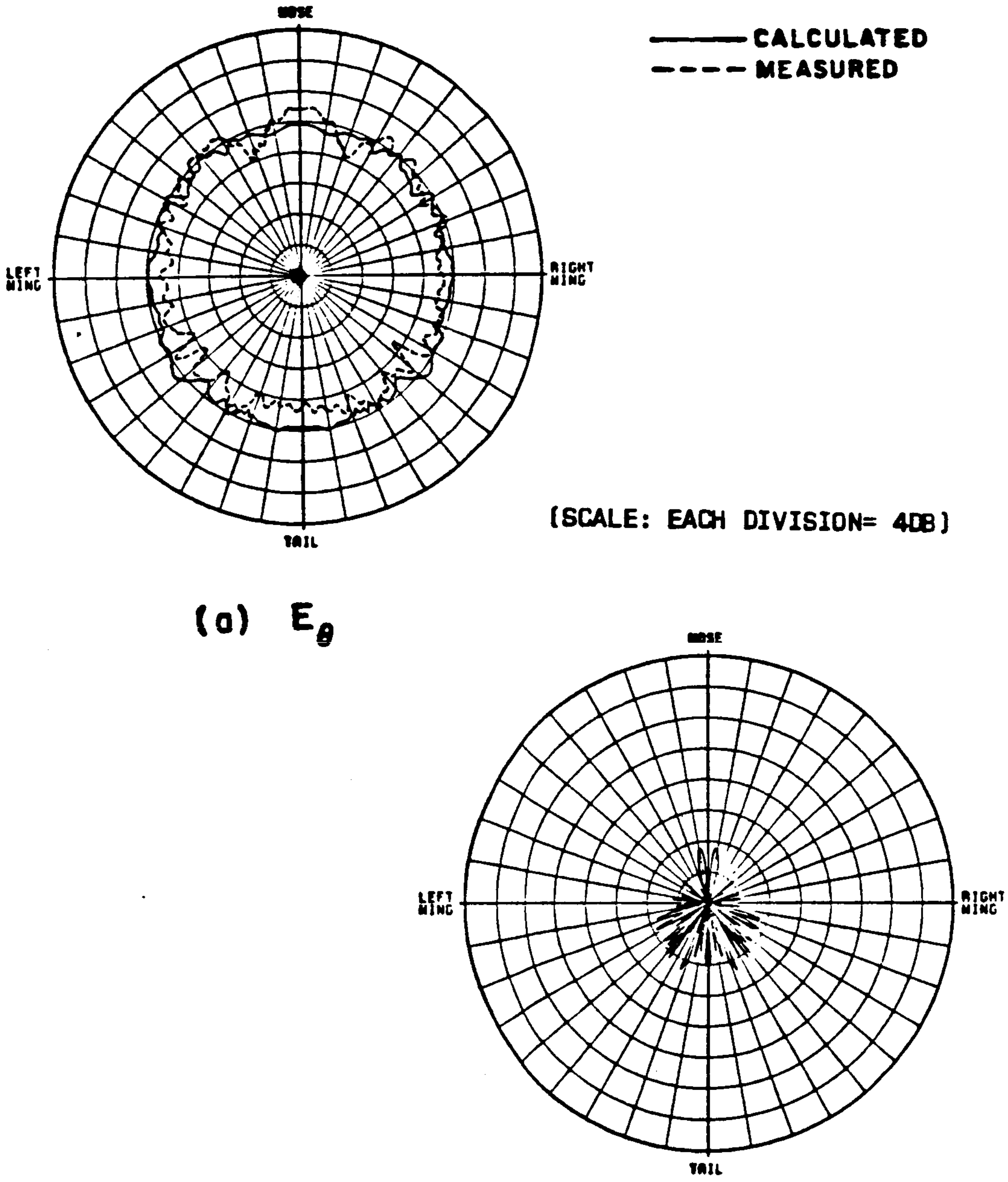

(a) E_θ

(b) E_ϕ

Figure 65. Azimuthal conical pattern (θ_p=30°) of a $\lambda/4$ monopole mounted on top of a F-16 fighter aircraft.

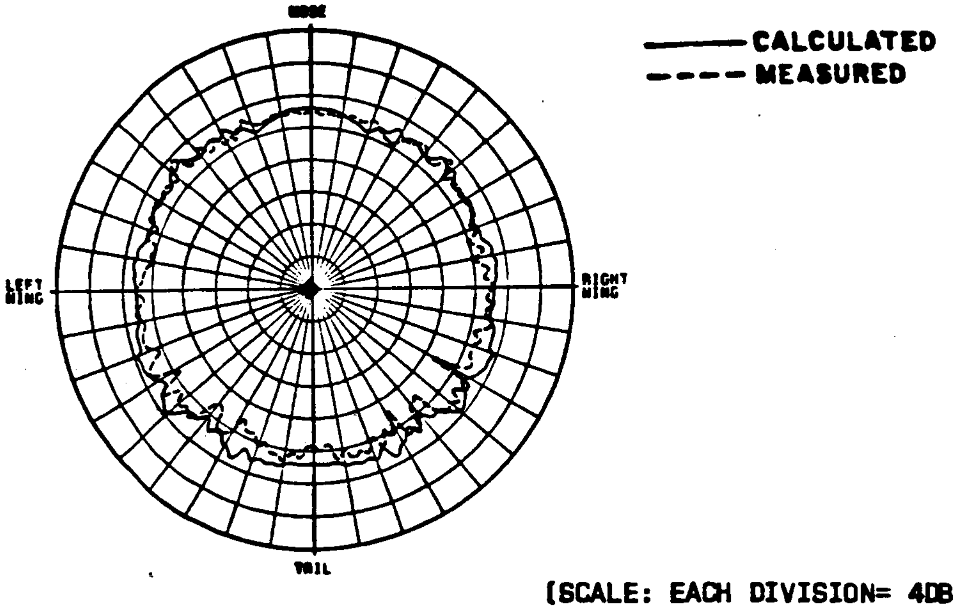

(a) E_θ

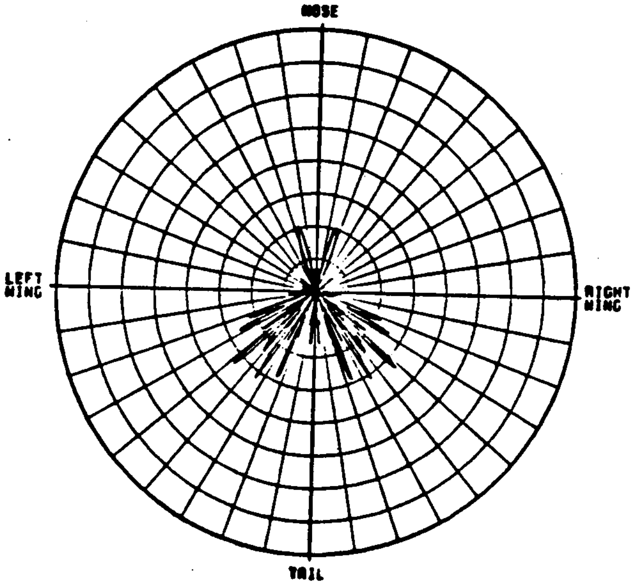

(b) E_ϕ

Figure 66. Azimuthal conical pattern (θ_p=40°) of a $\lambda/4$ monopole mounted on top of a F-16 fighter aircraft.

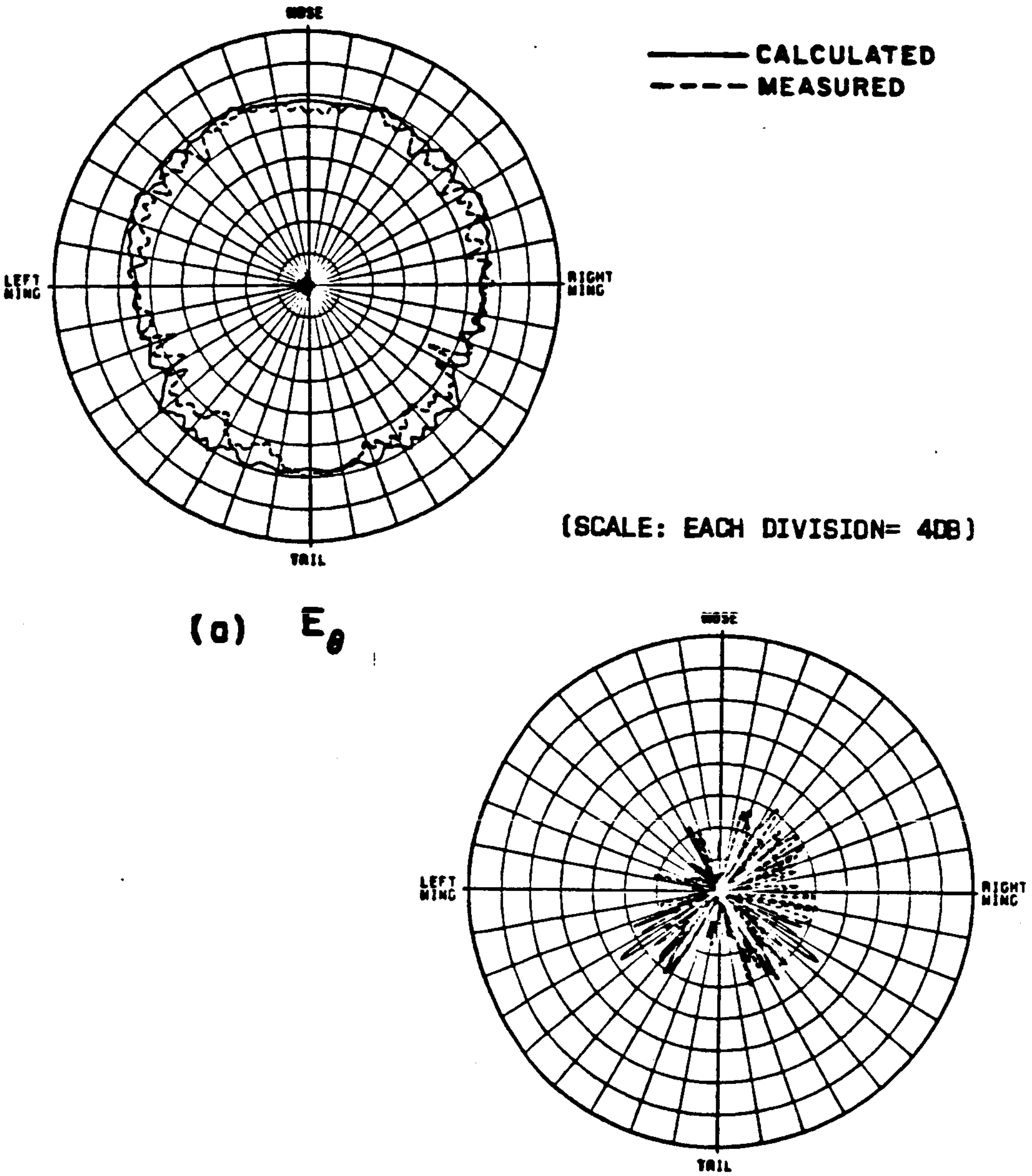

(a) E_θ

(b) E_ϕ

Figure 67. Azimuthal conical pattern (θ_p=45°) of a $\lambda/4$ monopole mounted on top of a F-16 fighter aircraft.

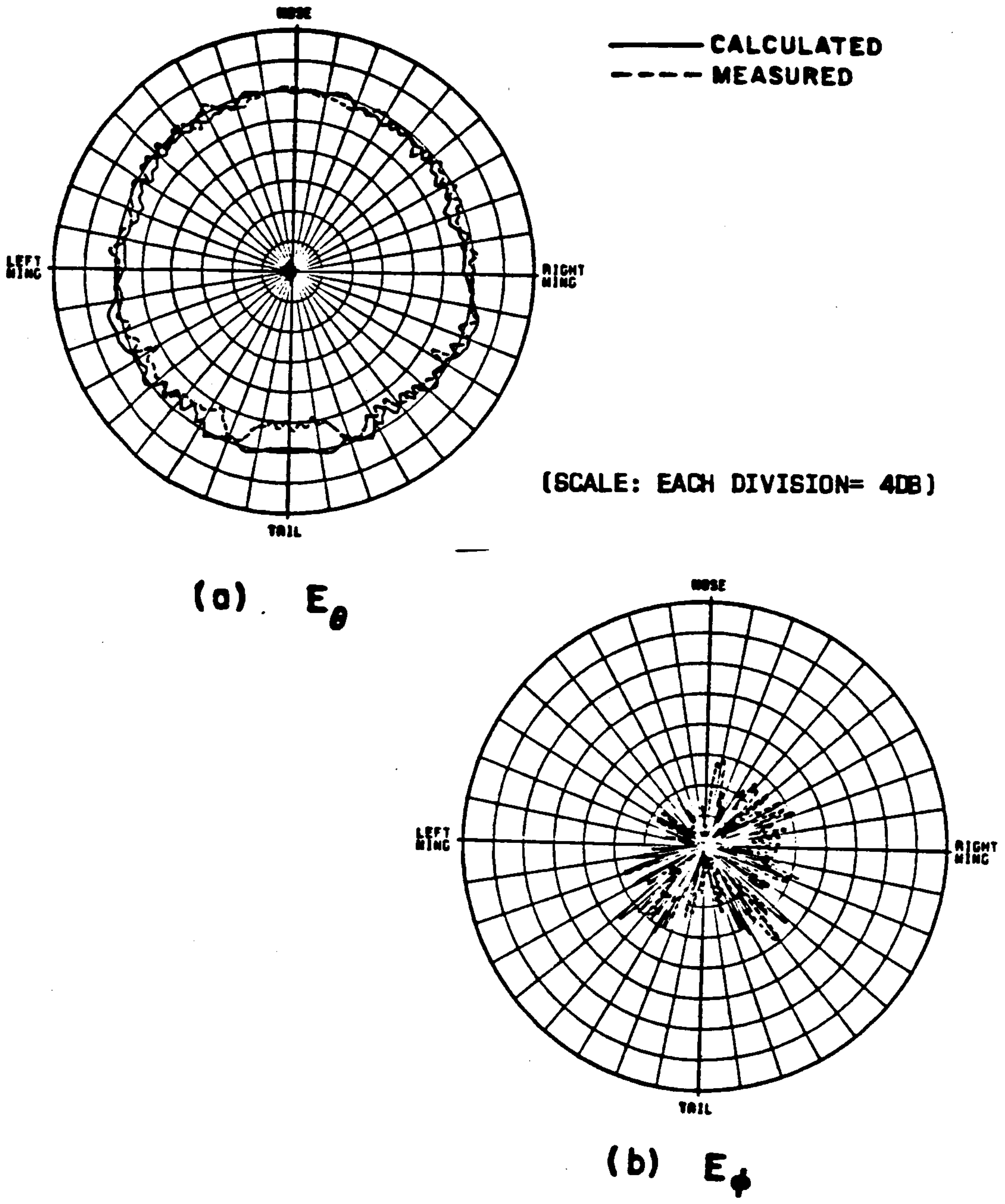

Figure 68. Azimuthal conical pattern (θ_p=50°) of a $\lambda/4$ monopole mounted on top of a F-16 fighter aircraft.

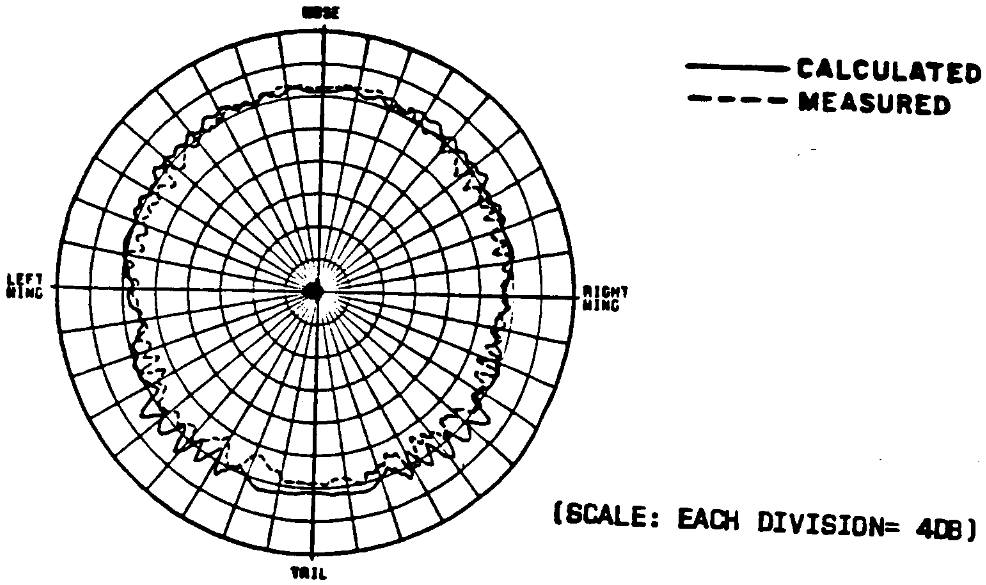

(a) E_θ

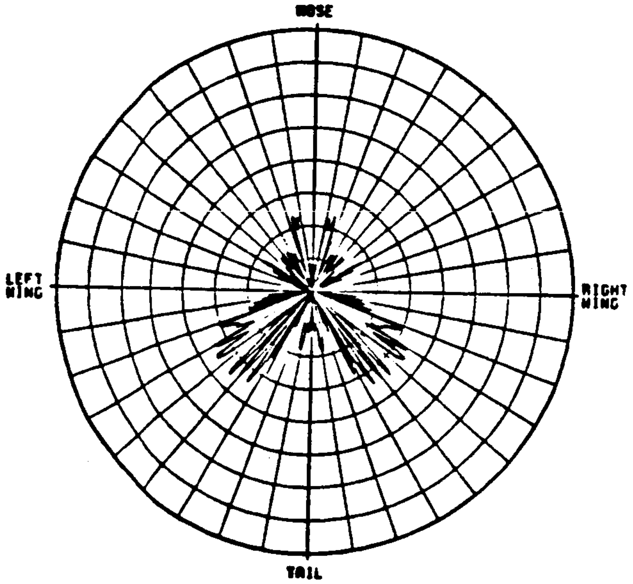

(b) E_ϕ

Figure 69. Azimuthal conical pattern (θ_p=55°) of a $\lambda/4$ monopole mounted on top of a F-16 fighter aircraft.

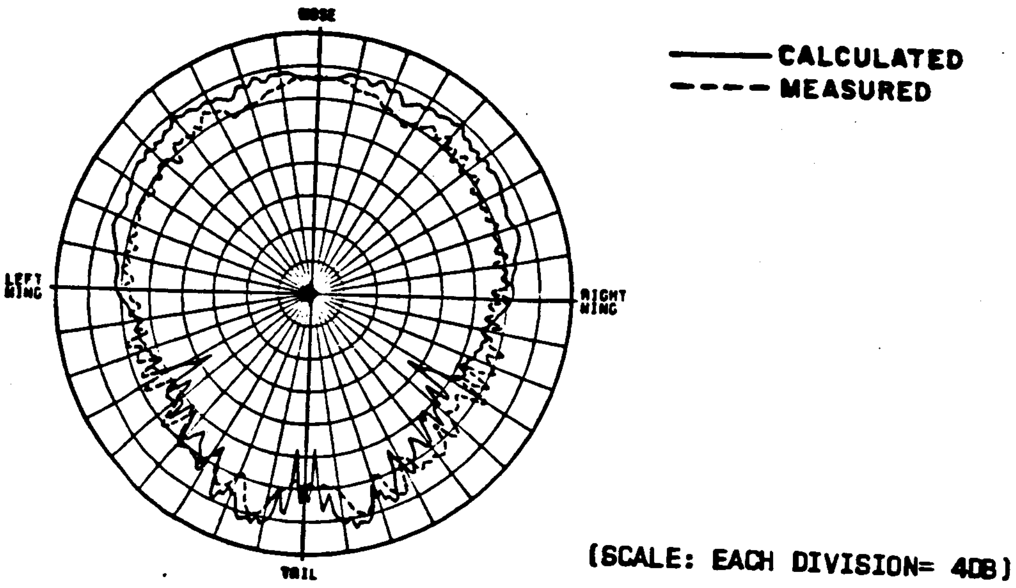

(a) E_θ

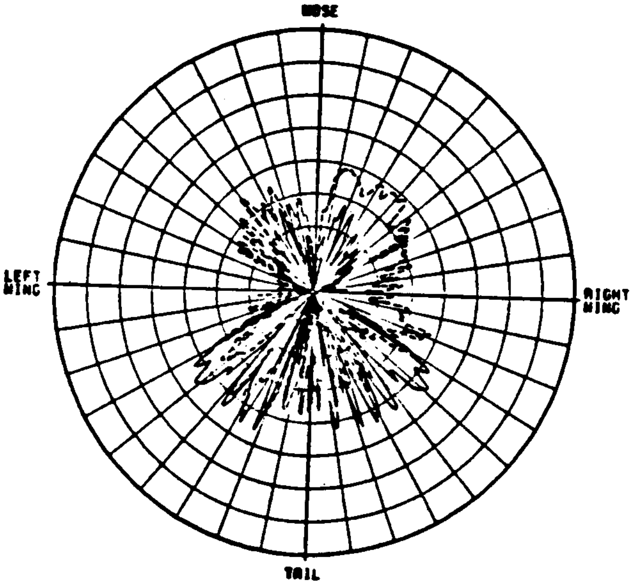

(b) E_ϕ

Figure 72. Azimuthal conical pattern (θ_p=70°) of a $\lambda/4$ monopole mounted on top of a F-16 fighter aircraft.

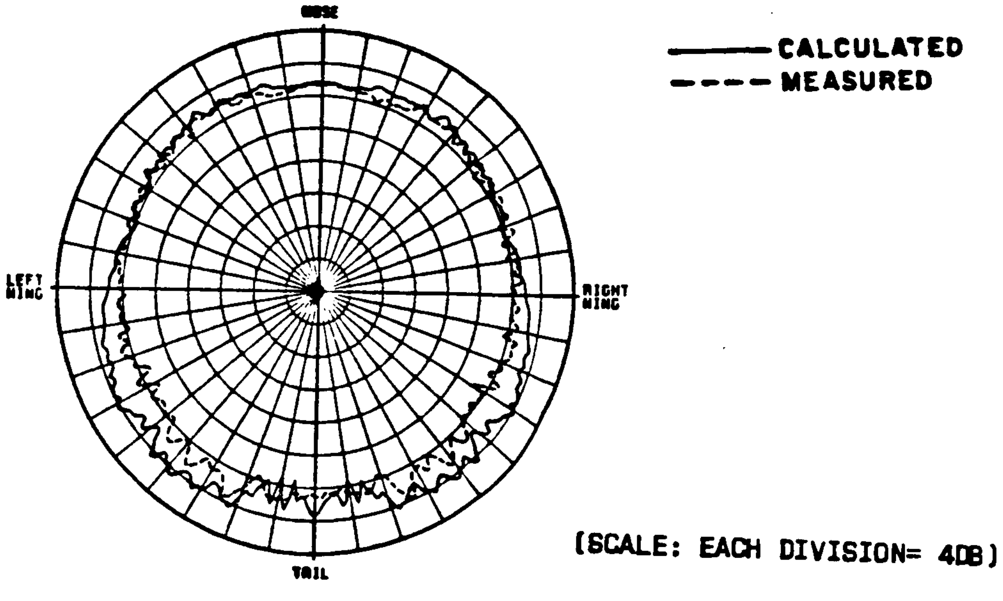

(a) E_θ

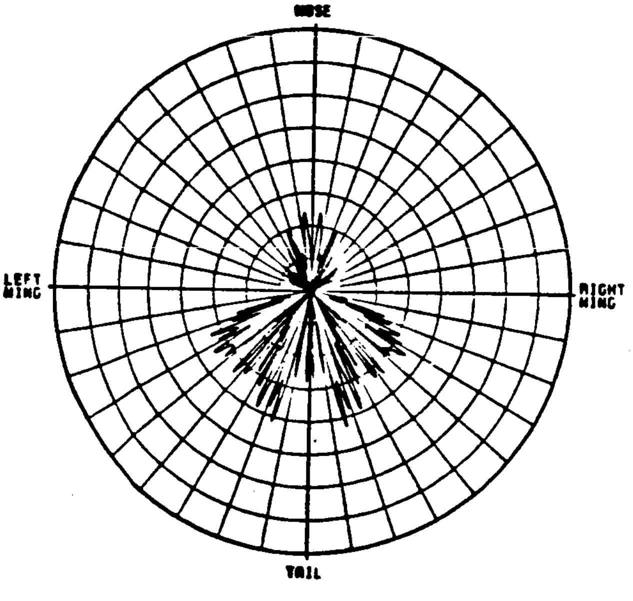

(b) E_ϕ

Figure 71. Azimuthal conical pattern (θ_p=65°) of a $\lambda/4$ monopole mounted on top of a F-16 fighter aircraft.

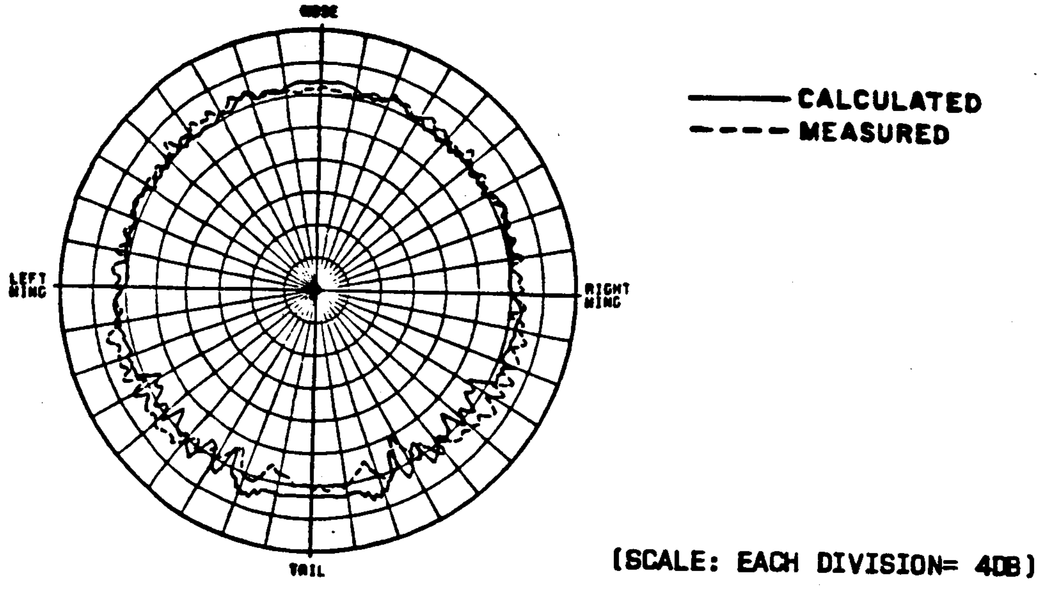

(a) E_θ

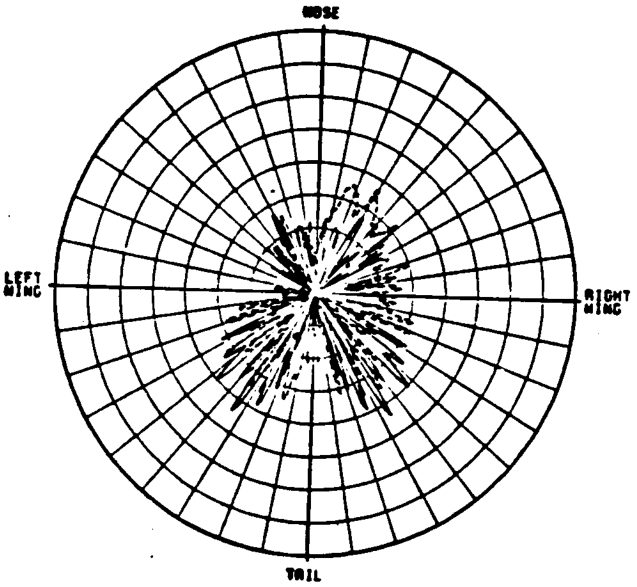

(b) E_ϕ

Figure 70. Azimuthal conical pattern (θ_p=60°) of a $\lambda/4$ monopole mounted on top of a F-16 fighter aircraft.

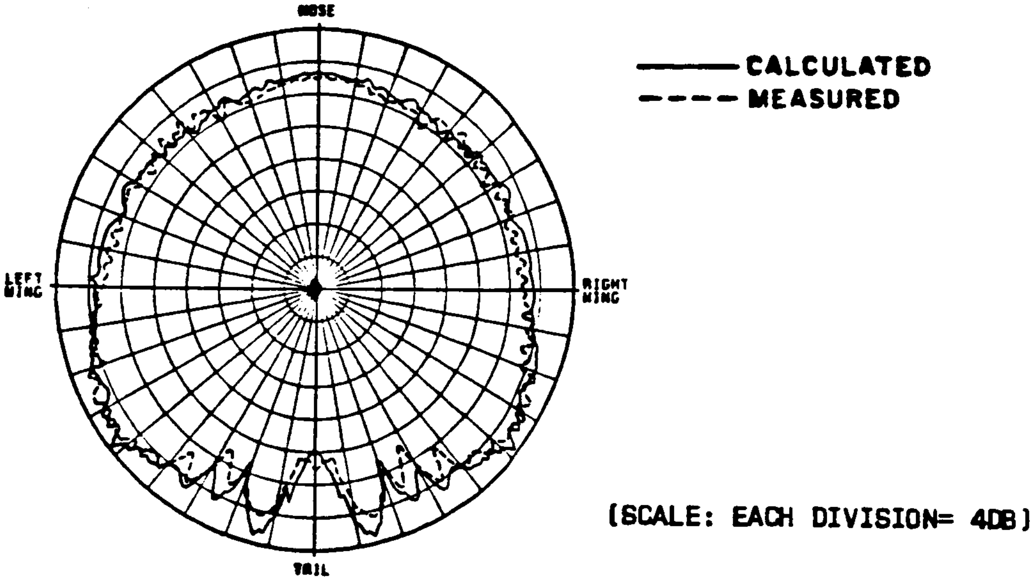

(a) E_θ

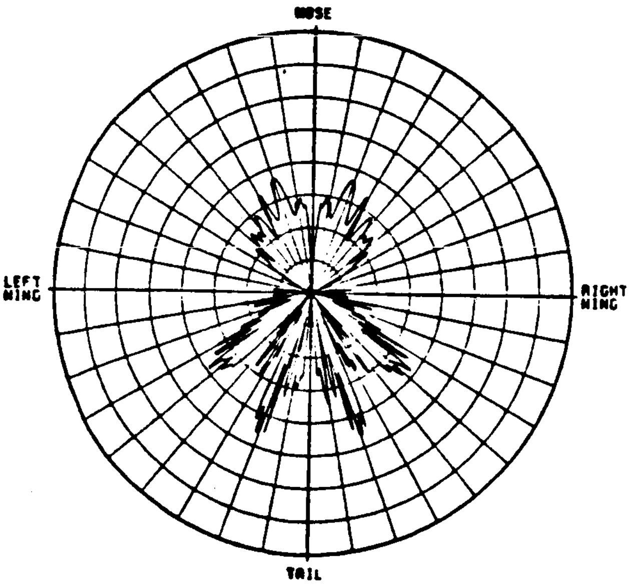

(b) E_ϕ

Figure 73. Azimuthal conical pattern (θ_p=75°) of a $\lambda/4$ monopole mounted on top of a F-16 fighter aircraft.

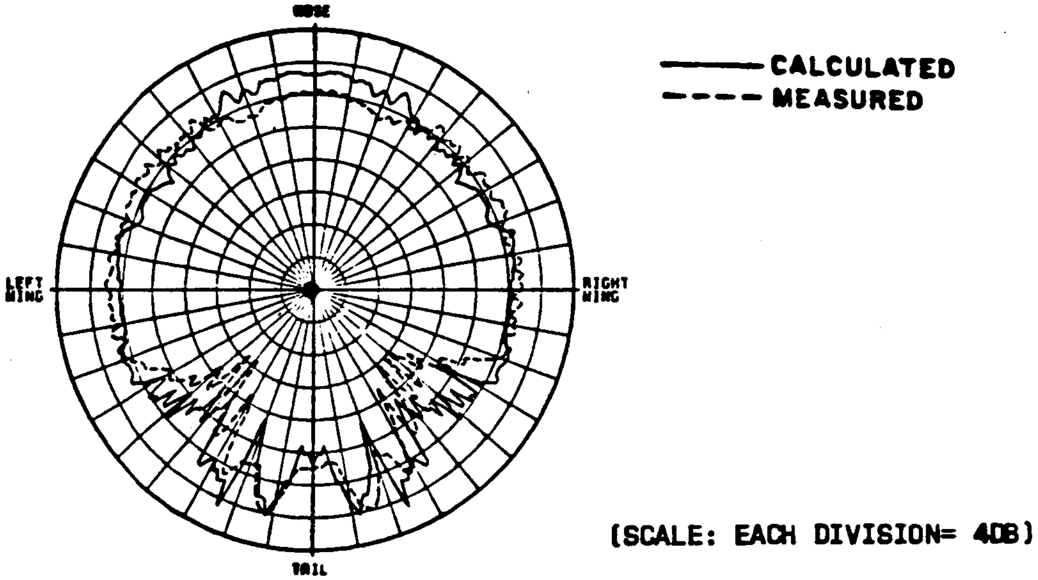

(a) E_θ

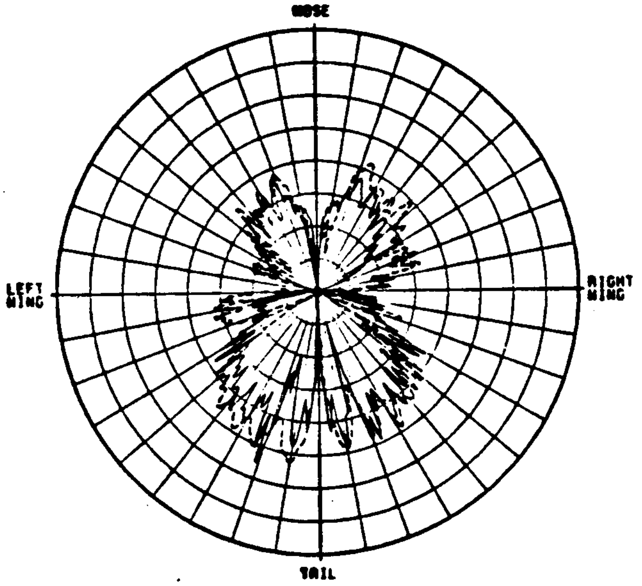

(b) E_ϕ

Figure 74. Azimuthal conical pattern (θ_p=80°) of a $\lambda/4$ monopole mounted on top of a F-16 fighter aircraft.

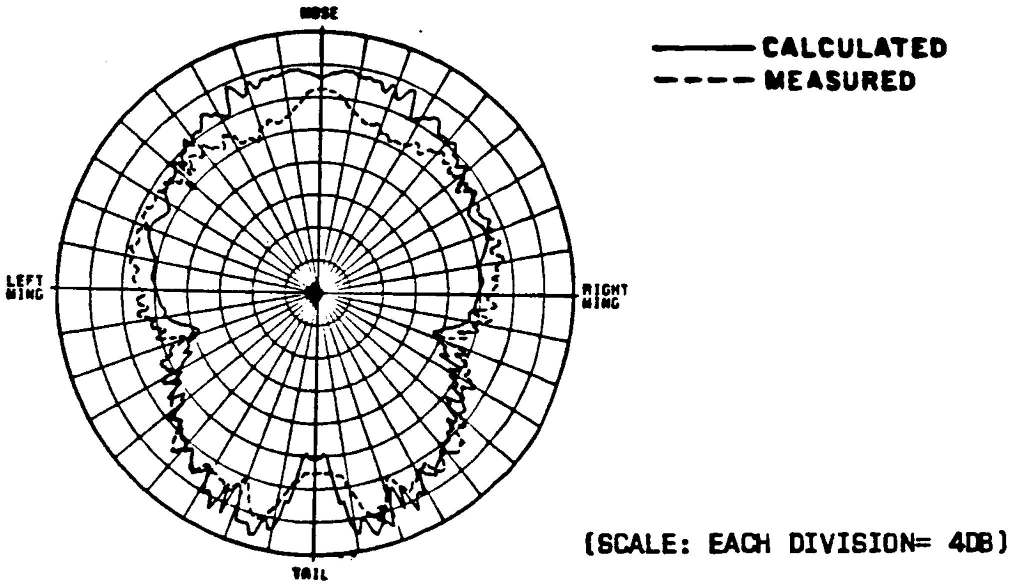

(a) E_θ

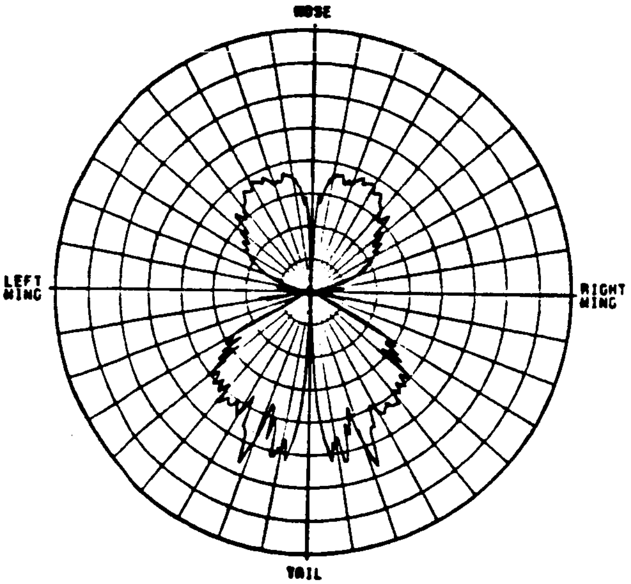

(b) E_ϕ

Figure 75. Azimuthal conical pattern (θ_p=85°) of a $\lambda/4$ monopole mounted on top of a F-16 fighter aircraft.

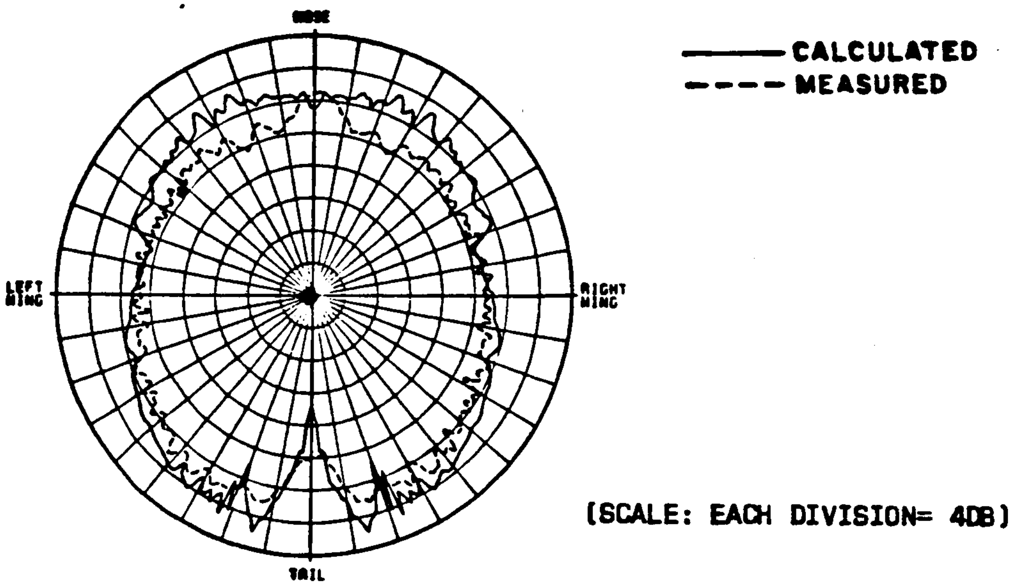

(a) E_θ

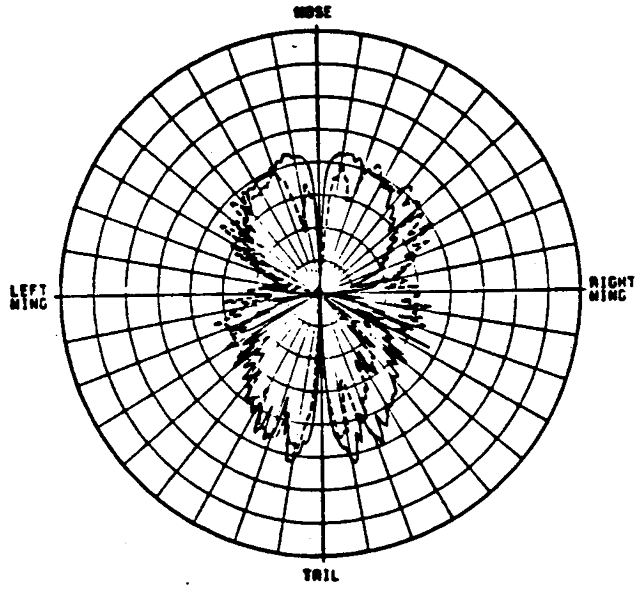

(b) E_ϕ

Figure 76. Azimuthal conical pattern (θ_p=90°) of a $\lambda/4$ monopole mounted on top of a F-16 fighter aircraft.

c-3

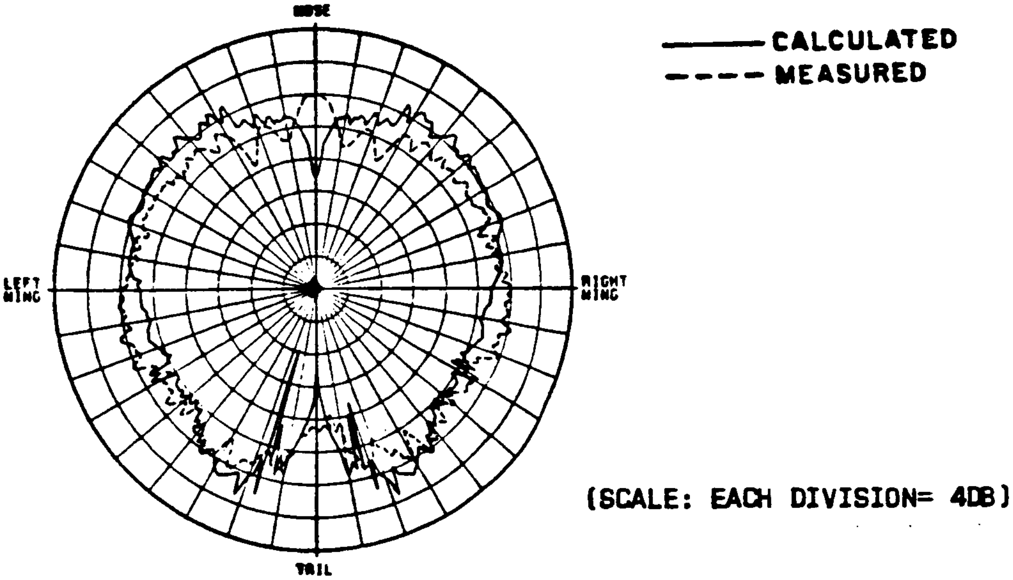

(a) E_θ

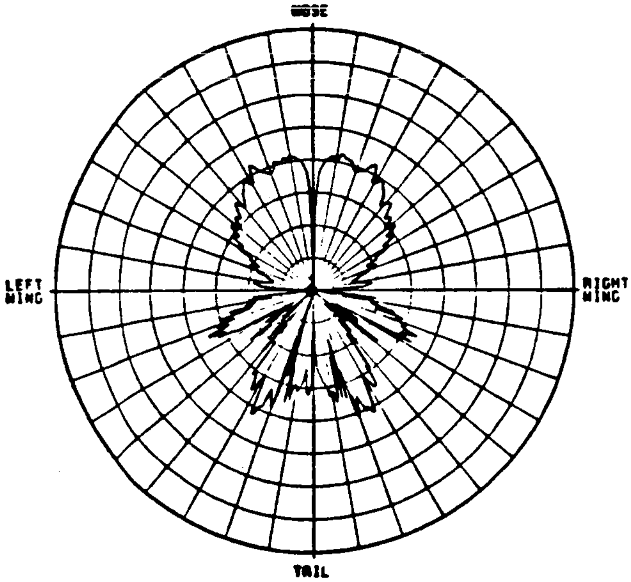

(b) E_ϕ

Figure 77. Azimuthal conical pattern (θ_p=95°) of a $\lambda/4$ monopole mounted on top of a F-16 fighter aircraft.

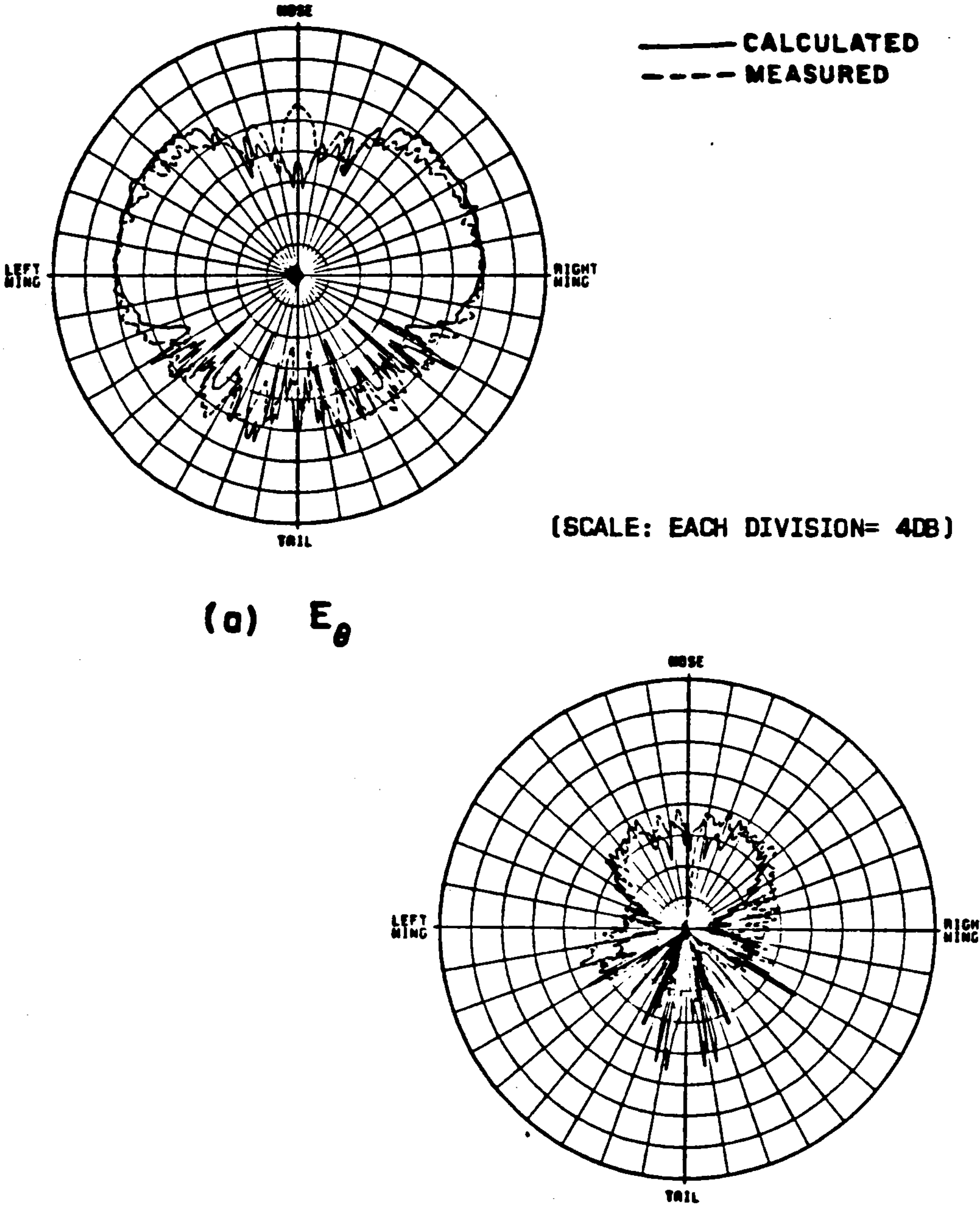

(a) E_θ

(b) E_ϕ

Figure 78. Azimuthal conical pattern (θ_p=100°) of a $\lambda/4$ monopole mounted on top of a F-16 fighter aircraft.

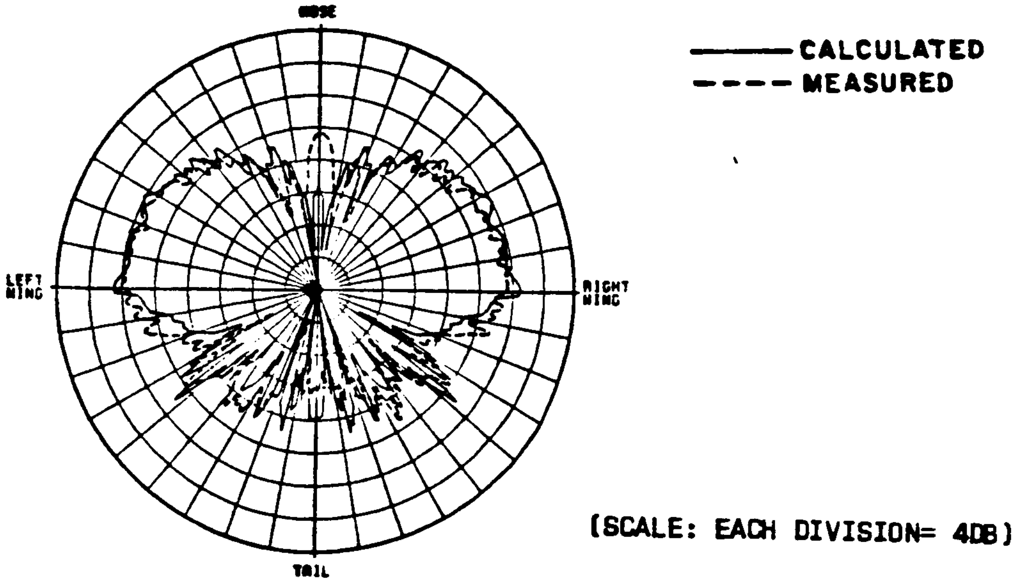

(a) E_θ

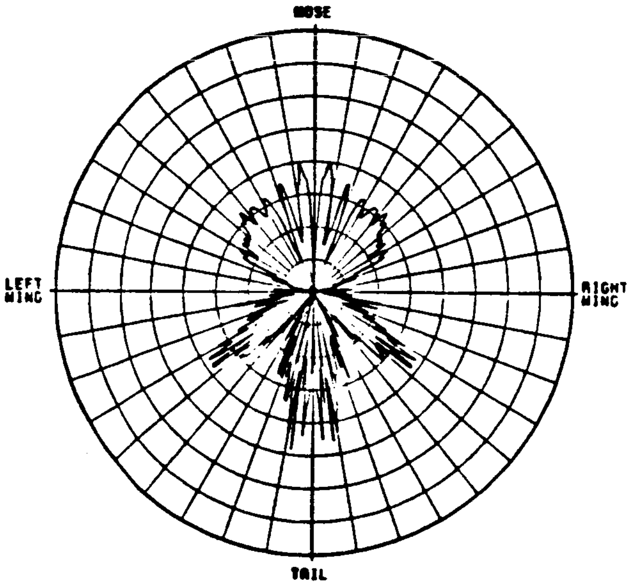

(b) E_ϕ

Figure 79. Azimuthal conical pattern (θ_p=105°) of a $\lambda/4$ monopole mounted on top of a F-16 fighter aircraft.

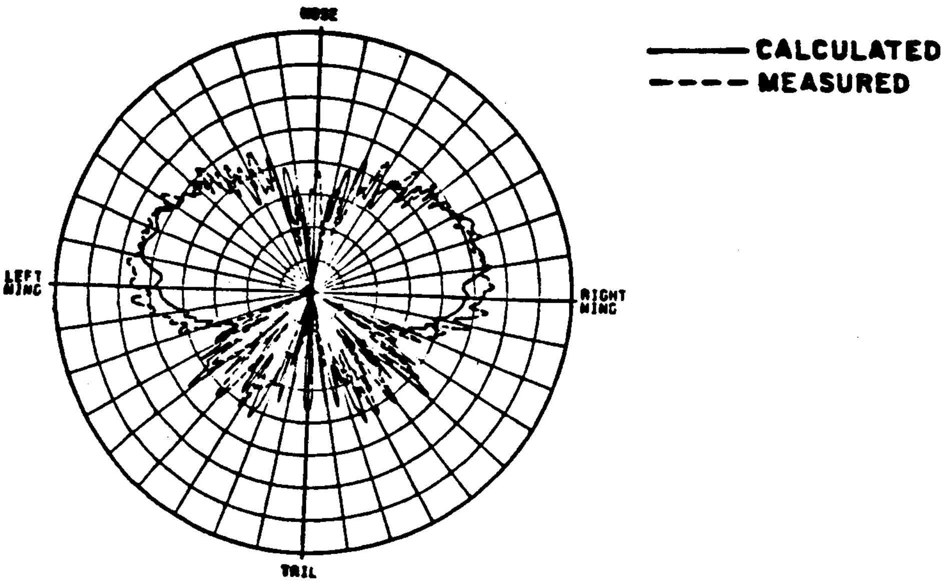

(a) E_θ

(SCALE: EACH DIVISION= 4DB)

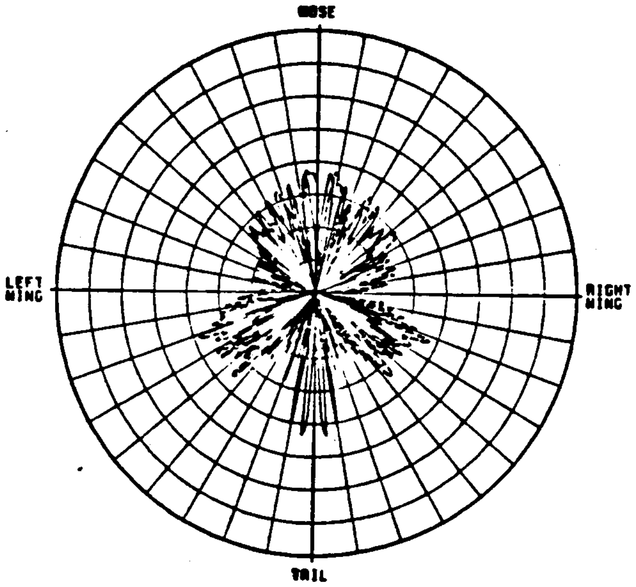

(b) E_ϕ

Figure 80. Azimuthal conical pattern (θ_p=110°) of a $\lambda/4$ monopole mounted on top of a F-16 fighter aircraft.

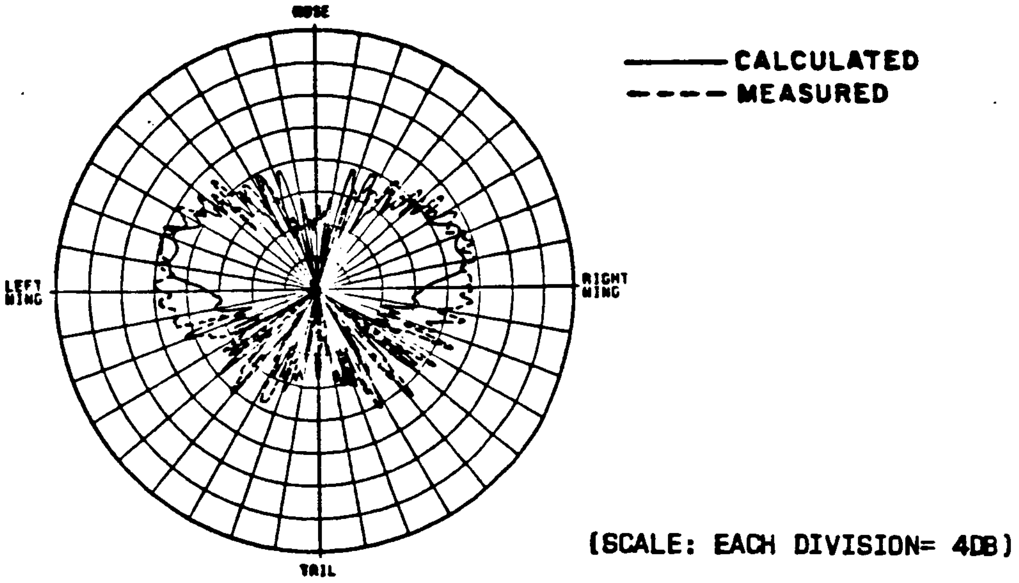

(a) E_θ

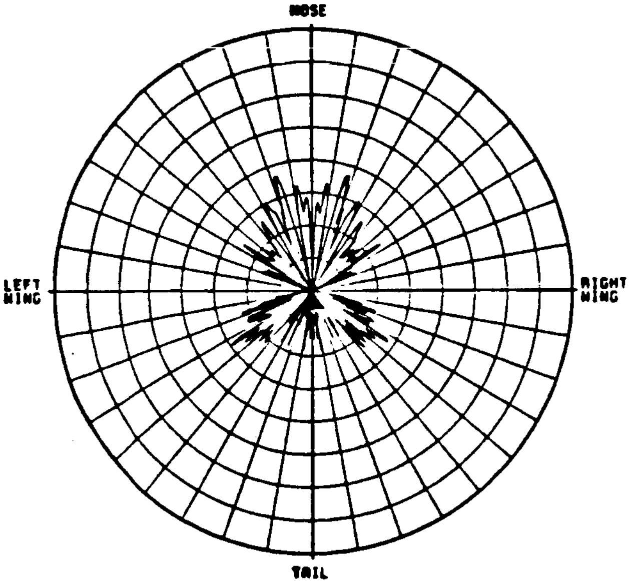

(b) E_ϕ

Figure 81. Azimuthal conical pattern (θ_p=115°) of a $\lambda/4$ monopole mounted on top of a F-16 fighter aircraft.

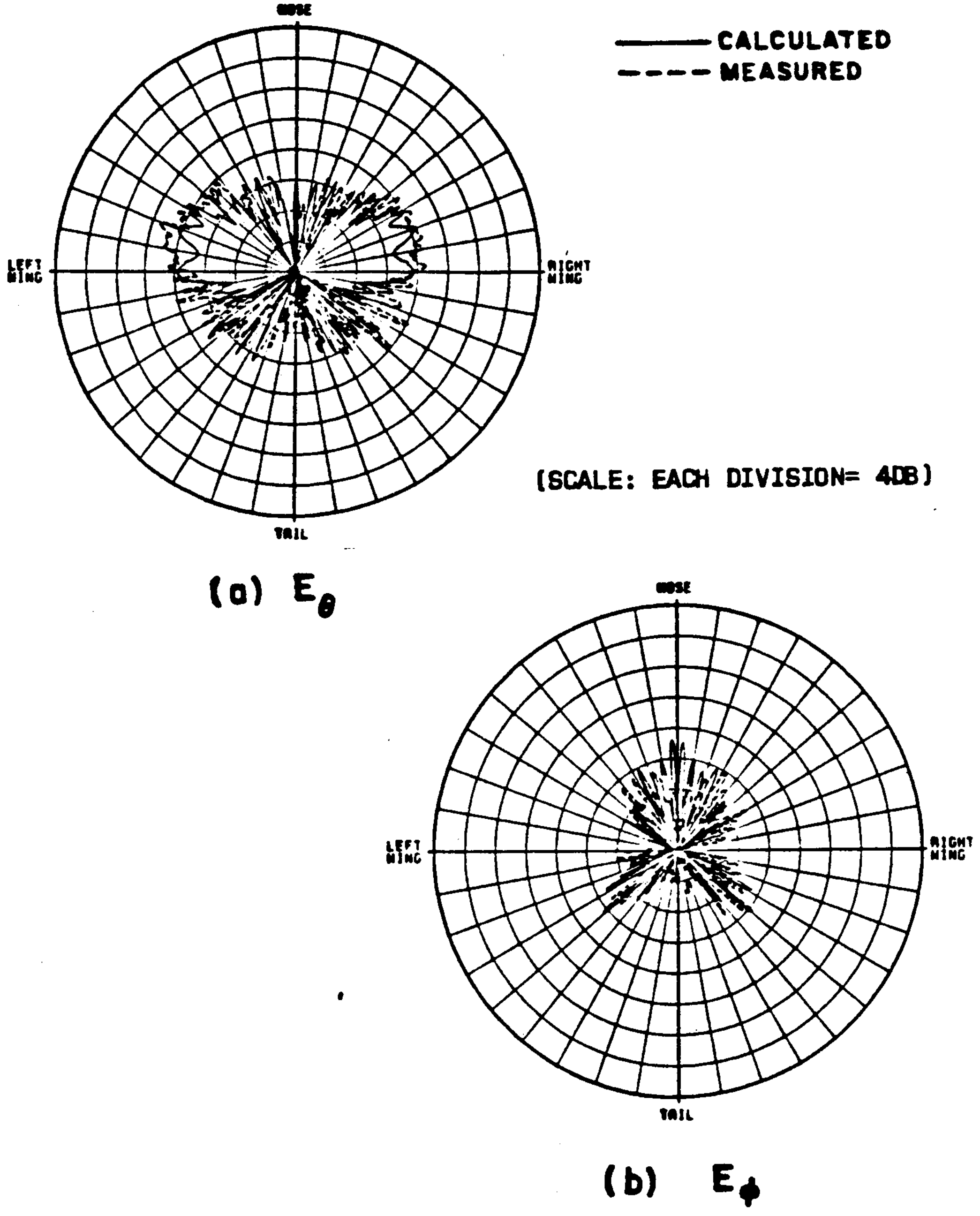

Figure 82. Azimuthal conical pattern (θ_p=120°) of a $\lambda/4$ monopole mounted on top of a F-16 fighter aircraft.

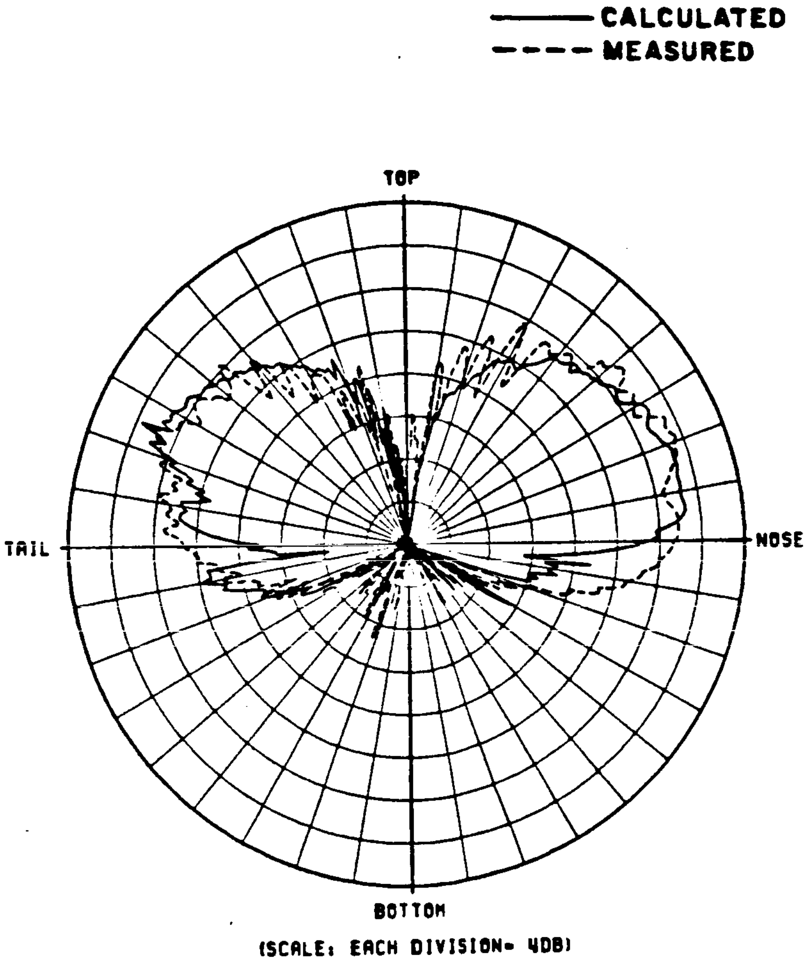

Figure 83. Elevation plane pattern of a λ/4 monopole mounted on top of a F-16 fighter.

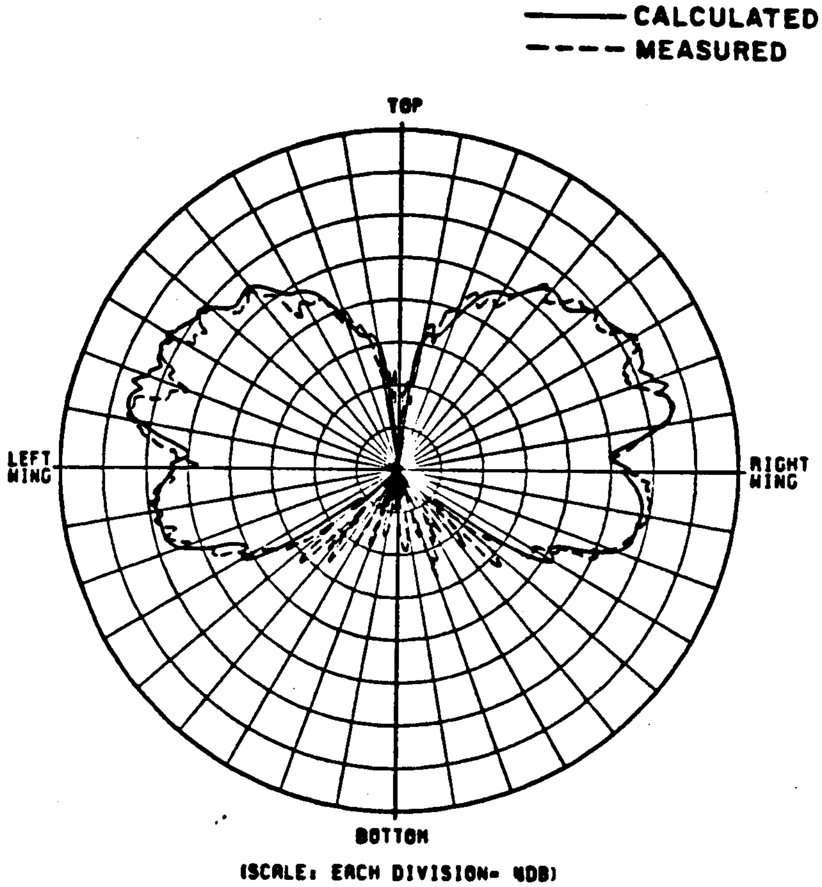

Figure 84. Roll plane pattern of a λ/4 monopole mounted on top of a F-16 fighter aircraft.

Example 10: Simulation of F-4 Fighter Aircraft

Consider a $\lambda/4$ monopole mounted on the bottom fuselage of an F-4 aircraft, which is loaded with armament, and operated at a frequency of .375 MHz. The measured data was obtained at the RADC Newport antenna range. The line drawings and the computer model of the F-4 aircraft are illustrated in Figure 85 and 86, respectively. Note that since the antenna is mounted on the belly of an aircraft, the coordinates are defined so as to associate with the bottom part of the aircraft. Consequently, the geometry of the F-4 in our computer model, as well as the pattern coordinate systems, are turned upside down. In fact, for the θ_p=75° pattern computed here, the actual pattern angle from the vertical is 180° - 75° or 105°. The input data is as follows:

```
UN: INCHES
3
FQ: FREQUENCY 375 MHZ
1,.375,1.
FG: F-4 FUSELAGE
5.,20.,300.,250.
F
0.,0.,0.
SG: MONOPOLE
0.,-200.
1
0.,0.
.414,.828,0.,7.87,3
1.,0.
PG: LEFT WING
6,T
-2.,18.,-133.
-2.,50.,-133.
-2.,50.,-70.
-2.,230.,119.
-2.,230.,167.
-2.,18.,136.
```

```
PG: RIGHT WING
6,T
-2.,-18.,136.
-2.,-230.,167.
-2.,-230.,119.
-2.,-50.,-70.
-2.,-50.,-133.
-2.,-18.,-133.
PG:LEFT ENGINE INTAKE
4,T
-2.,18.,-133.
-2.,50.,-133.
-4.,50.,-133.
-4.,18.,-133.
PG:RIGHT ENGINE INTAKE
4,T
-4.,-18.,-133.
-4.,-50.,-133.
-2.,-50.,-133.
-2.,-18.,-133.
```

```
PG:FUSELAGE BLOCKAGE
6,T
4.,9.,-50.
15.,13.,-50.
25.,6.,-50.
25.,-6.,-50.
15.,-13.,-50.
4.,-9.,-50.
PG:LEFT ENGINE INTAKE
4,F
-4.,50.,-133.
-52.,50.,-133.
-52.,18.,-133.
-4.,18.,-133.
PG: RIGHT ENGINE INTAKE
4,F
-4.,-18.,-133.
-52.,-18.,-133.
-52.,-50.,-133.
-4.,-50.,-133.
PG: LEFT MISSILE PYLON
4,F
20.,72.,-45.
0.,72.,-45.
0.,72.,-117.
20.,72.,-117.
```

```
PG: RIGHT MISSILE PYLON
4,F
20.,-72.,-117.
0.,-72.,-117.
0.,-72.,-45.
20.,-72.,-45.
PG:LEFT FUEL TANK
4,F
36.,127.,148.
0.,127.,148.
0.,127.,-77.
36.,127.,-77.
PG: RIGHT FUEL TANK
4,F
36.,-127.,-77.
0.,-127.,-77.
0.,-127.,148.
36.,-127.,148.
PP: POLAR PLOT
T
1,2.9,3
PD:AZIMUTH CONICAL PATTERN
90.,0.,75.
0,360,1
F,5000.
EX:
```

The azimuthal conical pattern is compared with measured data in Figure 87. Although there exists some discrepancy, the general shape of the two patterns are in good agreement.

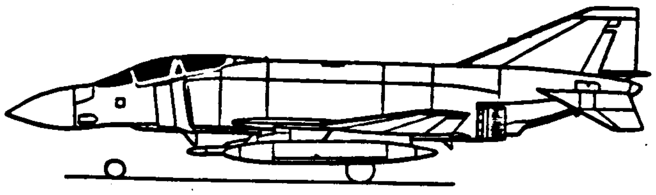

(a) SIDE VIEW

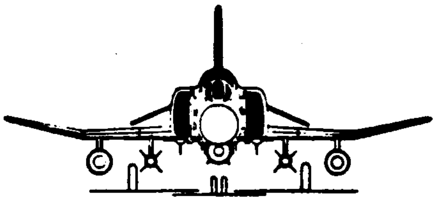

(b) FRONT VIEW

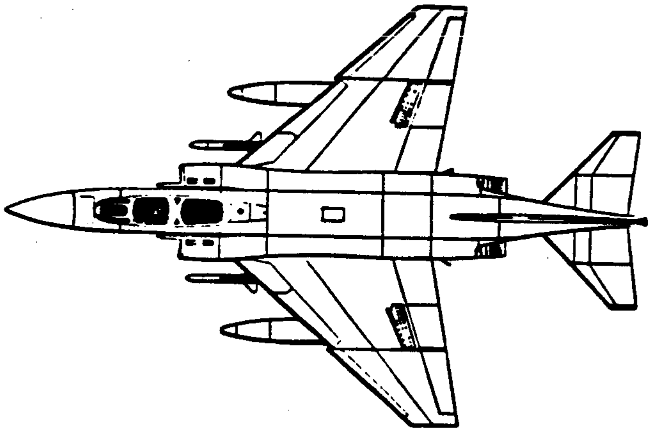

(c) TOP VIEW

Figure 85. F-4 (Phantom) fighter aircraft.

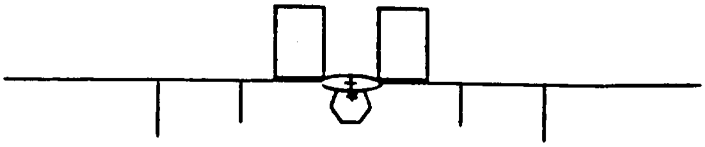

(a) FRONT VIEW

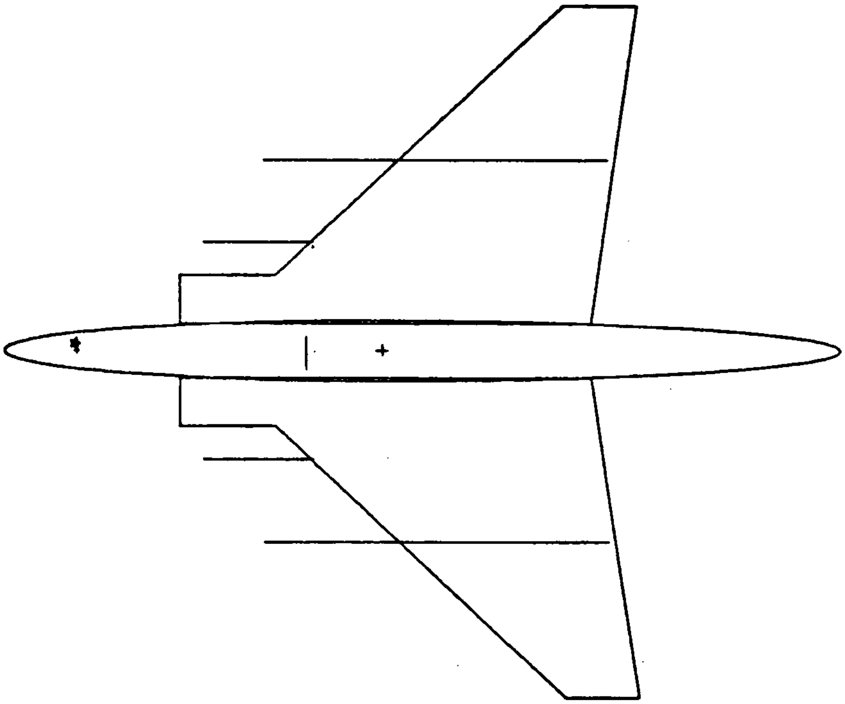

(b) BOTTOM VIEW

Figure 86. Computer simulated model of a F-4 Phantom fighter aircraft.

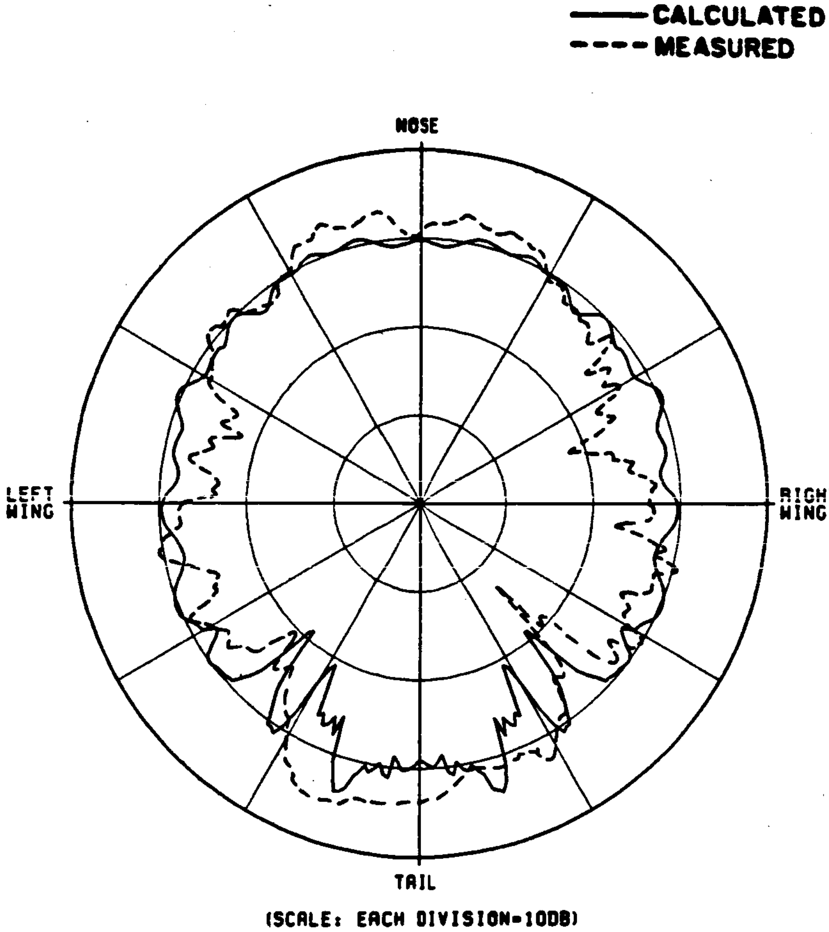

Figure 87. Azimuthal conical pattern (θ_p=105°) of a $\lambda/4$ monopole mounted on the belly of a F-4 fighter aircraft.

Example 11: Simulation of an A-10 Aircraft

Consider four monopoles mounted on the belly of an A-10 aircraft as shown in Figure 88. Each monopole is spaced a half wavelength apart. The mutual coupling between the monopoles is significant and cannot be neglected in the pattern calculations. The excitation including the coupling effect on the radiators is obtained using the thin-wire moment method [4]. The computer model based on the input data is shown in Figure 89. The input data is as follows:

```
UN: INCHES
3
FQ: 17.576 GHZ
1,17.576,1
FG: A-10 FUSELAGE
0.117,0.425,8.05,2.62
F
0.,0.,0.
SG: MONOPOLE ARRAY WITH COUPLING EFFECT INCLUDED IN CURRENT VALUE
0.,-1.29
4
.336,180.
0.,0.,0.,0.168,3
.272,14.
.336,0.
0.,0.,0.,0.168,3
.272,14.
.168,270.
0.,0.,0.,0.168,3
1.0,-3.0
.504,270.
0.,0.,0.,0.168,3
.272,14.
PG: LEFT WING INNER PLATE
4,T
0.05,.425,.07
0.05,1.86,.07
0.05,1.86,2.
0.05,.425,2.
PG: RIGHT WING INNER PLATE
4,T
0.05,-.425,2.
0.05,-1.86,2.
0.05,-1.86,.07
0.05,-.425,.07
```

ORIGINAL PAGE IS
OF POOR QUALITY

```
PG: LEFT WING OUTER PLATE
4,F
0.05,1.86,.07
-.45,5.6,.49
-0.45,5.6,1.77
0.05,1.86,2.
PG: RIGHT WING OUTER PLATE
4,F
0.05,-1.86,2.
-.45,-5.6,1.77
-.45,-5.6,.49
0.05,-1.86,.07
PG: LEFT FUEL TANK
4,F
0.05,1.58,-.6
.30,1.58,-.6
.30,1.58,2.
0.05,1.58,2.
PG:LEFT FUEL TANK
4,F
.30,1.58,-.6
.59,1.86,-.6
.59,1.86,2.
.30,1.58,2.
PG: RIGHT FUEL TANK
4,F
.30,-1.58,2.
.59,-1.86,2.
.59,-1.86,-.6
.30,-1.58,-.6
PG: RIGHT FUEL TANK
4,F
0.05,-1.58,2.
.30,-1.58,2.
.30,-1.58,-.6
0.05,-1.58,-.6
```

```
PG: PYLON 1
4,F
.4,0.53,1.61
.05,0.53,1.61
.05,0.53,.56
.4,0.53,.33
PG: PYLON 2
4,F
.4,-.53,.33
.05,-.53,.56
.05,-.53,1.61
.4,-.53,1.61
PG: PYLON 3
4,F
.4,1.05,1.61
.05,1.05,1.61
.05,1.05,.56
.4,1.05,.3
PG: PYLON 4
4,F
.4,-1.05,.3
.05,-1.05,.56
.05,-1.05,1.61
.4,-1.05,1.61
PD: AZIMUTH CONICAL PATTERN
90.,0.,75.
0,360,1
T,6000.
PP:
T
1,2.5,3
EX:
```

The azimuthal conical patern (θ_p=105°) is compared with the measured data obtained at the RADC Newport site in Figure 90. The result shows good engineering agreement.

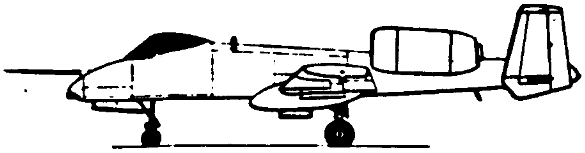

(a) SIDE VIEW

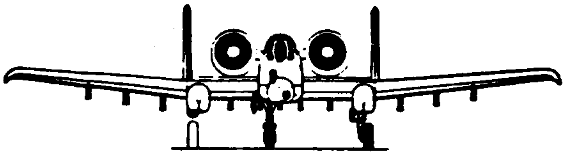

(b) FRONT VIEW

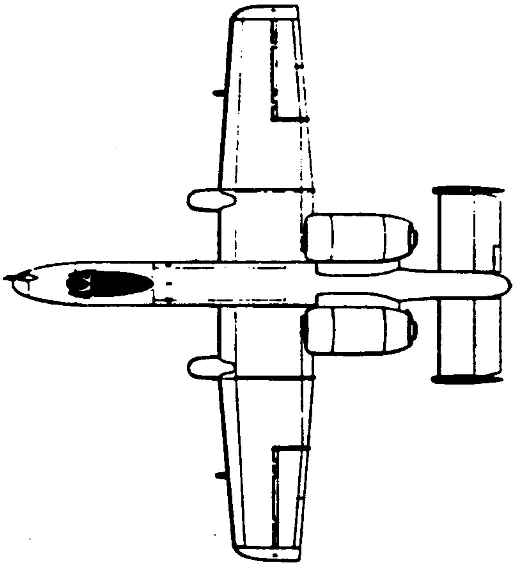

(c) TOP VIEW

Figure 88. A-10 aircraft.

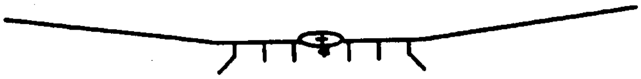

(a) FRONT VIEW

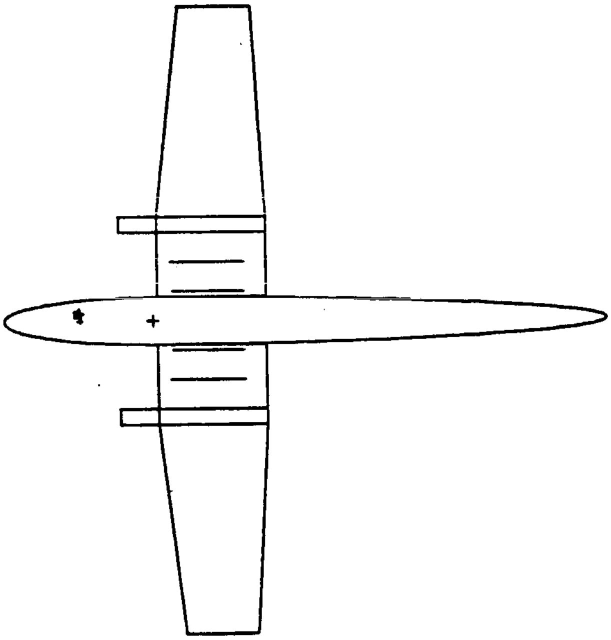

(b) BOTTOM VIEW

Figure 89. Computer simulated model of an A-10 aircraft.

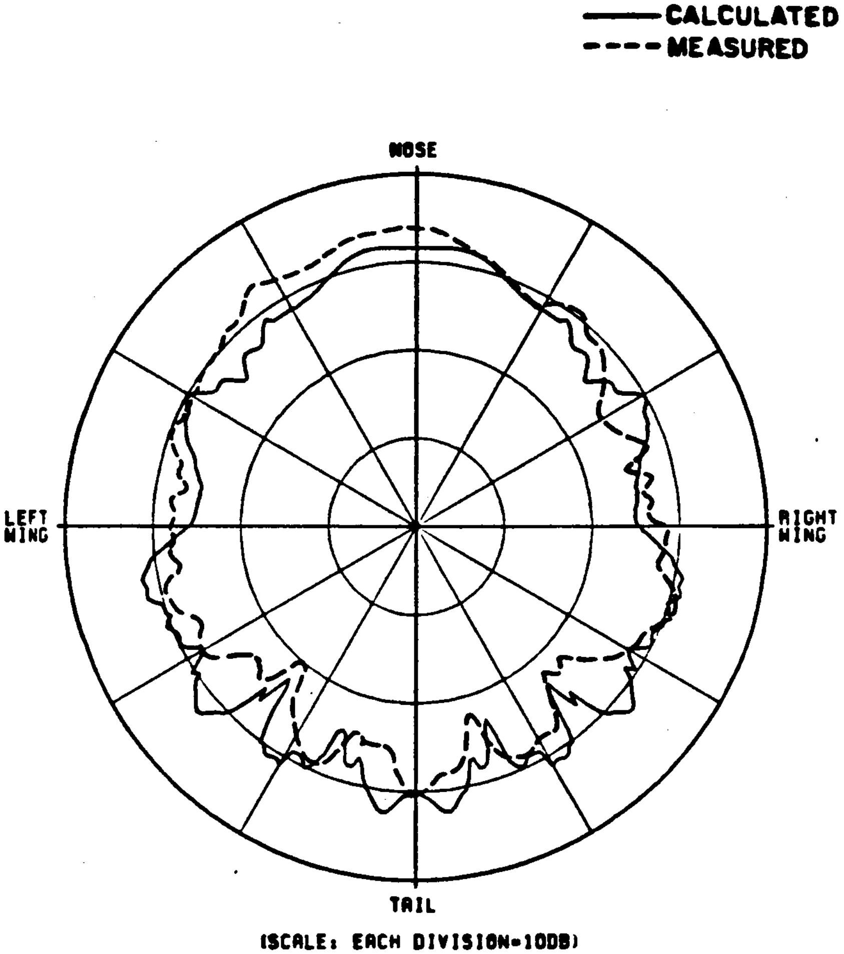

Figure 90. Azimuthal conical pattern (θ_p=105°) of four monopoles mounted on the belly of a A-10 aircraft.

Example 12: Simulation of C-141 Aircraft

Consider a monopole mounted on the top of a C-141 aircraft. The line drawings and the computer model of the C-141 are shown in Figures 91 and 92, respectively. The input data is as follows:

```
UN: FEET
2
FG: C141 FUSELAGE GEOMETRY
7.37,8.37,90.,46.05
F
0.,0.,0.
FQ: 2.52 GHZ
1.,2.52,1.
SG: SOURCE GEOMETRY
0.,0.
1
0.,0.
0.2,0.5,0.,0.09,3
1.,0.
PG: WING ON POSITIVE SIDE
5,T
6.0,7.37,-7.4
6.0,78.6,27.04
6.0,78.6,36.86
6.0,30.7,24.6
6.0,7.37,23.1
PG: WING ON NEGATIVE SIDE
5,T
6.0,-7.37,23.1
6.0,-30.7,24.6
6.0,-78.6,36.86
6.0,-78.6,27.04
6.0,-7.37,-7.4
PG: VERTICAL STABILIZER POSITIVE SIDE
4,T
7.5,1.6465,88.11
24.58,1.,92.81
24.58,0.,77.45
7.5,0.,62.82
PG: VERTICAL STABILIZER NEGATIVE SIDE
4,T
7.5,0.,62.82
24.58,0.,77.45
24.58,-1.,92.81
7.5,-1.6465,88.11
```

```
PG: T-TAIL POSITIVE SIDE
4,F
24.58,1.,92.81
24.58.25.3,98.22
24.58,25.3,92.05
24.58,0.,77.45
PG: T-TAIL NEGATIVE SIDE
4,F
24.58,0.,77.45
24.58,-25.3,92.05
24.58,-25.3,98.22
24.58.-1.,92.81
PP: POLAR PLOT IN DB
T
1,1.42,3
PD: AZIMUTH PLANE PATTERN
90.,0.,90.
0,360,1
F,1000.
EX:
```

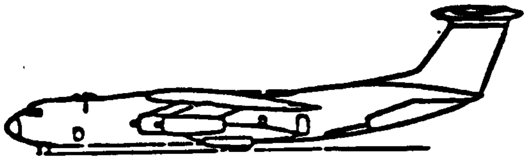

(a) SIDE VIEW

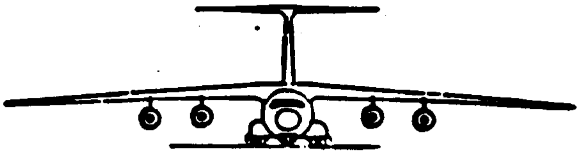

(b) FRONT VIEW

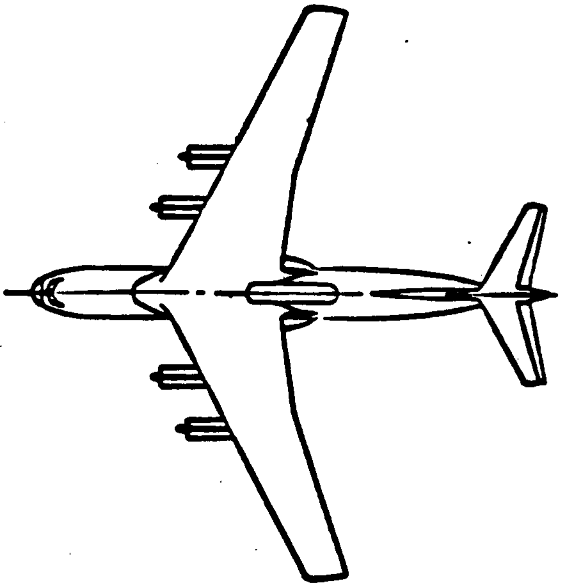

(c) TOP VIEW

Figure 91. C-141 aircraft.

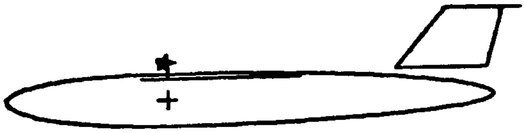

(a) SIDE VIEW

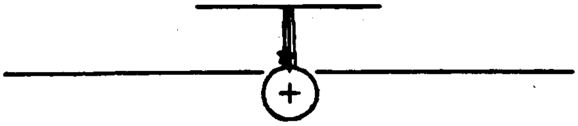

(b) FRONT VIEW

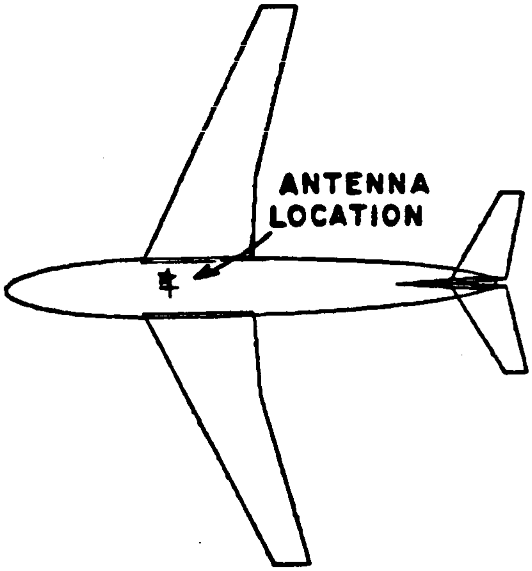
ANTENNA
LOCATION

(c) TOP VIEW

Figure 92. Computer simulated model of a C-141 aircraft.

Various azimuthal conical patterns (10°, 20°, 30°, 40°, 50°, 60°, 70°, 80°, 90°, 100°, see Figure 10(c)) and the elevation plane pattern are computed and compared with measured results as shown in Figures 93 and 94, respectively. The experimental work was performed at General Dynamics (San Diego, California) using a 1/10 scale model of a C-141 aircraft. The calculated results compare very favorably with the scale model measurements.

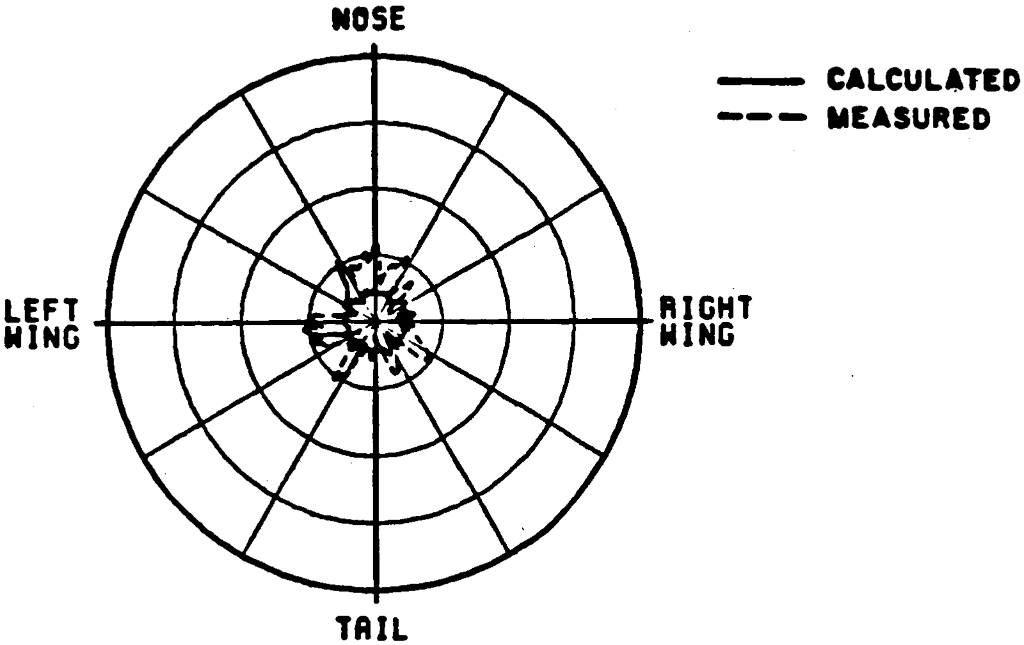

(a) $\theta_p = 10°$

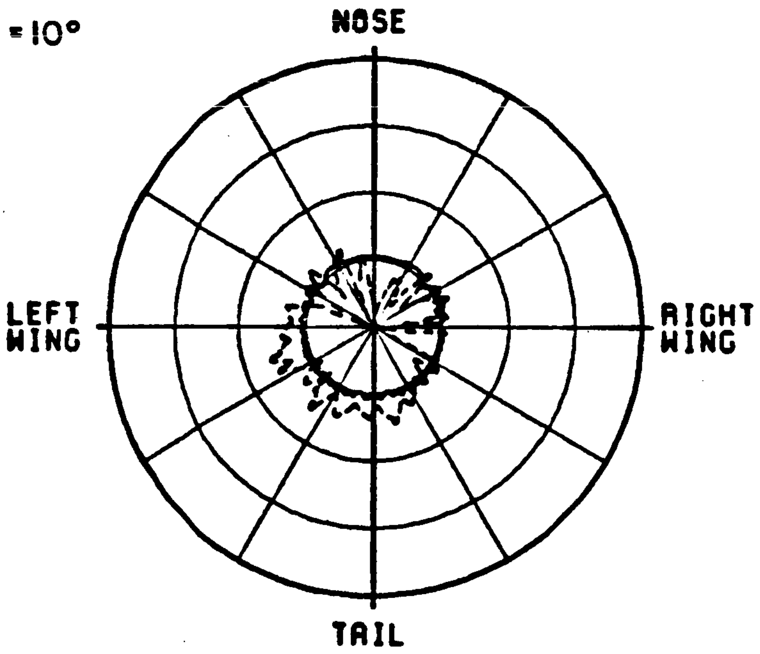

(SCALE: EACH DIVISION=10DB)

(b) $\theta_p = 20°$

Figure 93. Azimuthal conical patterns of a $\lambda/4$ monopole mounted on a C-141 aircraft.

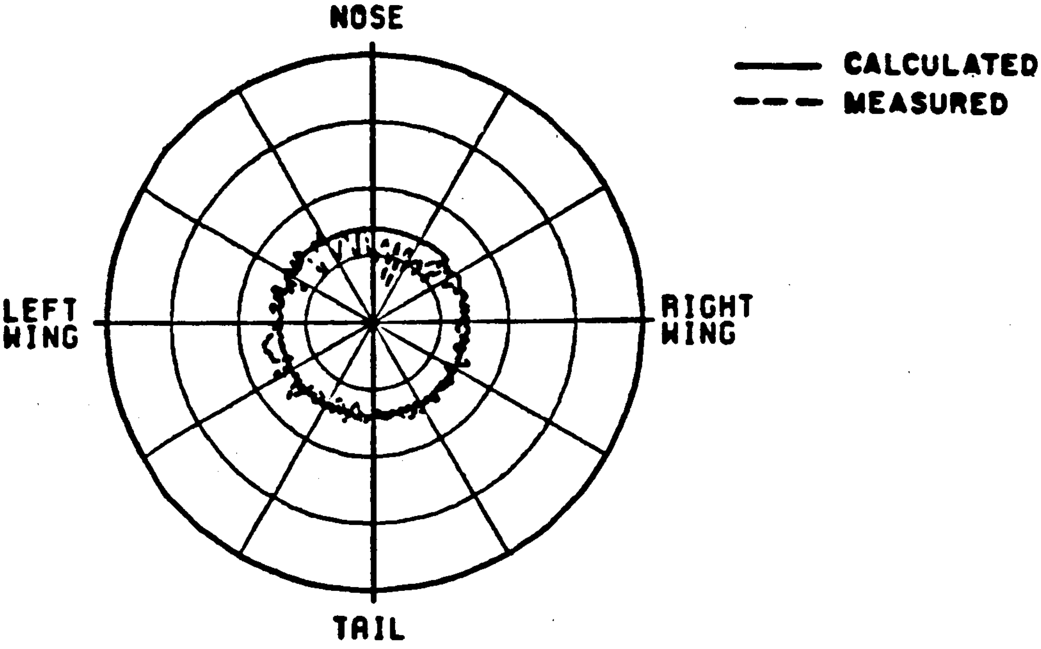

(c) $\theta_p = 30°$

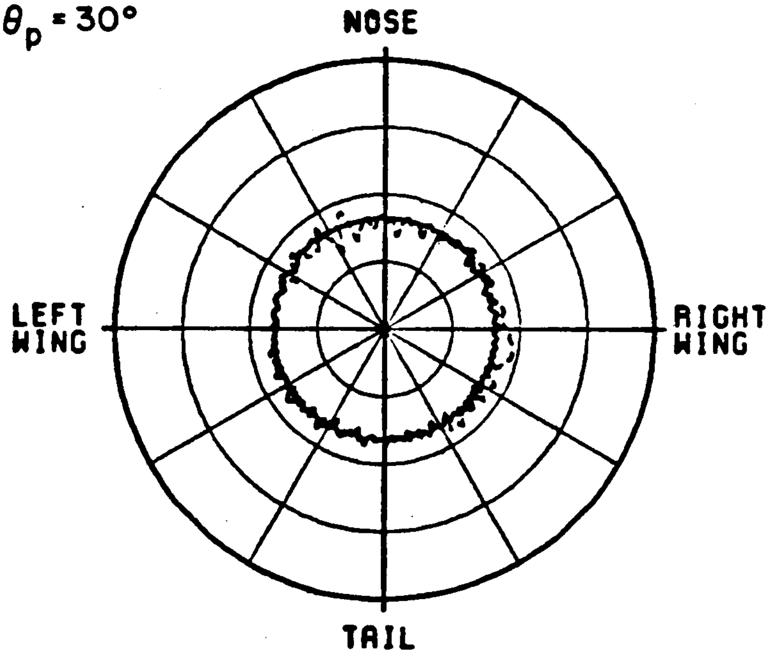

(SCALE: EACH DIVISION=10DB)

(d) $\theta_p = 40°$

Figure 93. (Continued).

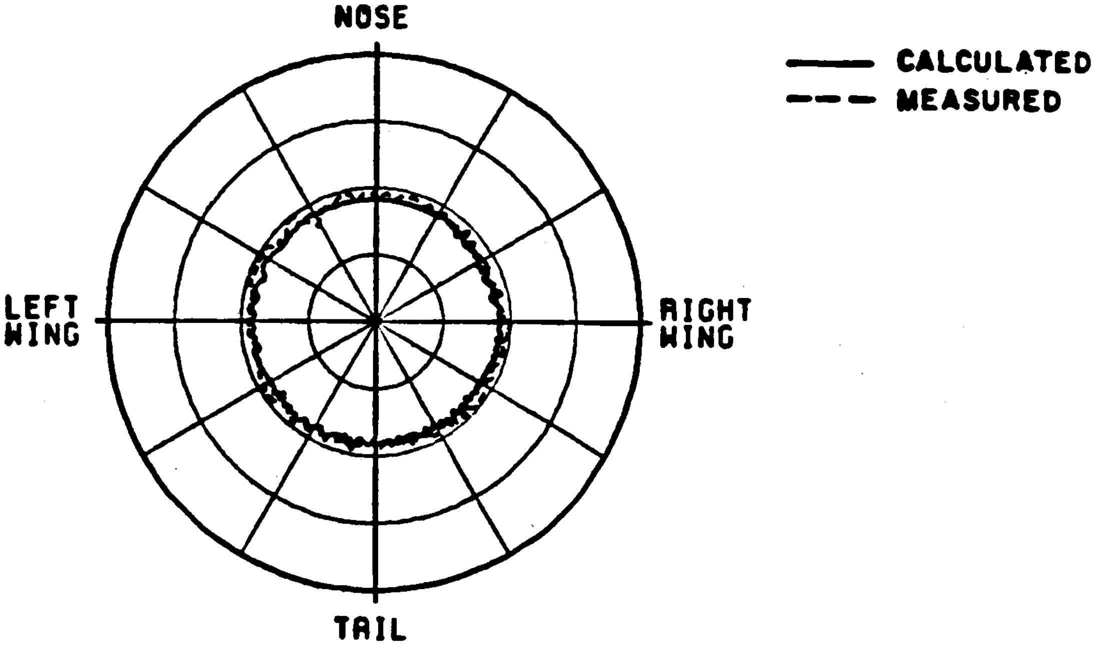

(e) θ_p = 50°

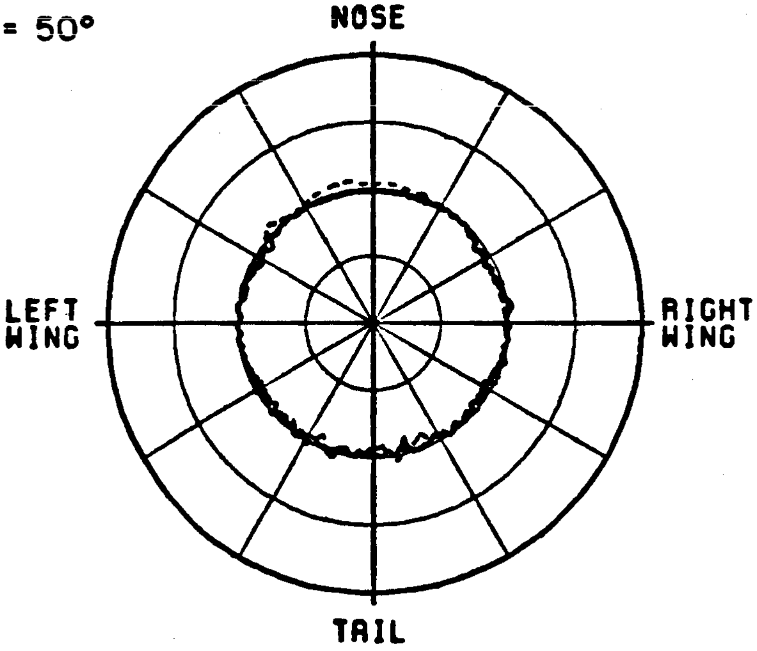

(SCALE: EACH DIVISION=10DB)

(f) θ_p = 60°

Figure 93. (Continued).

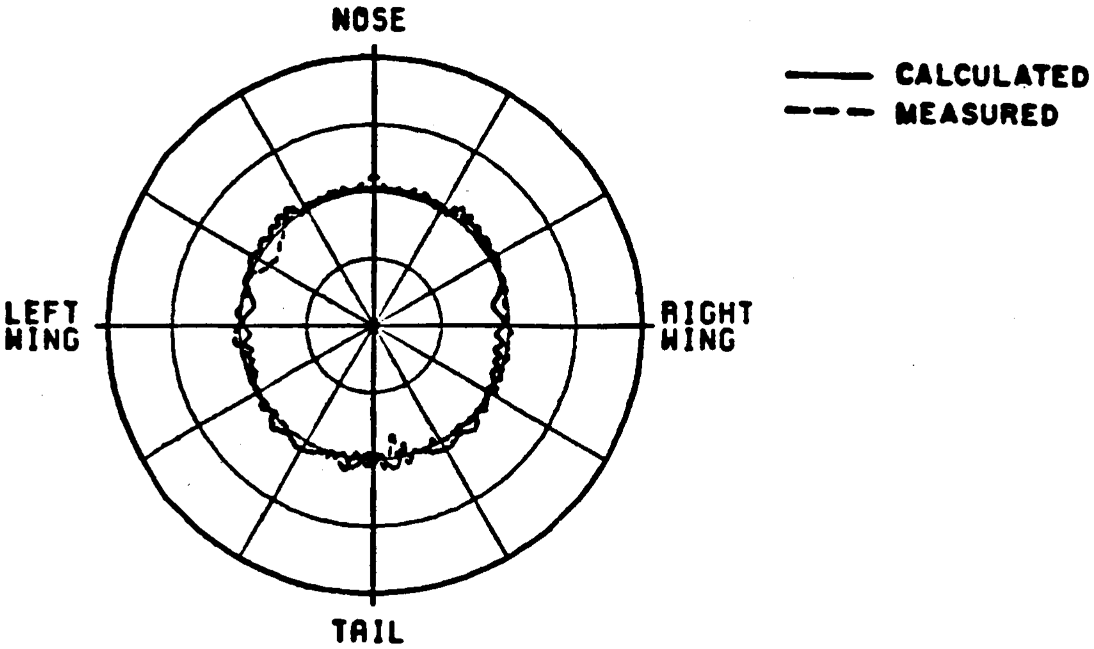

(g) $\theta_p = 70°$

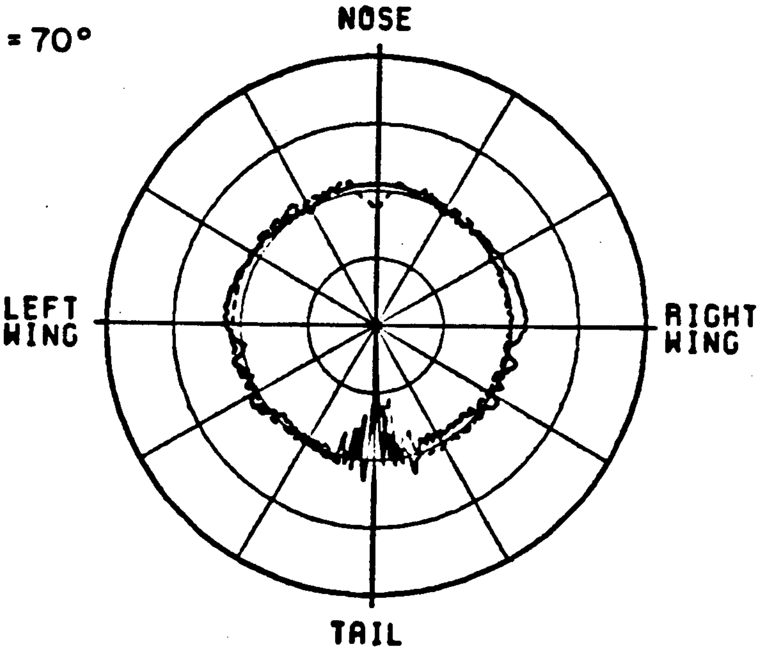

(SCALE: EACH DIVISION=10DB)

(h) $\theta_p = 80°$

Figure 93. (Continued).

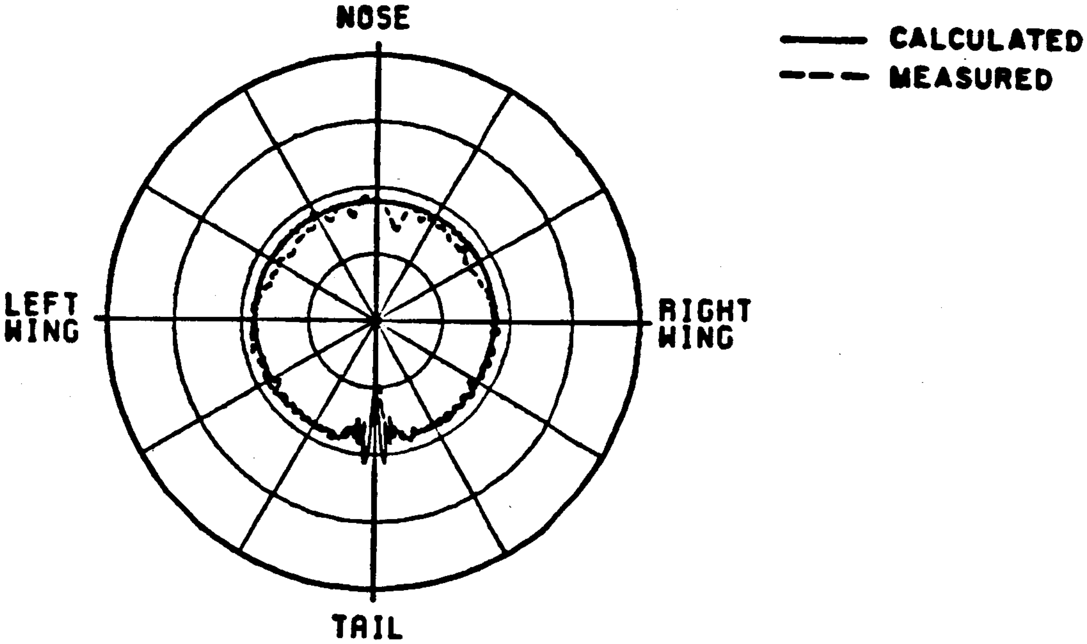

(i) $\theta_p = 90°$

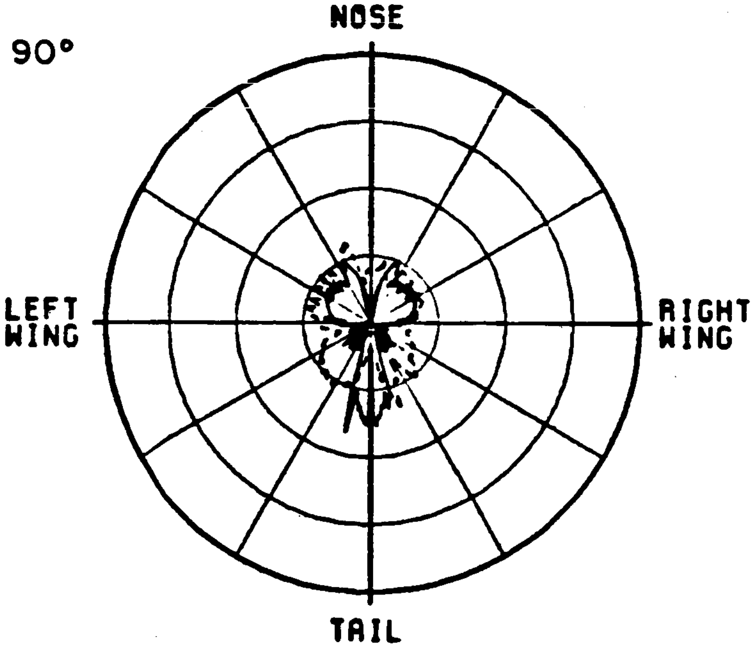

(SCALE: EACH DIVISION=10DB)

(j) $\theta_p = 100°$

Figure 93. (Continued).

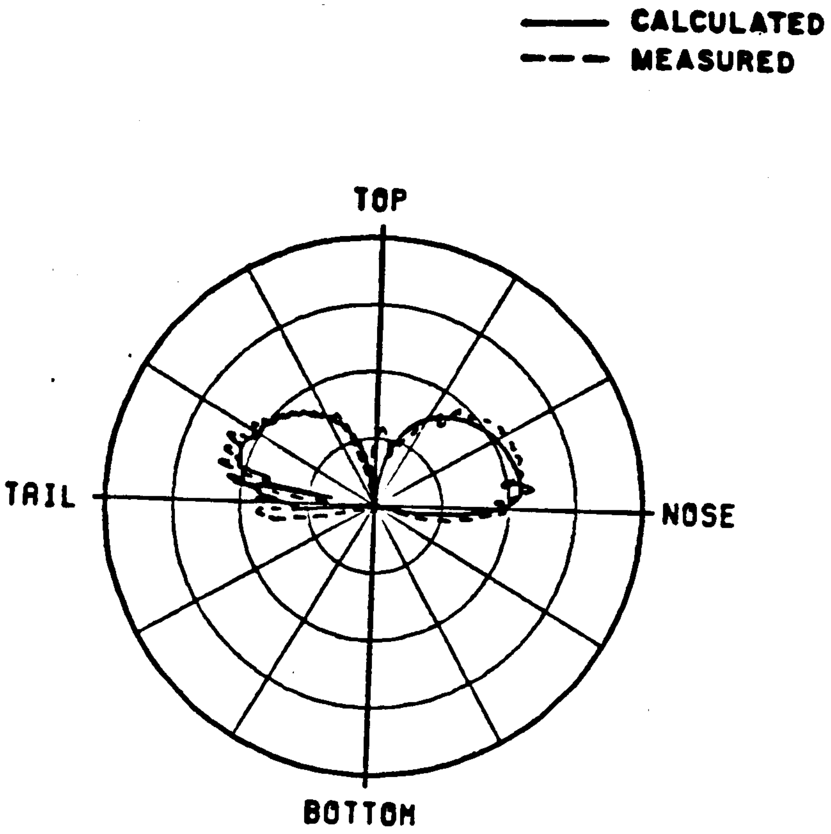

(SCALE: EACH DIVISION=10DB)

Figure 94. Elevation plane pattern of a $\lambda/4$ monopole mounted on top of a C-141 aircraft.

Example 13: Simulation of Missiles

Consider an axial slot antenna mounted between two large ram jets on a missile. The front view of the missile and the computer model are shown in Figure 95. The fuselage is simulated as a composite ellipsoid and only two side walls of the ram jets are simulated with two flat plates. A fuselage blockage plate is also added in the computer model and is shown as a dash line in the corresponding figure. This feature is added in the code to prevent the rays from passing through the fuselage and contributing to the field calculations. The roll and elevation plane patterns are compared with the measured results in Figure 96 and 97, respectively. Again, the calculated and measured results are in good agreement. The input data is as follows:

```
UN: IN INCHES
3
FG: FUSELAGE GEOMETRY FOR THE ANTENNA MOUNTED BETWEEN TWO RAM JETS CASE
6.75,6.75,100.,100.
F
0.,0.,0.
FC:
T,T
21.,-21.
FQ: FREQUENCY
1,12.,1.
SG: SOURCE
1.32,0.
1
0.,0.
0.024,0.153,0.,0.075,1
1.,0.
FB: FUSELAGE BLOCKAGE
1
4
6.1,8.3,-20.
6.1,8.3,20.
6.1,-8.3,20.
6.1,-8.3,-20.
```

```
PG: RIGHT AIR DUCT #1
4,T
6.147,2.788,-20.
7.826,4.467,-20.
7.826,4.467,10.
6.147,2.788,10.
PG: RIGHT AIR DUCT #2
4,T
6.147,-2.788,10.
7.826,-4.467,10.
7.826,-4.467,-20.
6.147,-2.788,-20.
PG: LEFT AIR DUCT #1
4,T
6.147,2.788,10.
7.826,4.467,10.
7.826,4.467,20.
6.147,2.788,20.
PG: LEFT AIR DUCT #2
4,T
6.147,-2.788,20.
7.826,-4.467,20.
7.826,-4.467,10.
6.147,-2.788,10.
PD: ROLL PLANE PATTERN
0.,1.32,90.
0,360,1
F,600.
PP: PEN PLOT
T
1,3.,3
EX: EXECUTE
PD: ELEVATION PLANE PATTERN
90.,91.32,90.2
0,360,1
F,600.
EX: EXECUTE
```

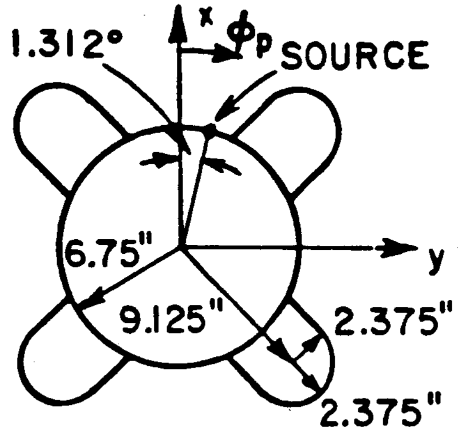
1.312°
x
ϕ_p
SOURCE
6.75"
y
9.125"
2.375"
2.375"

(a) MISSILE MODEL

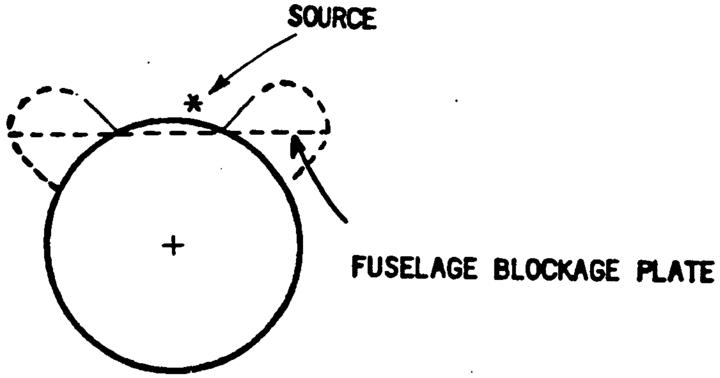
SOURCE
FUSELAGE BLOCKAGE PLATE

(b) COMPUTER SIMULATED MODEL

Figure 95. Missile model for an axial slot mounted between two ram jets.

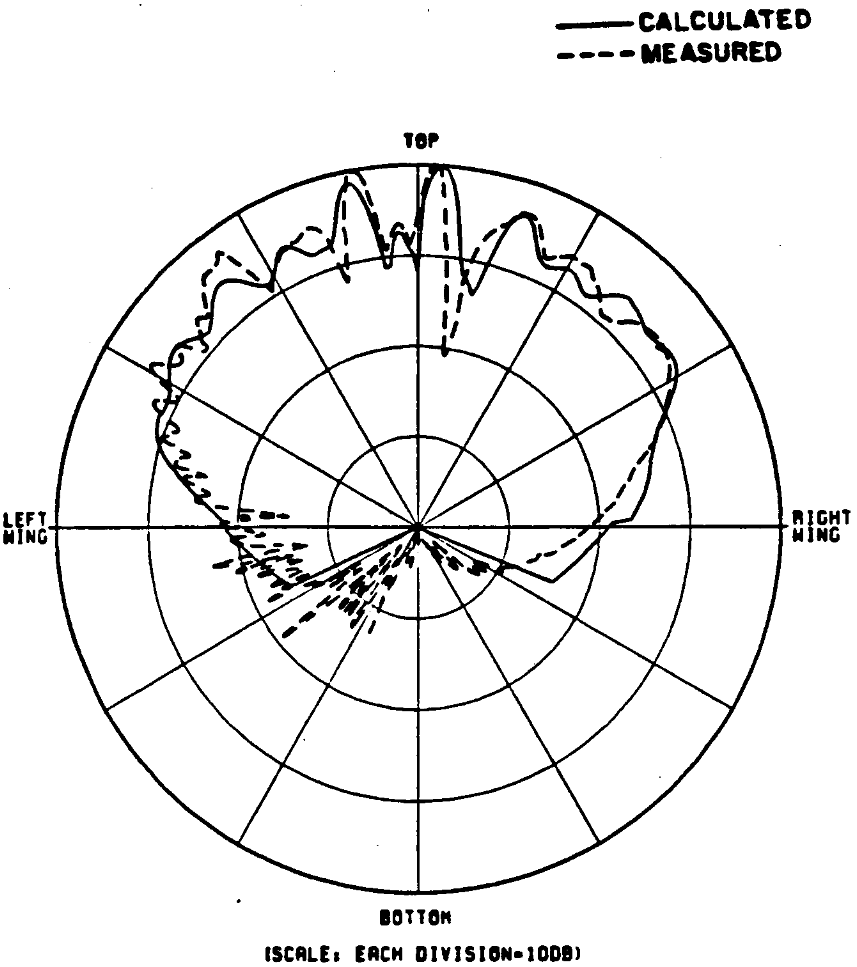

Figure 96. Roll plane pattern for an axial slot mounted between two ram jets.

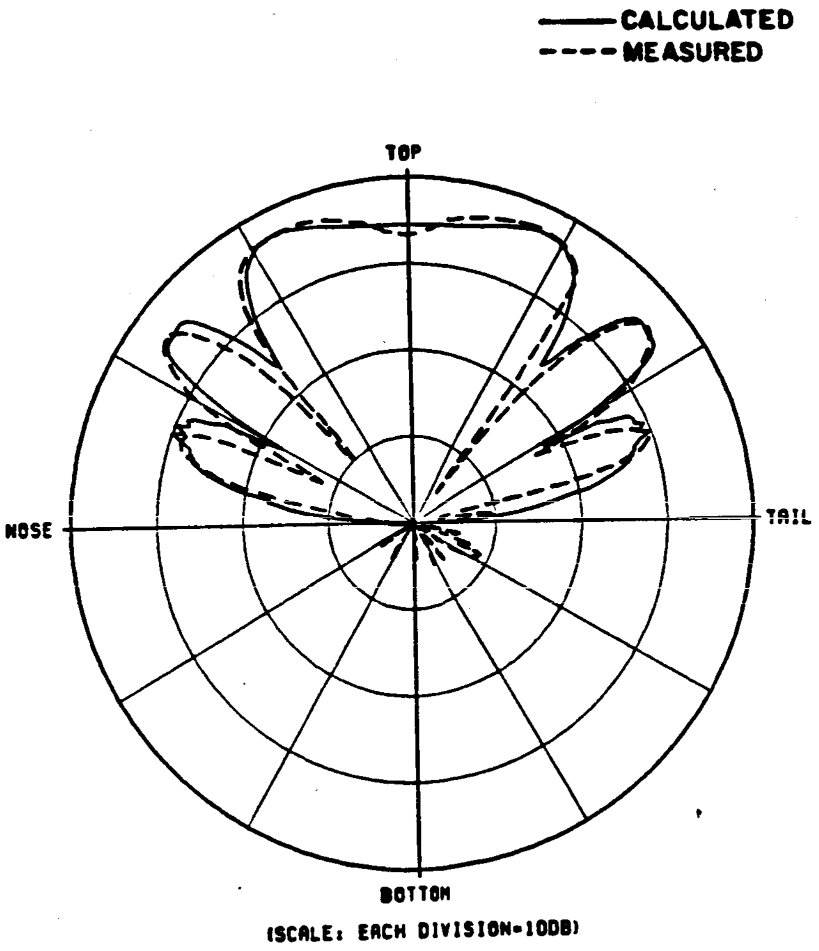

Figure 97. Elevation plane pattern for an axial slot mounted between two ram jets.

In this case, an axial slot antenna is mounted on the ram jet instead of the fuselage as shown in Figure 98. The ram jet is simulated as a composite ellipsoid and the other structures are simulated by multiple flat plates. The roll and elevation plane patterns are compared with measured data in Figure 99 and 100, respectively. The input data is as follows:

```
UN: IN INCHES
3
FG: FUSELAGE GEOMETRY FOR THE ANTENNA MOUNTED ON THE RAM JET CASE
2.375,2.375,100.,100.
F
0.,0.,0.
FC:
T,T
16.,-16.
FQ: FREQUENCY
1,12.,1.
SG: SOURCE GEOMETRY
0.,0.
1
0.,0.
0.024,0.153,0.,0.075,1
1.,0.
PG: LEFT SIDE WALL
4,T
-0.3,-2.3,15.
-1.9541,-2.375,15.
-1.9541,-2.375,-15.
-0.3,-2.3,-15.
PG: LEFT SIDE SLOPE
4,F
-1.9541,-2.375,15.
-6.75,-7.1709,15.
-6.75,-7.1709,-15.
-1.9541,-2.375,-15.
PG: LEFT AIR DUCT
4,F
-6.75,-7.1709,15.
-6.75,-9.5,15.
-6.75,-9.5,-15.
-6.75,-7.1709,-15.
PG: RIGHT SIDE WALL
4,T
-0.3,2.3,-15.
-1.9541,2.375,-15.
-1.9541,2.375,15.
-0.3,2.3,15.
PG: RIGHT SIDE SLOPE
4,F
-1.9541,2.375,-15.
-6.75,7.1709,-15.
-6.75,7.1709,15.
-1.9541,2.375,15.
PG: RIGHT AIR DUCT
4,F
-6.75,7.1709,-15.
-6.75,9.5,-15.
-6.75,9.5,15.
-6.75,7.1709,15.
PD: ROLL PLANE PATTERN
0.,0.,90.
0,360,1
F,600.
PP: PEN PLOT
T
1,3.,3
EX: EXECUTE
PD: ELEVATION PLANE PATTERN
90.,93.76,90.
0,360,1
F,600.
EX: EXECUTE
```

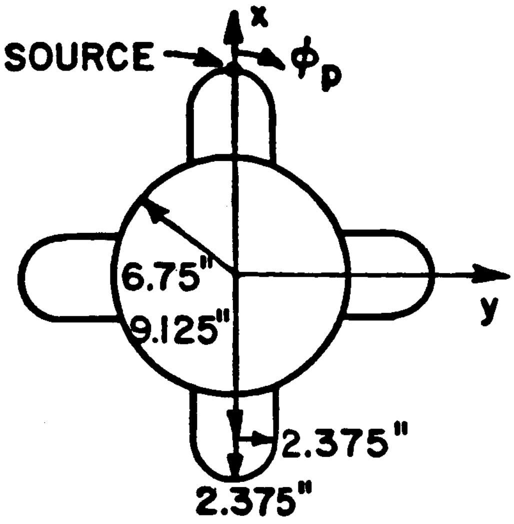
x
SOURCE
ϕ_p
6.75"
9.125"
y
2.375"
2.375"

(a) MISSILE MODEL

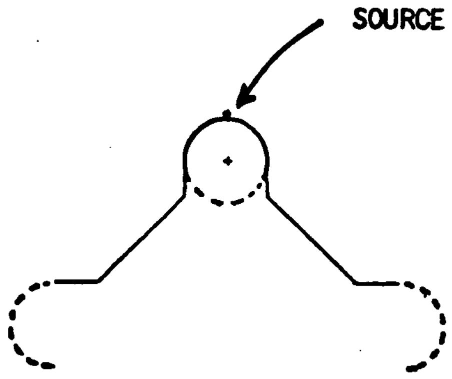

(b) COMPUTER SIMULATED MODEL

Figure 98. Missile model for an axial slot mounted on a ram jet.

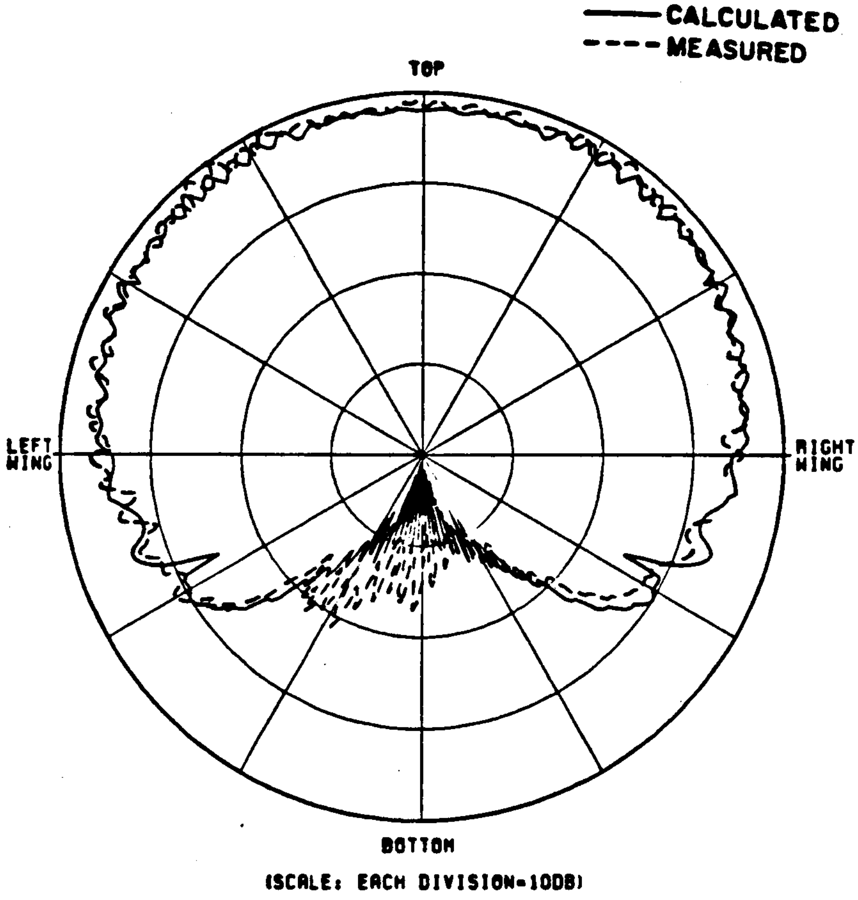

Figure 99. Roll plane pattern for an axial slot mounted on a ram jet.

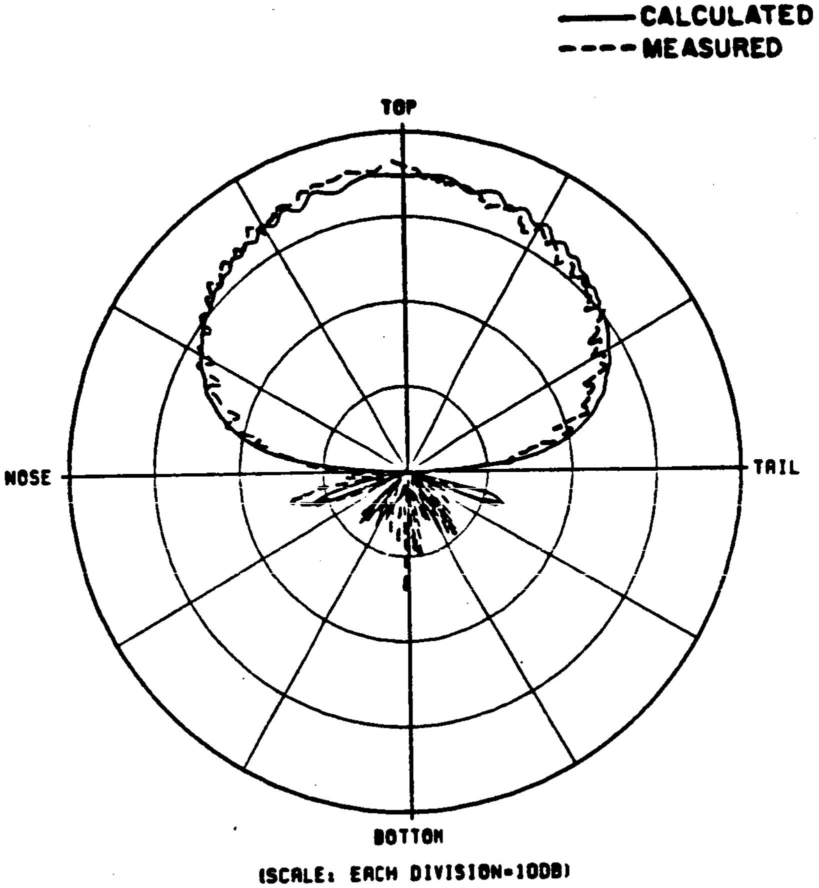

Figure 100. Elevation plane pattern for an axial slot mounted on a ram jet.

Example 14: Simulation of Space Shuttle

Consider an S-band Quad antenna (crossed-slot antenna with a 90° phase difference between the two slots) mounted on the top of a Space Shuttle Orbiter as shown in Figure 101. The computer model of the Space Shuttle Orbiter based on the input data is illustrated in Figure 102. The three principal plane patterns and a 45° roll conical pattern are computed as shown in Figures 103 to 106. The input data is as follows:

```
UN:IN INCHES
3
FG:SPACE SHUTTLE FOR THE TOP MOUNTED ANTENNA WITH CLOSED PAYLOAD DOORS CASE
75.,104.,1500.,130.
F
0.,0.,0.
FC:
T,F
944.3,0.
FQ:FREQUENCY (2 GHZ)
1,2.,1.
SG:CROSSED SLOT(.39 *.78 WAVELENGTH)
62.5,-10.
2
0.,0.
2.3,4.6,0.,1.476,1
1.,0.
0.,0.
2.3,4.6,90.,1.476,1
1.,90.
PG:SIDE WALL SIMULATED PLATE #1 ON POS. Y-SIDE
4,T
0.,101.1928,-30.
-120.,102.3928,-30.
-109.35,110.58,100.
-5.,109.54,100.
PG:SIDE WALL SIMULATED PLATE #2 ON POS. Y-SIDE
4,T
-5.,109.54,100.
-109.35,110.58,100.
-78.77,117.94,381.
-5.,117.2,381.
```

```
PG:SIDE WALL SIMULATED PLATE #3 ON POS. Y-SIDE
4,T
-5.,117.2,381.
-78.77,117.94,381.
-120.,118.84,458.13
-5.,117.69,458.13
PG:SIDE WALL SIMULATED PLATE #4 ON POS. Y-SIDE
4,T
-5.,117.69,458.13
-120.,118.84,458.13
-147.,106.07,944.3
-5.,104.65,944.3
PG:WING SIMULATED PLATE #1 ON POS. Y-SIDE
3,F
-120.,102.3928,-30.
-120.,125.192,100.
-109.35,110.58,100.
PG:WING SIMULATED PLATE #2 ON POS. Y-SIDE
4,F
-109.35,110.58,100.
-120.,125.192,100.
-120.,188.,458.13
-78.77,117.94,381.
PG:WING SIMULATED PLATE #3 ON POS. Y-SIDE
3,F
-78.77,117.94,381.
-120.,188.,458.13
-120.,118.84,458.13
PG:WING SIMULATED PLATE #4 ON POS. Y-SIDE
5,F
-120..118.84.458.13
-120.,188.,458.13
-135.083,468.34,729.72
-142.739,468.34,867.57
-147.,106.07,944.3
PG:VERTICAL STABILIZER ON POS. Y-SIDE
4,T
83.,14.1,884.5
390.7,5.8,1098.7
390.7,0.,1033.6
83.,0.,725.9
PG:VERTICAL STABILIZER ON NEG. Y-SIDE
4,T
83.,0.,725.9
390.7,0.,1033.6
390.7,-5.8,1098.7
83.,-14.1,884.5
```

```
PG:NOSE SIMULATED PLATE ON POS. Y-SIDE
4,F
-65.,50.,-322.
-105.,50.4,-322.
-120.,102.3928,-30.
0.,101.1928,-30.
PG:NOSE SIMULATED PLATE #1 ON TOP
4,T
-22.26,0.,-130.
-65.,0.,-322.
-65.,50.,-322.
0.,101.1928,-30.
PG:NOSE SIMULATED PLATE #2 ON TOP
4,T
0.,-101.1928,-30.
-65.,-50.,-322.
-65.,0.,-322.
-22.26,0.,-130.
PG:NOSE SIMULATED PLATE ON FRONT
5,F
-105.,50.4,-322.
-65.,50.,-322.
-65.,0.,-322.
-65.,-50.,-322.
-105.,-50.4,-322.
PG:NOSE SIMULATED PLATE ON NEG. Y-SIDE
4,F
0.,-101.1928,-30.
-120.,-102.3928,-30.
-105.,-50.4,-322.
-65.,-50.,-322.
PG:SIDE WALL SIMULATED PLATE #1 ON NEG. Y-SIDE
4,T
-5.,-109.54,100.
-109.35,-110.58,100.
-120.,-102.3928,-30.
0.,-101.1928,-30.
PG:SIDE WALL SIMULATED PLATE #2 ON NEG. Y-SIDE
4,T
-5.,-117.2,381.
-78.77,-117.94,381.
-109.35,-110.58,100.
-5.,-109.54,100.
PG:SIDE WALL SIMULATED PLATE #3 ON NEG. Y-SIDE
4,T
-5.,-117.69,458.13
-120.,-118.84,458.13
-78.77,-117.94,381.
-5.,-117.2,381.
```

```
PG:SIDE WALL SIMULATED PLATE #4 ON NEG. Y-SIDE
4,T
-5.,-104.65,944.3
-147.,-106.07,944.3
-120.,-118.84,458.13
PG:WING SIMULATED PLATE #1 ON NEG. Y-SIDE
3,F
-109.35,-110.58,100.
-120.,-125.192,100.
-120.,-102.3928,-30.
PG:WING SIMULATED PLATE #2 ON NEG. Y-SIDE
4,F
-78.77,-117.94,381.
-120.,-188.,458.13
-120.,-125.192,100.
-109.35,-110.58,100.
PG:WING SIMULATED PLATE #3 ON NEG. Y-SIDE
3,F
-120.,-118.84,458.13
-120.,-188.,458.13
-78.77,-117.94,381.
PG:WING SIMULATED PLATE #4 ON NEG. Y-SIDE
5,F
-147.,-106.07,944.3
-142.739,-468.34,867.57
-135.083,-468.34,729.72
-120.,-188.,458.13
-120.,-118.84,458.13
PP: POLAR PLOT IN DB
T
1,2.766,3

PD:ELEVATION PLANE CUT
90.,90.,90.
0,360,1
T,50000.
EX:EXECUTE
PD:AZIMUTH PLANE CUT
90.,0.,90.
0,360,1
T,50000.
EX: EXECUTE
PD:ROLL PATTERN CUT
0.,0.,90.
0,360,1
T,50000.
EX:EXECUTE
PD:ROLL CONICAL PLANE CUT
0.,0.,45.
0,360,1
T,50000.
EX: EXECUTE
```

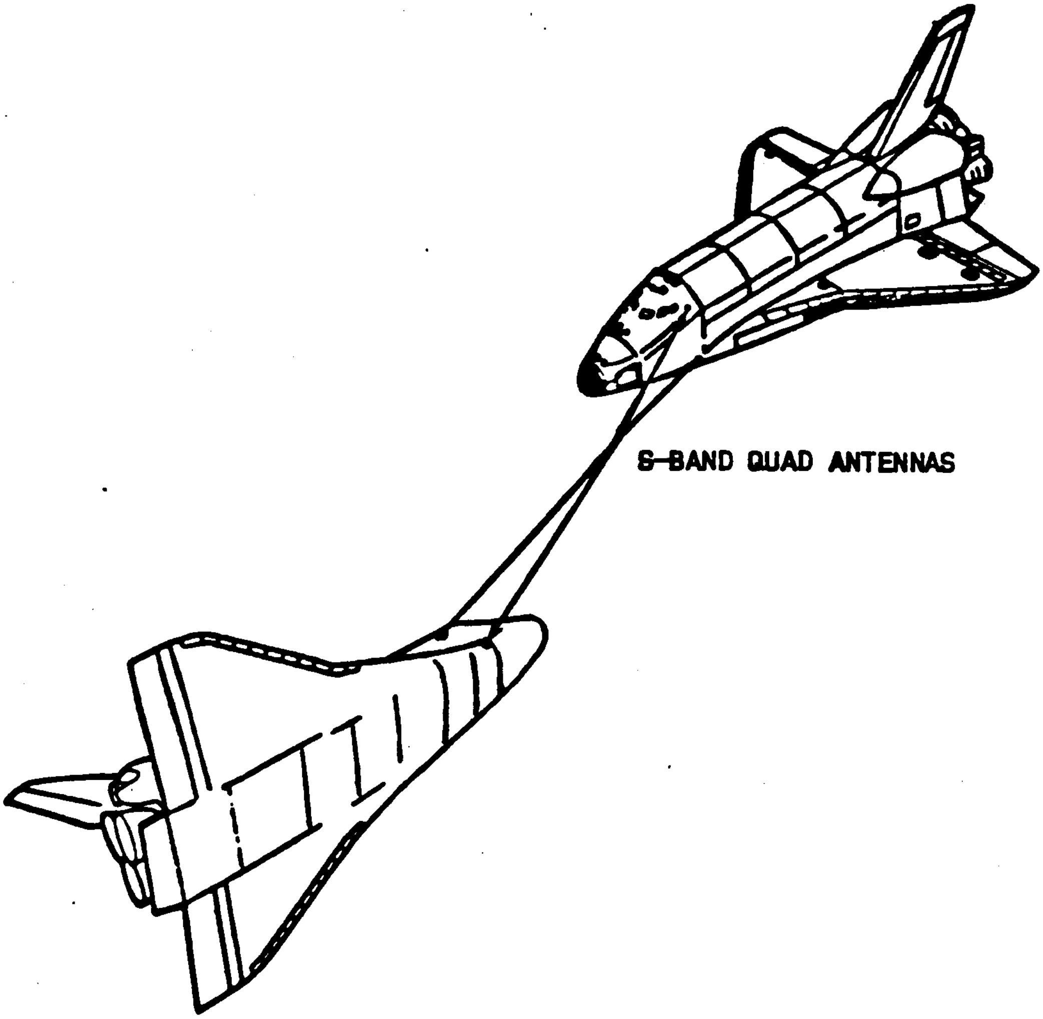
S-BAND QUAD ANTENNAS

Figure 101. S-band quad antenna locations on the Space Shuttle.

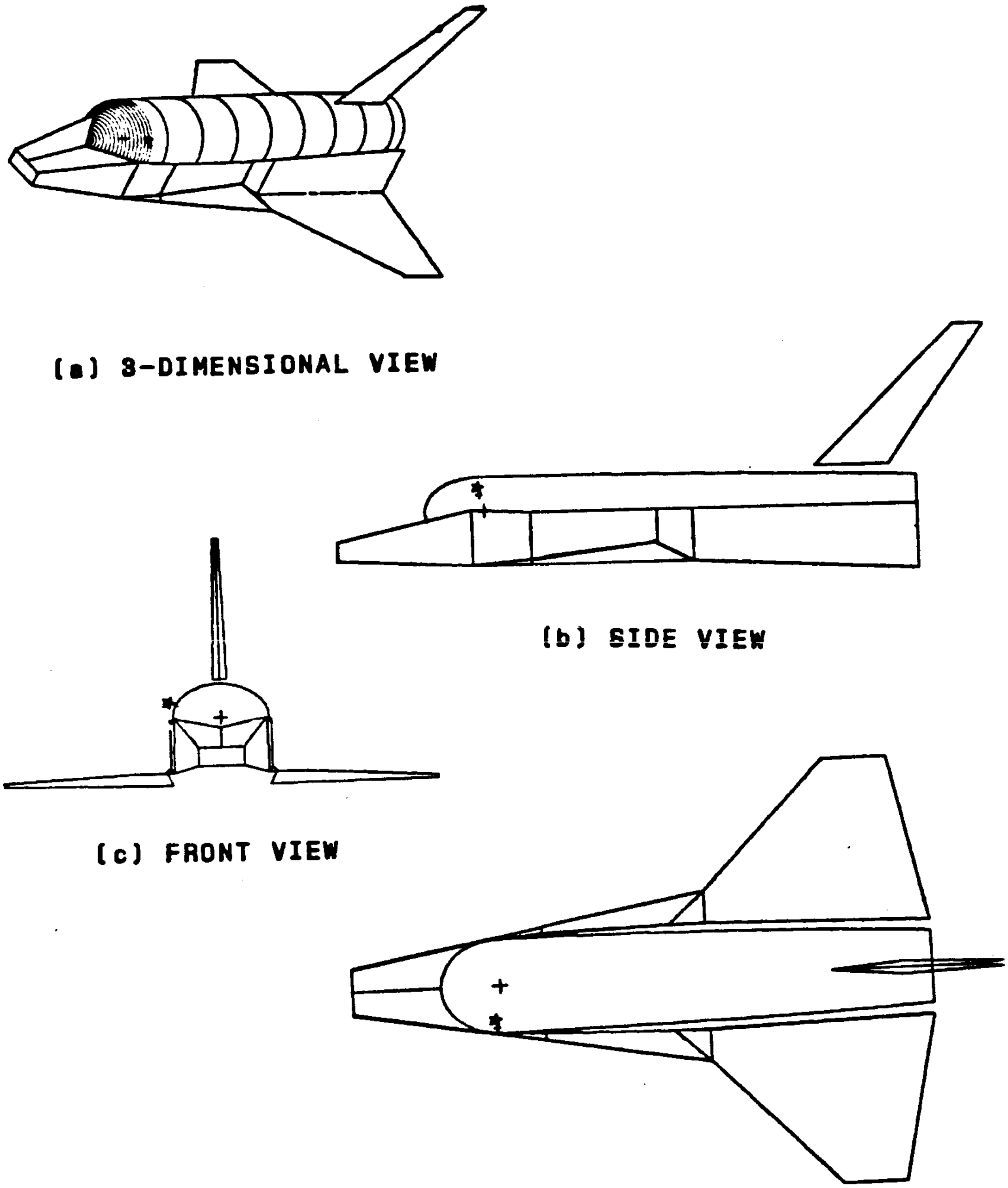

(a) 3-DIMENSIONAL VIEW

(b) SIDE VIEW

(c) FRONT VIEW

(d) TOP VIEW

Figure 102. Computer simulated model for a crossed-slot antenna mounted on top of a Space Shuttle Orbiter.

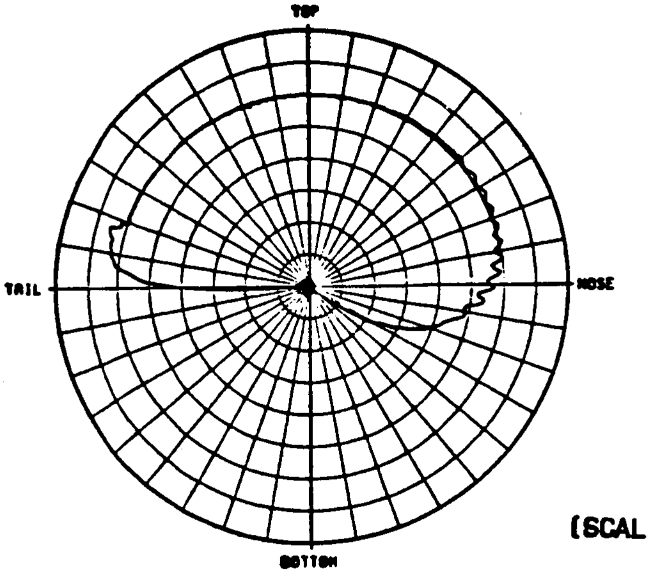

(SCALE: EACH DIVISION= 4DB)

(a) E_ϕ

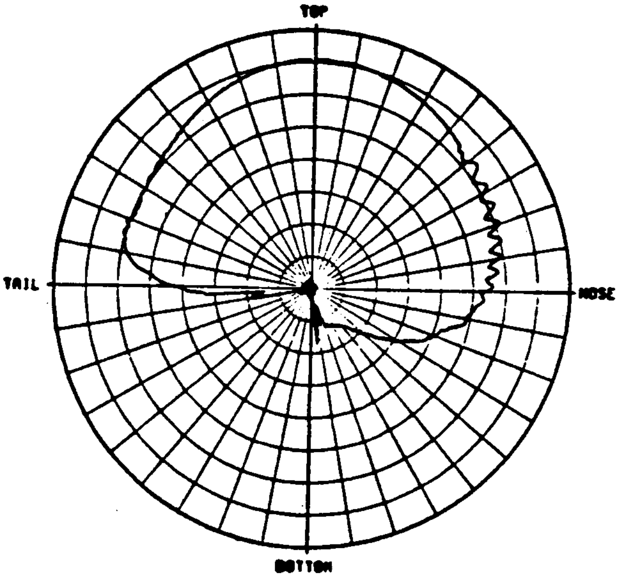

(b) E_θ

Figure 103. Elevation plane patterns for a crossed-slot antenna mounted on top of a Space Shuttle Orbiter.

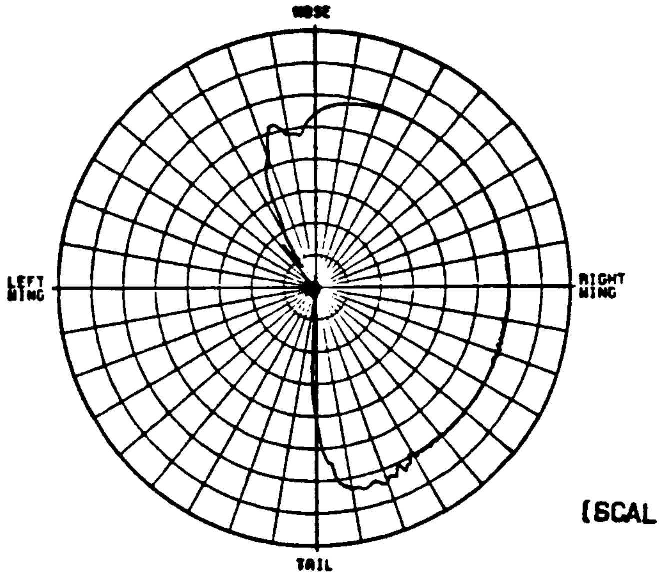

(SCALE: EACH DIVISION= 4DB)

(a) E_ϕ

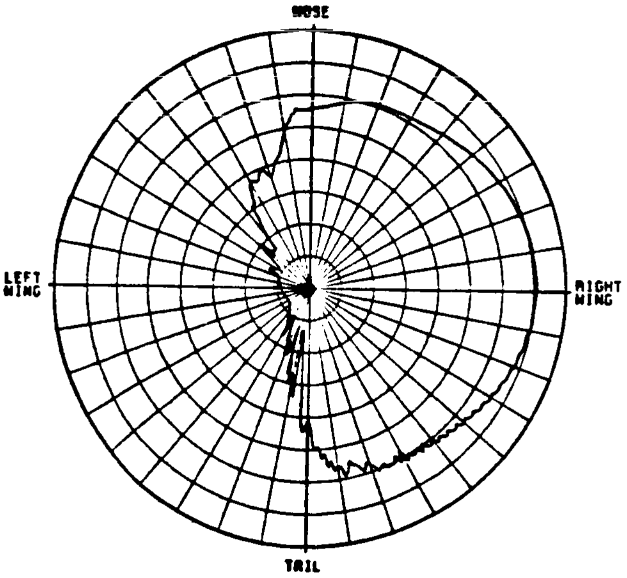

(b) E_θ

Figure 104. Azimuth plane patterns for a crossed-slot antenna mounted on top of a Space Shuttle Orbiter.

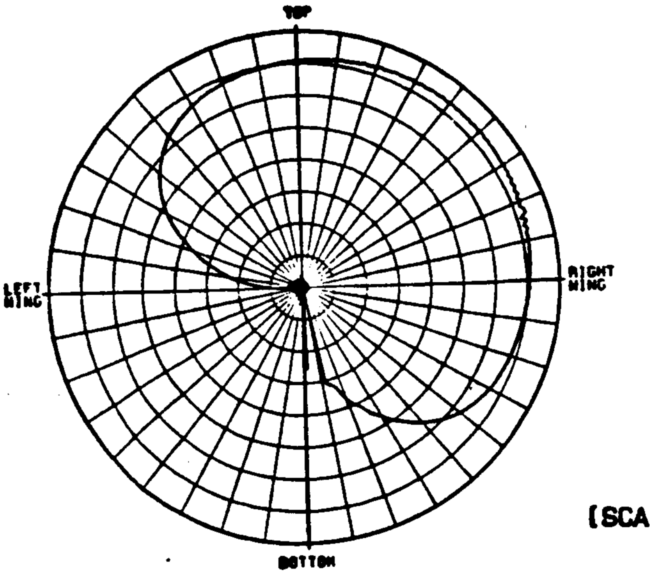

(SCALE: EACH DIVISION= 4DB)

(a) E_ϕ

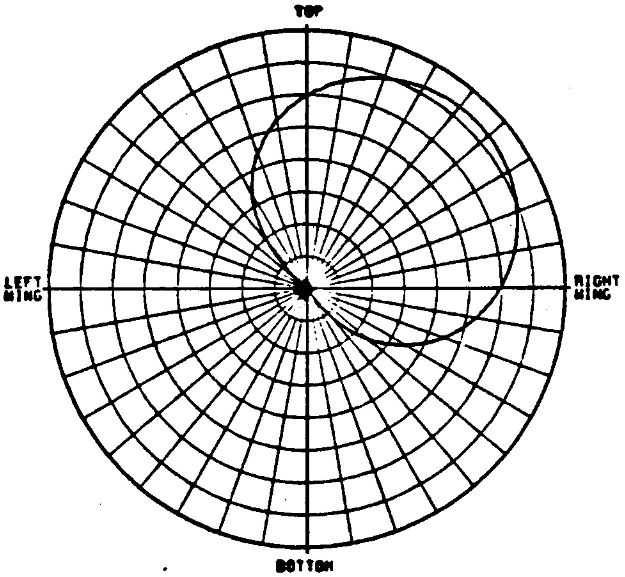

(b) E_θ

Figure 105. Roll plane radiation patterns for a crossed-slot antenna mounted on top of a Space Shuttle Orbiter.

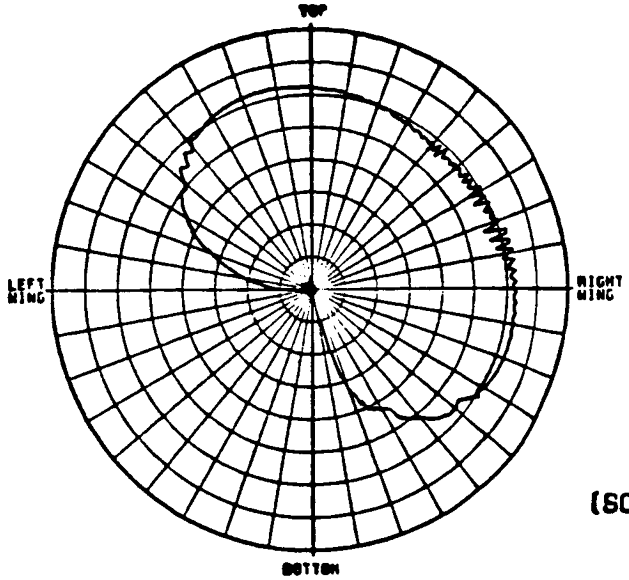

(SCALE: EACH DIVISION= 4DB)

(a) E_ϕ

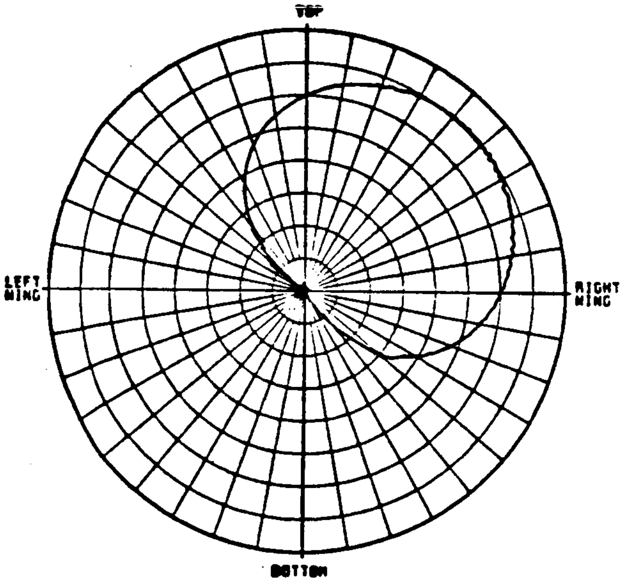

(b) E_θ

Figure 106. Roll conical patterns (θ_p=45°) for a crossed-slot antenna mounted on top of a Space Shuttle Orbiter when the payload bay doors are closed.

When the payload doors of the Orbiter are open, six more plates are used to simulate the heat radiators inside the payload doors, but at the same time ten plates are removed from the model since these plates are in the shadow region of the payload doors. The computer model of the Orbiter with open payload doors is shown in Figure 107.

In order to analyze the blocking and reflection effect of the heat radiators, the roll conical patterns (θ_p=45°) are computed and then compared with the roll conical patterns obtained when the payload doors were closed. The input data for this case is as follows:

```
UN:IN INCHES
3
FG:SPACE SHUTTLE FOR THE TOP MOUNTED ANTENNA WITH OPEN PAYLOAD DOORS CASE
75.,104.,1500.,130.
F
0.,0.,0.
FC:
T,F
19.,0.
FQ:FREQUENCY (2 GHZ)
1,2.,1.
SG:CROSSED SLOT(.39 *.78 WAVELENGTH)
62.5,-10.
2
0.,0.
2.3,4.6,0.,1.476,1
1.,0.
0.,0.
2.3,4.6,90.,1.476,1
1.,90.
FB:
2
4
-5.,104.37,19.
-5.,104.37,720.
-5.,-104.37,720.
-5.,-104.37,19.
4
83.,104.37,720.
83.,-104.37,720.
-83.,-104.37,720.
-83.,104.37,720.
```

```
PG:SIDE WALL SIMULATED PLATE #1 ON POS. Y-SIDE
5,T
0.,101.1928,-30.
-120.,102.3928,-30.
-109.35,110.58,100.
-5.,109.54,100.
-5.,104.37,19.
PG:DOOR #1 ON POS. Y-SIDE
4,F
-5.,104.37,19.
-37.1,130.1,19.
-37.1,130.1,720.
-5.,104.37,720.
PG:DOOR #2 ON POS. Y-SIDE
4,F
-37.1,130.1,19.
-37.1,187.9,19.
-37.1,187.9,720.
-37.1,130.1,720.
PG:DOOR #3 ON POS. Y-SIDE
4,F
-37.1,187.9,19.
-5.,245.8,19.
-5.,245.8,720.
-37.1,187.9,720.
PG:WING SIMULATED PLATE #1 ON POS. Y-SIDE
3,F
-120.,102.3928,-30.
-120.,125.192,100.
-109.35,110.58,100.
PG:WING SIMULATED PLATE #4 ON POS. Y-SIDE
5,F
-120.,118.84,458.13
-120.,188.,458.13
-135.083,468.34,729.72
-142.739,468.34,867.57
-147.,106.07,944.3
PG:VERTICAL STABILIZER ON POS. Y-SIDE
4,F
83.,14.1,884.5
390.7,5.8,1098.7
390.7,0.,1033.6
83.,0.,725.9
PG:VERTICAL STABILIZER ON NEG. Y-SIDE
4,F
83.,0.,725.9
390.7,0.,1033.6
390.7,-5.8,1098.7
83.,-14.1,884.5
```

```
PG:NOSE SIMULATED PLATE ON POS. Y-SIDE
4,F
-65.,50.,-322.
-105.,50.4,-322.
-120.,102.3928,-30.
0.,101.1928,-30.
PG:NOSE SIMULATED PLATE #1 ON TOP
4,T
-22.26,0.,-130.
-65.,0.,-322.
-65.,50.,-322.
0.,101.1928,-30.
PG:NOSE SIMULATED PLATE #2 ON TOP
4,T
0.,-101.1928,-30.
-65.,-50.,-322.
-65.,0.,-322.
-22.26,0.,-130.
PG:NOSE SIMULATED PLATE ON FRONT
5,F
-105.,50.4,-322.
-65.,50.,-322.
-65.,0.,-322.
-65.,-50.,-322.
-105.,-50.4,-322.
PG:NOSE SIMULATED PLATE ON NEG. Y-SIDE
4,F
0.,-101.1928,-30.
-120.,-102.3928,-30.
-105.,-50.4,-322.
-65.,-50.,-322.
PG:SIDE WALL SIMULATED PLATE #1 ON NEG. Y-SIDE
5,T
-5.,-104.37,19.
-5.,-109.54,100.
-109.35,-110.58,100.
-120.,-102.3928,-30.
0.,-101.1928,-30.
PG:DOOR #1 ON NEG. Y-SIDE
4,F
-5.,-104.37,720.
-37.1,-130.1,720.
-37.1,-130.1,19.
-5.,-104.37,19.
```

```
PG:DOOR #2 ON NEG. Y-SIDE
4,F
-37.1,-130.1,720.
-37.1,-187.9,720.
-37.1,-187.9,19.
-37.1,-130.1,19.
PG:DOOR #3 ON NEG. Y-SIDE
4,F
-37.1,-187.9,720.
-5.,-245.8,720.
-5.,-245.8,19.
-37.1,-187.9,19.
PG:WING SIMULATED PLATE #1 ON NEG. Y-SIDE
3,F
-109.35,-110.58,100.
-120.,-125.192,100.
-120.,-102.3928,-30.
PG:WING SIMULATED PLATE #4 ON NEG. Y-SIDE
5,F
-147.,-106.07,944.3
-142.739,-468.34,867.57
-135.083,-468.34,729.72
-120.,-188.,458.13
-120.,-118.84,458.13
PP:POLAR PLOT IN DB
T
1,2.766,3
PD:ROLL PLANE CUT
0.,0.,45.
0,360,1
T,50000.
EX:EXECUTE
```

The computed results are shown in Figure 108, however, measured results are not available. Comparing the two roll conical patterns, one can see that the blocking effect of the heat radiator causes large disturbances in the 30° to 60° and in the 100° to 160° range. This is due to the strong direct reflections from the heat radiator in the main beam region of the top mounted antenna.

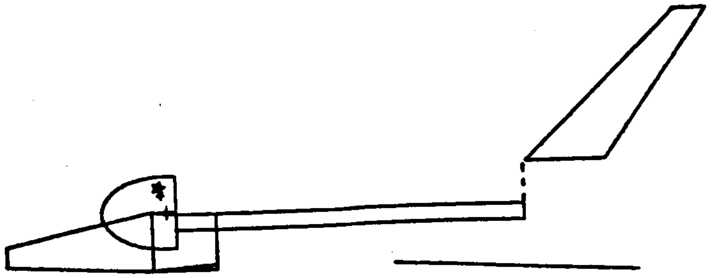

(a) SIDE VIEW

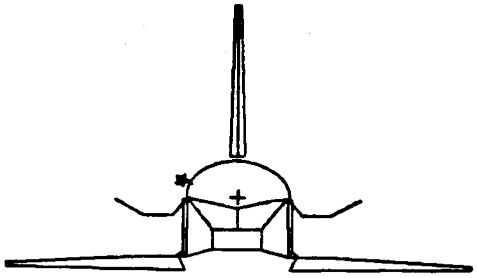

(b) FRONT VIEW

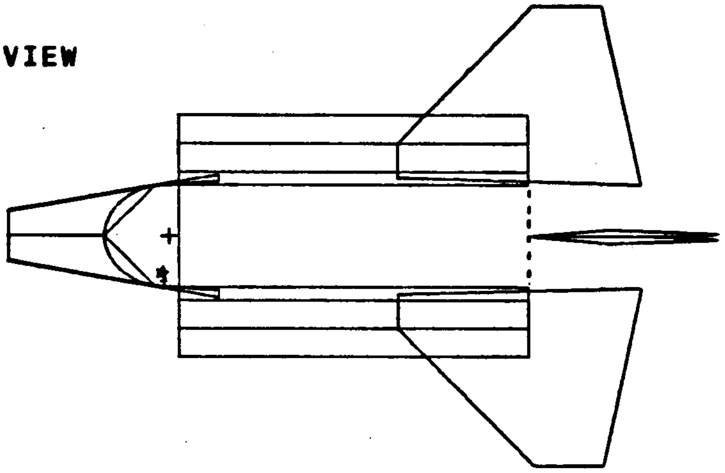

(c) TOP VIEW

Figure 107. Computer simulated model for a crossed-slot antenna mounted on top of a Space Shuttle Orbiter when the payload bay doors are open.

ORIGINAL PAGE IS
OF POOR QUALITY

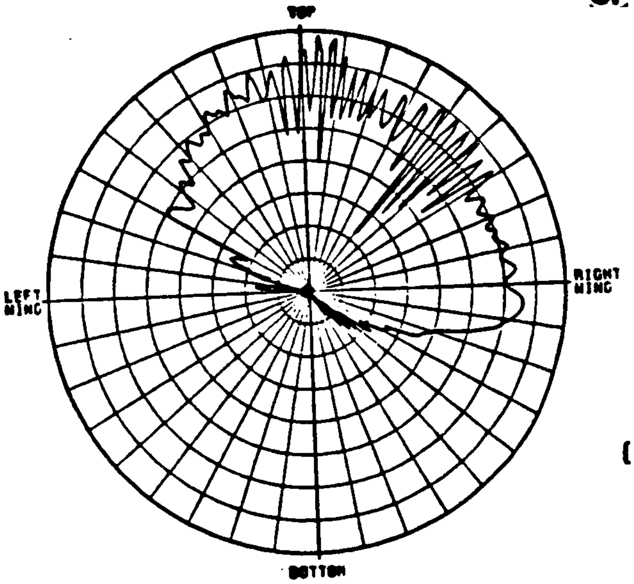

(SCALE: EACH DIVISION= 4DB)

(a) E_ϕ

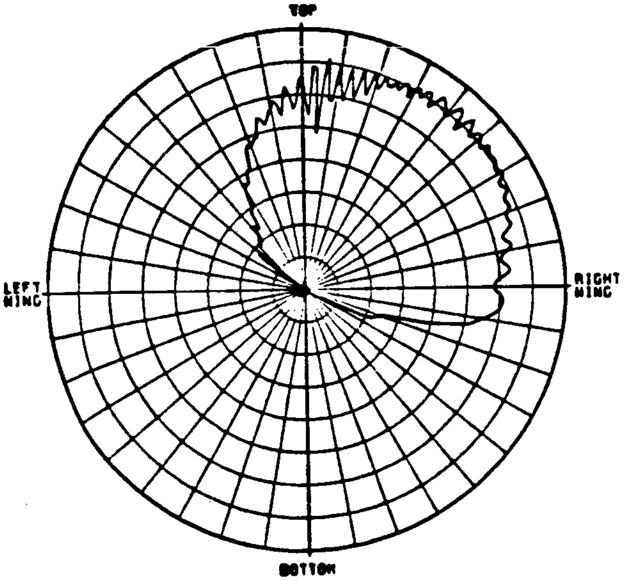

(b) E_θ

Figure 108. Roll conical patterns (θ_p=45°) for a crossed-slot antenna mounted on top of a Space Shuttle Orbiter when the payload bay doors are open.

For the bottom mounted antenna case, a composite ellipsoid and 16 plate model are used to simulate the basic structure. A computer simulated model and the resulting patterns are shown in Figures 109 and 110, respectively. The input data is as follows:

```
UN:IN INCHES
3
FG:SPACE SHUTTLE FOR THE BOTTOM MOUNTED ANTENNA WITH CLOSED PAYLOAD DOORS CASE
40.,108.,2500.,325.
F
0.,0.,0.
FC:
T,F
1055.,0.
FQ:FREQUENCY (2 GHZ)
1,2.,1.
SG:CROSSED SLOT(.39 *.78 WAVELENGTH)
80.,-4.
2
0.,0.
2.3,4.6,0.,1.476,1
1.,0.
0.,0.
2.3,4.6,90.,1.476,1
1.,90.
PG:SIDE WALL SIMULATED PLATE #1 ON POS. Y-SIDE
3,T
-1.,41.5,-300.
-155.,109.,-30.
-5.,107.5,-30.
PG:SIDE WALL SIMULATED PLATE #2 ON POS. Y-SIDE
4,T
-5.,107.5,-30.
-155.,109.,-30.
-165.,109.6,18.
-5.,108.,18.
PG:SIDE WALL SIMULATED PLATE #3 ON POS. Y-SIDE
4,T
-5.,108.,18.
-165.,109.6,18.
-165.,109.29,458.
-5.,107.69,458.
PG:SIDE WALL SIMULATED PLATE #4 ON POS. Y-SIDE
4,T
-5.,107.69,458.
-165.,109.29,458.
-165.,102.17,1055.
-5.,100.57,1055.
```

```
PG:WING SIMULATED PLATE #1 ON POS. Y-SIDE
3,T
1.,108.5,8.
1.,188.,458.
1.,108.5,458.
PG:WING SIMULATED PLATE #2 ON POS. Y-SIDE
5,T
1.,108.5,458.
1.,188.,458.
1.,468.,730.
1.,468.,867.
1.,107.,944.
PG:BOTTOM SIMULATED PLATE #1
4,T
-1.,-41.5,-300.
-155.,-109.,-30.
-155.,109.,-30.
-1.,41.5,-300.
PG:BOTTOM SIMULATED PLATE #2
4,F
-155.,-109.,-30.
-165.,-109.6,18.
-165.,109.6,18.
-155.,109.,-30.
PG:BOTTOM SIMULATED PLATE #3
4,F
-165.,-109.6,18.
-165.,-109.29,458.
-165.,109.29,458.
-165.,109.6,18.
PG:BOTTOM SIMULATED PLATE #4
4,F
-165.,-109.29,458.
-165.,-102.17,1055.
-165.,102.17,1055.
-165.,109.29,458.
PG:SIDE WALL SIMULATED PLATE #1 ON NEG. Y-SIDE
3,T
-5.,-107.5,-30.
-155.,-109.,-30.
-1.,-41.5,-300.
PG:SIDE WALL SIMULATED PLATE #2 ON NEG. Y-SIDE
4,T
-5.,-108.,18.
-165.,-109.6,18.
-155.,-109.,-30.
-5.,-107.5,-30.
PG:SIDE WALL SIMULATED PLATE #3 ON NEG. Y-SIDE
4,T
-5.,-107.69,458.
-165.,-109.29,458.
-165.,-109.6,18.
-5.,-108.,18.
PG:SIDE WALL SIMULATED PLATE #4 ON NEG. Y-SIDE
4,T
-5.,-100.57,1055.
-165.,-102.17,1055.
-165.,-109.29,458.
-5.,-107.69,458.
PG:WING SIMULATED PLATE #1 ON NEG. Y-SIDE
3,T
1.,-108.5,458.
1.,-188.,458.
1.,-108.5,8.
PG:WING SIMULATED PLATE #2 ON NEG. Y-SIDE
5,T
1.,-107.,944.
1.,-468.,867.
1.,-468.,730.
1.,-188.,458.
1.,-108.5,458.
PP:POLAR PLOT IN DB
T
1,2.766,3
PD:ROLL PLANE CUT
0.,0.,45.
0,360,1
T,50000.
EX:EXECUTE
```

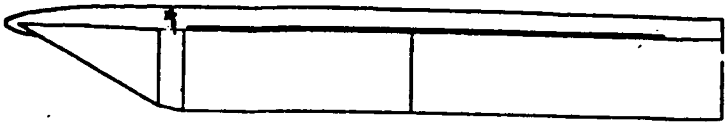

(a) SIDE VIEW

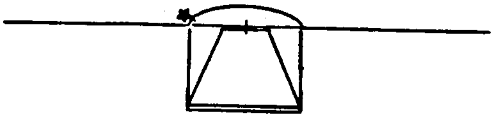

(b) FRONT VIEW

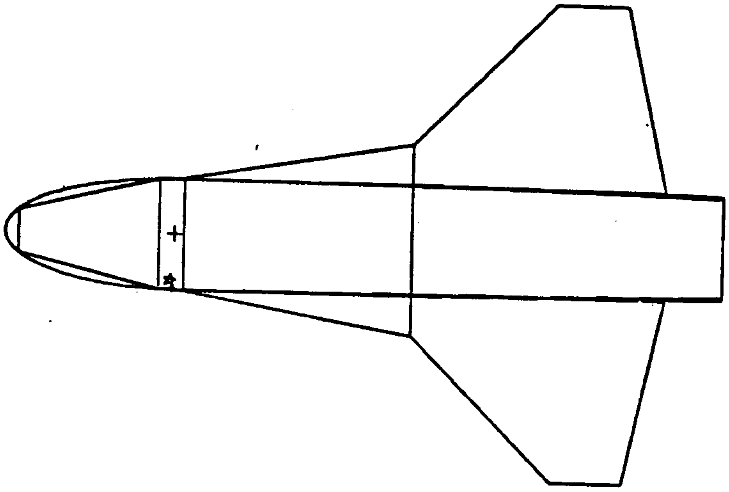

(c) BOTTOM VIEW

Figure 109. Computer simulated model for a crossed-slot antenna mounted on bottom of a Space Shuttle Orbiter.

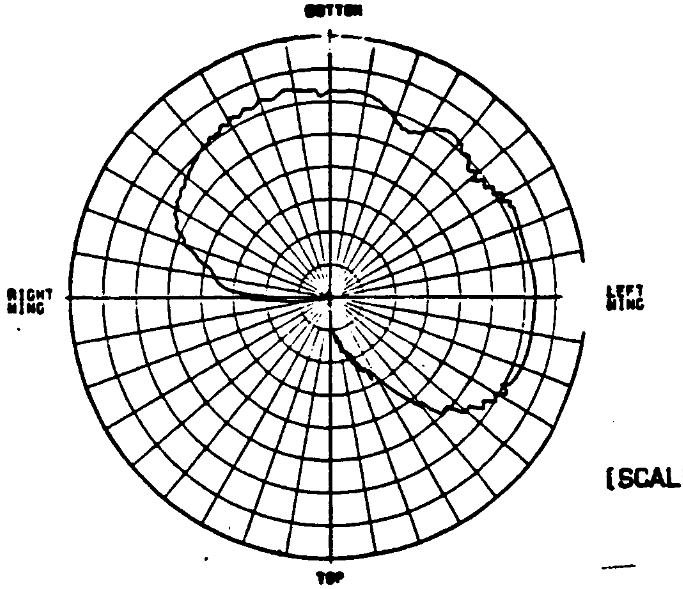

(SCALE: EACH DIVISION= 4DB)

(a) E_ϕ

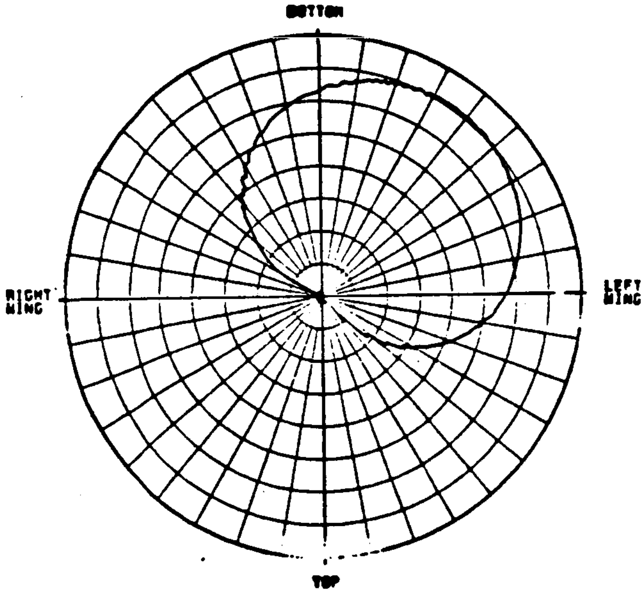

(b) E_θ

Figure 110. Roll conical patterns (θ_p=45°) for a crossed-slot antenna mounted on bottom of a Space Shuttle Orbiter when the payload bay doors are closed.

When the payload doors are open, the whole structure is still simulated by 16 plates as shown in Figure 111, although some of these plates are different from those obtained from the closed payload doors case. A roll conical pattern (θ_p=45°) is computed and then compared with that obtained with the payload doors are closed. The input data is as follows:

```
UN:IN INCHES
3
FG:SPACE SHUTTLE FOR THE BOTTOM MOUNTED ANTENNA WITH OPEN PAYLOAD DOORS CASE
40.,108.,2500.,325.
F
0.,0.,0.
FC:
T,F
1055.,0.
FQ:FREQUENCY (2 GHZ)
1,2.,1.
SG:CROSSED SLOT(.39 *.78 WAVELENGTH)
80.,-4.
2
0.,0.
2.3,4.6,0.,1.476,1
1.,0.
0.,0.
2.3,4.6,90.,1.476,1
1.,90.
FB:
1
6
0.,41.5,-300.
0.,107.5,-30.
0.,107.,760.
0.,-107.,760.
0.,-107.5,-30.
0.,-41.5,-300.
PG:SIDE WALL SIMULATED PLATE #1 ON POS. Y-SIDE
3,T
-1.,41.5,-300.
-155.,109.,-30.
-5.,107.5,-30.
```

```
PG:SIDE WALL SIMULATED PLATE #2 ON POS. Y-SIDE
5,T
-5.,107.5,-30.
-155.,109.,-30.
-165.,109.29,18.
-80.,108.44,18.
-5.,107.69,18.
PG:SIDE WALL SIMULATED PLATE #3 ON POS. Y-SIDE
4,T
-5.,107.69,18.
-80.,108.44,18.
-80.,108.44,458.
-5.,107.69,458.
PG:DOOR SIMULATED PLATE #1 ON POS. Y-SIDE
4,F
-80.,108.44,18.
-43.2,153.6,18.
-43.2,153.6,458.
-80.,108.44,458.
PG:DOOR SIMULATED PLATE #2 ON POS. Y-SIDE
4,F
-43.2,153.6,18.
-30.4,217.6,18.
-30.4,217.6,458.
-43.2,153.6,458.
PG:WING SIMULATED PLATE #1 ON POS. Y-SIDE
3,T
1.,108.5,8.
1.,188.,458.
1.,108.5,458.
PG:WING SIMULATED PLATE #2 ON POS. Y-SIDE
5,T
1.,108.5,458.
1.,188.,458.
1.,468.,730.
1.,468.,867.
1.,107.,944.
PG:BOTTOM SIMULATED PLATE #1
4,T
-1.,-41.5,-300.
-155.,-109.,-30.
-155.,109.,-30.
-1.,41.5,-300.
PG:BOTTOM SIMULATED PLATE #2
4,F
-155.,-109.,-30.
-165.,-109.29,18.
-165.,109.29,18.
-155.,109.,-30.
```

```
PG:SIDE WALL SIMULATED PLATE #1 ON NEG. Y-SIDE
3,T
-5.,-107.5,-30.
-155.,-109.,-30.
-1.,-41.5,-300.
PG:SIDE WALL SIMULATED PLATE #2 ON NEG. Y-SIDE
5,T
-5.,-107.69,18.
-80.,-108.44,18.
-165.,-109.29,18.
-155.,-109.,-30.
-5.,-107.5,-30.
PG:SIDE WALL SIMULATED PLATE #3 ON NEG. Y-SIDE
4,T
-5.,-107.69,458.
-80.,-108.44,458.
-80.,-108.44,18.
-5.,-107.69,18.
PG:DOOR SIMULATED PLATE #1 ON NEG. Y-SIDE
4,F
-80.,-108.44,458.
-43.2,-153.6,458.
-43.2,-153.6,18.
-80.,-108.44,18.
PG:DOOR SIMULATED PLATE #2 ON NEG. Y-SIDE
4,F
-43.2,-153.6,458.
-30.4,-217.6,458.
-30.4,-217.6,18.
-43.2,-153.6,18.
PG:WING SIMULATED PLATE #1 ON NEG. Y-SIDE
3,T
1.,-108.5,458.
1.,-188.,458.
1.,-108.5,8.
PG:WING SIMULATED PLATE #2 ON NEG. Y-SIDE
5,T
1.,-107.,944.
1.,-468.,867.
1.,-468.,730.
1.,-188.,458.
1.,-108.5,458.
PP:POLAR PLOT IN DB
T
1,2.766,3
PD:ROLL PLANE CUT
0.,0.,45.
0,360,1
T,50000.
EX:EXECUTE
```

The results shown in Figure 112 also indicate severe disturbances of the pattern due to the strong reflections from the payload doors. The above results indicate why one can lose use of his communication channel when the shuttle payload doors are open.

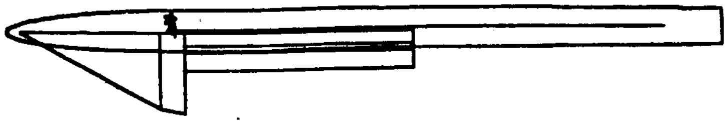

(a) SIDE VIEW

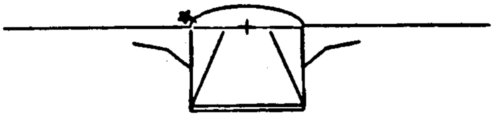

(b) FRONT VIEW

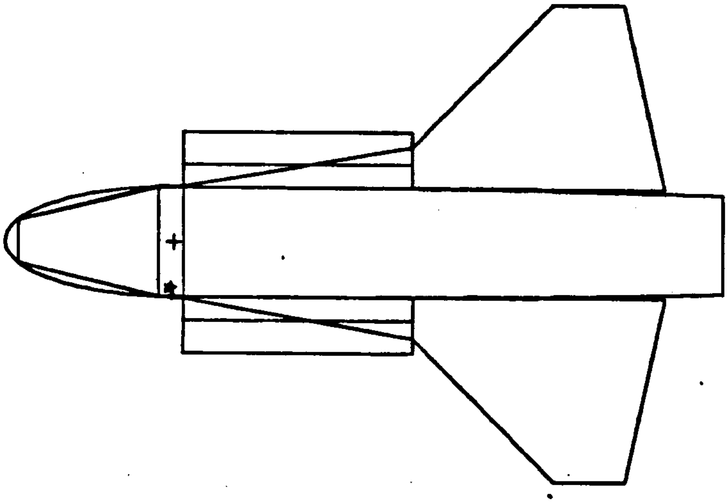

(c) BOTTOM VIEW

Figure 111. Computer simulated model for a crossed-slot antenna mounted on bottom of a Space Shuttle Orbiter when the payload bay doors are open.

ORIGINAL PAGE IS
OF POOR QUALITY

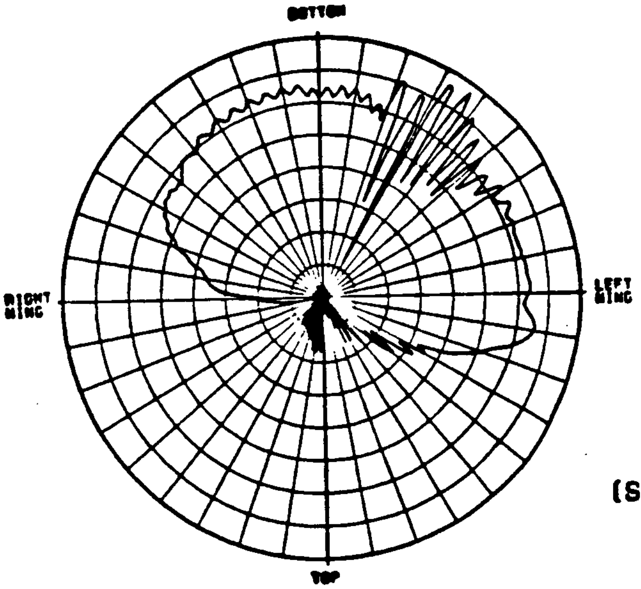

(SCALE: EACH DIVISION= 4DB)

(a) E_ϕ

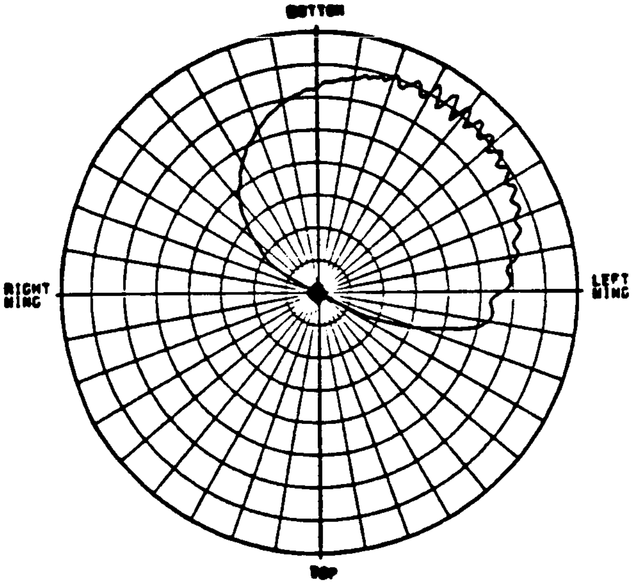

(b) E_θ

Figure 112. Roll conical patterns (θ_p=45°) for a crossed-slot antenna mounted on bottom of a Space Shuttle Orbiter when the payload bay doors are open.

REFERENCES

[1] R.G. Kouyoumjian and P.H. Pathak, "A Uniform Geometrical Theory of Diffraction for an Edge in a Perfectly-Conducting Surface," Proc. IEEE, Vol. 62, November 1974, pp. 1448-1461.

[2] R.G. Kouyoumjian, P.J. Pathak and W.D. Burnside, "A Uniform GTD for the Diffraction by Edges, Vertices and Convex Surfaces," Theoretical Methods for Determining the Interaction of Electromagnetic Waves with Structures, edited by J.K. Skwirynski, Sijthoff and Noordhoff, Netherlands, 1979.

[3] P.H. Pathak, N. Wang, W.D. Burnside and R.G. Kouyoumjian, "A Uniform GTD Solution for the Radiation from Sources on a Convex Surface," IEEE Trans. on Antenna Propagation, Vol. AP-29, No. 4, July 1981, p. 609-622.

[4] J.H. Richmond, "Radiation and Scattering by Thin-Wire Structures in the Complex Frequency Domain," Report 2902-10, July 1973, The Ohio State University ElectroScience Laboratory, Department of Electrical Engineering; prepared under Grant No. NGL 36-008-138 for National Aeronautics and Space Administration.

[5] W.D. Burnside, M.C. Gilreath, R.J. Marhefka, and C.L. Yu, "A Study of KC-135 Aircraft Antenna Patterns," IEEE Trans. on Antennas and Propagation, Vol. AP-23, No. 3, May 1975, pp. 309-316.

[6] R.J. Marhefka, "Analysis of Aircraft Wing-Mounted Antenna Patterns" Report 2902-25, June 1976, The Ohio State University ElectroScience Laboratory, Department of Electrical Engineering; prepared under Grant No. NGL 36-008-138 for National Aeronautics and Space Administration.

[7] W.D. Burnside, E.L. Pelton, N. Wang, "Analysis of Aircraft Simulations Using an Elliptic Cylinder and Multiple Plate," Report 711305-1, April 1979, The Ohio State University ElectroScience Laboratory, Department of Electrical Engineering; prepared under Contract N00019-78-C-0524 for Naval Air Systems Command.

[8] W.D. Burnside, N. Wang, and E.L. Pelton, "Near Field Analysis of Airborne Antennas," IEEE Trans. on Antenna and Propagation, Vol. AP-28, No. 3, May 1980, p. 318-327.

[9] W.D. Burnside and T. Chu, "Airborne Antenna Pattern Code User's Manual," Report 711588-2, March 1980, The Ohio State University ElectroScience Laboratory, Department of Electrical Engineering; prepared under Contract N62269-78-C-0379 for Naval Air Development Center.

[10] H.H. Chung and W.D. Burnside, "General 3D Airborne Radiation Pattern Code User's Manual", Technical Report 711679-10, July 1982, The Ohio State University ElectroScience Laboratory, Department of Electrical Engineering; prepared under Contract No. F30602-79-C-0068 for the Department of the Air Force, Rome Air Development Center.

[11] W.D. Burnside, R.G. Kouyoumjian, R.J. Marhefka, R.C. Rudduck, and C.H. Walter, "Asymptotic High Frequency Techniques for UHF and Above Antennas," Annual Report 4508-6, August 1977, The Ohio State University ElectroScience Laboratory, Department of Electrical Engineering; prepared under Contract N00123-76-C-1371 for Naval Regional Procurement Office.

[12] W.D. Burnside, "User's Manual Flat Plate Program," Report 4508-4, May 1977, The Ohio State University ElectroScience Laboratory, Department of Electrical Engineering; prepared under Contract N00123-76-C-1371 for Naval Regional Procurement Office, Long Beach, California.

[13] R.J. Marhefka, User's Manual for Plates and Cylinder Computer Code," Report 4508-8, March 1978, The Ohio State University ElectroScience Laboratory, Department of Electrical Engineering; prepared under Contract N00123-76-C-1371 for Naval Regional Procurement Office, Long Beach, California.

[14] J.J. Kim, N. Wang, and C.D. Chuang, "Geodesic Paths of an Ellipsoid-Mounted Antenna", Technical Report 713321-3, March 1982, The Ohio State University ElectroScience Laboratory, Department of Electrical Engineering; prepared under Contract No. N00019-80-PR-RJ015 for the Department of the Navy, Naval Air Systems Command.

[15] J.J. Kim and W.D. Burnside, "Geodesic Paths for Side-Mounted Antenna on an Ellipsoid Model", Technical Report 714215-1, October 1982, The Ohio State University ElectroScience Laboratory, Department of Electrical Engineering; prepared under Contract No. N00019-81-C-0424 for the Department of the Navy, Naval Air Systems Command.

[16] J.J. Kim, "Simulation and Analysis of Airborne Antenna Radiation Patterns", Technical Report 716199-1, December 1984, The Ohio State University ElectroScience Laboratory, Department of Electrical Engineering; prepared under Grant No. NSG 1498 for the National Aeronautics and Space Administration. Also a Ph.D. dissertation, The Ohio State University, 1984.

[17] C.A. Lindberg, "A Shallow-Cavity UHF Crossed-Slot Antenna", IEEE Trans. AP-17, September 1969, pp. 558-563.